

**Advancing Alkali Metal Dihydropyridine
Chemistry: Syntheses, Structures and
Applications**

Samantha Alana Orr

A thesis submitted to the Department of Pure and Applied Chemistry, University of Strathclyde in part fulfilment of the requirements for the degree of Doctor of Philosophy.

June 2017

This thesis is the result of the author's original research. It has been composed by the author and has not been previously submitted for examination which has led to the award of a degree.

The copyright of this thesis belongs to the author under the terms of the United Kingdom Copyright Acts as qualified by University of Strathclyde Regulation 3.50. Due acknowledgement must always be made of the use of any material contained in, or derived from, this thesis.

Dedicated to my Late Grandad

Acknowledgements

Being the first in my family to undertake a PhD was overwhelming, you have no idea what to expect, nobody has been through the rollercoaster of a PhD to pass on advice and share their experience. But as I sat in the library reading my PhD acceptance email, the excitement and optimism I had assured me I was on the right path! Now at the end of the journey I can honestly say my answer to the next person in my family, is, without hesitation, do it!!! It was the best experience of my life; along with some lows I have had exceptional highs, memories that will live with me for the rest of my life and for that I am truly grateful.

First and foremost I must thank my supervisor Prof. Robert Mulvey who I owe this whole experience to! I have been extremely fortunate to work with someone who saw something in me, that most of the time I didn't see myself! Rab has always encouraged me and pushed me to be the best I could possibly be, and for that I could never thank him enough. His lengthy discussions in coffee shops (even if we got distracted talking about Nobu), help and guidance have shaped me into the researcher I am today. Not only does it feel like you are part of his research group, you are part of the Mulvey family!

Following that, I must thank George Fraser and his wife, whose generosity has helped fund this PhD and made this research possible.

My extended thanks must go to the other supervisors within the group. Prof. Eva Hevia, whose wealth of knowledge and encouragement has been invaluable throughout my years. Dr Charlie O'Hara who must have special mention, as he was the one who introduced me to this chemistry as an undergraduate with a summer placement, an opportunity that has helped direct me to where I am today! And finally Dr Stuart Robertson has been priceless throughout the past three years, along with many insightful discussions on my projects, he has always been there with a pink jammy to celebrate our victories.

Thanks must go to the entire extended Mulvey/Hevia/O'Hara/Robertson groups past and present for making the lab such an enjoyable place to be. As the group was so

large there are too many people to mention individually and at risk of missing someone out, I would like to thank you all as a whole, I have shared great memories with you all over the years! To name a few, I must mention my morning tea pals Leonie and Marina, I have gained two sisters with you crazy pair. Laia must also be mentioned; we started our journey together and have been through the peaks and troughs of the PhD as a team. We have shared so many memories (organising USIC, the shark song, Barca vs Celtic), I was very fortunate to have a friend like you to experience it all with! I must also thank Ross for all his help and advice on the dihydropyridine work, and for doing all the X-ray crystallography within this thesis! I have also been fortunate enough to have the opportunity to mentor some undergraduate students who have been great fun to work with. Andreas must be thanked for his help with the work in chapter 5, and my current summer student Neil (who might support the wrong team) but is currently working on the aluminium based dihydropyridine work.

Many people in my day-to-day lab life must be acknowledged. To start, a very special lady who makes me laugh everyday...Isabel my wee adopted granny!! Thank you for always being there, looking after me! You spoil me rotten...I mean who else could make my Halloween costumes as good as you – Best Bride of Chucky costume ever!! Janie-Anne, our little lab hero, I greatly appreciate all your help making the lab run smoothly for us. I don't know what we would do without you! Paul and Billy who spoil us with our liquid nitrogen deliveries!! Craig Irving at NMR for his tolerance of my one million and one questions, I'm sure he'll be glad when the day comes that he doesn't have me popping my head in asking "Craig, have you got a wee second"! Alan Kennedy must also be mentioned for all his time he has dedicated to my nightmare X-ray crystallographic data over the years!!

To name a few people, outside of my chemistry world that put up with me on a daily basis, I must start with thanking my bestie Megan! Your attitude to life motivates me everyday, you have always been supportive of your lil Bill Nye and I love you so much for that!! I'm very lucky to have a friend like you cheering me on...one day we'll get that mermaid room!! And last but not least, a late entry to the PhD journey, Callum! Thank you for always putting a smile on my face and keeping me going! I am very fortunate to have someone as supportive as you....the best "Stillie" Coupling in 2017.

Finally, I have no words to explain how grateful I am of my Mum and Dad's support. Everything that I am today is because you both always went the extra mile for me so I could have this opportunity. I will never forget the journey to get me here, tutors, B&Q car parks, stationary shops...I am so proud of what we have achieved. Anyone that knows me will understand how special my Mum and Dad are to me. No matter the favour, whether it be running to McDonalds to get me brain food, helping making jars of sweets for our USIC conference, joining me on a trip to work at midnight to monitor NMRs, or just being my personal taxi service, they have been there through it all doing anything they can to help!! I am forever grateful to have such loving, supportive and crazy fun parents to keep me smiling.

Abstract

This project develops the chemistry of Group 1 dihydropyridines, a class of compound previously largely confined to lithium. A synthetic approach to sodium and potassium derivatives has been optimised via metathesis, the new compounds have been thoroughly characterised and the catalytic ability of the family has been assessed.

Firstly, the previously reported lithium dihydropyridine (LiDHP) proved a valuable precursor to access five new s-block dihydropyridines that have been isolated and characterised by X-ray crystallography and NMR spectroscopy. The isomerisations of the 1,2- to the 1,4- isomeric forms have been monitored by NMR spectroscopy. Thermal studies on the non-solvated derivatives were performed and related to their ability to release metal hydride. Their proficiency to act as metal hydride surrogates was confirmed in reactions reducing benzophenone.

Secondly, the first catalytic role of LiDHPs was established in the successful catalysed dehydrogenative cyclisation of diamine boranes. It was found that the LiDHP catalyst could compete with a ruthenium catalyst to prepare desired 1,3,2-borolidines. A three-step mechanism has been suggested, (deprotonation, β -hydride elimination and intramolecular hydrogen loss) supported by crystallographically characterised intermediates and extensive NMR studies. Formed in situ, the borolidines were further functionalised to more synthetically useful phenylborane derivatives.

The LiDHP was next subjected to a further catalytic screening for hydroboration of carbonyls. This also proved successful for preparing boronate esters, from a range of aldehydes and ketones with pinacolborane. The reaction was thought to proceed akin to that reported in the literature, namely a hydrometallation followed by a metathesis step. However, an acceptor-donor adduct of pyridine and pinacolborane, characterised by X-ray crystallography, provided insight to a potential alternative pathway in the catalytic cycle.

Finally, expanding on the monometallic dihydropyridines, six new heterobimetallic dihydropyridine complexes, Li/Al, K/Al and K/Zn, have been synthesised and crystallographically characterised. Their structural assembly is contrasted with similar literature complexes.

Publications

[1] S. A. Orr, A. R. Kennedy, J. J. Liggat, R. McLellan, R. E. Mulvey and S. D. Robertson, Accessible heavier s-block dihydropyridines: structural elucidation reactivity of isolable molecular hydride sources, *Dalton Trans.*, **2016**, 45, 6234-6240.
Main group transformations

[2] R. McLellan, A. R. Kennedy, S. A. Orr, S. D. Robertson and R. E. Mulvey, Lithium Dihydropyridine Dehydrogenation Catalysis: A Group 1 Approach to the Cyclization of Diamine Boranes, *Angew. Chem. Int. Ed.*, **2017**, 56, 1036-1041.

[3] R. McLellan, A. R. Kennedy, S. A. Orr, S. D. Robertson and R. E. Mulvey, Lithium Dihydropyridine Catalysed Hydroboration of carbonyls, *Accepted Chem. Eur. J.*

Conference Presentations

[4] Developing group 1 dihydropyridine chemistry: from transient intermediates to isolable compounds, Oral Presentation, *West Brewery Inorganic Chemistry Postgraduate Presentations*, Glasgow, June **2015**

[5] Developing group 1 dihydropyridine chemistry: from transient intermediates to isolable compounds, Oral Presentation, *Universities of Scotland Inorganic Chemistry Conference*, Heriot-Watt University, August **2015**

[6] Developing group 1 dihydropyridine chemistry, *Poster Presentation, Annual Main Group Interest Group Meeting and AGM*, RSC London September **2015**

[7] Developing group 1 dihydropyridine chemistry: from transient intermediates to isolable compounds, Oral Presentation, *The international chemical congress of pacific basin societies*, Honolulu, Hawaii, December **2015**

[8] Advancing Group 1 Dihydropyridine Chemistry: from Isolable compounds to catalytic applications, Poster presentation, *Universities of Scotland Inorganic Chemistry Conference*, University of Strathclyde, August **2016**

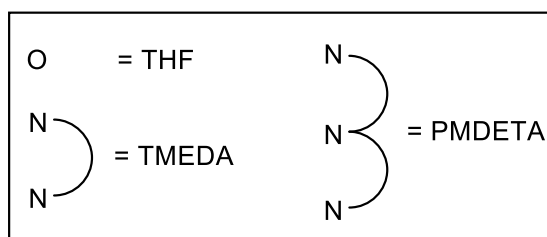
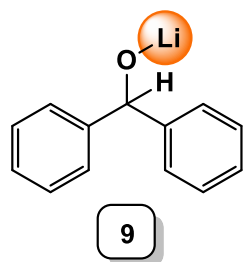
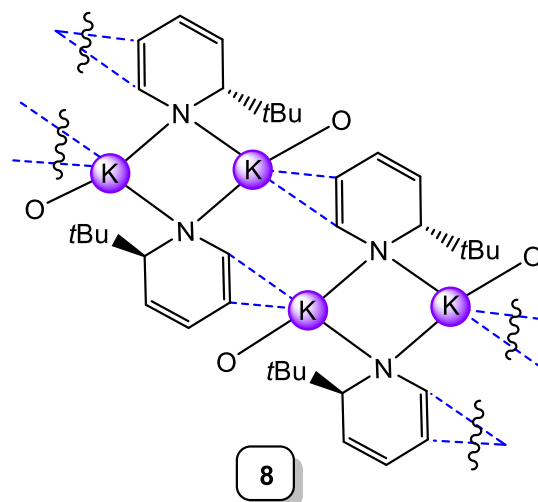
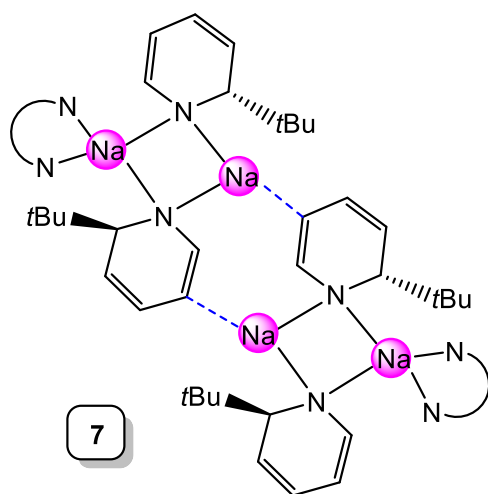
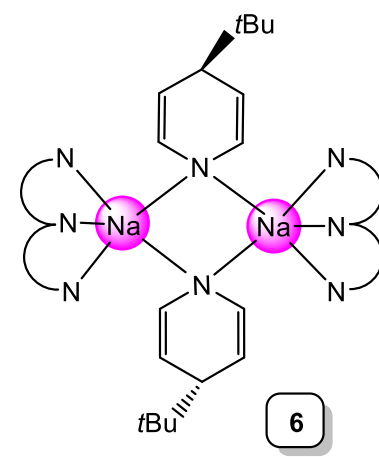
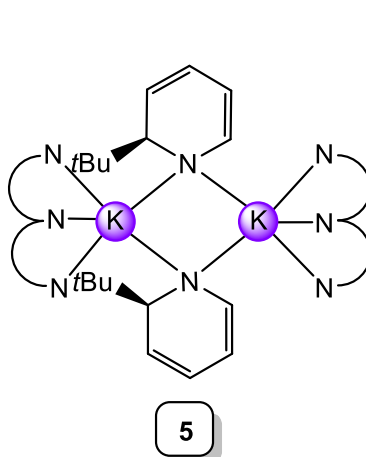
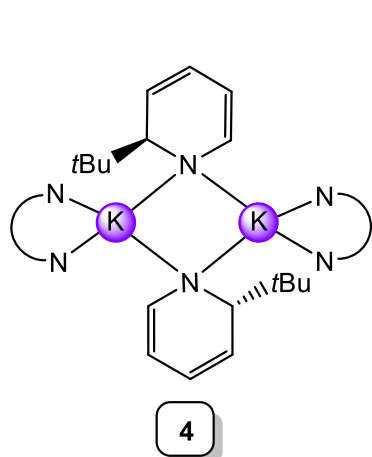
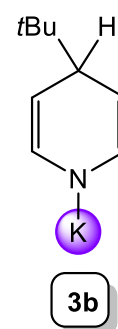
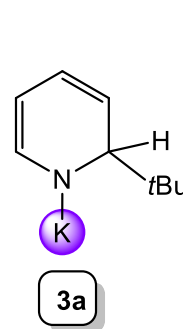
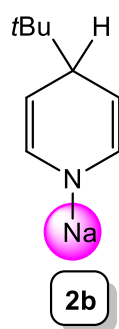
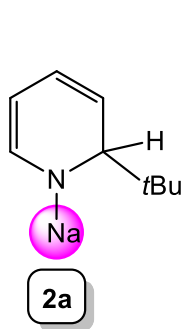
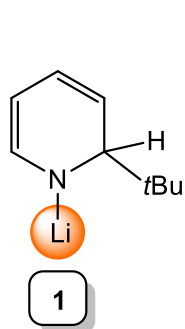
[9] Alkali Metal Dihydropyridines: Synthesis, Structures and Catalytic Applications, Oral presentation, *WestCHEM research day*, University of Strathclyde, August **2016**

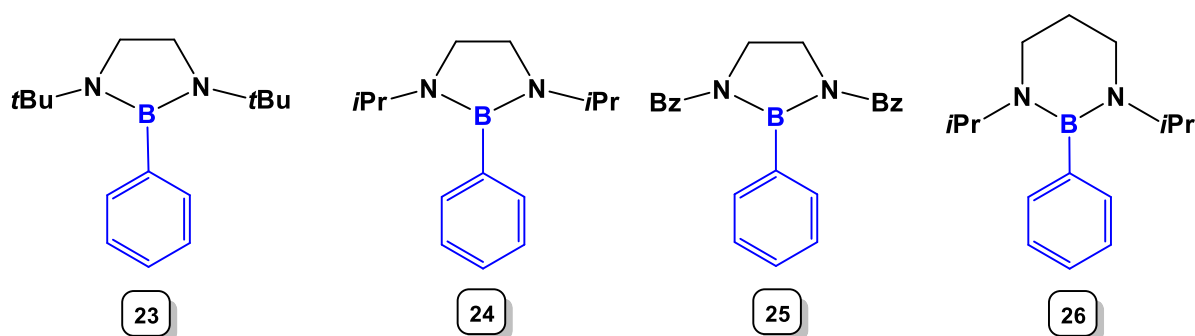
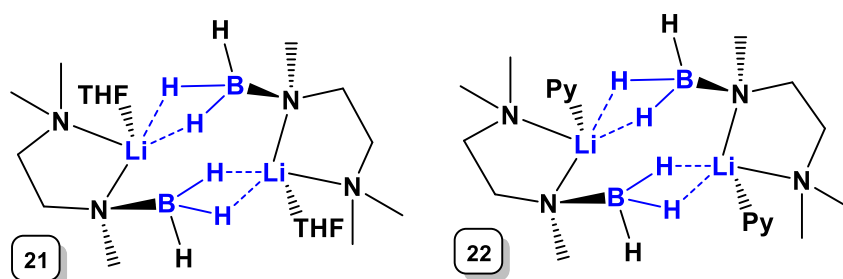
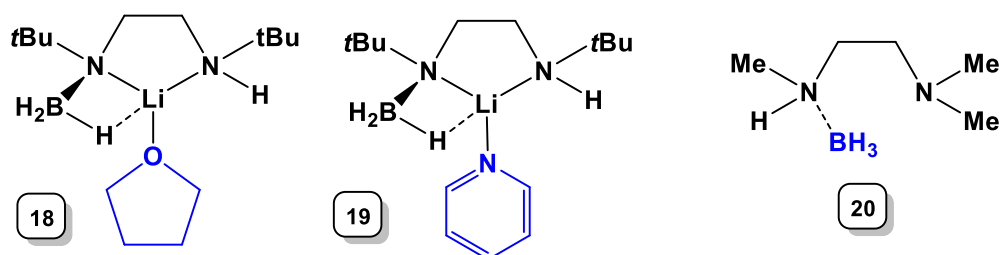
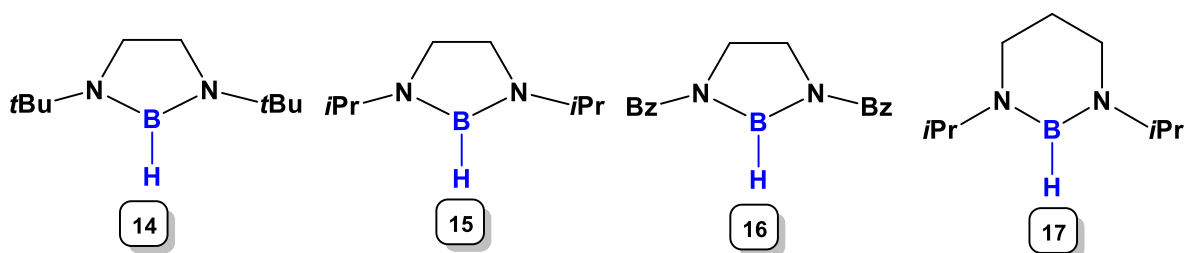
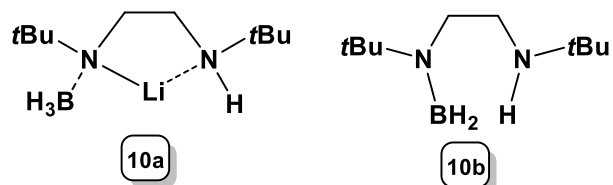
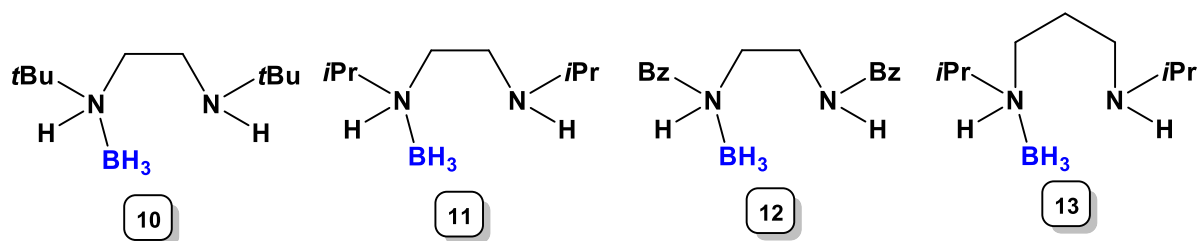
List of Common Abbreviations

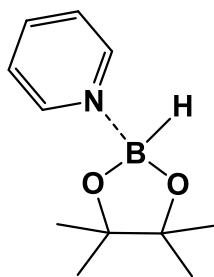
AM	Alkali Metal
AMMAI	Alkali-Metal-Mediated Aluminatation
AMMMg	Alkali-Metal-Mediated Magnesiatio
AMMZn	Alkali-Metal-Mediated Zincation
<i>i</i> -Bu	iso-butyl
<i>n</i> Bu	n-butyl
<i>n</i> BuLi	n-butyl lithium
<i>t</i> Bu	tert-butyl
<i>t</i> BuLi	tert-butyl lithium
<i>t</i> BuOK	Potassium tert-butoxide
<i>t</i> BuONa	Sodium tert-butoxide
CCDB	Cambridge Crystallographic Database
C ₆ D ₆	Deuterated benzene
CDCl ₃	Deuterated chloroform
C ₆ D ₁₂	Deuterated cyclohexane
CIP	Contact Ion Pair
COSY	Correlation Spectroscopy
DA	Diisopropylamide
DA(H)	Diisopropylamine
DFT	Density Functional Theory
DHP	dihydropyridine
DIBAL(H)	Diisobutylaluminium hydride
DoM	Directed <i>ortho</i> -metallation
DOSY	Diffusion Ordered Spectroscopy
Et	Ethyl
Fe	Ferrocene
HMDS	1,1,1,3,3,3-hexamethyldisilazide
HMDS(H)	1,1,1,3,3,3-hexamethyldisilazane
HSQC	Heteronuclear Single Quantum Correlation Spectroscopy
KDHP	Potassium dihydropyridine
LDA	Lithium diisopropylamide

LICKOR	Alkyl lithium/potassium alkoxide superbases
LiDHP	Lithium dihydropyridine
Me	Methyl
Me ₆ -TREN	tris[2-(dimethylamino)ethyl]amine
MW	Molecular weight
NaDHP	Sodium dihydropyridine
NMR	Nuclear Magnetic Resonance
Ph	Phenyl
PhN	Phenylnaphthalene
PMDETA	N,N,N',N'',N'''-pentamethyldiethylenetriamine
ppm	parts per million
Py	pyridine
iPr	<i>iso</i> -propyl
R	Generic alkyl group
RLi	Generic alkyl lithium reagent
RMgX	Generic Grignard reagent
SSIP	Solvent Separated Ion Pair
THF	Tetrahydrofuran
TMEDA	<i>N,N,N',N'</i> -tetramethylethylenediamine
TMP	2,2,6,6-tetramethylpiperidide
TMP(H)	2,2,6,6-tetramethylpiperidine
TMS	Tetramethylsilane
TMT	Trans-Metal Trap

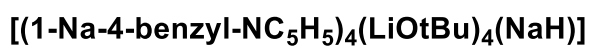
Numbered Compounds



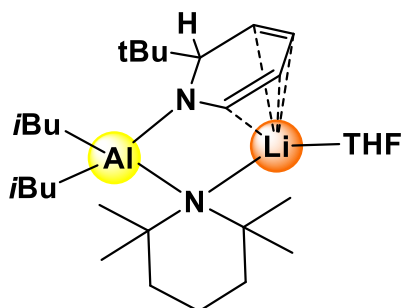




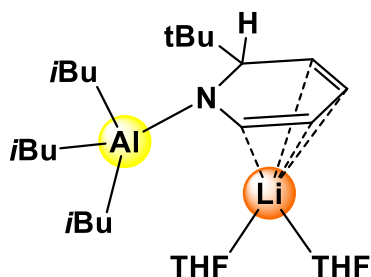
27



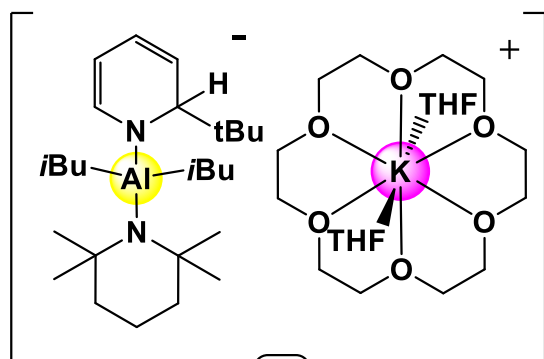
28



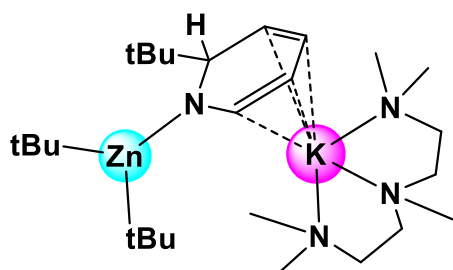
29



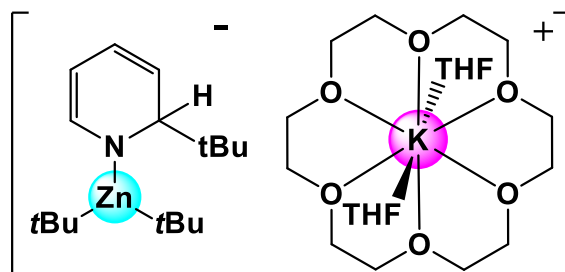
30



31



32



33

Table of Contents

ACKNOWLEDGEMENTS	IV
ABSTRACT	VII
PUBLICATIONS	VIII
CONFERENCE PRESENTATIONS	IX
LIST OF COMMON ABBREVIATIONS	X
NUMBERED COMPOUNDS	XII
TABLE OF CONTENTS	XV
CHAPTER 1: INTRODUCTION TO POLAR ORGANOMETALLIC CHEMISTRY	1
1.1 Organolithium chemistry	1
1.1.1 Organolithiums	2
1.1.2 Preparation of Organolithium Compounds	3
1.1.3 Lithium amides	6
1.2 Cooperative mixed-metal chemistry	9
1.2.1 LICKOR superbase	9
1.2.2 Development of Grignard reagents	12
1.2.3 Alkali-metal-mediated metallation (AMMM)	15
1.2.4 Trans-Metal-Trapping (TMT)	19
1.3 References	23
CHAPTER 2: DEVELOPMENT OF S-BLOCK DIHYDROPYRIDINES	29
2.1 Summary	29
2.2 Introduction	30
2.2.1 Metallodihydropyridines	31
2.2.2 s-Block dihydropyridines	34

2.2.3 Group 1 dihydropyridines	38
2.3 Aims of this chapter	41
2.4 Result and discussion	41
2.4.1 Synthetic approach to isolable sodium and potassium dihydropyridines	41
2.4.2 Solid state structures	46
2.4.3 Solution state structures	56
2.4.4 Thermal Volatility Analysis (TVA) studies	58
2.4.5 Preliminary hydrometallation studies	61
2.5 Conclusions and future work	61
2.6 Experimental	62
2.6.1 Synthesis	62
2.6.2 TVA collection	67
2.6.3 Reduction of benzophenone	67
2.6.4 Crystallographic data and refinement details for compounds 4-8	68
2.7 References	69
CHAPTER 3: LITHIUM DIHYDROPYRIDINE CATALYSED DEHYDROGENATIVE CYCLISATION OF DIAMINE BORANES	75
3.1 Summary	75
3.2 Introduction	76
3.2.1 Dehydrocoupling catalysis	76
3.2.2 Dehydrogenative cyclisation	78
3.3 Aims of this chapter	79
3.4 Results and discussion	79
3.4.1 Preliminary optimization studies	79
3.4.2 Extension to other diamine boranes	83
3.4.3 Reaction mechanism by NMR spectroscopic studies	85
3.4.4 Structural evidence to support reaction mechanism	91
3.4.5 Reactivity studies of isolated intermediates	99
3.3.6 Postsynthetic functionalization of 1,3,2-diazaborolidine	101
3.5 Conclusions and future work	104
3.6 Experimental	106

3.6.1 General catalytic procedure	106
3.6.2 Synthesis of starting materials and characterisation of new compounds	106
3.6.3 Crystallographic data and refinement details for compounds 18 , 19 , 21 , 22 and 23 .	113
3.7 References	114
CHAPTER 4: LITHIUM DIHYDROPYRIDINE CATALYSED HYDROBORATION OF CARBONYLS	116
4.1 Summary	116
4.2 Introduction	117
4.2.1 Summary of catalysed hydroboration reactions	120
4.2.2 Catalysed hydroboration of carbonyls	123
4.3 Aims of this chapter	124
4.4 Results and discussion	125
4.4.1 Hydroboration of ketones	125
4.4.2 Hydroboration of aldehydes	129
4.4.3 Proposed reaction pathway	132
4.5 Conclusions and future work	136
4.6 Experimental	137
4.6.1 General catalytic hydroboration procedure	137
4.6.2 Characterisation of hydroborated aldehydes	137
4.6.3 Characterisation of hydroborated ketones	139
4.6.4 Crystallographic data and refinement details of compound 27	142
4.7 References	143
CHAPTER 5: BIMETALLIC DIHYDROPYRIDINES: SYNTHETIC APPROACH AND STRUCTURAL EXPLORATION	147
5.1 Summary	147
5.2 Introduction	148
5.3 Aims of this chapter	148
5.4 Results and discussion	148
5.4.1 X-ray crystallographically characterised s-block bimetallic dihydropyridines	148

5.4.2 Mixed alkali metal-aluminium dihydropyridines	152
5.4.3 Mixed alkali metal - zinc dihydropyridines	158
5.5 Conclusions and future work	162
5.6 Experimental	164
5.6.1 Synthesis of compounds 28-33	164
5.6.2 Crystallographic data and refinement details for compounds 28-33 .	167
5.7 References	168
CHAPTER 6: CLOSING REFLECTIONS	171
CHAPTER 7: GENERAL EXPERIMENTAL TECHNIQUES AND PROCEDURES	174
7.1 Schlenk techniques	174
7.2 Glovebox manipulation	175
7.3 Solvent and reagent purification	175
7.4 Analytical procedures	176
7.4.1 NMR Spectroscopy	176
7.4.2 X-ray Crystallography	177
7.4.3 Elemental Analysis	177
7.5 Preparation of common starting materials	177
7.5.1 Preparation of <i>n</i> BuNa	177
7.5.2 Preparation of KCH ₂ SiMe ₃	177
7.5.3 Preparation of <i>t</i> Bu ₂ Zn	177
7.5.4 Preparation of <i>i</i> Bu ₂ AlTMP	178
7.6 References	178

Chapter 1: Introduction to polar organometallic chemistry

Organometallic chemistry as a field is extremely vast, being prevalent in many applied research areas including pharmaceuticals, agrochemical, dyes and polymers, as well as in fundamental academic research where synthesis is a major component. The scope is therefore outside the confines of this thesis. However, a few monumental landmarks in the history of organometallics^[1] have been highlighted in figure 1.1. This chapter aims to provide a brief summary of organolithium chemistry and discuss the significant developments of second-generation bimetallic ‘ate’ complexes and how these exhibit extraordinary synergic reactivity. This will set the scene for the research discussed herein, with each chapter following having a brief, but more specific introduction.

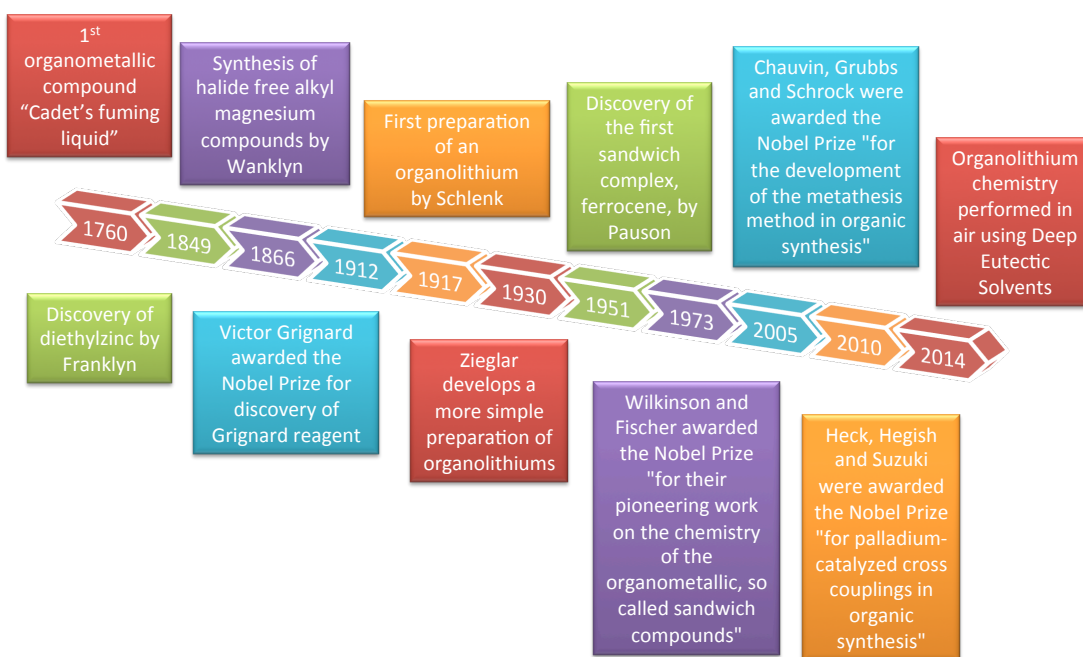


Figure 1.1: A selection of highlights in organometallic chemistry.

1.1 Organolithium chemistry

Wilhelm Schlenk, a German scientist, reported the seminal breakthrough of the first preparations of organolithium (RLi) compounds in 1917.^[2] The specific compounds made were methyl lithium, ethyllithium and phenyllithium in addition to the organosodium analogues. Schlenk's contribution was acknowledged, yet not fully realised, by receiving a Nobel Prize nomination for this ground-breaking work. A

century later, Schlenk's name is found today in air- and moisture sensitive laboratories worldwide due to his creativity and development of such innovative inert atmosphere apparatus designs and techniques. For the safe handling and manipulation of these air- and moisture-sensitive organometallic materials, synthetic chemists routinely employ Schlenk techniques. Of no surprise, in the early years organolithium compounds were deemed too unstable to be of much practical use, given Schlenk's description "...the numerous yellow-glowing sparks thrown out by the red flame make the burning of methyllithium a magnificent sight".

However, in reality and in time these reagents have become indispensable to the synthetic chemist, in particular alkyl and amido-lithium compounds which are utilised widely.^[3-7] Collum, highlighted their exploitation in organic synthesis, proposing that well over 95% of natural products syntheses rely upon lithium based reagents at some stage in their preparations.^[8] This is not surprising when organolithium metallation or addition followed by an electrophilic quench is one of the world's most practiced synthetic methodologies.

With this year marking a century since Schlenk's initial organolithium discovery, it can only be said that the transformation of a carbon-hydrogen bond to a more polar, reactive, carbon-metal bond is as important as ever, allowing synthetic chemists access to a vast library of new carbon-carbon or carbon-heteroatom bond formations.

1.1.1 Organolithiums

Considering one of the most common alkyllithium reagents, *n*-butyllithium (*n*BuLi) it would be naïve to think about the structure as a simplistic monomeric carbon-lithium unit. Dietrich revealed the first structural characterisation of an organolithium compound, ethyllithium, as solvent-free tetrameric aggregates.^[9,10] Structural reports emerged in following years as X-ray crystallographic equipment advanced, deducing the structural complexity of the class of alkyllithium and related organolithium compounds. The aggregation state of one of the most common alkyllithium reagents, butyllithium, demonstrates the influence of steric factors.^[11] By simply moving from the *n*butyl to *t*butyl isomer, a hexameric versus a tetrameric electron deficient arrangement is observed in the solid state (Figure 1.2). A consequence of these

molecular architectures is that the compounds exhibit solubility in hydrocarbon solvents. However, for methyllithium^[12] and phenyllithium^[13] this is not the case due to supramolecular structures featuring significant intermolecular interactions, so donor solvents that destroy these intermolecular contacts are required for solubility. Thus the degree of association observed is correlated to the solvent choice and ultimately related to the reactivity.

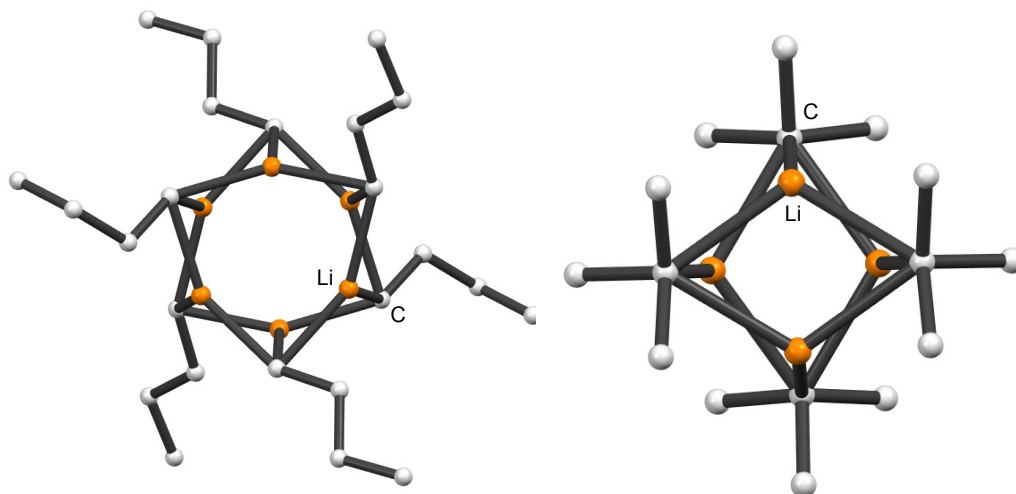
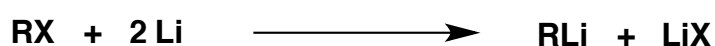


Figure 1.2: Comparison of the discrete molecular structures of non-solvated hexameric *n*BuLi (left) and tetrameric *t*BuLi (right).

1.1.2 Preparation of Organolithium Compounds

One of the reasons for their popularity in synthetic chemistry is that to date a wide range of organolithium reagents are commercially available from companies such as Sigma Aldrich, Tokyo Chemical industry and Boc Sciences. The most important reagent *n*-BuLi is made via a redox reaction from the elemental metal^[14] as in eqn 1.1.

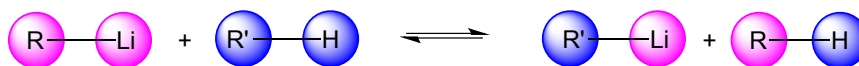


Equation 1.1: Preparation of *n*BuLi via a redox reaction.

Those compounds not available for purchase can be accessed via a range of preparative methods typically involving metallation or metal-halogen exchange, which still require the use of commercially available reagents. Representative examples of these exchange methodologies are now highlighted.

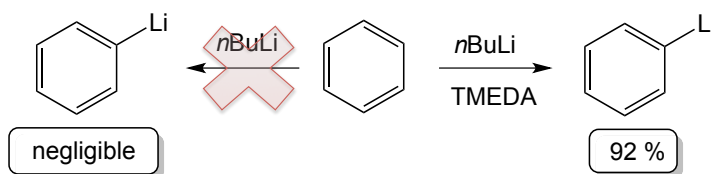
1.1.2.1 Deprotonative Metallation

Deprotonative metallation is the most versatile method and most important for functionalizing aromatic compounds as shown in [scheme 1.1](#), where RLi is typically an alkyllithium reagent and R'H is the organic species to be metallated.



Scheme 1.1: Schematic of a typical deprotonative metallation reaction.

The acid-base equilibria reaction is to an extent predictable from pK_a patterns. In essence, the most acidic hydrogen atom will be removed (deprotonated) and replaced with lithium. However if the R'H co-product is more acidic, that is has a lower pK_a than RH, then the equilibrium will reverse to the starting materials. For this reason, pK_a has a detrimental effect on the reaction equilibrium and has to be considered when planning this type of synthesis. A problem is that organolithium reactions cannot be carried out in water and many tabulated pK_a values of organic substrates have been experimentally determined in water.^[15] Solvent can also have a profound effect on the outcome of the metallation reaction with regards to reactivity. For example the participation of Lewis base donors can accelerate and catalyse lithiation. [Scheme 1.2](#) shows an example that illustrates the influence of Lewis donors on the reaction outcome. In the absence of *N,N,N',N'*-tetramethylethylenediamine (TMEDA), even the strong base *n*-butyllithium cannot deprotonate benzene to any appreciable extent. However, upon the addition of TMEDA, benzene is metallated in a near quantitative yield.^[16]

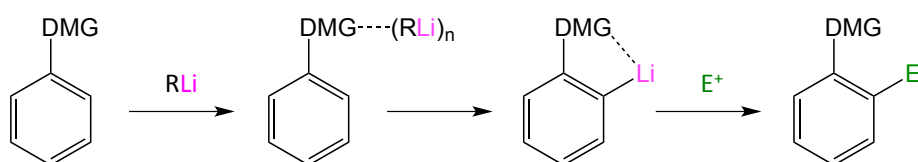


Scheme 1.2: Influence of Lewis base donors in the lithiation reaction of benzene.

1.1.2.2 Directed *ortho* Metallation (DoM)

A special subcategory of metal-hydrogen exchange is Directed *ortho* Metallation (DoM), in particular directed *ortho* lithiation^[17,18] ([Scheme 1.3](#)). The methodology is

based on a pre-installed directing metallating group (DMG) controlling the position of metallation to functionalise aromatic rings (Figure 1.3). Gilman and Wittig independently discovered this extremely useful methodology in the 1940s.^[19,20] The long established alternative method, electrophilic aromatic substitution can give rise to *ortho* and *para* substitutions, whereas DoM provides a superior method to exclusively substitute at the position *ortho* to the DMG.



Scheme 1.3: Chemdraw representation of Directed *ortho* Lithiation and subsequent electrophilic interception.

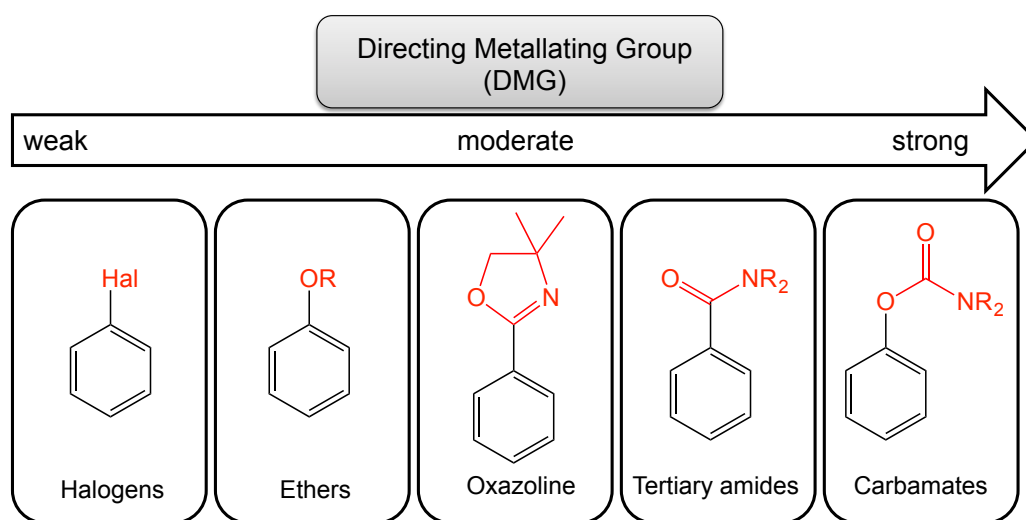
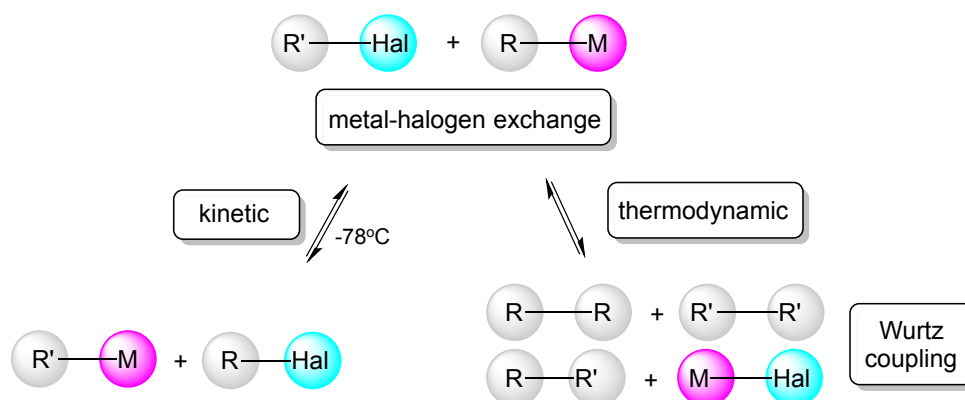
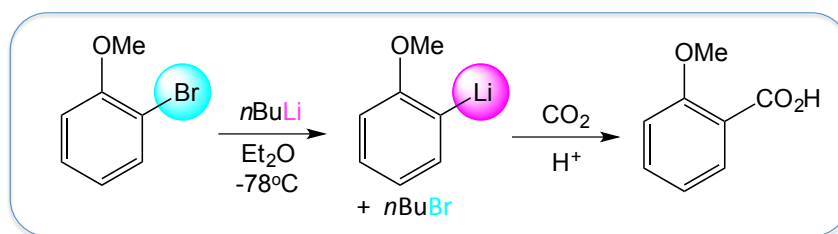


Figure 1.3: Common examples illustrating the directing ability of different *ortho* directing groups.

1.1.2.3 Metal-Halogen exchange

This approach is similar to the deprotonative metallation; and like this approach it has its advantages and disadvantages. Firstly, the reaction equilibrium has to be considered (Scheme 1.4) as the reaction will favour the side with the carbanion most capable of accommodating and stabilizing a negative charge.



Scheme 1.4: Example of a lithium-halogen exchange reaction (top) and (bottom) the importance of kinetic control to avoid Wurtz coupling.

A key advantage this halide-based approach has over general metallation is that it is regioselective to the position of the halogen in the organic halide starting material. This is a practical development for carrying out a selective metallation on compounds that contain many C-H bonds of similar strength. The drawback to this of course is the halogenated compound has to be available or synthesised beforehand. The downfall of this reaction is that potential side reactions can occur including Wurtz coupling resulting in a homocoupled product R-R, and the thermodynamic metal halide precipitate.^[21] However, if the reaction is carried out at -78°C to work under kinetic control, the side reactions can be overcome by the speed of the metal-halogen exchange. This only applies if a weakly bound carbon-halogen bond is used, for example C-Br/C-I. If Br was replaced with Cl or F, the bond would be stronger, harder to break than C-H bonds, and consequently side reactions would occur, including most notably Wurtz coupling (Scheme 1.4).

1.1.3 Lithium amides

Derivatives of secondary amines of general formula $\text{RR}'\text{NH}$, alkali metal amides $\{[\text{RR}'\text{NLi}]\}$, are amongst the most widely used polar metal reagents for various

important organic transformations including the generation of enolates, condensation reactions and Wittig reactions to name but a few.^[22] This use of alkali metal amides is due to their complementary characteristics of strong Brønsted basicity (though not as strong as that of *n*- or *t*-butyllithium) and weak nucleophilicity, making them effective strong bases with a high degree of chemoselectivity. Whilst there are many amido derivatives which have been studied, the three of utmost importance^[23] from a synthetic point of view are lithium diisopropylamide (LDA), lithium 2,2,6,6-tetramethylpiperidide (LiTMP) and lithium 1,1,1,3,3,3-hexamethyldisilazide (LiHMDS) (Figure 1.4).

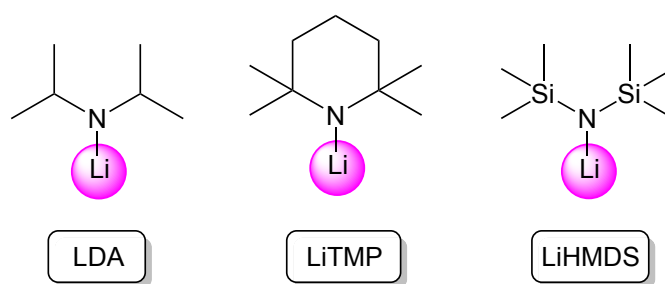
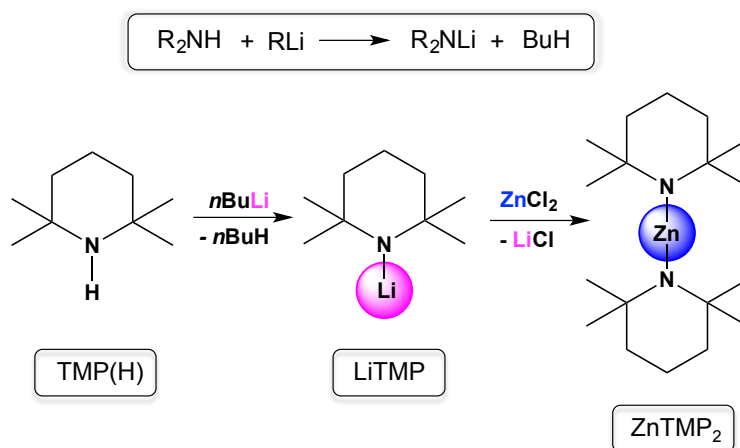


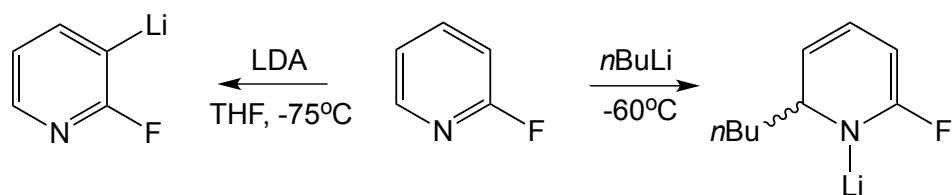
Figure 1.4: Three of the most employed lithium amides in the synthetic toolbox.

Some common alkali metal amides including LDA and LiHMDS are commercially available, and thus it is economical and time effective to purchase them instead of preparing them in the laboratory. However, the synthesis of lithium amide compounds in general is essentially based on the deprotonative metallation reaction. Starting with the parent amine and reacting with an alkyl lithium, most commonly *n*-BuLi, butane is produced as a gaseous by-product and the lithiated amine is collected. It is common to use these *in-situ*, though many have been isolated from solution and completely characterised.^[24-26] Due to the simplicity of preparing lithium amides, they can also be used as precursors to prepare other metal amides such as the zinc bis(amide),^[27] Zn(TMP)₂ via salt metathesis upon reaction with a less polar metal halide (Scheme 1.5).



Scheme 1.5: General reaction scheme for preparing lithium amides (top) and example of their use in the preparing other metal amides such as Zn(TMP)_2 (bottom).

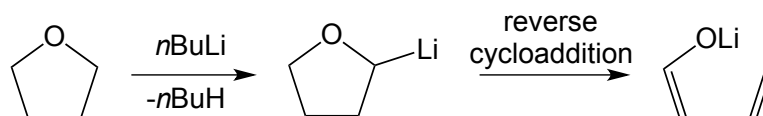
In the case of lithium, LDA, LiTMP and LiHMDS, have been described as the *utility amides* due to their key place within a synthetic chemist's toolbox.^[23] These sterically demanding secondary amides provide the exemplary alternative to their more nucleophilic alkyl lithium reagent congeners, allowing the deprotonation of a substrate without causing much if any nucleophilic addition side reaction. This can be illustrated upon comparing the reactivity of the most common alkyl reagent, *n*-BuLi and the most widely used lithium amide, LDA with 2-fluoropyridine^[28,29] (Scheme 1.6).



Scheme 1.6: Comparison of LDA versus *n*-BuLi reactivity with 2-fluoropyridine.

To complement the advantages of their high deprotonative reactivity, there are benefits from a practical perspective. These amides offer a reagent that is safer to handle in comparison with alkyl reagents such as *n*-BuLi. There is not the same requirement to perform reactions at sub-ambient temperatures to avoid attack of solvents, which have been reported to have cost implications of over £250k per annum per batch tonne process.^[30] Scheme 1.7 depicts a typical example of this involving *n*-BuLi with the

common Lewis base solvent tetrahydrofuran (THF), where the cyclic ether undergoes decomposition through a ring opening process.^[31-34]



Scheme 1.7: Ring opening of THF via α -lithiation induced by *n*-BuLi.

It is therefore understandable that alkali metal amides have been studied to a meticulous standard in order to have a full knowledge of their structures^[35-39] in both solid state (mainly by X-ray crystallography) and solution state (mostly by NMR spectroscopic studies), given the intimate connection of structure with their reactivity. A simplified representation of donor-free LDA, LiTMP and LiHMDS are illustrated in Table 1.1.

Table 1.1: Simplified graphical representation of the three utility lithium amides.

LiHMDS	LiTMP	LDA
Cyclic trimer	Cyclic trimer or tetramer	Polymeric helix

1.2 Cooperative mixed-metal chemistry

1.2.1 LICKOR superbase

Lochmann-Schlosser's base,^[40-42] commonly written as LICKOR, has been given the abbreviation based on its composition, alkyllithium (LiC) and potassium alkoxide (KOR). However, it is the enhancement in the deprotonative ability of *n*-butyllithium when combined with potassium *tert*butoxide along with the observed regioselectivity that has truly coined it and related formulations as "superbases". The properties of the new basic mixture contain the assets of both fragments, combined as one powerful metallating entity. An intermediate level of reactivity is exhibited, somewhat between less reactive *n*-butyllithium and more reactive butylpotassium. It is this that makes

superbases a desirable alternative to conventional organolithium or Grignard reagents. An illustrative example that highlighted the special synergic effect of this reagent was when it was successfully employed to deprotonate benzene^[43] (note its pK_a is 43), in a transformation that *n*-butyllithium is not capable of in the absence of Lewis base donors. Simplistic model systems of potential superbase motifs were reported,^[44] though there remained no identified molecular structure of the LiCKOR base. It was the reaction of the superbase *n*BuLi/KOtBu with excess benzene in THF at -78°C that led to the first crystallographic characterisation of a Lochman-Schlosser superbase type compound.^[45] A mixed-metal cluster $[(\text{PhK})_4(\text{PhLi})(t\text{BuOLi})(\text{THF})_6(\text{C}_6\text{H}_6)_2]$ was revealed bearing all LICKOR fragments; lithium, potassium, alkoxide and aryl as this was post metallation (Figure 1.5).

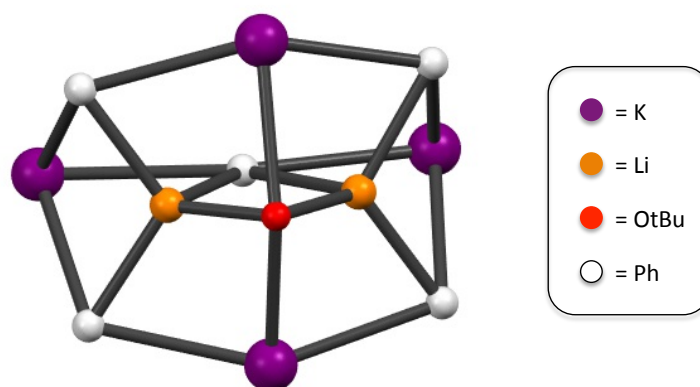


Figure 1.5: Inner scaffold of mixed-metal cluster

$[(\text{PhK})_4(\text{PhLi})\text{LiOtBu}(\text{THF})_6(\text{C}_6\text{H}_6)_2]$ containing all ‘superbase’ components, THF and benzene molecules have been omitted for clarity.^[45]

However, as this does not contain any butyl anions – a key component of the LICKOR superbase – the true constitution of the superbase remains to be ascertained. Efforts are continually being made to expose the black box of superbase chemistry. A report of a neopentyl lithium/potassium *tert*-butoxide Lochmann-Schlosser superbase $[\text{Li}_4\text{K}_4\text{Np}_3(\text{OtBu})_5]$ emerged in the last year highlighting the difficulty in isolating X-ray quality crystals of such compounds. The collected X-ray crystallographic data was not good enough quality to report bonding parameters, only the atom connectivity of the molecular structure was conclusive.^[46] As shown in figure 1.6, there is an alkyl

potassium ring in a roof-shaped arrangement with two dimeric lithium *tert*-butoxide units positioned into place above and below the plane of the four potassium atoms.

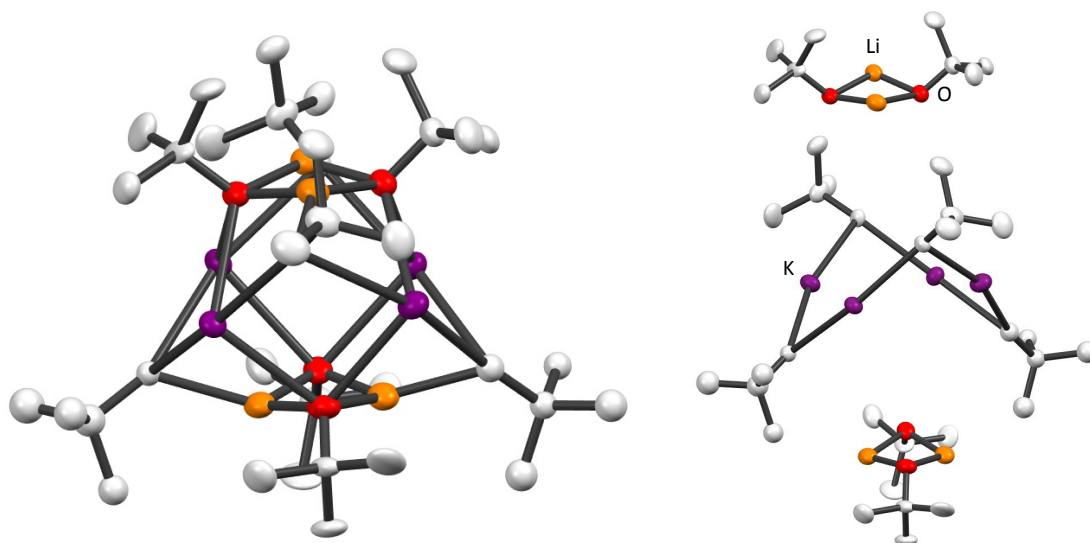
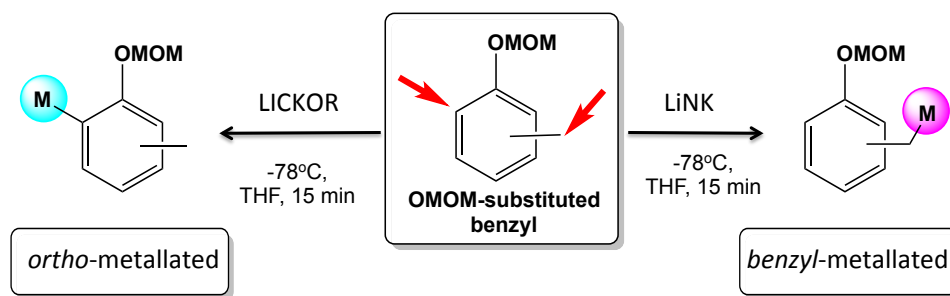


Figure 1.6: Neopentyl variant of Lochmann-Schlosser superbase (left) and fragmented into simplistic units (right).

Developing on this work, O'Shea unveiled a second generation LICKOR base incorporating the secondary amine TMP(H). The composition $n\text{BuLi}/\text{KO}t\text{Bu}/\text{TMP}(\text{H})$, commonly referred to as LiNK, is akin to the Lochmann-Schlosser superbase in that its active arrangement has yet to be unequivocally established. However, some attractive chemistry can be exploited, overriding the *ortho*-directing effect when metallating *o*-, *m*- and *p*-substituted toluenes^[47,48] bearing a methoxymethoxy (OMOM) [$-\text{OCH}_2\text{OCH}_3$] group. Two possible sites can be considered for metallation as highlighted by red arrows in [scheme 1.8](#). In the case of traditional LICKOR base the *ortho*-directing group will dominate the metallation site. However, employing the LiNK base *in-situ* under the same reaction conditions, the selective metallation of benzyl species is possible via a controlled anion migration. This is attributed to the role of TMP(H). Caubere also describes a unimetal derivative,^[49] RLi/LOR , based on the same principle as the LICKOR superbase.

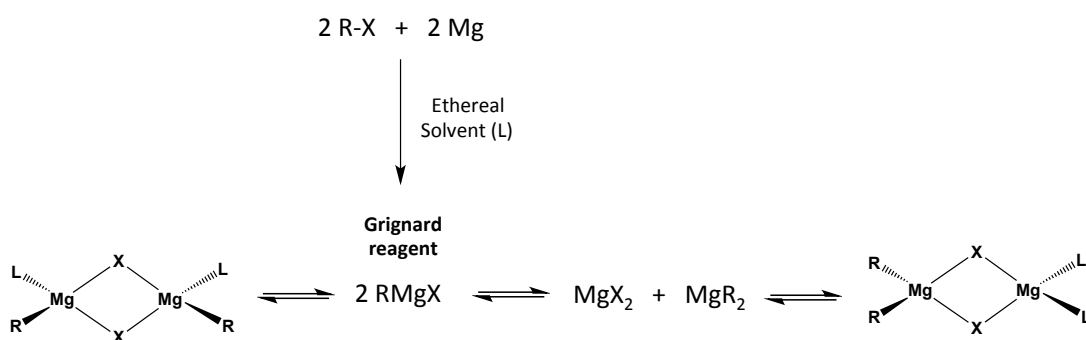


Scheme 1.8: Comparison of LICKOR versus LiNK in metallation reactions of OMOM-substituted toluenes.

1.2.2 Development of Grignard reagents

The significance of the Grignard reagent, of general formula RMgX where R is an organic group and X is a halide, was recognised in 1912 when Victor Grignard was awarded the Nobel Prize. The synthetic applications to date are vast as they provide a good alternative to organolithium reagents, primarily due to some advantages they have over their Group 1 rivals. Some of the most important advantages include improved functional group tolerance; the ability to withstand higher reaction temperatures due to their higher kinetic stability and the absence of a requirement for cryogenic reaction conditions to eliminate side reactions reflecting their more modest reactivity.

Akin to the previous structural discussions on organolithium compounds, RMgX is a very simplistic generic description of Grignard reagents. In reality they exist as a complicated mixture of different aggregated assemblies. Another crucial factor to consider is the Schlenk equilibrium.^[1] To elaborate, Grignard reagents are generally prepared from an organic halide (commonly a chloride or bromide) and magnesium turnings in ethereal solvent as shown in [Scheme 1.9](#). However, once the heteroleptic Grignard reagent RMgX is formed it can undergo disproportionation, also known as Schlenk equilibria, to its homoleptic components of a diorganomagnesium (R_2Mg) compound and a magnesium salt (MgX_2). This equilibrium can be desirable to prepare diorganomagnesium reagents, as adding a donor ligand such as dioxane can induce the precipitation of a $[\text{MgX}_2\text{dioxane}]$ complexed salt, the position of the equilibrium can be controlled.

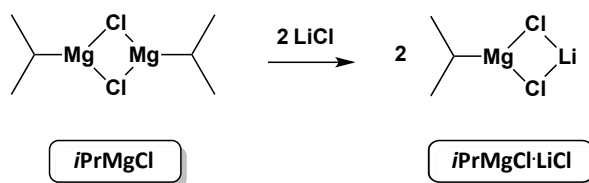


Scheme 1.9: Synthesis of Grignard reagent and Schlenk equilibria.

In 1947, Hauser introduced an amido variant of the Grignard reagent to the market.^[50,51] Although these halomagnesium amides, of the general formula $[\text{R}_2\text{NMgX}]_n$, were first mentioned by Meunier,^[52] it was the work by Hauser that provided a platform for these compounds in synthesis. From the straightforward approach of preparing these, an amine and a Grignard reagent, other research groups soon added to the range of reagents of this type including Eaton's incorporation of the exceedingly bulky TMP to prepare the bromide TMPMgBr ,^[53,54] followed by Mulzer's preparation of the chloro derivative TMPMgCl .^[55]

As a result of their influential role in C-H cleavage methodology, huge research efforts have been focussed on understanding these reagents and as a result major developments have emerged. Pioneering work by Knochel beginning in 2004, described a synergic effect when incorporating stoichiometric LiCl into Grignard reagents^[56] and Hauser bases^[57] to reveal a superior class of compounds termed as 'turbo-Grignard reagent, $[\text{RMgX}\cdot\text{LiCl}]$ ' or 'turbo Hauser, $[\text{R}_2\text{NMgX}\cdot\text{LiCl}]$ ' bases. These displayed increased reactivity, improved regioselectivity and functional group tolerance and in the case of turbo Hauser better solubility, ultimately outperforming their non-salt-containing ancestors.^[58,59] It is well known that turbo Grignard reagents are favoured for metal-halogen exchange, whilst turbo Hauser reagents are more commonly employed in metal hydrogen exchange. For example, both of these reagent types could magnesiate sensitive polyfunctionalised aryl derivatives^[60] that would be susceptible to attack with a conventional reagent. This enhanced reactivity is attributed

to the LiCl deaggregating the structural assembly to realise a more reactive, more soluble magnesiate species [$i\text{PrMgCl}_2\cdot\text{Li}^+$] (Scheme 1.10).



Scheme 1.10: Representative deaggregation of Grignard reagents by lithium chloride to form turbo derivatives.

Although the molecular structures of turbo Grignard reagents has yet to be fully elucidated, studies probing the solid and solution state^[61,62] are present in the literature. The structural insight of turbo Hauser reagents on the other hand have been unravelled in more detail through X-ray crystallographic evidence^[63,64] (Figure 1.7) and more recently diffusion ordered spectroscopy (DOSY) NMR studies^[65] have been reported describing their solution state structures.

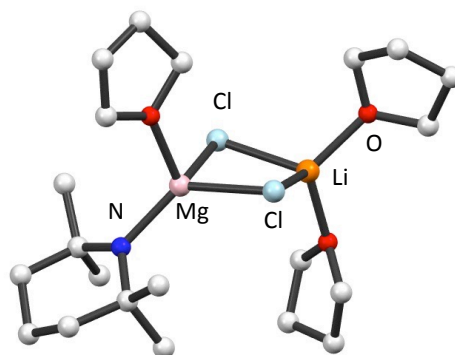


Figure 1.7: X-ray crystallography study of an example turbo Hauser base.

Although there are four main categories of Grignard reagents as summarised in figure 1.8, it comes as no surprise that the two most common turbo variants, $i\text{PrMgCl}\cdot\text{LiCl}$ and $\text{TMPMgCl}\cdot\text{LiCl}$, have gained themselves a place in the commercial chemical catalogue, with $i\text{PrMgCl}\cdot\text{LiCl}$ being awarded the EROS (Encyclopedia of Reagents for Organic Synthesis) Best Reagent Award 2011.^[66] Moving to the future of these reagents, their use has recently been implemented in flow chemistry^[67] (for example, the magnesiation of functionalised heterocycles and acrylates with $\text{TMPMgCl}\cdot\text{LiCl}$), and they are currently utilised in the synthesis of natural products and pharmaceuticals

highlighting their ability to be employed on a large scale. The concept of incorporating lithium chloride with conventional metal reagents to enhance their reactivity^[68] has been significantly expanded, not only for various magnesium reagents, but also for other softer metals, most notably zinc or aluminium.^[59]

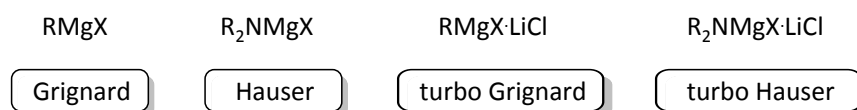


Figure 1.8: Schematic of the developments in Grignard type reagents.

1.2.3 Alkali-metal-mediated metallation (AMMM)

Heterobimetallic multicomponent mixtures have opened up a new world of metallation chemistry with several research groups from over the world developing the field including Knochel (Germany), Kondo (Japan), Mongin (France), Mulvey (Scotland), O'Shea (Ireland), Uchiyama (Japan) and Wheatley (England). The unique synergic enhanced reactivity that can be observed is reliant on the cooperative effects of the two metal components, a hard alkali metal (Li, Na or K) with a subordinate (in the sense of much weaker metallating ability) soft divalent (Mg, Zn or Mn) or a trivalent (Al or Ga) metal when combined in a bimetallic complex. (Figure 1.9). Most of these bimetallic combinations come under the category of a metallate, or “ate” for short.

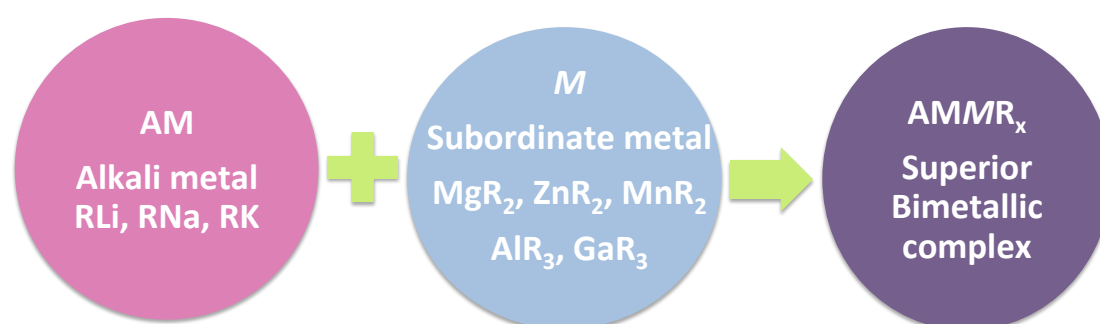
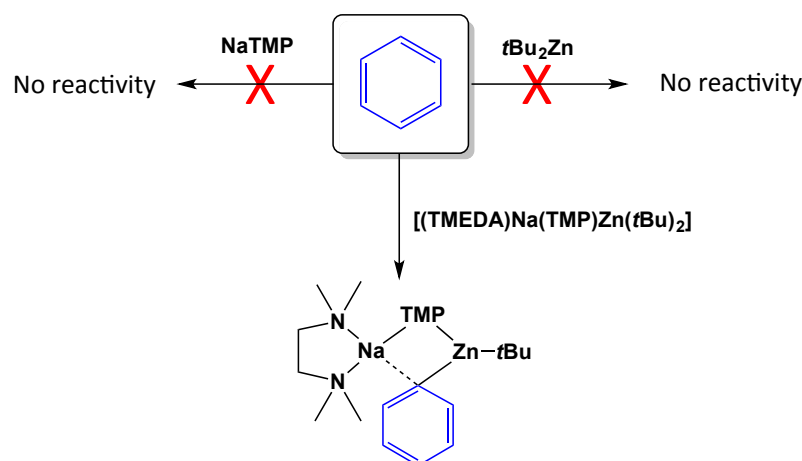


Figure 1.9: Simplistic representation of the components in a heterobimetallic species.

It was as long ago as 1858 that Wanklyn reported the synthesis of the bimetallic sodium zincate species $[\text{NaZnEt}_3]$.^[69] However, although this was the first zincate reported, almost a century passed before Wittig proclaimed the terminology of these

bimetallic systems as ‘ates’, when he unveiled a lithium trisphenylmagnesiates and lithium trisphenylzincates, $[\text{LiMgPh}_3]$ and $[\text{LiZnPh}_3]$.^[70] The label ‘ates’ was based on the predicted arrangement that the negative charge lies towards the softer less electropositive metal (Zn , $\chi = 1.6 > \text{Mg}$, $\chi = 1.2 > \text{Li}$, $\chi = 1.0$)^[71] giving an anionic natured fragment such as MgPh_3^- and ZnPh_3^- , counterbalanced by the alkali metal Li^+ .

Somewhat counter-intuitively, it is thought to be the normally less reactive metal that performs the C-H to C-M deprotonative metallation, though the presence of the more reactive alkali metal is imperative for any reactivity. In the case of the monometallic components, these are generally incapable of metallating in the same manner independently. An example of this phenomenon is shown with the well studied sodium zincate^[72] $[(\text{TMEDA})\text{Na}(\mu\text{-TMP})(\mu\text{-}t\text{Bu})\text{Zn}(t\text{Bu})]$ (Scheme 1.11). For this reason this second generation metallation has been labelled Alkali-Metal-Mediated Metallation (AMMM).



Scheme 1.11: Contrasting reactivity of monometallic components versus the bimetallic combination in attempted metallations of benzene.^[72]

A wide range of sophisticated cooperative bimetallic systems have now been designed and studied.^[73-75] Typically they conform to the formula $[\text{AMMR}_x]$, where AM is an alkali metal, M is a divalent or trivalent metal, R is the anionic fragments that can be alkyl or amido, and x is the number of anionic fragments to balance the valency of the species. These can then be further categorised as homoleptic or heteroleptic, depending on whether they have a set of the same anions or different anions respectively. The

ratio of AM: M can often also be varied giving rise to ‘ates’ termed as lower order in the case of 1:1 or higher order for 2:1 as illustrated in figure 1.10.

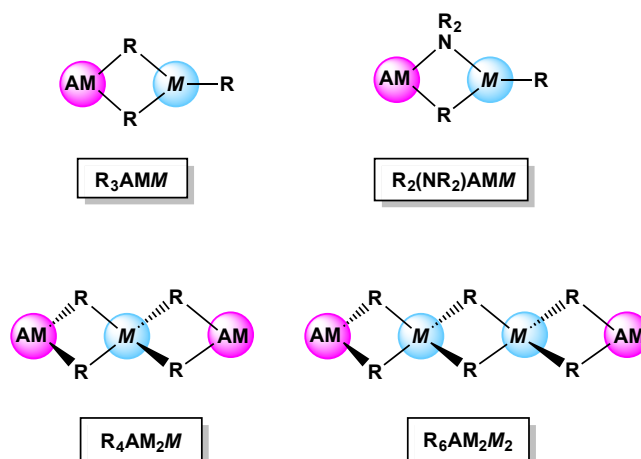
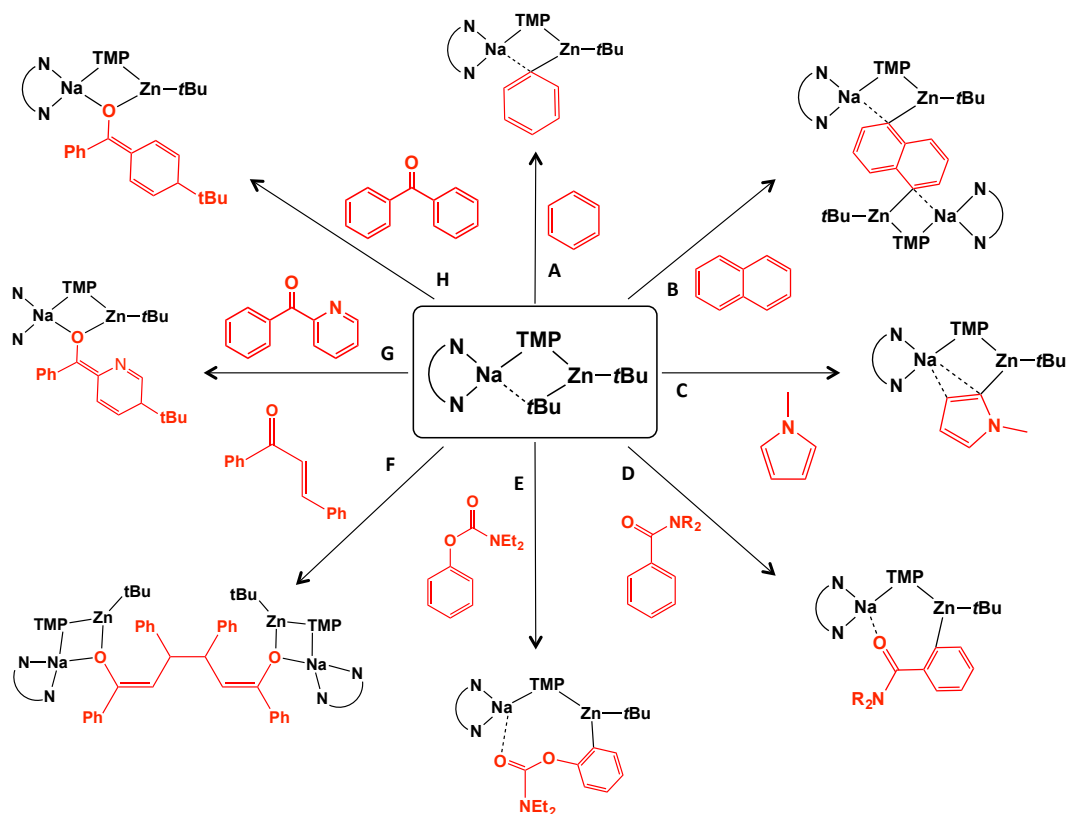


Figure 1.10: Simplistic representation of a selection of ate metallating agents.

Considering all the factors that can be varied, to discuss them all would be out of the scope of this thesis though some landmarks along the way have been mentioned below. Zincates were first structurally characterised in the 1960s by Weiss,^[76] a pioneer of X-ray crystallographic studies of polar organometallic compounds,^[77] who revealed the structure of the higher order lithium tetraorganozincate $[\text{Li}_2\text{ZnMe}_4]$. Kondo and Uchiyama meticulously developed the reactivity of the related bisalkyl-monoamidozincate “ $\text{LiZn}(\text{TMP})(t\text{Bu})_2$ ”.^[78,79] Structural studies by the Mulvey group followed,^[80] which unveiled the molecular arrangement to be $[(\text{THF})\text{Li}(\mu\text{-TMP})(\mu\text{-}t\text{Bu})\text{Zn}(t\text{Bu})]$ (Figure 1.11A). Subsequent characterisation of the sodium amidozincate derivative, $[(\text{TMEDA})\text{Na}(\mu\text{-TMP})(\mu\text{-}t\text{Bu})\text{Zn}(t\text{Bu})]$ (Figure 1.11C) emerged and its reactivity was studied in extensive detail. This sodium TMP-zincate was found to display an extraordinary breadth of reactivity, ranging from unusual metallation patterns (a-e),^[81-84] nucleophilic addition (g and h)^[85,86] and single electron transfer (f)^[87] abilities as summarised in scheme 1.12.



Scheme 1.12: Selection of examples showcasing the reactivity of the sodium-TMP zincate, $[(\text{TMEDA})\text{Na}(\mu\text{-TMP})(\mu\text{-}t\text{Bu})\text{Zn}(t\text{Bu})]$.^[81-87]

AMMZn featured in *Science* for the “synergic sedation of sensitive anions” employing the silyl-containing sodium zincate^[88] $[(\text{TMEDA})\text{Na}(\mu\text{-TMP})(\mu\text{-CH}_2\text{SiMe}_3)\text{Zn}(\text{CH}_2\text{SiMe}_3)]$ (Figure 1.11D), whilst moving to the related magnesium and manganese analogues highlighted the diverse reactivity. For example, as published in *Nature Chemistry* the related complexes, $[(\text{TMEDA})\text{Na}(\text{TMP})(\text{CH}_2\text{SiMe}_3)\text{Mg}(\text{TMP})]$ and $[(\text{TMEDA})\text{Na}(\text{TMP})(\text{CH}_2\text{SiMe}_3)\text{Mn}(\text{TMP})]$, induced controlled fragmentation of tetrahydrofuran.^[89]

Inspired by its large abundance in the earth’s crust, aluminium has also been studied in the context of synergistic ate chemistry. Uchiyama and Kondo^[90-92] established a position for lithium aluminates in the field with their heteroleptic derivative $[(\text{THF})\text{Li}(\mu\text{-TMP})(\mu\text{-}i\text{Bu})\text{Al}(i\text{Bu})_2]$ (Figure 1.11B), which was found to be an excellent metallating agent for sensitive aromatic substrates in possession of halogen substituents. Mulvey expanded this area by introducing a dialkyl-diamido composition

“LiAl(TMP)₂(*i*Bu)₂”.^[93] Further systematic studies by Mulvey explored the contents of the “black box” of AMMAI in an enlightening publication, where an in depth understanding was gained of how these metallating agents operate – not through an aluminations (C-H to C-Al) process as originally proposed by Uchiyama expected but instead following a *trans-metal-trapping* (TMT) route.^[94] This will be discussed in more detail in section 1.2.4. Another recent ground-breaking addition to this field is the sodium magnesiate complex “Na₄Mg₂(TMP)₆(*n*Bu)₂”. The molecular structure of this complex still remains to be formally determined, though from related complexes and NMR studies it is presumed to have the structure shown in figure 1.11E. Published in 2014 in *Science*,^[95] the chemistry of this complex unleashed a newfound “template metallation” approach to performing directed *ortho-meta*’ dimetallations of some common arene substrates including anisole, trifluorobenzene, phenyl-*N,N*,diethyl-*O*-carbamate or *meta-meta*’ dimetallations of *N,N*-dimethylaniline and *t*butybenzene.

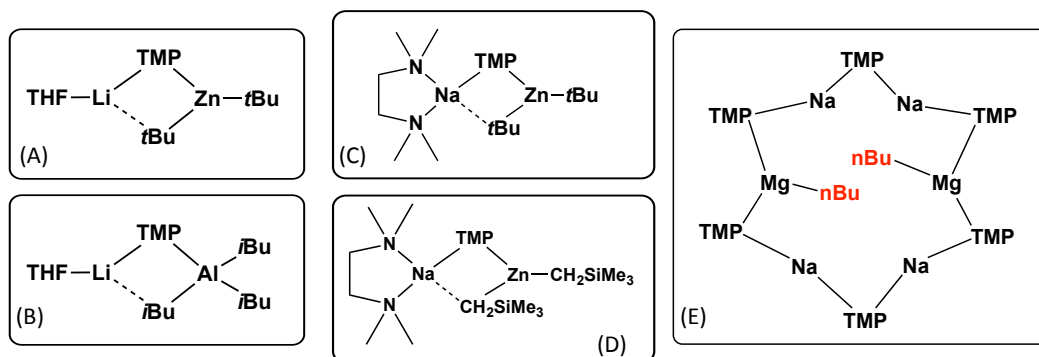


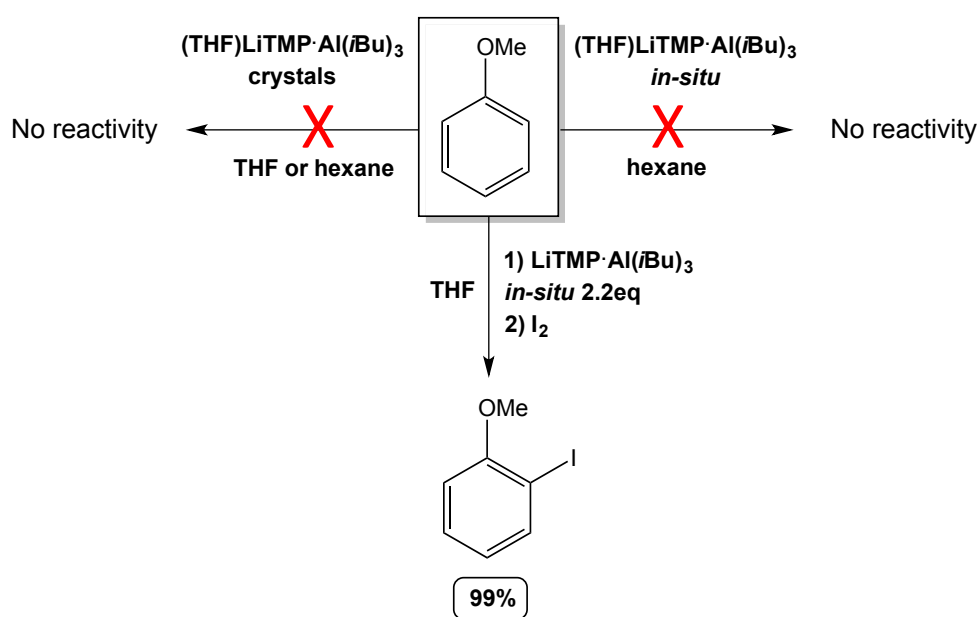
Figure 1.11: Some key ate metallating agents from the literature.^[72, 78-79, 88, 90-92, 95]

1.2.4 Trans-Metal-Trapping (TMT)

As mentioned in section 1.2.3, Uchiyama, Kondo and Wheatley have reported extensive studies of the monoamido-triaklyl-lithium aluminate “LiTMP·Al(*i*Bu)₃”. However, the underlying Pandora’s box of what species is responsible for the reactivity remained a topic for debate. Two of the most important lithium aluminates in the literature the mono-TMP complex “LiTMP·Al(*i*Bu)₃” and the bis-TMP analogue “LiTMP·Al(TMP)(*i*Bu)₂” were subjected to a thorough NMR study to gain insight to their solution state, and hopefully elucidate their metallation pathway. Since the reactions are typically performed in bulk THF it raised the questions – does the base

exist as a single species in solution? Is it an aluminating reaction with a direct C-H to C-Al exchange or is it in fact a two-stage process featuring a lithiation followed by a rapid trapping of the carbanion by the triorganoaluminium species?

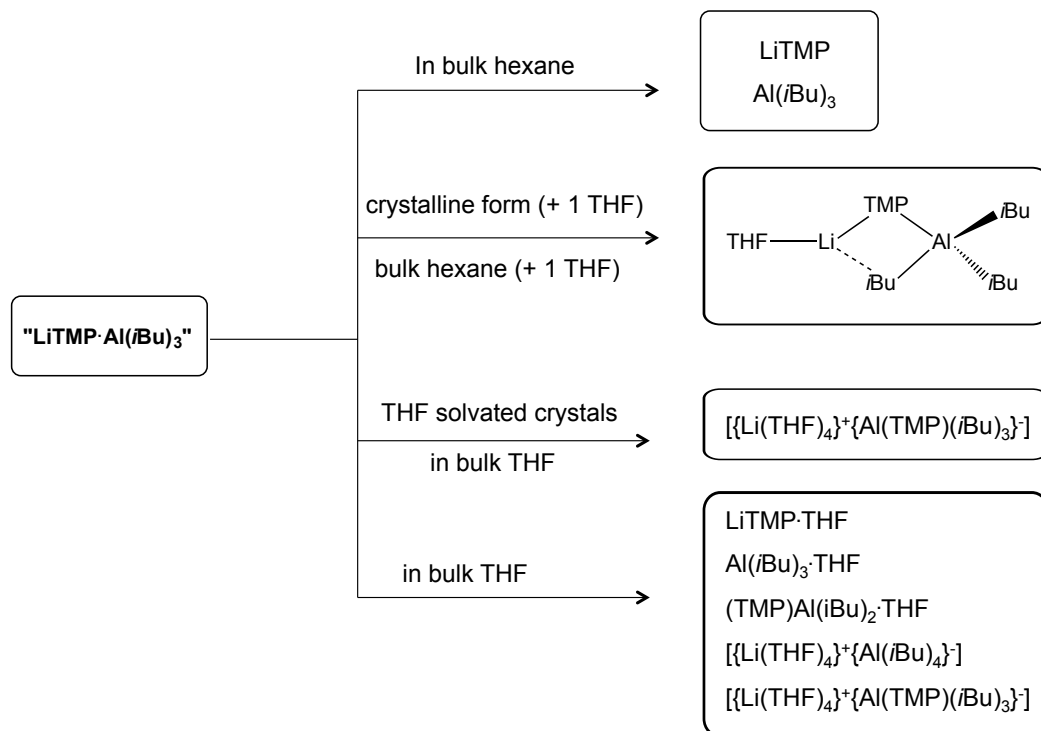
Uchiyama, Kondo and Wheatley have characterised by X-ray crystallography a range of contacted ion pair structural motifs of LiTMP and Al(*i*Bu)₃ with different solvating Lewis base donors on the lithium atom. However, the contacted ion pair complex [(THF)LiTMP·Al(*i*Bu)₃] with one solvating molecule of THF is proposed to be the active base for these AMMAI reactions. But in reality, the reactions are performed in bulk THF – a reaction media that can influence the solution state composition.



Scheme 1.13: Comparative reactivities of in-situ “LiTMP·Al(*i*Bu)₃” versus [(THF)LiTMP·Al(*i*Bu)₃] with anisole.^[90-92, 94]

Mulvey’s studies with the benchmark reagent anisole highlighted this influence (Scheme 1.13) whereby the *in-situ* reaction mixture of “LiTMP·Al(*i*Bu)₃” in bulk THF yielded 99% of the desired product. However, reacting isolated crystals or an *in-situ* prepared mixture of the proposed active species [(THF)LiTMP·Al(*i*Bu)₃] with anisole in either THF or hexane resulted in no reactivity at all. When the solution states of the different crystalline and *in-situ* fragments were studied in the absence of anisole, the surprising complexity of the underlying composition was exposed. Remarkably it was

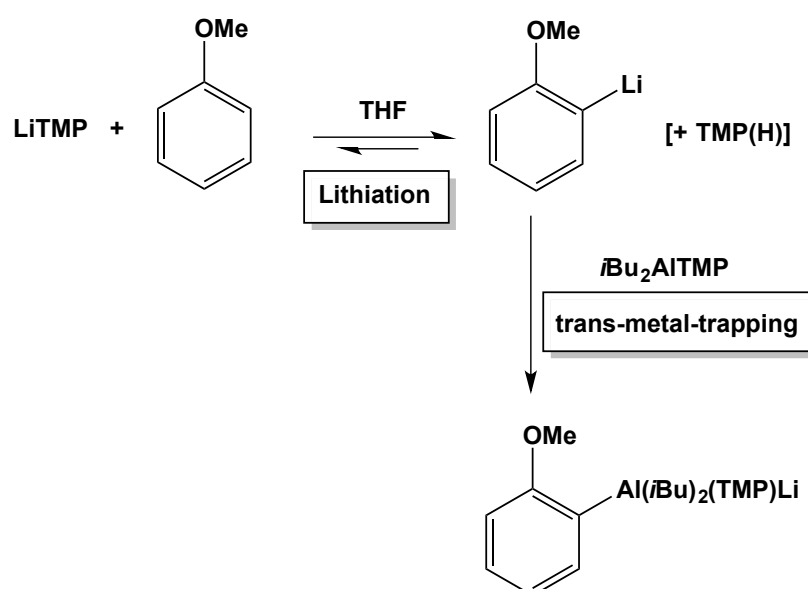
concluded that this putative base when dissolved in bulk THF gave rise to five different species identified by NMR spectroscopy (Scheme 1.14). Therefore, it was concluded that what was once deemed the active species is in fact not.



Scheme 1.14: Summary of composition of “LiTMP·Al(*i*Bu)₃” in various conditions.^[94]

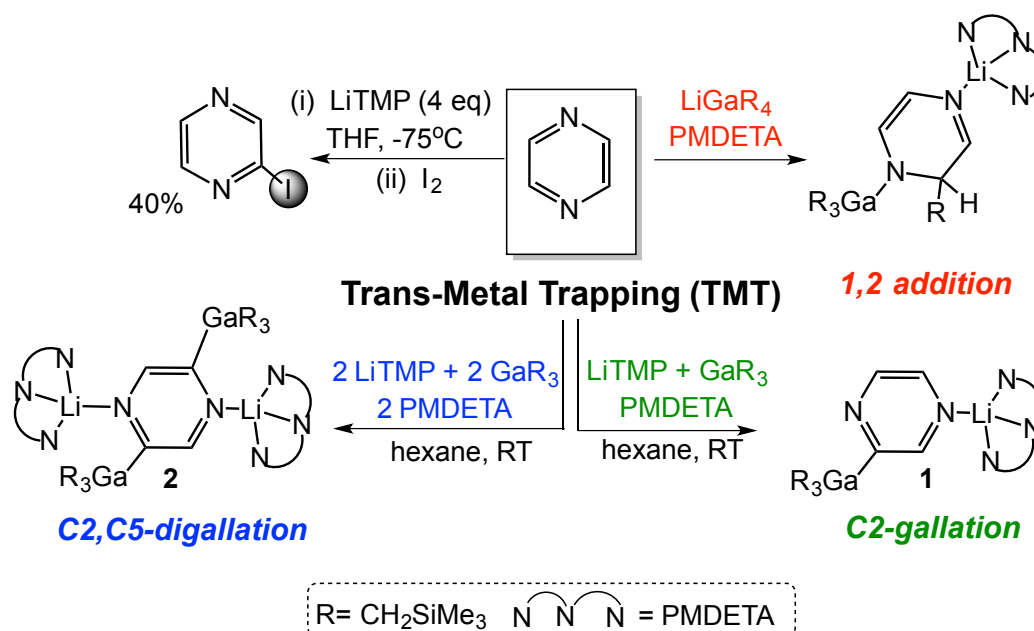
Performing the same investigation with “LiTMP·Al(TMP)(*i*Bu)₂” also proved to be insightful, and indeed more straightforward to study. From the reaction of anisole with this base, supported with extensive control studies, it could be determined that there was in fact no aluminium (C-H to C-Al) reaction occurring, but a tandem two-step lithiation/trans-metal-trapping procedure. Unlike the “LiTMP·Al(*i*Bu)₃” mixture where five species exist in bulk THF, LiTMP and Al(TMP)(*i*Bu)₂ still exist principally as two separate species in solution, namely the lithium amide LiTMP·THF and the alkylaluminium amide Al(TMP)(*i*Bu)₂·THF. It was established by studying these two species on their own that LiTMP performs the metallation of the organic substrate, then the emerging carbanion is trapped by the aluminium moiety (Scheme 1.15). The synergistic role of Al(TMP)(*i*Bu)₂ is crucial, not only in that it stabilises the carbanion formed, but its lack of interaction with LiTMP (due to bulky steric effects) aids in driving the equilibrium to the desired metallated anisole product. This type of two-step

pathway is not unprecedented, as it has been previously observed with comparable homoleptic tris-TMP lithium-zinc^[96] and -cadmium systems.^[97] Akin to the lithium aluminate, these do not cocomplex in solution, the LiTMP performs the metallation with the neutral diamido-metal species stabilising the carbanion. Note that Knochel also reports a similar approach but as this uses the halide species *i*Bu₂AlCl to trap aromatic carbanions after lithium halogen exchange, it proceeds with lithium halide elimination and thus gives neutral Al-trapped species as opposed to the ate species observed with the Al(TMP)(*i*Bu)₂ trapping agent.^[98]



Scheme 1.15: Proposed *trans-metal trapping* two-step pathway for the ‘aluminum’ of anisole.

The influence of this *trans-metal-trapping*, TMT, discovery has been monumental in that it has opened up a new approach to complex metallations.^[99] Recently, a new lithium and gallium TMT system was developed based on a mixture of LiTMP and the trialkylgallium [Ga(CH₂SiMe₃)₃, GaR₃]. This has been successfully applied to the metallation and stabilisation of diazines more specifically, pyrazine, pyrimidine and pyridazine, allowing the isolation of rare crystal structures of such metallodiazines. Interestingly the TMP system shows novel reactivity in contrast to the tetraalkyl lower order lithium gallate^[100] [LiGaR₄] as summarised in [Scheme 1.16](#).



Scheme 1.16: Comparison of typical ‘ate’ reactivity versus trans-metal-trapping with pyrazine.^[99-100]

1.3 References

- [1] C. Elschenbroich, in *Organometallics*, Wiley-VCH, Weinheim, Germany, **2006**.
- [2] W. Schlenk and J. Holtz, *Ber. Dtsch. Chem. Ges.* **1917**, *50*, 262–274.
- [3] V. H. Gessner, C. Däschlein and C. Strohmam, *Chem. Eur. J.* **2009**, *15*, 3320–34.
- [4] G. Wu and M. Huang, *Chem. Rev.* **2006**, *106*, 2596–616.
- [5] M. Pérez, M. Fañanás-Mastral, P. H. Bos, A. Rudolph, S. R. Harutyunyan and B. L. Feringa, *Nat. Chem.* **2011**, *3*, 377–81.
- [6] M. Schlosser, in *Organometallics in synthesis*, 2nd Ed., Wiley: Chichester, U.K., 2002.
- [7] J. Clayden, in *Organolithiums: Selectivity for Synthesis*, Vol 23, Tetrahedron Organic Chemistry Series; Permagon, Elsevier Science; Oxford, U.K., 2002.
- [8] D. B. Collum, *Acc. Chem. Res.* **1993**, *26*, 227–234.
- [9] H. Dietrich, *Acta Cryst.*, **1963**, *16*, 681-689
- [10] H. Dietrich, *J. Organomet. Chem.*, **1981**, *205*, 291-299
- [11] T. Kottke and D. Stalke, *Angew. Chem. Int. Ed.*, **1993**, *32*, 580-582.
- [12] E. Weiss and E. A. C. Lucken, *J. Organomet. Chem.*, **1964**, *2*, 197-205.
- [13] R. E. Dinnebier, U. Behrens and F. Olbrich, *J. Am. Chem. Soc.*, **1998**, *120*, 1430-1433.

- [14] H. Yamamoto and K. Oshima, in *Main Group Metals in Organic Synthesis*, Wiley VCH: Weinheim, Germany, **2004**.
- [15] <http://www.chem.wisc.edu/areas/reich/pkatable/> (20/06/2017).
- [16] D. W. Slocum, T. K. Reinscheld, C. B. White, M. D. Timmons, P. A. Shelton, M. G. Slocum, R. D. Sandlin, E. G. Holland, D. Kusmic, J. A. Jennings, K. C. Tekin, Q. Nguyen, S. J. Bush, J. M. Keller and P. E. Whitley, *Organometallics* **2013**, *32*, 1674–1686.
- [17] P. Beak and V. Snieckus, *Acc. Chem. Res.*, **1982**, *15*, 306-312.
- [18] V. Snieckus, *Chem. Rev.* **1990**, *90*, 879–933.
- [19] H. Gilman and R. L. Bebb, *J. Am. Chem. Soc.*, **1939**, *61*, 109-112.
- [20] G. Wittig and G. Fuhrmann, *Ber. Dtsch. Chem. Ges.*, **1940**, *73*, 1197-1218.
- [21] D. E. Applequist and D. F. O'Brien, *J. Am. Chem. Soc.*, **1963**, *85*, 743-748.
- [22] P. Knochel and G. A. Molander, in *Comprehensive Organic Synthesis*, 2nd Ed., Elsevier, **2014**.
- [23] R. E. Mulvey and S. D. Robertson, *Angew. Chem. Int. Ed.*, **2013**, *52*, 11470–87.
- [24] R. E. Mulvey, *Chem. Soc. Rev.* **1998**, *27*, 339-346.
- [25] R. E. Mulvey, *Chem. Soc. Rev.* **1991**, *20*, 167–209.
- [26] K. Gregory, P. von Ragué Schleyer and R. Snaith, *Adv. Inorg. Chem.* **1991**, *37*, 47-142.
- [27] W. S. Rees, O. Just, H. Schumann and R. Weimann, *Polyhedron* **1998**, *17*, 1001–1004.
- [28] F. Marsais, P. Granger and G. Quéguiner, *J. Org. Chem.*, **1981**, *46*, 4494-4497.
- [29] T. Güngör, F. Marsais and G. Quéguiner, *J. Organomet. Chem.*, **1981**, *215*, 139-150.
- [30] L. S. Bennie, W. J. Kerr, M. Middleditch and A. J. B. Watson, *Chem. Commun.*, **2011**, *47*, 2264-2266.
- [31] H. Gilman and B. J. Gaj, *J. Org. Chem.*, **1957**, *22*, 1165–1168.
- [32] S. C. Honeycutt, *J. Organomet. Chem.* **1971**, *29*, 1–5.
- [33] J. Clayden and S. A. Yasin, *New J. Chem.* **2002**, *26*, 191–192.
- [34] R. B. Bates, L. M. Kroposki and D. E. Potter, *J. Org. Chem.*, **1972**, *37*, 560-562.
- [35] M. Lappert, A. Protchenko, P. Power and A. Seeber, in *Metal Amide Chemistry*, Wiley: Chichester, U.K. **2009**.
- [36] N. D. R. Barnett, R. E. Mulvey, W. Clegg and P. A. O'Neill, *J. Am. Chem. Soc.*, **1991**, *113*, 8187-8188.

- [37] A. Mootz, A. Zinnius and B. Bottcher, *Angew. Chem. Int. Ed.*, **1969**, *8*, 378-379.
- [38] M. F. Lappert, M. J. Slade, A. Singh, J. L. Atwood, R. D. Rogers and R. Shakir, *J. Am. Chem. Soc.*, **1983**, *105*, 302-304.
- [39] E. Hevia, A. R. Kennedy, R. E. Mulvey, D. L. Ramsay and S. D. Robertson, *Chem. Eur. J.*, **2013**, *19*, 14069-14075.
- [40] M. Schlosser, *J. Organomet. Chem.*, **1967**, *8*, 9-16.
- [41] L. Lochmann, J. Pospisil and D. Lim, *Tett. Lett.*, **1966**, *7*, 257-262.
- [42] M. Schlosser, *Pure Appl. Chem.*, **1988**, *60*, 1627-1634.
- [43] M. Schlosser, H. C. Jung and S. Takagishi, *Tetrahedron*, **1990**, *46*, 5633-5658.
- [44] W. Clegg, A. M. Drummond, S. T. Liddle, R. E. Mulvey and A. Robertson, *Chem. Commun.*, **1999**, 1569 – 1570.
- [45] C. Unkelbach, D. F. O'Shea and C. Strohmann, *Angew. Chem. Int. Ed.*, **2014**, *53*, 553-556.
- [46] P. Benrath, M. Kaiser, T. Limbach, M. Mondeshki and J. Klett, *Angew. Chem. Int. Ed.* **2016**, *55*, 10886-10889.
- [47] P. Fleming and D. F. O'Shea, *J. Am. Chem. Soc.* **2011**, *133*, 1698-1701.
- [48] A. Manvar, P. Fleming and D. F. O'Shea, *J. Org. Chem.*, **2015**, *80*, 8727-8738.
- [49] P. Caubere, *Chem. Rev.*, **1993**, *93*, 2317-2334.
- [50] C. R. Hauser and H. G. Walker, *J. Am. Chem. Soc.*, **1947**, *69*, 295-297.
- [51] F. C. Frostick and C. R. Hauser, *J. Am. Chem. Soc.*, **1949**, *71*, 1350-1352.
- [52] L. Meunier, *C. R. Hebd. Seances Acad. Sci.*, **1903**, *136*, 758-759.
- [53] P. E. Eaton, C. H. Lee and Y. Xiong, *J. Am. Chem. Soc.*, **1989**, *111*, 8016-8018.
- [54] P. E. Eaton, Y. Xiong and R. Gilardi, *J. Am. Chem. Soc.*, **1993**, *115*, 10195-10202.
- [55] W. Schlecker, A. Huth, E. Ottow and J. Mulzer, *Synthesis*, **1995**, 1225-1227.
- [56] A. Krasovskiy and P. Knochel, *Angew. Chem. Int. Ed.*, **2004**, *43*, 3333-3336.
- [57] A. Krasovskiy, V. Krasovskaya and P. Knochel, *Angew. Chem. Int. Ed.*, **2006**, *45*, 2958-2961.
- [58] P. Knochel, W. Dohle, N. Gommermann, F. F. Kneisel, F. Kopp, T. Korn, I. Sapountzis and V. A. Vu, *Angew. Chem. Int. Ed.*, **2003**, *42*, 4302-4320.
- [59] B. Haag, M. Mosrin, V. Malakhov and P. Knochel, *Angew. Chem. Int. Ed.*, **2011**, *50*, 9794-9824.
- [60] W. Lin, O. Baron and P. Knochel, *Org. Lett.*, **2006**, *8*, 5673-5676.

- [61] F. Blasberg, M. Bolte, M. Wagner and H.W. Lerner, *Organometallics*, **2012**, *31*, 1001-1005.
- [62] C. Schnegelsberg, S. Bachmann, M. Kolter, T. Auth, M. John, D. Stalke and K. Koszinowski, *Chem. Eur. J.*, **2016**, *22*, 7752-7762.
- [63] P. García-Álvarez, D. V. Graham, E. Hevia, A. R. Kennedy, J. Klett, R. E. Mulvey, C. T. O'Hara and S. Weatherstone, *Angew. Chem. Int. Ed.*, **2008**, *47*, 8079-8081.
- [64] D. R. Armstrong, P. García-Álvarez, A. R. Kennedy, R. E. Mulvey and J. A. Parkinson, *Angew. Chem. Int. Ed.*, **2010**, *49*, 3185-3188.
- [65] R. Neufeld, T. L. Teuteberg, R. Herbst-Irmer, R. A. Mata and D. Stalke, *J. Am. Chem. Soc.*, **2016**, *138*, 4796-4806.
- [66] R. Li-Yuan Bao, R. Zhao and L. Shi, *Chem. Commun.*, **2015**, *51*, 6884-6900.
- [67] T. P. Petersen, M. R. Becker and P. Knochel, *Angew. Chem. Int. Ed.*, **2014**, *53*, 7933-7937.
- [68] E. Hevia and R. E. Mulvey, *Angew. Chem. Int. Ed.*, **2011**, *50*, 6448-6450.
- [69] J. A. Wanklyn, *Justus Liebigs Ann. Chem.*, **1858**, *107*, 125-128.
- [70] G. Wittig, F. J. Meyer and G. Lange, *Justus Liebigs Ann. Chem.*, **1951**, *571*, 167-201.
- [71] L. Pauling, in *General Chemistry An Introduction to Descriptive Chemistry and Modern Chemical Theory*, W. H. Freeman, San Francisco, California, **1947**.
- [72] P. C. Andrikopoulos, D. R. Armstrong, H. R. L. Barley, W. Clegg, S. H. Dale, E. Hevia, G. W. Honeyman, A. R. Kennedy and R. E. Mulvey, *J. Am. Chem. Soc.*, **2005**, *127*, 6184-6185.
- [73] R. E. Mulvey, *Dalton Trans.*, **2013**, *42*, 6676-6693.
- [74] R. E. Mulvey, *Acc. Chem. Res.*, **2009**, *42*, 743-755.
- [75] R. E. Mulvey and S. D. Robertson, in *FascinATES : mixed-metal ate compounds that function synergistically*, Organo-di-metallic compounds (or reagents), Topics in Organometallic Chemistry, Springer, **2014**.
- [76] E. Weiss and R. Wolfrum. *Chem. Ber.*, **1968**, *101*, 35-40.
- [77] E. Weiss, *Angew. Chem. Int. Ed.*, **1993**, *32*, 1501-1523.
- [78] Y. Kondo, M. Shilai, M. Uchiyama and T. Sakamoto, *J. Am. Chem. Soc.*, **1999**, *121*, 3539-3540.
- [79] M. Uchiyama, Y. Masimoto, D. Nobuto, T. Furuyama, K. Yamaguchi and K. Morokuma, *J. Am. Chem. Soc.*, **2006**, *128*, 8748-8750.

- [80] W. Clegg, S. H. Dale, E. Hevia, G. W. Honeyman and R. E. Mulvey, *Angew. Chem. Int. Ed.*, **2006**, *45*, 2370-2374.
- [81] W. Clegg, S. H. Dale, R. W. Harrington, E. Hevia, G. W. Honeyman and R. E. Mulvey, *Angew. Chem. Int. Ed.*, **2006**, *45*, 2374-2377.
- [82] W. Clegg, S. H. Dale, E. Hevia, G. W. Honeyman, R. E. Mulvey and C. T. O'Hara, *Angew. Chem. Int. Ed.*, **2006**, *45*, 6548-6550.
- [83] B. Conway, E. Hevia, A. R. Kennedy and R. E. Mulvey, *Chem. Commun.*, **2007**, 2864-2866.
- [84] L. Balloch, A. R. Kennedy, R. E. Mulvey, T. Rantanen, S. D. Robertson and V. Snieckus, *Organometallics*, **2011**, *30*, 145-152.
- [85] E. Hevia, G. W. Honeyman, A. R. Kennedy and R. E. Mulvey, *J. Am. Chem. Soc.*, **2005**, *127*, 13106-13107.
- [86] J. J. Crawford, B. J. Fleming, A. R. Kennedy, J. Klett, C. T. O'Hara and S. A. Orr, *Chem. Commun.*, **2011**, *47*, 3772-3774.
- [87] D. R. Armstrong, L. Balloch, J. J. Crawford, B. J. Fleming, L. M. Hogg, A. R. Kennedy, J. Klett, R. E. Mulvey, C. T. O'Hara, S. A. Orr and S. D. Robertson, *Chem. Commun.*, **2012**, *48*, 1541-1543.
- [88] A. R. Kennedy, J. Klett, R. E. Mulvey and D. S. Wright, *Science*, **2009**, *326*, 706-708.
- [89] R. E. Mulvey, V. L. Blair, W. Clegg, A. R. Kennedy, J. Klett and L. Russo, *Nature Chem.*, **2010**, *2*, 588-591.
- [90] M. Uchiyama, H. Naka, Y. Matsumoto and T. Ohwada, *J. Am. Chem. Soc.*, **2004**, *126*, 10526-10527.
- [91] H. Naka, M. Uchiyama, Y. Matsumoto, A. E. H. Wheatley, M. McPartlin, J. V. Morey and Y. Kondo, *J. Am. Chem. Soc.*, **2007**, *129*, 1921-1930.
- [92] H. Naka, J. V. Morey, J. Haywood, D. J. Eisler, M. McPartlin, F. Garcia, H. Kudo, Y. Kondo, M. Uchiyama and A. E. H. Wheatley, *J. Am. Chem. Soc.*, **2008**, *130*, 16193-16200.
- [93] R. E. Mulvey, D. R. Armstrong, B. Conway, E. Crosbie, A. R. Kennedy and S. D. Robertson, *Inorg. Chem.*, **2011**, *50*, 12241-12251.
- [94] D. R. Armstrong, E. Crosbie, E. Hevia, R. E. Mulvey, D. L. Ramsay and S. D. Robertson, *Chem. Sci.*, **2013**, *5*, 3031-3045.
- [95] A. J. Martinez-Martinez, A. R. Kennedy, R. E. Mulvey and C. T. O'Hara, *Science*, **2014**, *346*, 834-837.

- [96] E. Nagaradja, F. Chevallier, T. Roisnel, V. Dorcet, Y. S. Halauko, O. A. Ivashkevich, V. E. Matulis and F. Mongin, *Org. Biomol. Chem.*, **2014**, *12*, 1475-1487; and references therein.
- [97] F. Chevallier, T. Blin, E. Nagaradja, F. Lassagne, T. Roisnel, Y. S. Halauko, V. E. Matulis, O. A. Ivashkevich and F. Mongin, *Org. Biomol. Chem.*, **2012**, *10*, 4878-4885; and references therein.
- [98] T. Klatt, K. Groll and P. Knochel, *Chem. Commun.*, **2013**, *49*, 6953-6955.
- [99] M. Uzelac, A. R. Kennedy, E. Hevia and R. E. Mulvey, *Angew. Chem. Int. Ed.*, **2016**, *55*, 13147-13150.
- [100] D. R. Armstrong, E. Brammer, T. Cadenbach, E. Hevia and A. R. Kennedy, *Organometallics*, **2013**, *32*, 480-489.

Chapter 2: Development of s-block dihydropyridines

2.1 Summary

This chapter aims to advance s-block dihydropyridine chemistry, more specifically that of group 1. This is an area that has only attracted sporadic attention until recently. The earlier synthesis of a 1-lithio-2-*t*-butyl-dihydropyridine, [1-Li-2-*t*-Bu(NC₅H₅)] **1a**, from pyridine and *t*-butyllithium provided the foundation for this work.

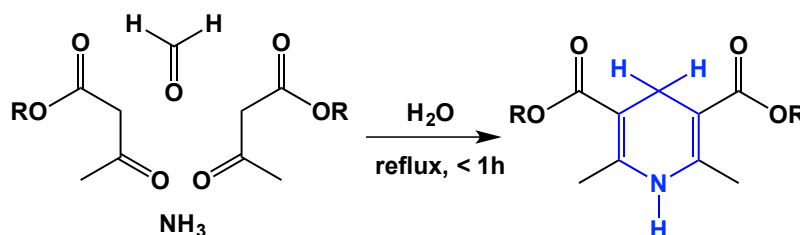
Herein, the synthesis, characterisation and reactivity of heavier alkali-metal dihydropyridines are discussed. A facile metathetical route of isolated **1a** with the alkali-metal *t*-butoxide NaOtBu or KOtBu, allowed the first preparation and isolation of the heavier alkali metal dihydropyridines, [1-Na-2-*t*-Bu(NC₅H₅)] **2a** and [1-K-2-*t*-Bu(NC₅H₅)] **3a**. Further studies on this work indicated the presence of a 1-lithio-4-*t*-butyl-dihydropyridine variant, [1-Li-4-*t*-Bu(NC₅H₅)] **1b**, in solution, hence *in-situ* studies were carried out. NMR spectroscopy determined that a one-pot synthesis, predominantly results in **2a** or **3a**, but also gives rise to the 1,4- isomers, **2b** or **3b**.

X-ray crystallographic studies revealed a series of group 1 metallodihydropyridine compounds. By employing the monodentate, bidentate and tridentate donors, THF, TMEDA and PMDETA respectively, five new structurally diverse compounds were isolated and fully characterised, [K(1,2-*t*-Bu-DHP)(TMEDA)]₂ **4**, [K(1,2-*t*-Bu-DHP)(PMDETA)]₂ **5**, [Na(1,4-*t*-Bu-DHP)(PMDETA)]₂ **6**, [Na(1,2-*t*-Bu-DHP)]₂(TMEDA)]₂ **7**, and [K(1,2-*t*-Bu-DHP)(THF)]_∞ **8**.

Thermal volatility analysis (TVA) studies were insightful for providing an explanation for the relative reactivity of these compounds. Both **2a** and **3a** underwent thermal decomposition to produce 2-*t*-butylpyridine and metal hydride, for **2a** this occurred around 124°C similar to **1** at 120°C. However, **3a** underwent decomposition at a considerably lower temperature of 99°C. This gave an early indication that these compounds could be utilised as isolable sodium or potassium hydride surrogates. Given this, preliminary hydrometallation studies with benzophenone were explored.

2.2 Introduction

The important members of the class of compounds known as N-heterocyclic organic compounds, dihydropyridines, are of great value to study. About thirty years after the 1849 discovery of pyridine and related aromatic CN heterocycles in Glasgow by Anderson,¹⁻³ Hantzsch serendipitously prepared dihydropyridines during his seminal synthetic development of a suite of substituted pyridines.⁴ This pioneering synthesis was a routine three component condensation reaction of an aldehyde with two equivalents of beta-keto ester in the presence of a nitrogen donor such as ammonia, that produced 1,4-dihydropyridine (Scheme 2.1).



Scheme 2.1: Reaction showing Hantzsch's original dihydropyridine synthesis.

In principle five different dihydropyridine isomers can exist, though the 1,2- and 1,4-isomers are commonplace in the literature with over 4000 distinct 1,2 and 1,4-DHP structures being reported on the Cambridge crystallographic data centre (CCDC).⁵ Today the landscape of DHP chemistry is panoramic extending into territories such as agriculture,^{6,7} biochemistry,⁸ pharmacology^{9,10} and synthesis.^{11,12}

Dihydropyridines became of greater significance through the discovery of the naturally occurring coenzyme nicotinamide adenine dinucleotide (NADH). This led to much more interest and activity in their isolation and redox chemistry. 1,4-DHP isomers have also commanded attention due to their prevalence in cardiovascular pharmaceuticals as in the calcium channel blockers Nifedipine, Norvasc and DynaCirc used to treat hypertension. Additionally, antihypertensive 1,4-DHPs have also been reported to be successful cystic fibrosis transmembrane conductance regulator (CFTR) correctors.¹³⁻¹⁵ Whilst the pharmacologically active 1,4-isomer has been extensively investigated, the 1,2-isomer has received relatively meagre attention though it is also a fundamental synthetic precursor to more sophisticated scaffolds; participating as a

diene in Diels-Alder reactions to construct isoquinuclidines and as useful intermediates to anti-cancer agents and flu remedies (e.g., Tamiflu).¹⁶

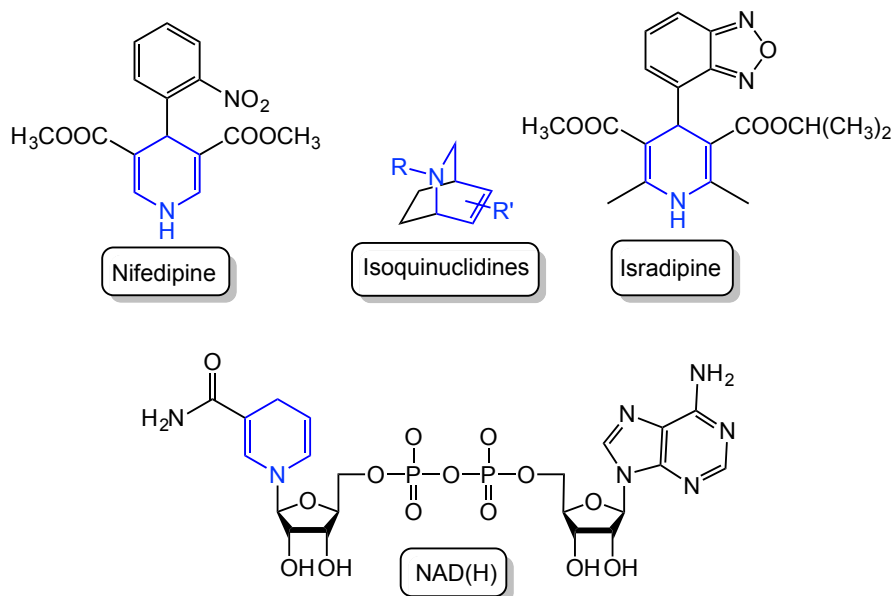


Figure 2.1: Representative examples of the dihydropyridine scaffold (highlighted in blue) in synthetic and naturally-occurring molecules.

2.2.1 Metallodihydropyridines

Given the scope of these compounds it may be surprising that less than 90 metallodihydropyridines have been structurally characterised to date. (Figure 2.2)⁵ Interestingly, these are not limited to one area of the periodic table, as an array of s, p, d and f-block congeners have been reported, though most of these involve transition metals.

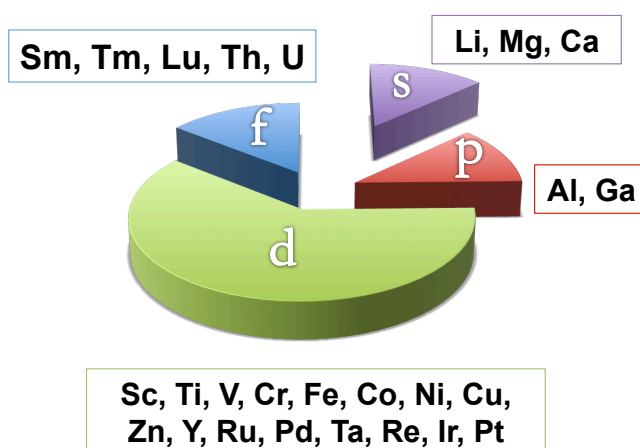


Figure 2.2: Structurally characterized metallodihydropyridines as a function of the metal position in the periodic table.⁵

The experimental work described in this chapter focuses on s-block metallodihydropyridines, hence a comprehensive discussion on this class of compound follows. However, some important comparable dihydropyridines must be mentioned. A stand out p-block example is the lithium tetrakis-(*N*-dihydropyridyl)-aluminate, more commonly known as Lansbury's reagent,¹⁷ employed as a selective reducing agent for aldehydes and ketones.^{18,19} An interesting point to note about the reaction producing Lansbury's reagent is the lack of isomeric selectivity that is found in the product. Albeit a fairly simple synthesis, the reaction of LiAlH₄ and pyridine results in five different isomers of a solvent separated ion pair species of formula LiAl(NR₂)₄ where NR₂ can be either the 1,2 or 1,4-dihydropyridyl ring (Figure 2.3a). This low selectivity was attributed to the conflict between kinetic and thermodynamic control where the 1,2-isomer is the former and 1,4-isomer the latter^{20,21} thus explaining the difficulty of isolating the 1,2-dihydropyridyl form of the reagent. Another group 13 dihydropyridine worth mentioning here is a boron example that is prepared via an s-block intermediate (Figure 2.3b).²² This relies on dimesitylfluoroborane (DMFB) coordinating to pyridine, which then undergoes a 1,2-nucleophilic addition with phenyllithium. However, the boron dihydropyridine is not limited to DMFB, since alternative routes can be employed, such as hydroboration of pyridine with pinacolborane (HBpin), which has been well studied and in recent years catalytic approaches have been reported. This aspect will be discussed in more detail in chapter 4: catalytic hydroboration.

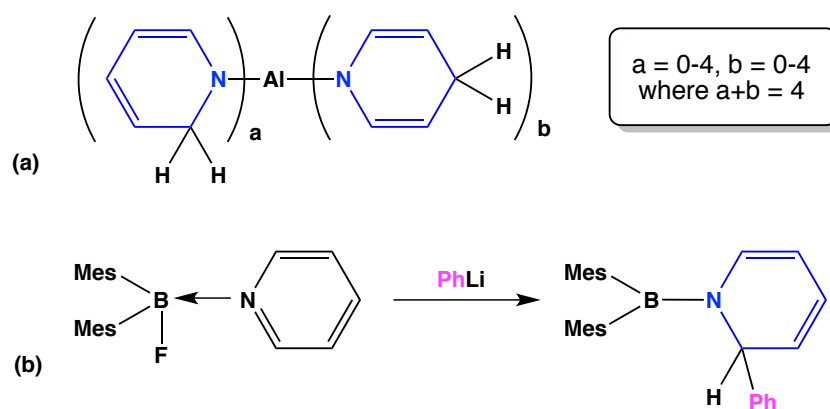
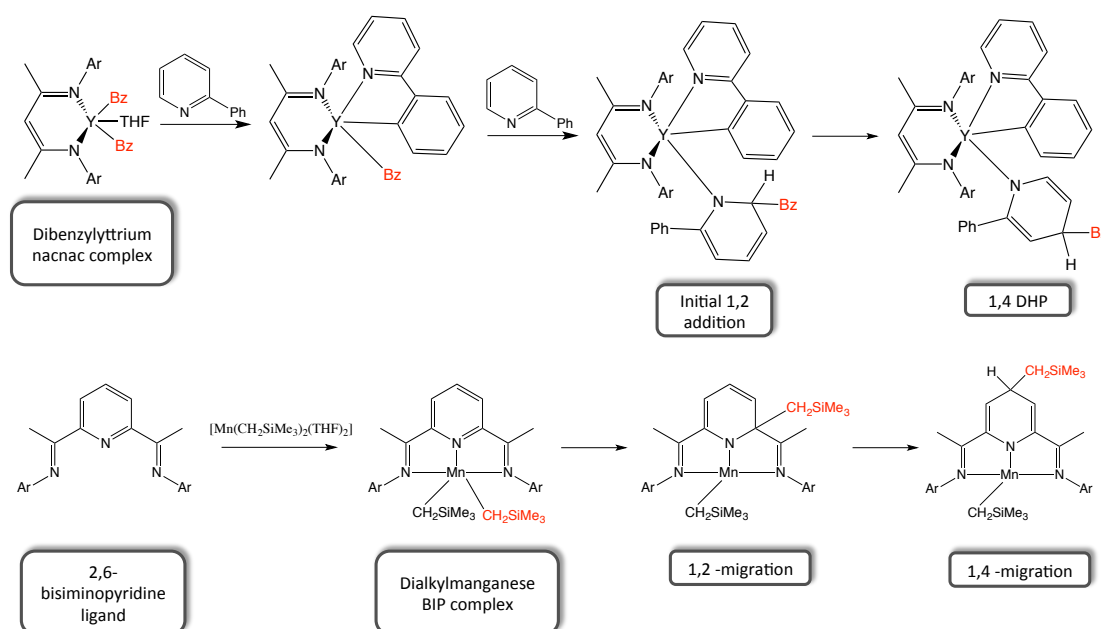


Figure 2.3: p-Block dihydropyridine examples: (a) Lansbury reagent and (b) boron dihydropyridine via an alkyl lithium synthesis.

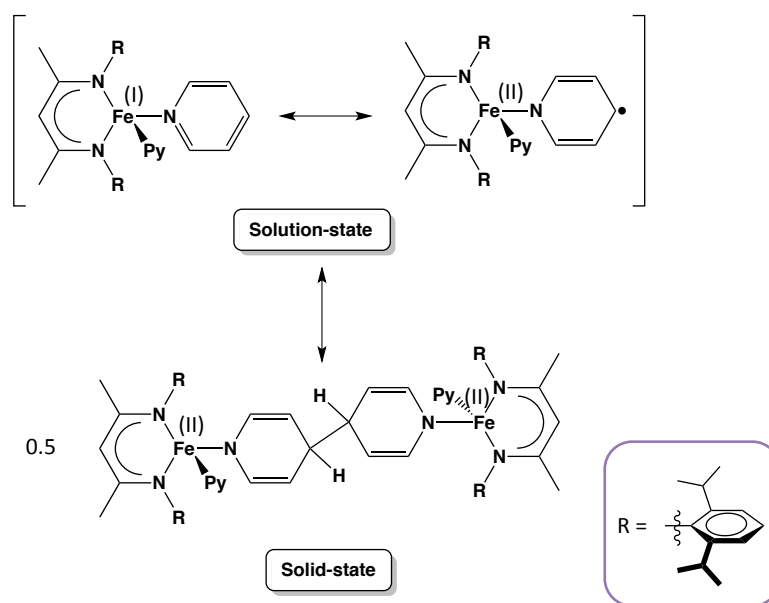
d-Block dihydropyridines are generally prepared via three routes, namely addition to pyridine from an alkylmetal complex,²³ alkyl migration from the dialkylmetal complex to the supporting pyridine based ligand²⁴ (typically a bisiminopyridine ligand, BIP) or more commonly via a metal hydride complex adding across pyridine.²⁵⁻²⁸ Interestingly these complexes still exhibit similar chemistry with most examples proceeding initially through a 1,2 intermediate before leading to the thermodynamic 1,4-dihydropyridine product. **Scheme 2.2** shows an example of each case. In the situation of direct addition with nacnac supported dibenzylttrium, 2-phenylpyridine coordinates and is deprotonated by one benzyl arm, followed by another equivalent of 2-phenylpyridine undergoing addition to give the resulting 1,2 benzyldihydropyridine, which over time converts to the thermodynamic product 1,4-DHP.²⁹ Similarly in the case of reacting the bisiminopyridine ligand with the dialkylmanganese complex, $[\text{Mn}(\text{CH}_2\text{SiMe}_3)_2(\text{THF})_2]$, the initial metal-ligand complex is formed followed by migration of the $(-\text{CH}_2\text{SiMe}_3)$ group from the 2-position to the 4-position.³⁰



Scheme 2.2: Dibenzylyttrium complex reacting with 2-phenylpyridine (top) and 2,6-bisiminopyridine reacting with dialkylmanganese (bottom).^[29, 30]

Recently there have been a few reported examples of d-block dihydropyridine related species arising from a different avenue. This involves using iron(I) pyridine complexes and exploiting the capabilities of pyridine as a redox-active ligand. Consequently reduction of pyridine results in a radical “DHP-like” species, which can dimerise to

give a bis(dihydropyridine) complex.^{31,32} Similar bi-dihydropyridine complexes have been reported utilising thulium³³ and samarium.³⁴ Interestingly these reductively coupled dihydropyridine species that have been characterised by X-ray crystallography have arisen from reactivity studies opposed to studying dihydropyridines in their own right. In f-block chemistry the reductive dimerization of pyridine is used as a test reaction to gauge the reactivities and stabilities of thulium and samarium complexes. The different supporting ligands on these complexes, cyclopentadienyls or phospholyls, largely control these factors hence the complexes are subjected to a reaction with pyridine. These reactions can result in a reductively coupled 1,2-dihydropyridine species, similar to that observed with iron in [scheme 2.3](#), or simply in no redox reactivity at all just simple pyridine coordination. This approach is not limited to pyridine as a similar protocol has been performed with acridine.



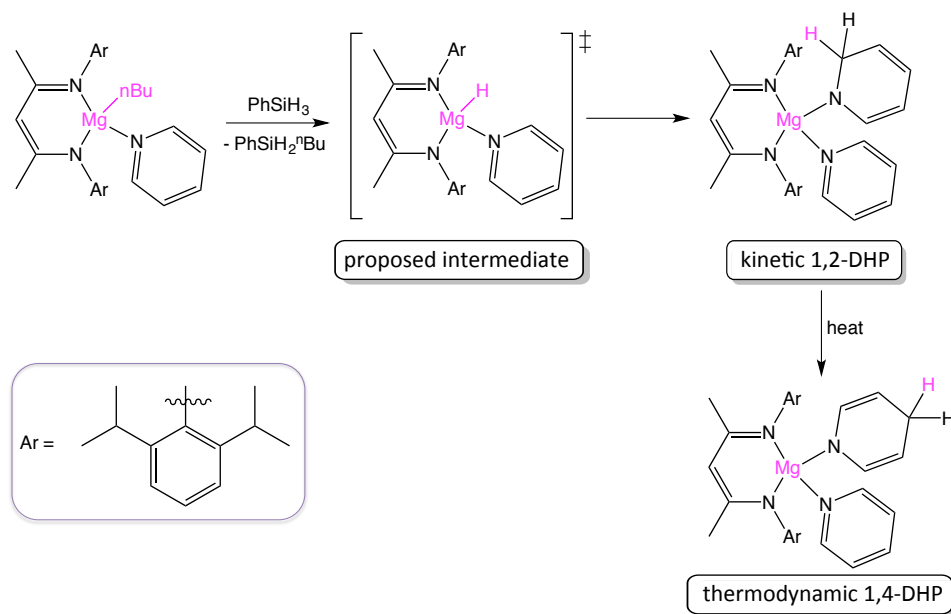
Scheme 2.3: Interconversions of iron(I) pyridine species in solution versus coupled dihydropyridine species formed in solid state.

2.2.2 s-Block dihydropyridines

Recent years have seen considerable upturn in the development of s-block DHP chemistry, in particular that of alkaline earth metals³⁵⁻⁴⁰ primarily due to the demand of attempting to mimic rare element chemistry with more abundant sustainable elements. Not only has a structural foundation been established, the resulting DHP compounds have shown ability for further reactivity⁴¹ and their presence as intermediates in

catalytic hydroboration^{42,43} and hydrosilylations⁴⁴ of pyridine mechanisms has been recognised.

Hill reported the earliest structurally characterised magnesium dihydropyridine³⁵ complex, by exploiting the reactivity of a pyridine adduct of the well defined β -diketiminato *n*-butyl magnesium precursor [(DIPPnacnac)Mg(*n*Bu)(pyridine)] (Scheme 2.4). It was proposed that upon reacting with phenylsilane, a hydride surrogate, an *in-situ* reactive ‘MgH’ species forms, although it was not observed - note that a similar reactivity has been previously seen with an yttrium analogue. The ‘MgH’ complex reacts with the coordinated pyridine resulting in a mixture of 1,2 and 1,4 dihydropyridyl species at room temperature. Analogous to the well-studied Lansbury reagent, and the previously reported reactivity of MgH₂ with pyridine,³⁶ this system also exhibits a temperature dependency with the thermodynamic 1,4-DHP product being obtained after heating the reaction mixture at 60°C for 12h.



Scheme 2.4: Formation of kinetic and thermodynamic magnesium dihydropyridine complexes from a nacnac supported magnesium alkyl precursor.

This work by Hill has been extended to various substituted pyridines and other heterocycles³⁷ as summarised in figure 2.4. These substrates have been selected to support the view that the 1,4-DHP is a thermodynamic product that proceeds via the kinetic 1,2-DHP intermediate. It was reported that with 2,6-lutidine where both sites at

the 2- and 6-position are blocked no reactivity was observed. However, with 2-methylpyridine, the reaction resulted in a 1,4-DHP, which would be plausible as there is an available 1,2 site for the intermediate addition step, to then convert to the 1,4 DHP. This was seen for 3-, 3,5-methylpyridine and quinoline where the initial addition is possible. From another perspective, blocking the 4-position with a substituent, as in 4-methyl pyridine and isoquinoline, resulted in isolable 1,2-DHPs, where no follow-on reactivity to the thermodynamic product has been witnessed. Interestingly, 4-dimethylaminopyridine (DMAP), although bearing a substituent at the 4-position still results in an isomeric mixture.

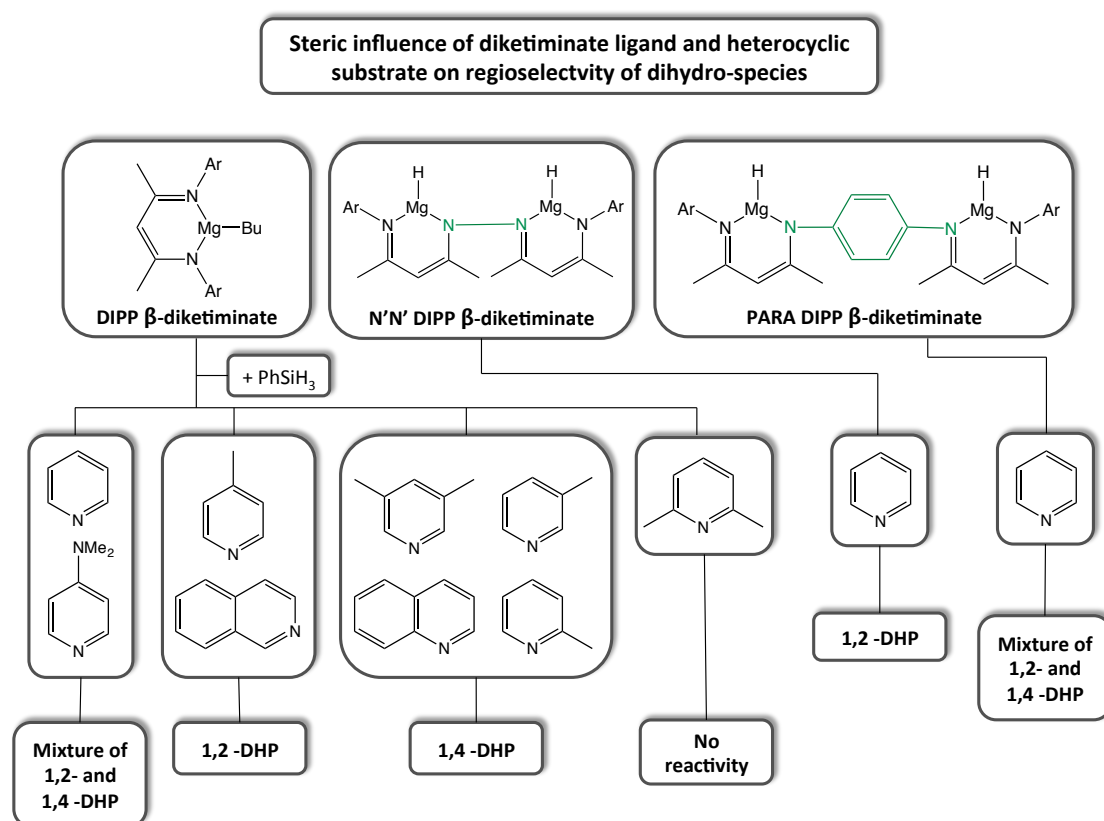
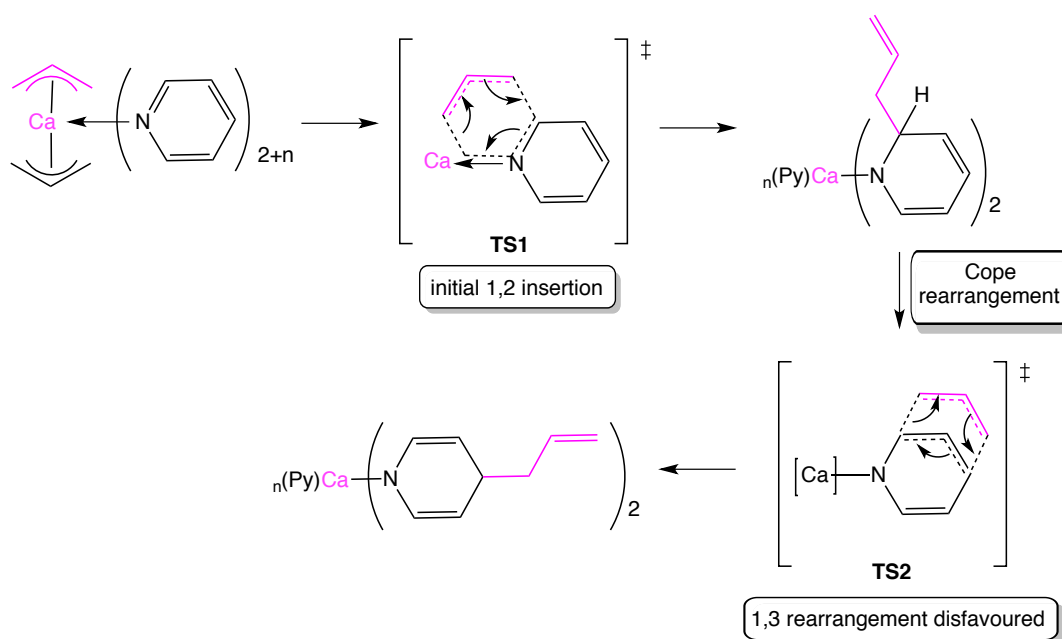


Figure 2.4: Summary of the influence of the steric ligand and heterocyclic substrate on the regioselective dihydro-product obtained.^[37, 38]

Recent work by the Harder group has highlighted the influence of the supporting ligand on the regioselective dearomatization of pyridine.³⁸ Keeping on the theme of β-diketiminate ligands, they explored distinctive tetranuclear $[\text{NN}(\text{MgH})_2]$ and octanuclear $[\text{PARA}_3\text{Mg}_3\text{H}_{10}]$ magnesium hydride clusters, which were supported by bis-β-diketiminate ligands, noting that the tetranuclear is N-N coupled and the octanuclear is phenylene bridged. They found that the tetranuclear cluster was the first

crystallographically authenticated example of selective 1,2 dearomatisation of pyridine by magnesium. The secondary intramolecular interactions within this species also made this stable enough to prevent rearrangement to the thermodynamic 1,4-isomer. It is suggested this is an outcome of the rigid N-N bridge in the ligand, as the phenylene bridged analogue displays no selectivity and performs in an analogous way to the monomeric β -diketiminato.

Okuda ventured into the heavier group 2 dihydropyridine arena, with calcium, reporting the first structurally characterised example, remarkably arising from a different synthetic approach than the typical metal hydride route.⁴⁰ Consequently, the nature of the dihydropyridyl species formed is slightly different. Instead of a metal hydride addition across pyridine, there is an insertion of pyridine within a Ca-C bond of an allyl calcium precursor $[\text{Ca}(\text{C}_3\text{H}_5)_2]$ (Scheme 2.5). Fascinatingly, this is followed by a clean regioselective transformation to the 1,4-allyl DHP. Again it is worth noting here the trend of the reaction proceeding through a 1,2 transition state at room temperature.



Scheme 2.5: Proposed mechanism for forming a regioselective 1,4-allyl calcium DHP.^[40]

2.2.3 Group 1 dihydropyridines

The original alkylation of pyridine with organolithium reagents is well known dating back to 1930.⁴⁵ For years it was postulated that the mechanism involved an addition step of 'RLi' followed by an elimination/rearomatisation step with the concurrent loss of LiH.^{46,47} Many studies followed this, investigating the isolation, characterisation and decomposition of the intermediate compound,⁴⁸⁻⁵⁰ and the reactivity of these compounds as a reducing agent.^{46,51} The first actual isolation and characterisation of a lithiodihydropyridine came in 1988 from the reaction of *n*BuLi and pyridine. This resulted in a 1-Li-2-*n*-butyldihydropyridine with two solvating pyridine ligands, (Figure 2.5a) highlighting that pyridine has a dual role of reactant and Lewis base donor stabilising the lithium centre.^{49,50} Although a crystalline complex was isolated, they were not single crystals hence X-ray diffraction could not be performed. Crystallographic structural authentication did not arrive until 1996 when a crystalline 1,4-lithiodihydropyridine was isolated (Figure 2.5b).⁵²

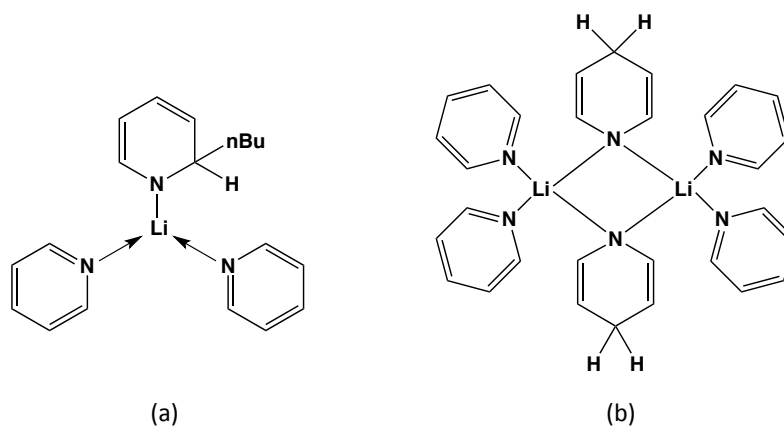
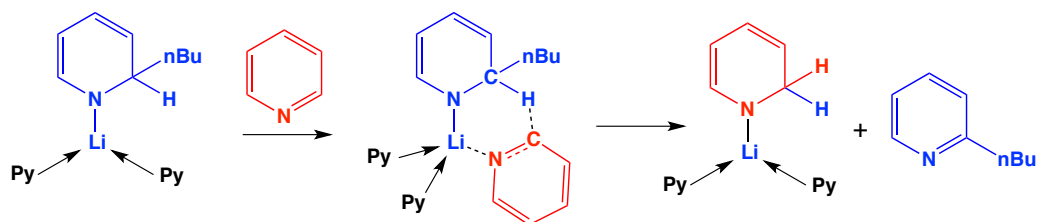


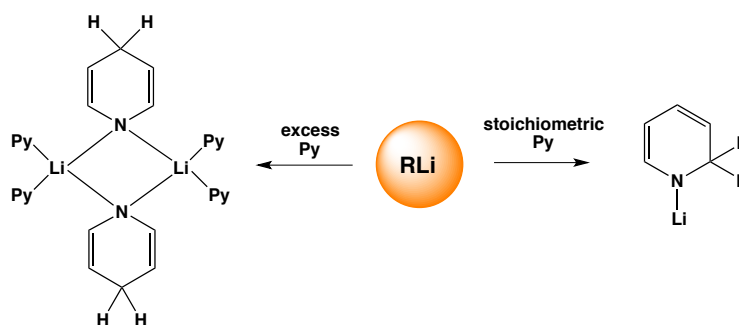
Figure 2.5: Chemdraw representations of (a) pyridine solvate adduct of 1,2-lithiodihydropyridyl intermediate and (b) pyridine solvate 1,4-lithiodihydropyridyl species.

Interestingly, this molecular structure revealed that the pyridine adduct of the 1-Li-2-*n*-butyldihydropyridine underwent a secondary reaction. The surrogate LiH unit of this complex reduced another molecule of pyridine resulting in 2-*n*-butylpyridine and a new dihydropyridyllithium complex (Scheme 2.6). Although the crystal structure defines a 1,4-dihydropyridine, ¹H NMR studies revealed that a mixture of 1,2- and 1,4-dihydropyridine ligands were present, showing a similar isomerisation process to that reported with Lansbury's reagent.^{20,21}



Scheme 2.6: Proposed mechanism of the formation of 1,2-lithiodihydropyridine and *n*-butylpyridine.

Since this work, this area of chemistry remained largely unexplored, with very few lithium dihydropyridine examples in the literature⁵³ and the closest example to a heavier group 1 dihydropyridine being a mixed metal K/Zn complex where the K atom sits in the outer sphere offering π -stabilisation to a zinc dihydropyridine.⁵⁴ Since alkali-metal dihydropyridines were yet to be studied in their own right, this initiated research within our group where the pioneering alkylation reaction of pyridine was revisited. The reaction of *t*-BuLi and pyridine (typically carried out in excess pyridine) was investigated. Surprisingly altering the pyridine ratio and performing the reaction stoichiometrically in *n*-hexane facilitated the crystallisation and isolation of 1-lithio-2-*t*-butyldihydropyridine as confirmed by NMR spectroscopic studies (scheme 2.7).⁵⁵ A remarkable feature of this intermediate is its excellent hexane solubility which it exhibits. However an interesting point to note here, is that when a linear alkyl group is used, *n*-butyllithium as opposed to *t*-butyllithium, a hexane insoluble precipitate forms instantly. Recently, there has been growing interest in isolating soluble LiH sources, with a stand out example in the literature being the arene soluble octanuclear complex, $[\{(DippNPPh_2)Li\}_4(LiH)_4]$, reported by Stasch.⁵⁶ As these DHP compounds are known to release LiH, it also doubles up as an extremely practical hexane soluble lithium hydride source, as was demonstrated in the reduction of benzophenone.⁵⁵



Scheme 2.7: Influence of pyridine ratio on DHP isomeric product.

From this method a Me₆TREN stabilised adduct of the 1-lithio-2-*t*-butyldihydropyridine was crystallised and its structure determined by X-ray diffraction. This revealed the first stable molecular structure of a 1,2-lithiodihydropyridyl intermediate (Figure 2.6).⁵⁵ Further work has established tridentate Lewis base donors such as PMDETA or Me₄AEE are equally as successful in monomerising and stabilising the 1,2-lithiodihydropyridyl intermediate. Due to the success of this method it was expanded to different butyl isomers, *i*-butyl and *s*-butyl, with the latter appearing to be the least stable analogue of the four, decomposing under ambient conditions.⁵⁷

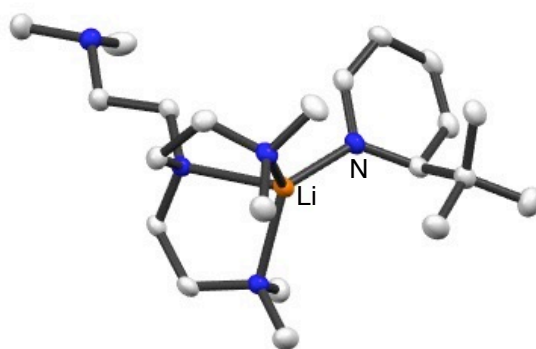
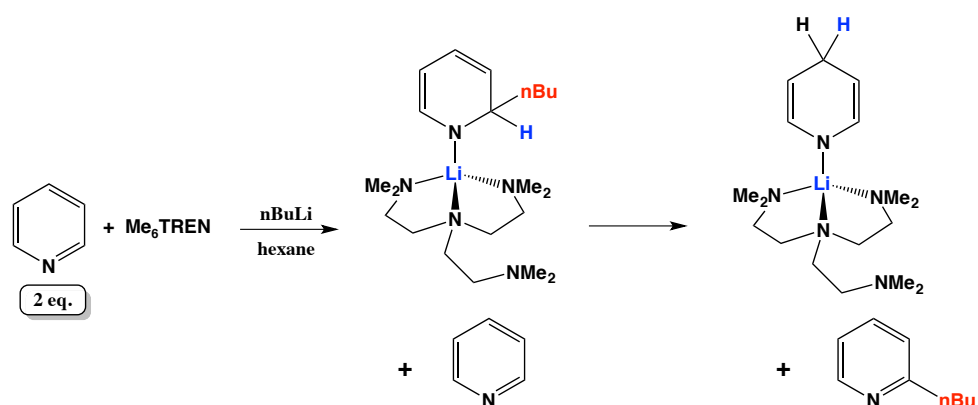


Figure 2.6: Monomeric structure of **1** with Me₆TREN, [1-Li-2-*t*-Bu(NC₅H₅)(Me₆TREN)]. Hydrogen atoms omitted for clarity.

To confirm the importance of the pyridine stoichiometry, studies were done replicating the same conditions, but using two equivalents of pyridine for the reaction with *n*-butyllithium, in the presence of the Lewis base donor Me₆TREN. This was in agreement with the mechanism proposed previously, where the initial addition takes place but is swiftly followed by the reduction of the second equivalent of pyridine to give a 1,4-lithiodihydropyridine species (Scheme 2.8).



Scheme 2.8: Reaction of *n*-BuLi with two molar equivalents of pyridine.

2.3 Aims of this chapter

Our primary aim was to extend the landscape of group 1 dihydropyridine chemistry to lithium and broaden our knowledge of heavier group 1 metals by:

- Optimising a synthetic strategy to isolate the more reactive heavier alkali metal dihydropyridines analogous to the reported lithium derivative.
- Characterise their solution state structure by NMR spectroscopy.
- Employ Lewis base donors in a bid to characterise these in the solid state by X-ray crystallography.
- Perform thermal volatility analysis (TVA) to determine their thermal properties.
- Evaluate their ability as a metal hydride surrogate in a test reaction.

2.4 Result and discussion

2.4.1 Synthetic approach to isolable sodium and potassium dihydropyridines

Initially the focus was on finding a viable synthetic route to prepare sodium and potassium derivatives that would allow the isolation of pure “intermediate” heavier metallodihydropyridines.

Direct nucleophilic addition

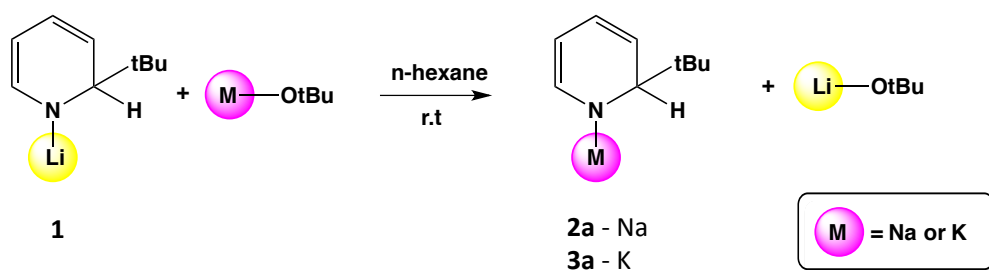
Predictably, the initial approach studied was a direct nucleophilic addition, as this had proved successful for the isolation of a 1-Li-2-*t*-Bu-DHP, **1**. As a starting point reactions were carried out with pyridine and a stoichiometric equivalent of an alkylsodium or alkylpotassium reagent such as BuNa, NaCH₂SiMe₃ or KCH₂SiMe₃ in a non-polar solvent such as *n*-hexane.

Disappointingly, this route only provided black intractable mixtures in all cases at room temperature, presumably due to the (too) highly reactive character of the alkyl metal reagent. Upon later consideration of this approach it was determined to be of limited use synthetically, as even if optimised to realise a pure product, the alkyl variant on the dihydropyridine would be restricted by the stability of the alkyl metal in

the first instance. For this reason it was decided to move forward with a different approach.

Metathesis reaction of lithium dihydropyridine

Due to the fact that crystalline **1** [1-Li-2-*t*-Bu(NC₅H₅)] can be straightforwardly isolated in excellent yields⁵⁵ of 80% it was decided to attempt a simple metathesis reaction with an alkali-metal-*t*-butoxide to access the sodium and potassium derivatives. Reacting isolated **1** in *n*-hexane with a stoichiometric equivalent of NaOtBu at room temperature, resulted immediately in an insoluble beige precipitate, which could be filtered and isolated in yields of 68% (Scheme 2.9). Performing the same reaction with KOtBu resulted in a yellow suspension, the solid of **3a** could be isolated with ease in a good yield of 73%.



Scheme 2.9: Metathesis reaction of crystalline **1** with MOtBu in hexane solution.

Subjecting both samples to ¹H NMR spectroscopy in d₈-THF solution (due to the lack of solubility in C₆D₆) it was confirmed that in the case of sodium and potassium, [1-Na-2-*t*-Bu(NC₅H₅)] **2a** and [1-K-2-*t*-Bu(NC₅H₅)] **3a** were obtained respectively. In each ¹H NMR spectrum five equal intensity resonances were observed corresponding to the dihydropyridine ring and one corresponding to the nine equivalent hydrogen atoms of the *t*-Bu group, as illustrated in figure 2.7. The shifts of the ¹H NMR signals of the dihydropyridine ring are also in agreement with the loss of aromaticity. The ¹H NMR resonances of each alkali metal dihydropyridine variant has been summarised in table 2.1.

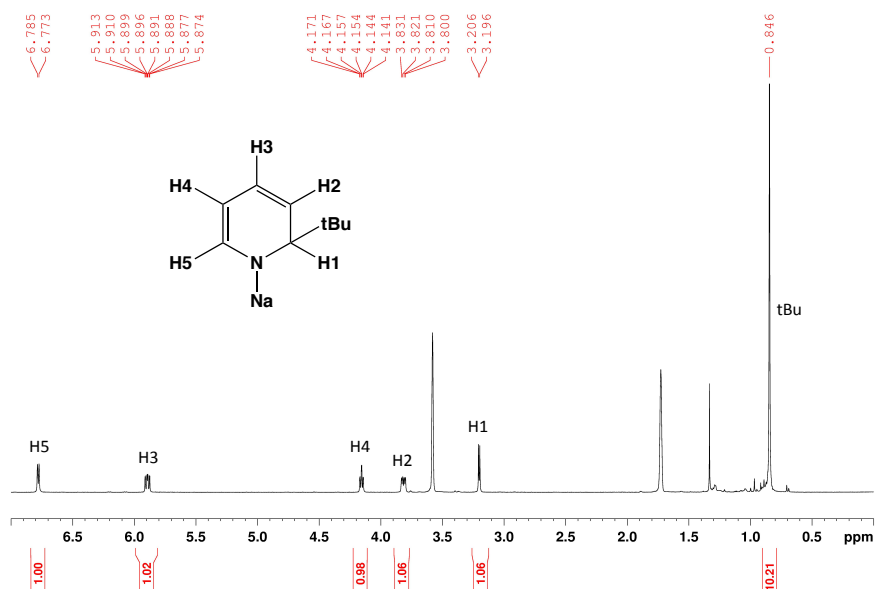


Figure 2.7: ^1H NMR spectrum of **2a** in d_8 -THF solution.

Table 2.1: ^1H NMR resonances of 1-M-2-*t*-Bu-DHP in d_8 -THF solution.

Chemical shifts in d_8 -THF (ppm)						
Compound	H1	H2	H3	H4	H5	tBu
1	3.51	3.85	5.79	3.90	6.60	0.79
2a	3.20	3.82	5.89	4.16	6.78	0.85
3a	3.16	3.69	5.86	4.22	6.77	0.86

Interestingly when **1** was prepared *in-situ*, by the addition of *t*-BuLi to pyridine followed by the addition of NaOtBu, a beige suspension was still observed. This was isolated in 87% yield, a slightly higher yield than that achieved in the previous method using isolated **1**. However, the ^1H NMR spectrum indicated the presence of a second dihydropyridine species. Again, five equal intensity resonances were observed corresponding to the dihydropyridine ring of the asymmetric 1,2-isomer, with 3 new signals at 2.91, 3.81 and 6.20 ppm which were attributed to the dihydropyridine ring of the symmetric 1,4-isomer [1-Na-4-*t*-Bu(NC₅H₅)] **2b** (Figure 2.8). A similar mixture of 1,2- and 1,4-DHP isomers was also observed with potassium.

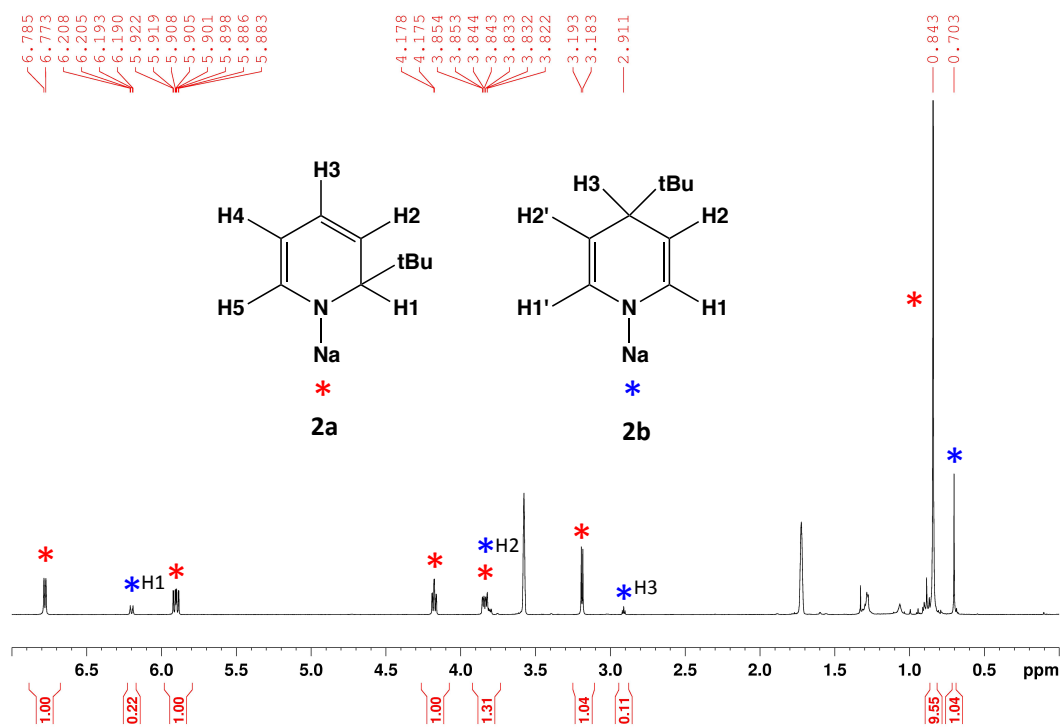


Figure 2.8: ^1H NMR spectrum of product mixture **2a** and **2b** from reaction of pyridine, $t\text{BuLi}$ and NaOtBu *in-situ* in d_8 -THF solution.

When the isolated yields of product from both the isolated and *in-situ* routes are compared a correlation can be made. Compound **1** has a crystalline yield of 80%, when the reaction to obtain **2** and **3** were performed *in-situ* the total isolated yields are 87% and 93% respectively. However, if we look at the NMR ratio of 1,2 to 1,4 within the isolated solid it is consistent that the 1,2 isomer is the major product, with a 4:1 ratio being observed (approximately 80% of the 1,2 isomer).

Table 2.2: Isolated yields of dihydropyridine compounds **1-3**.

Compound	Isolated 1 route – yield of pure 1,2-isomer (%)	<i>In-situ</i> route – total yield of mixture of 1,2 and 1,4 isomer (%)	NMR ratio of 1,2:1,4 isomer in mixture (%)
1	83	-	-
2a	67	87	82:18
3a	73	93	80:20

In the literature there is precedence for a conversion from the 1,2 kinetic isomer to the 1,4 thermodynamic isomer.³⁵ It was decided to investigate the possibility of this being the pathway to isolating the 1,4-isomer with the sodium and potassium dihydropyridines - although there was no indication of this happening with **1**. Most examples in the literature observe the thermodynamic product as a result of heating the sample for a period of time, hence it was decided to subject isolated **2a** to similar conditions and observe if **2b** would form. In a J. Young's NMR tube, compound **2a** was dissolved in d_8 -THF solution and monitored over time whilst being subjected to prolonged heating at 55°C (Figure 2.9). From the ^1H NMR spectra it can be concluded that there is no sign of alkyl transfer to give rise to the 1,4-isomer. Instead aromatic resonances corresponding to 2-*t*-butylpyridine started to appear at 7.04, 7.33, 7.58 and 8.46 ppm, indicating the rearomatisation of the pyridine ring with the concomitant loss of NaH. There was no evidence of **2b** forming. Upon revisiting the synthesis of **1**, it was found that the 1,2-isomer selectively crystallised from hexane. However, analysis of the filtrate confirmed the presence of the 1,4 isomer. This explains why an *in-situ* preparation of **2** and **3** lead to mixtures of products. Since the 1,4-isomers of sodium and potassium are less soluble in *n*-hexane they co-precipitate with the 1,2 isomer.

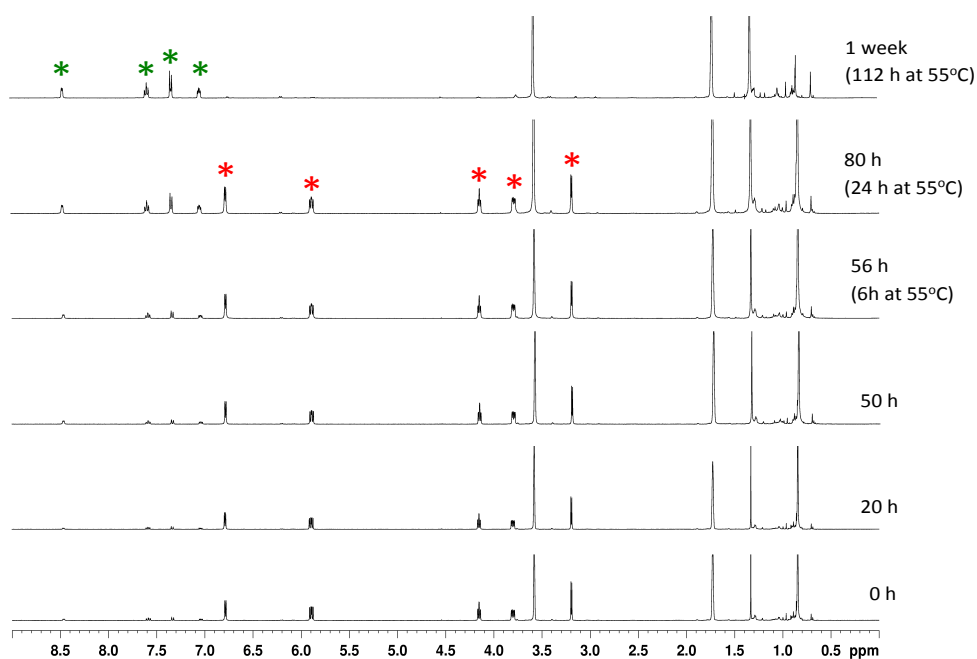


Figure 2.9: ^1H overlay of **2a** monitored over time with heating where the red asterisk represents **2a** and the green asterisk 2-*tert*-butylpyridine.

2.4.2 Solid state structures

As the solid-state structures of **2a** and **3a** could not be determined, common Lewis base donors TMEDA, PMDETA and THF were employed with the hope of isolating X-ray quality crystals of solvated derivatives to divulge more structural information. Using these donors five new metallodihydropyridines [$\{\text{K}(1,2\text{-}t\text{-Bu-DHP})(\text{TMEDA})\}_2$] **4**, [$\{\text{K}(1,2\text{-}t\text{-Bu-DHP})(\text{PMDETA})\}_2$] **5**, [$\{(\text{PMDETA})\text{Na}(1,4\text{-}t\text{-Bu-DHP})\}_2$] **6**, [$\{\{\text{Na}(1,2\text{-}t\text{-Bu-DHP})\}_2(\text{TMEDA})\}_2$] **7**, and [$\{\text{K}(1,2\text{-}t\text{-Bu-DHP})(\text{THF})\}_\infty$] **8** were prepared and crystallographically characterised displaying three manifestly different structural motifs, a dimer, dimer of dimers and a novel polymeric dihydropotassium.

Complexes **4**, **5** and **6** exhibit a dimeric assembly with the general formula [$\{(\text{donor})\text{M}(\text{DHP})\}_2$] ($\text{M} = \text{K}$ for **4** and **5**; $\text{M} = \text{Na}$ for **6**). This is a common motif found in alkali metal amide chemistry.⁵⁸ Sodium and potassium amide closed dimeric structures with TMEDA and PMDETA are surprisingly rare with only single figures of each type existing in the CSD library compared with the large repertoire of lithium examples.^{5,58} All three of these discrete dimers contain the archetypal 4-membered M_2N_2 core, with the coordination sphere of each metal being satisfied by one bidentate or tridentate chelating Lewis base donor, (donor = TMEDA for **4**; and PMDETA for **5** and **6**).

X-ray crystallographic quality crystals of [$\{\text{K}(1,2\text{-}t\text{-Bu-DHP})(\text{TMEDA})\}_2$] **4** revealed a centrosymmetric dimeric assembly (Figure 2.10). The four-atom KNKN core ring, where the bridging amide is a 2-*t*-Bu-substituted dihydropyridine unit, is strictly planar with endocyclic angles totalling 360° . The two symmetry equivalent K atoms connect the two dihydropyridine bridges anti relative to the *t*-butyl groups with the $(\text{KN})_2$ plane.⁵⁹⁻⁶² The structure is completed by a datively bonded neutral bidentate Lewis base donor TMEDA protecting the outer sphere of each cation.

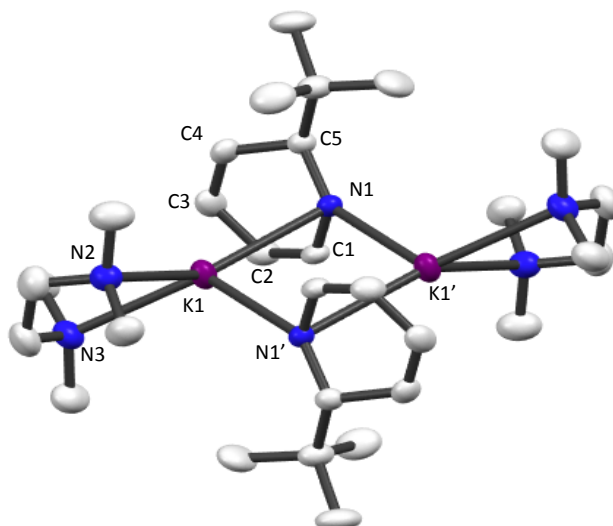


Figure 2.10: Molecular structure of **4**, R,S-enantiomer is shown with displacement ellipsoids at 50% probability level, hydrogen atoms, π -interactions and minor disordered component of dihydropyridine ring and *t*Bu group have been omitted for clarity. Symmetry transformations used to generate equivalent atoms labelled ‘: 0.5-*x*, 1.5-*y*, -*z*. Selected bond lengths (Å) and bond angles (°): K1-N1, 3.002(3); K1-N1’, 2.749(2); K1-N2, 2.877(2); K1-N3, 2.860(2); N1-C1, 1.321(4); C1-C2, 1.378(4); C2-C3, 1.425(4); C3-C4, 1.339(4); C4-C5, 1.507(3); N1-C5, 1.469(3); K1-N1-K1’, 94.91(7); N1-K1-N1’, 85.09(7); N1-K1-N2, 146.32(6); N1-K1-N3, 145.20(6); N1’-K1-N2, 119.94(6); N1’-K1-N3, 88.49(6); N2-K1-N3, 63.62(5).

The K-N_(amide) bonding within **4** resembles that found in the literature. The (KN)₂ ring exhibits a rhomboidal arrangement where K1-N1’ [2.749(2)] is shorter than K1-N1 [3.002(3)] by 0.253 Å. This variation in bond length has been seen before in K amide examples though not to this extent.⁶³⁻⁶⁵ Moving to the K-N_(TMEDA) dative bonds, there are no remarkable differences when comparing the bond lengths [2.877(2) and 2.860(2)] with comparable reported examples ranging from 2.825-2.950Å.^{59,63,64,66}

The geometry of the K atom is not easily defined due to its soft nature allowing it to engage in π interactions with C2, C3 and C4 of the pyridyl ring (Figure 2.11a). However if we generate a centroid in the dihydropyridine ring and consider the nitrogen and π -system as a single coordination point, it can be described as being four coordinate with a pseudo-tetrahedral geometry (Figure 2.11b). The distortions in bond angles around the metal centre can be attributed to potassium’s desire to form a cation- π interaction with the dihydropyridine ligand. The bond angles have been summarised

and compared using N1 as the bonding point versus the centroid (C*) of the NC₅H₅ ring in table 2.3.

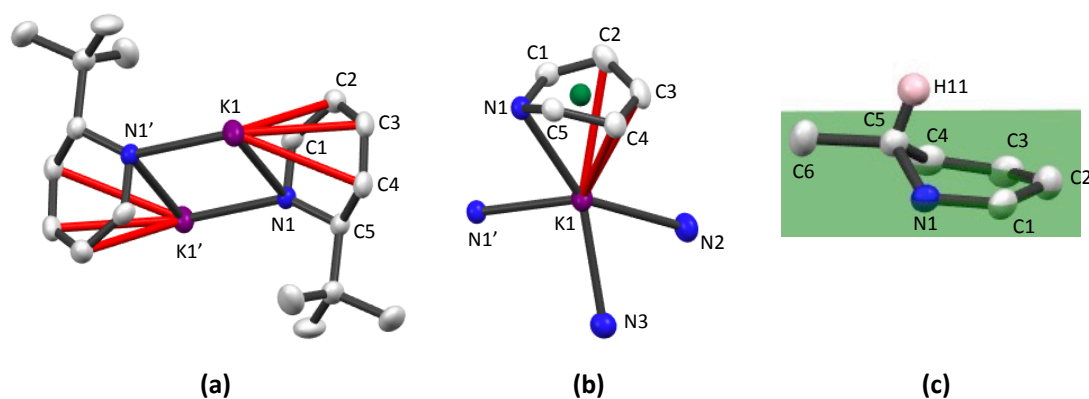


Figure 2.11: Fragments of the molecular structure of **4**, (a) with removal of TMEDA and π -interactions highlighted in red; (b) core geometry around potassium with a centroid highlighted in green and (c) plane through 5 atoms of dihydropyridine ring. Selected bond lengths (\AA): K1-C2, 3.226(3); K1-C3, 3.194(3); K1-C4, 3.280(2); K1-C*, 2.918.

Table 2.3: Bond angles comparing distortion around K in **4** in pseudo-tetrahedral geometry using the N bond versus centroid (C*) of dihydropyridine ring.

Angle	Bond angle ($^{\circ}$) using nitrogen (N1)	Bond angle ($^{\circ}$) using centroid (C*)
N2-K1-N3	63.62(5)	63.62(5)
N2-K1-N1'	119.94(6)	119.94(6)
N3-K1-N1'	88.49(6)	88.49(6)
N1/C* - K1 - N2	146.32(6)	119.68
N1/C* - K1 - N3	145.20(6)	149.67
N1/C* - K1 - N1'	85.09(7)	110.70

Examining the dihydropyridine ring in more detail, the bonding is distinguished where the C-C bond lengths are concordant with their carbon atoms being either sp^3 or sp^2 . It supports the presence of conjugation within C1-C4 having bonds lengths in the range of 1.339-1.425 \AA , whereas C4-C5 is more characteristic of sp^3 bonding with a bond length of 1.507 \AA .⁵⁷ Another nice feature of the ring is the manner that sp^3 C5 bearing

the *t*-butyl group is puckered from the plane by 0.646 Å in a distorted tetrahedral geometry (Figure 2.11c).

Exchanging the bidentate ligand TMEDA for tridentate PMDETA allowed the isolation of **5**, [$\{K(1,2\text{-}t\text{-Bu-DHP})(\text{PMDETA})\}_2$]. This dimer possesses an essentially planar four-atom KNKN core ring (Figure 2.12). Again, the dihydropyridine anions occupy the bridging positions. However, this time in contrast to **4** the *t*-butyl group finds itself in a rare *syn* orientation relative to the KNKN plane, sharing similar features to the first *syn* Na-amido dimeric structure (Figure 2.13a).⁶⁷ Interestingly, the molecular structure of **5** demonstrates the metal's ability to accept supplementary stabilisation within its coordination sphere accommodating tridentate PMDETA whilst maintaining a dimeric molecular constitution.

Analogous to that encountered in **4**, the geometry around the metal centre is distorted due to the K- π interactions with the neighbouring dihydropyridine ring. Looking at the geometry of potassium, again due to the cation- π interactions, it is difficult to place this in a common geometry classification. However, removing the shrubbery from the metal centre, it perhaps finds best similarity with a trigonal bipyramidal geometry albeit one extremely distorted at equatorial positions N2 and N4 (Figure 2.13b).⁶⁵

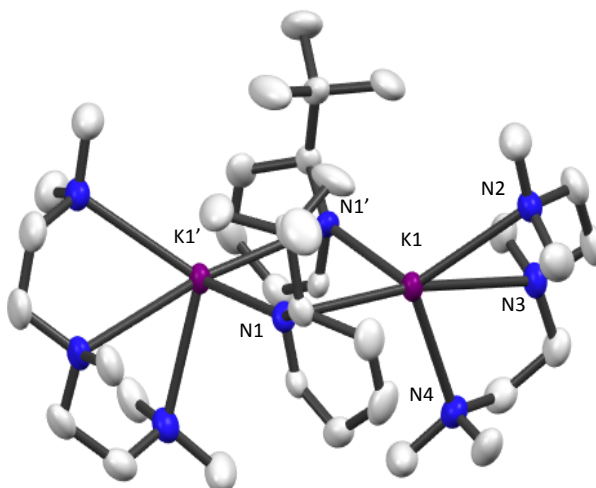


Figure 2.12: Molecular structure of **5**, R,R-enantiomer is shown with displacement ellipsoids at 50% probability level, hydrogen atoms and minor disordered component of dihydropyridine ring and *t*Bu group have been omitted for clarity. Symmetry transformations used to generate equivalent atoms labelled ‘: 1.5-x, y, 1.5-z. Selected

bond lengths (Å) and bond angles (°): K1-N1, 3.056(2); K1-N1', 2.774(13); K1-N2, 2.980(1); K1-N3, 2.990(1); K1-N4, 2.956(2); N1-C1, 1.336(9); C1-C2, 1.371(8); C2-C3, 1.422(7); C3-C4, 1.347(8); C4-C5, 1.497(6); N1-C5, 1.468(14); N1-K1-N1', 82.87(5); K1-N1-K1', 96.29(5); N2-K1-N1, 127.41(2); N2-K1-N3, 59.93(4); N2-K1-N4, 110.13(4); N2-K1-N1', 117.52(4); N3-K1-N1, 171.0(2); N3-K1-N4, 59.19(4); N3-K1-N1', 97.6(3); N4-K1-N1, 111.8 (2); N4-K1-N1', 105.8(4).

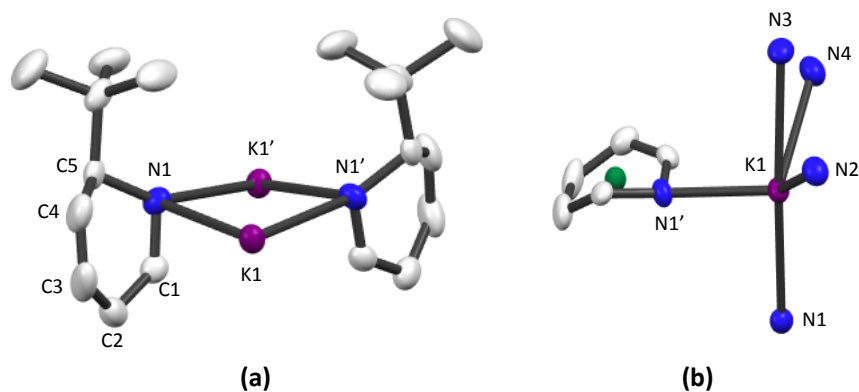


Figure 2.13: Different perspectives of the molecular structure of **5**, (a) with removal of PMDETA and (b) core geometry around potassium with a centroid highlighted in green. Selected bond lengths (Å) and bond angles (°): N1-K1-C*, 80.96; N2-K1-C*, 131.43; N3-K1-C*, 97.53; N4-K1-C*, 87.13.

Unsurprisingly, the geometry of the dihydropyridine ring chimes with that in **4**, exhibiting similar features. The ring displays a puckering at C5, 0.640Å from the plane due to the sp^3 nature of the carbon. Whilst C1-C2, C2-C3 and C3-C4 have bond lengths in the range of 1.347(8)-1.422(7) Å indicating the delocalisation within this region of the ring, C4-C5 has an appreciably longer bond length of 1.497(6) Å owing to the aliphatic nature at this carbon.

The molecular structure of $[\{(PMDETA)Na(1,4-t\text{-Bu-DHP})\}_2]$ **6** was found to be a centrosymmetric closed dimer possessing an essentially planar Na_2N_2 ring completed by two PMDETA ligands, which datively bonds in a tridentate fashion to sodium resulting in a coordination number of five for the metal (Figure 2.14).

Of the three dimers **6** is anomalous having its *t*-butyl group at the 4-position of the dihydropyridine ring whereas the others have the *t*-butyl group at the 2-position. When

all three of the dimeric structures are compared, a striking difference in having the *t*-butyl group at the 4-position is observed - the lack of π -interactions between the cation and the dihydropyridine ring. Although the conjugation remains present within the ring as can be distinguished by comparing the bond lengths of C1-C2 [1.342(3)Å] with C2-C3 [1.508(3)Å], there are no secondary interactions with the sodium atom. Consequently, in this example no tilting of the dihydropyridine ring towards the metal was observed, opposite to that seen in **4** and **5**. This is supported when the M-C_(DHP) and M-C'_(DHP) bond lengths are reviewed (Table 2.4).

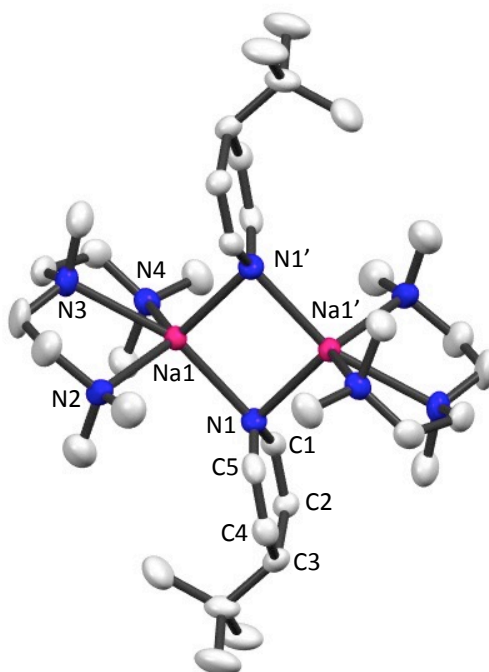


Figure 2.14: Molecular structure of [{(PMDETA)Na(1,4-*t*Bu-DHP)}₂] **6** with displacement ellipsoids at 50% probability level and hydrogen atoms omitted for clarity. Symmetry transformations used to generate equivalent atoms labelled ‘: -x, -y, 1-z. Selected bond lengths (Å) and bond angles (°): Na1-N1, 2.420(2), Na1-N1’, 2.451(2); Na1-N2, 2.608(2); Na1-N3, 2.555(2); Na1-N4, 2.620(2); Na1-N1-Na1’, 84.93(6); N1-Na1-N1’, 95.07(6); N2-Na1-N1’, 103.05(6); N2-Na1-N3, 70.40(6); N2-Na1-N4, 127.57(6); N3-Na1-N1, 106.57(6); N3-Na1-N1’, 103.05(6); N3-Na1-N4, 70.62(6); N4-Na1-N1, 114.16(6); N4-Na1-N1’, 100.43(6).

Moving to the impact this has on the (MN)₂ dimeric core, compound **6** differs from compounds **4** and **5** considerably. In **4** and **5** two types of bonding can be seen within the KNKN core. For example in **4**, M1-N1 [3.0014(1)] is longer than M1-N1’ [2.7492(1)] indicating a shorter σ -bond and longer π -interaction. However in **6**, both

Na-N bond lengths are comparable [2.4204(2) and 2.4511(2)] and in agreement with typical σ -Na-N_(amide) bonds lengths.⁶⁸ This can be attributed to **4** and **5** having a conjugated π -system interacting with the metal cation whereas in **6** this does not occur. There is precedence for this, in a PMDETA solvated sodium-pyrrole dimer, the metal engages exclusively with the nitrogen, opting not to participate in secondary interactions.⁶⁹ However, it has been noted that with sodium, this can also be an influence of the Lewis base donor. Moving from TMEDA to PMDETA in a sodium-indole dimer suppressed the σ/π difference in the NaNNaN core, resulting in a more symmetrical σ -natured core with almost identical Na-N bond lengths.⁶⁸ The significance of the π -interactions on the structure is emphasised when we compare the M1-N1-M1' bond angles. Typical σ -amido dimers, such as (donor.MTMP)₂ and (donor.MHMDS)₂, display an acute bond angle in the region of 75-85°, ⁷⁰ which **6** obeys [84.92(2)]. However, **4** and **5** do not conform to this trend, instead they expand into obtuse angles [94.91(1) and 96.2(4)°] as a result of the additional intramolecular interactions.

Table 2.4 Bond distances [Å] for **4**, **5** and **6** of the metal to each atom of the DHP ring.

Bond	4	5	6
M1-N1	3.0014(1)	3.056(16)	2.4204(2)
M1-N1'	2.7492(1)	2.774(13)	2.4511(2)
M1-C1	2.9532(1)	3.122(7)	3.2105(2)
M1-C1'	3.2447(1)	3.193(7)	2.9452(2)
M1-C2	3.2257(1)	3.479(5)	4.4538(3)
M1-C2'	4.6165(2)	4.559(5)	4.0334(4)
M1-C3	3.1939(1)	3.416(6)	5.1915(4)
M1-C3'	5.3856(3)	5.385(6)	4.8529(4)
M1-C4	3.2796(2)	3.423(6)	4.6351(4)
M1-C4'	5.1315(3)	5.191(6)	4.3195(4)
M1-C5	3.6589(2)	3.722(3)	3.4470(3)
M1-C5'	4.0529(2)	4.096(3)	3.3015(2)

Interestingly compounds **7** and **8** do not adopt the conventional dimer motif. Instead the dimer acts as the basic building block of higher aggregated, intricate assemblies, each of which is distinct. Employment of the bidentate donor TMEDA with **2** gave **7**, which X-ray crystallographic studies established was [$\{\{\text{Na}(1,2-t\text{-Bu-DHP})\}_2$

(TMEDA)}₂], a discrete, centrosymmetric tetranuclear dimer of dimers (Figure 2.15). Its molecular framework is composed of two simple (NaN)₂ dimeric rings. These dinuclear subunits are connected by cation- π interactions between the inner sodium atoms (Na1) and the carbon atom (C11') of the neighbouring dihydropyridyl ring. The outermost sodium atoms Na2/2' are capped by TMEDA molecules that prevent further aggregation.

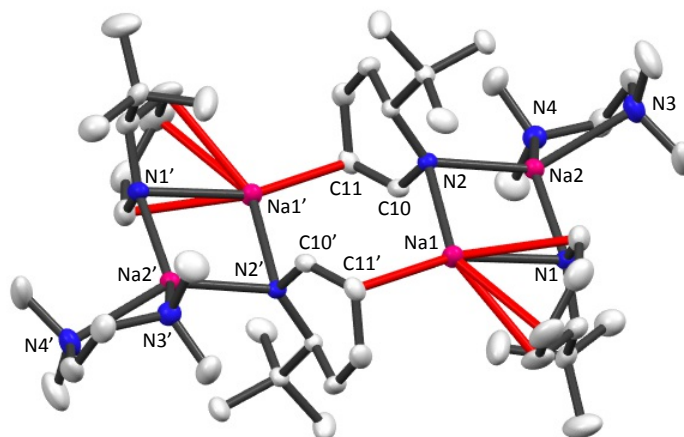


Figure 2.15: Molecular structure of [{{Na(1,2-*t*-Bu-DHP)}₂(TMEDA)}₂], **7** with displacement ellipsoids at 50% probability level, hydrogen atoms and minor disordered component of dihydropyridine ring have been omitted for clarity. Symmetry transformations used to generate equivalent atoms labelled '': 1-x, 2-y, 1-z. Selected bond lengths (Å) and bond angles (°): Na1-N1, 2.631(2); Na1-N2, 2.4465(15); Na2-N1, 2.343(2); Na2-N2, 2.4472(14); Na2-N3, 2.440(2); Na2-N4, 2.496(2); Na1-C11', 2.606(2); C10-C11, 1.387(3); N2-C10, 1.331(2); Na1-N2-Na2, 86.92(5); N2-Na1-N1, 90.44(6); Na2-N1-Na1, 84.98(6); N1-Na1-N2, 90.43(6); C11'-Na1-N2, 109.18(6); C11'-Na1-N1, 160.30(7); N1-Na2-N3, 133.63(7); N1-Na2-N4, 103.07(7); N2-Na2-N3, 110.95(5); N2-Na2-N4, 142.78(6); N3-Na2-N4, 75.50(6).

Examining the dimeric subunits in more detail (Figure 2.16a), the NaNNaN ring is strictly planar (endocyclic angles: 360°), and akin to **4** and **5** the nature of the bonding within is distinguishable. The bond lengths of Na1-N2, Na2-N1 and Na2-N2 [2.4465(15), 2.343(2) and 2.4472(14) Å respectively] are consistent with those in **6**, and consequently typical sigma Na-N_(amide) bonds. The anomaly is Na1-N1 with a significantly extended length of 2.631(2) Å, which is more characteristic of Na being

engaged in a π -interaction with the ring. This side-on bonding mode exhibits Na1- $C_{(\text{ring})}$ interactions spanning 2.710(3)-2.996(3) Å which are in agreement with reported Na-C π -interactions.⁷¹⁻⁷³

These dinuclear subunits are sewn together by further cation π -interactions between Na1-C11' [2.6055(17) Å], to form an eight atom (NaNCC)₂ ring centrepiece (Figure 2.16b). This ring is essentially planar through six atoms, Na1-C10-C11-Na1'-C10'-C11', with the N2 puckered out of the ring, residing 1.038 Å out of the plane. There is novelty in this type of aggregation via secondary interactions,⁷⁴ opposed to the typical Na-N aggregation,⁷⁵⁻⁷⁸ with few examples in the literature. The most relatable example is a 2,3,4,5-tetramethyl-1-sodiopyrrole complex where the π -coordination between the dienyl pyrrole and the sodium acts as a bridge to generate a polymeric motif.⁷⁹ Both the dihydropyridyl rings within this complex agree with the loss of aromaticity and an sp³- α C which is corroborated by the bond lengths of the dihydropyridyl ring and C5 being puckered out of the sp² hybridised plane of carbon atoms (C1-C4).

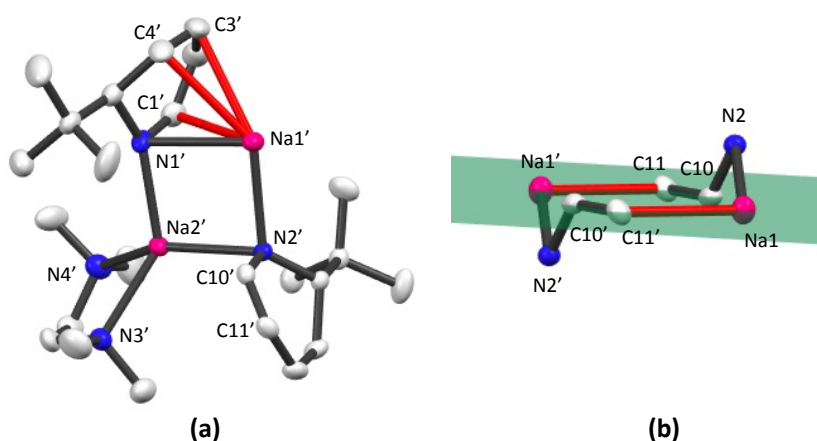


Figure 2.16: Fragments of 7, (a) dimeric building block and (b) eight-membered core aggregation unit with a plane through six atoms; π -interactions highlighted in red. Selected bond lengths (Å): Na1-C1, 2.710(3); Na-C3, 2.834(3); Na1-C4, 2.825(2).

Deaggregation to a dimer could also be suppressed in the K analogue by switching to the popular non-chelating monodentate Lewis base THF. The structure of crystalline **8** was determined by X-ray diffraction studies to be an unprecedented polymeric dihydropyridine, [$\{K(1,2-t\text{-Bu-DHP})(\text{THF})\}_\infty$], **8** (Figure 2.17). Dimeric (KN)₂ rings make up the backbone of the structure, resembling that in **4**, which are linked up

through intermolecular cation π -interactions. Each K atom has one THF molecule datively bound.

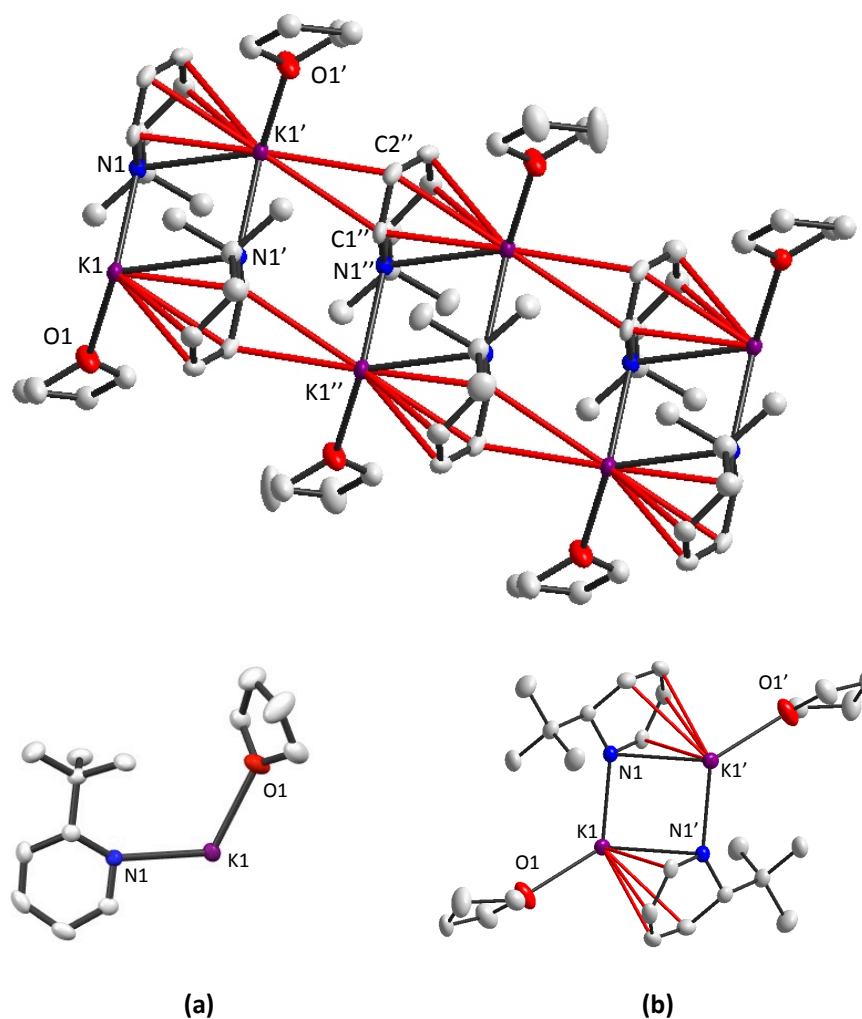


Figure 2.17: Fragment of the X-ray characterised polymeric structure of $[\{K(1,2-t\text{-Bu-DHP})(\text{THF})\}_\infty]$, **8** (top), monomeric unit and dimeric unit (bottom) with displacement ellipsoids at 50% probability level, hydrogen atoms and minor disordered component of the THF molecule have been omitted for clarity. Symmetry transformations used to generate equivalent atoms labelled ‘: 1-x, 2-y, 1-z, labelled’: -1+x, y, z. Selected bond lengths (Å) and bond angles (°): K1-N1, 2.722(1); K1-N1’, 3.113(1); K1-O1, 2.7171(14); K1’-C1’’, 3.119(2); K1’-C2’’, 3.350(2); K1-C1’, 2.990(1); K1-C2’, 3.194(2); K1-C3’, 3.099(2); K1-C4’, 3.254(2). K1-N1-K1’, 97.58(4); N1-K1-N1’, 82.42(4); N1-K1-O1, 116.86(4); N1’-K1-O1, 122.73(4).

This striking assembly can be dismantled to its basic monomeric unit (Figure 2.17 bottom). This contains one K atom engaging in a K-N bond with the dihydropyridyl ring and a K-O_(THF) bond. These monomeric units aggregate into (KN)₂ dimers, in an essentially identical bonding mode to that in **4**, with K1-N1', [3.1128(13) Å] deviating considerably from K1-N1, [2.7220(14) Å] owing to increased π -character in the dimerization interaction (Figure 2.17 bottom). The K-C_(ring) distances suggest an η^4 coordination, [K1-C1'/C2'/C3'/C4'; mean length 3.1342 Å],⁸⁰ with these stabilising π -contacts with the metal having a geometrical consequence on both the tilting of the dihydropyridine ring and the K coordination geometry. It is the bonding preference of the soft K metal to a soft arene π -system that results in this novel dihydropotassium polymer.⁶⁵ The dimers link up through intermolecular η^2 π -type interactions between K' and the olefinic C1'' and C2'' atoms [3.3498(15) and 3.1190(19) Å] of the dihydropyridine ring in a neighbouring dimeric unit (Figure 2.17). The propagation of this polymeric motif relies solely upon these modest K- π interactions. Totally unique in dihydropyridine chemistry, this polymeric structure can be compared with a select few potassium polymers containing other amido and related ligands,⁸¹ though these generally exhibit zigzag arrangements.^{82,83}

2.4.3 Solution state structures

Due to the poor solubility of compounds **4**, **5**, **7** and **8** in d₆-benzene these compounds were fully assigned by NMR spectroscopy in a d₈-THF solution. The ¹H NMR spectra displayed assignments completely in agreement with the solid-state structure, and no remarkable features were noted. Since compound **6** was also soluble in C₆D₁₂, a non-coordinating solvent, this was also subjected to a DOSY NMR study⁸⁴⁻⁸⁷ as shown in figure 2.18 in an attempt to determine its solution structure.

This technique has recently been receiving a lot of attention in organometallic chemistry, more specifically for alkali metal complexes, to determine their solution state structures by molecular weight prediction.⁸⁸⁻⁹¹ DOSY studies of complex **6** revealed an estimated molecular weight of 633.28 g/mol as determined from a logarithmic plot of diffusion coefficient versus formula weight based on the well-defined dihydropyridine hydrogen resonances (Figure 2.19). Given that this molecular weight is higher than the heaviest internal standard, 1,2,3,4-tetraphenyl-naphthalene

(432.55 g/mol), the results must be interpreted with caution. The expected molecular weight for dimeric compound **6** [$\{\text{Na}(1,4\text{-}t\text{-Bu-DHP})(\text{PMDETA})\}_2$] would be 665.02 g/mol (table 2.5), hence the predicted value is within 5% error suggesting the dimeric molecule is retained in solution. However, considering all various combinations, the possibility of an unsolvated tetrameric complex [$\{1\text{-Na-}2\text{-}t\text{-Bu}(\text{NC}_5\text{H}_5)\}_4$] cannot be ruled out, as this has an even better fit with an error of 0.56%.

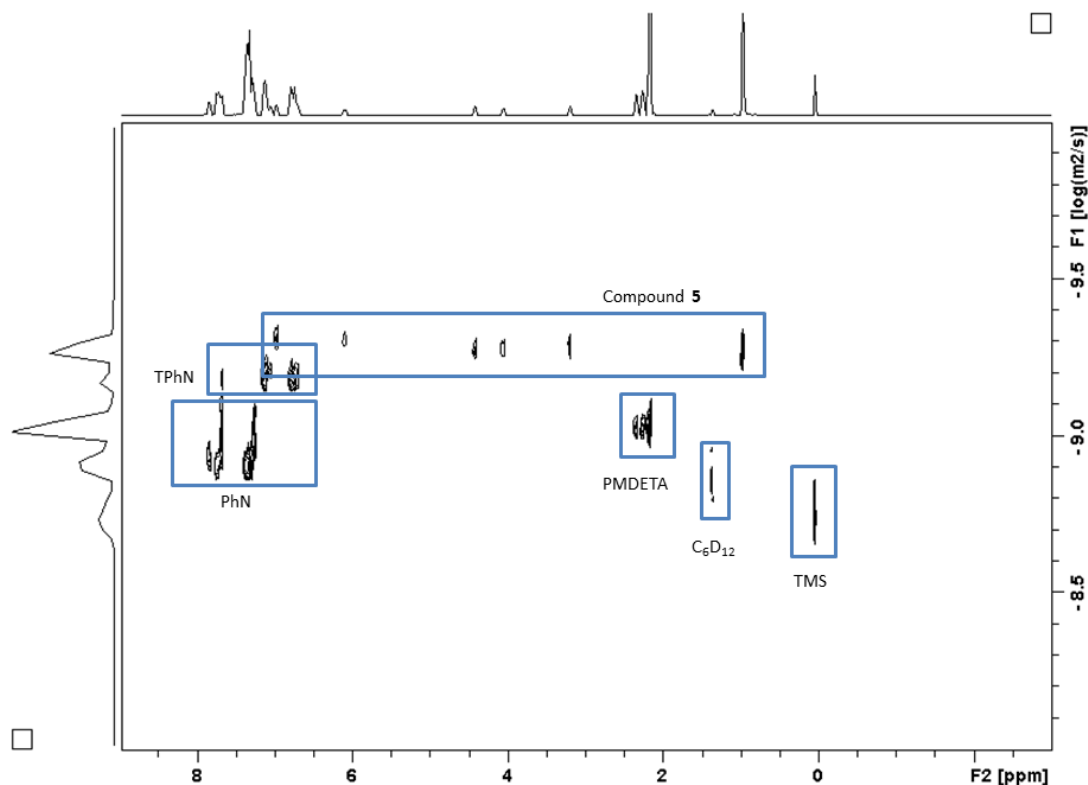


Figure 2.18: ^1H DOSY NMR spectrum of **6** in C_6D_{12} solution.

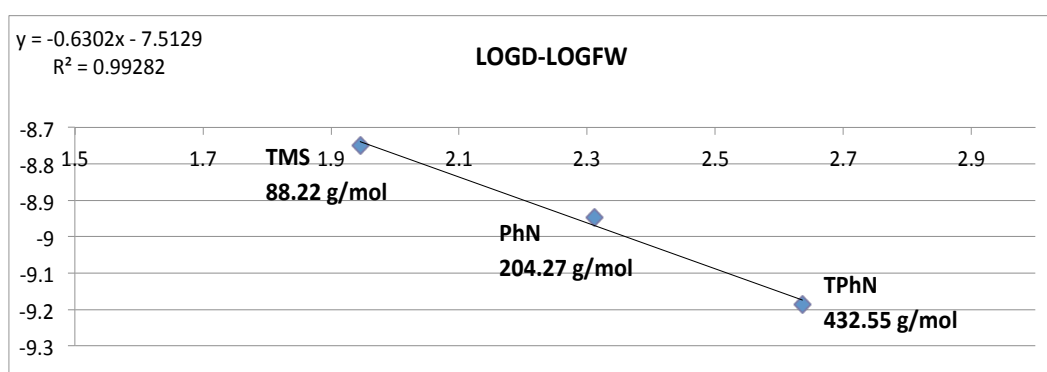


Figure 2.19: Plot of $\log D$ versus $\log FW$ from ^1H DOSY NMR data of the mixture of **6** and inert standards TPhN, PhN and TMS in C_6D_{12} solution at 300K.

Table 2.5: D-FW analysis from the ¹H DOSY NMR data of the mixture of **6** and standards TPhN, PhN and TMS in C₆D₁₂ solution at 300K.

Compound	D _{AV} (m ² s ⁻¹)	Log D _{AV}	FW (g/mol)	Log FW
TPhN	6.53x10 ⁻¹⁰	-9.18541948	432.55a	2.63603632
PhN	1.13x10 ⁻⁹	-8.9474343	204.27a	2.31020459
TMS	1.78x10 ⁻⁹	-8.7490923	88.22a	1.94556705
6	5.03x10 ⁻¹⁰	-9.29820759	633.28b	2.80159377

^a = Theoretical FW ^b= FW calculated from [log D = -0.6302·logFW-7.5129 (r²=0.9928)]

Although, combining previous knowledge with the ¹H NMR spectrum, a more conclusive answer can be drawn. If the unsolvated tetrameric complex was the solution state structure, it would be expected to see concomitantly free PMDETA would be observed in the ¹H NMR spectrum and in this case the PMDETA resonances in the spectrum do not correlate with free PMDETA, thus suggesting it is still bound to the Lewis acidic metal. It was noted that PMDETA has a different diffusion coefficient than the organometallic fragment to which it is bound. However, this has been reported with other Lewis donor: acceptor adducts.⁹²⁻⁹⁴ This is suspected to be due to dissociation/association of the donor ligand to the metal occurring and in this case when the molecular weight of the ‘free’ PMDETA was calculated it was considerably larger (260.25 g/mol) than its uncoordinated state (173.3 g/mol), hence it can be assumed that the PMDETA is loosely coordinated in solution. Also, if we acknowledge the insolubility of **2** in hexane, requiring d₈-THF to obtain solubility for NMR studies, it is unlikely that an unsolvated tetrameric complex would be soluble in a similar medium. Taking in all these factors it can be reasonably concluded that in solution **6** remains true to its solid-state arrangement.

2.4.4 Thermal Volatility Analysis (TVA) studies

Thermal volatility analysis (TVA) is a technique generally employed in polymer chemistry to investigate thermal degradation, with particular focus on polymer flammability stability. The Strathclyde system, built in-house, is based upon the

apparatus and techniques originally described by I.C. McNeill in 1966 and developed subsequently (Figure 2.20).⁹⁵⁻⁹⁹

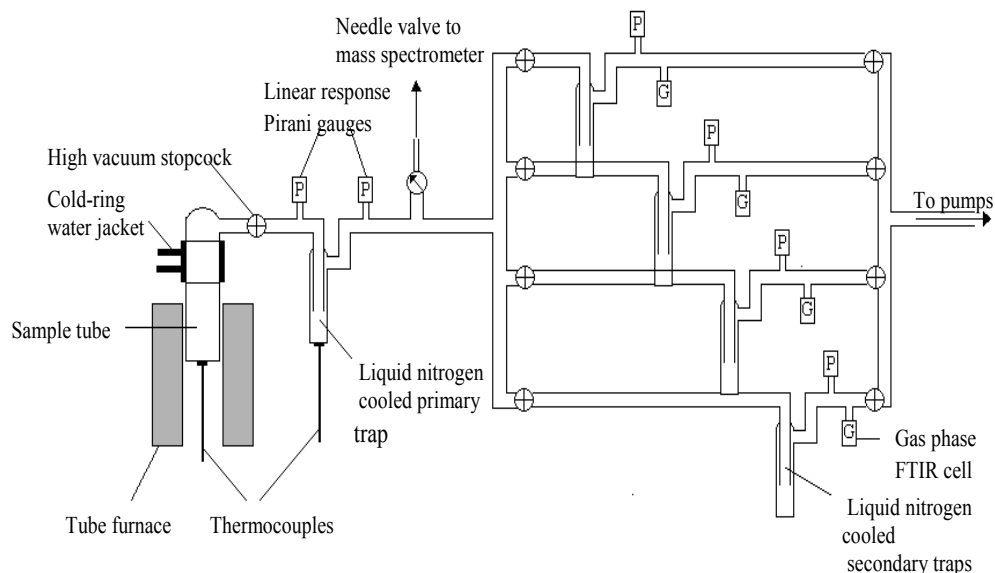


Figure 2.20: Schematic of Thermal Volatility Analysis setup.

A key benefit of this technique is that the sample can be controlled and analysed in real time to study its thermal properties. By collecting the consequent volatiles of thermolysis in a cryogenically cooled trap, they can be subjected to further analysis such as infrared spectroscopy, NMR spectroscopy and mass spectrometry, to determine the degradation components. It was decided to employ this versatile technique to determine the thermal stability of donor-free molecular **2a** and **3a**, to probe their potential as metal-hydride carriers.

Upon adapting the glassware slightly to facilitate air sensitive samples, it was subjected to a gradient heating program starting from room temperature increasing to 140°C in 2.5 °C min⁻¹ increments. As evidenced in figure 2.21, for compound **2a** the evolution of volatiles spanned a range of 60 to 140°C with the maximum loss rate at 124°C. The decomposition volatiles corresponding to this signal were collected and identified by ¹H NMR spectroscopy to be the anticipated alkylpyridine, 2-*t*-butylpyridine, intimating the release of NaH and concomitant rearomatisation of the dihydropyridine ring.

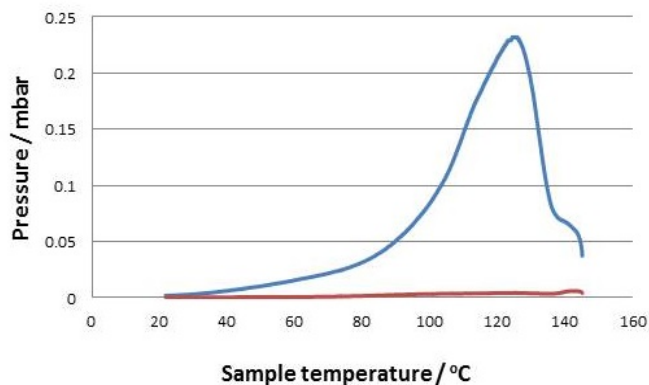


Figure 2.21: Thermal volatility analysis thermogram for **2a** where the blue line represents total volatile products and red line the non-condensable volatile products.

For **3**, there were two broad signals in the graph (figure 2.22), implying the loss of two species, one ranging from 20 to 70°C and the second from 70 to 120°C, with some overlap. When the decomposition volatiles were subjected to ^1H NMR spectroscopic analysis, the alkylpyridine was again observed, whilst the second product in the thermolysis curve was assigned as *n*-hexane. This can be attributed to *n*-hexane being trapped in the solid sample. Considering the boiling point of *n*-hexane is in the region of the initial broad signal, it can be concluded that the maximum rate of loss of KH occurred at a noticeably lower temperature of 99°C. Noting that **1** has a maximum rate of loss at 120°C,⁵⁵ similar to that of **2**, these results reflect the enhanced reactivity of potassium compared with the two smaller alkali metals lithium and sodium. Another advantage of TVA is the monitoring of products that are non-condensable; hence it can be assured that no other products were evolved during this process. It can be seen in both cases, **2** and **3**, only MH and 2-*t*-butylpyridine were produced.

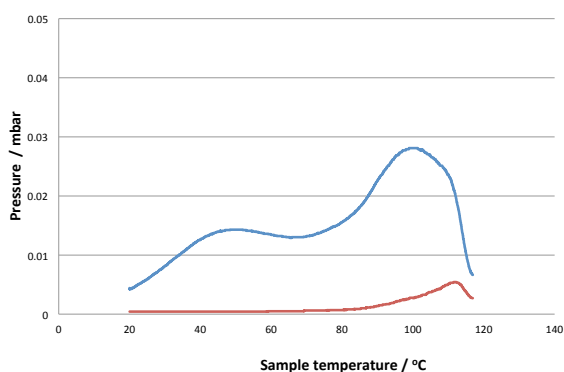


Figure 2.22: Thermal volatility analysis thermogram for **3a** where the blue line represents total volatile products and red line the non-condensable volatile products.

2.4.5 Preliminary hydrometallation studies

Due to the simplicity of preparation of these compounds and the promising results from the TVA studies highlighting their ability to release metal hydrides, the next avenue to explore was their ability as alternative metal hydride reagents.

Given their many desirable features over commercial metal hydrides such as solubility, safety and practicality working on intricate scales, if they performed in a similar manner to current 'LiH' reagents, these dihydropyridine complexes would make highly competitive novel metal-hydride sources. A straightforward reduction of benzophenone was selected as a benchmark reaction as there has been precedence for this as a control test reaction with other new synthetic LiH derivatives.⁵⁶

Since comparable studies have been performed with the original LiDHP **1** to isolate $[\text{Ph}_2\text{CO}(\text{H})\text{Li}]$, **9**, the same method was adopted. On a stoichiometric scale reacting isolated **2** with benzophenone in hexane resulted in an aqua blue solution, which, unlike the lithium example where a precipitate of the reduced metalobenzophenone was collected, did not yield any precipitate. This change can be attributed to the highly soluble nature of the product.¹⁰⁰ To overcome this an internal standard, hexamethylbenzene, was added and a ^1H NMR spectroscopic yield of 48% was obtained. Moving to compound **3**, mimicking the same reaction conditions produced a precipitate that could be collected and quantified in a more generous yield of 76%, identical to the lithium version isolated in a 76% yield.

2.5 Conclusions and future work

This work has provided a platform for alkali metal dihydropyridines in the literature with five new structurally characterized sodium and potassium examples. The structural diversity displayed upon moving from mono- to bi- to tridentate donors also provides a new range of complexes that rely on π -interactions for their aggregation, emphasizing the structural novelty possible with soft alkali metal atoms.

Now these simple synthetically accessible dihydropyridine compounds have been extensively characterized, they need to establish their place in the synthetic toolbox. The thermal studies and preliminary hydrometallation reactions would hint at their

unique selling point being a soluble metal-hydride surrogate source. Due to the elimination of the metal-hydride resulting in concomitant rearomatisation of 2-*tert*butylpyridine, it would be interesting to explore its capability to re-uptake the metal-hydride. If this was possible alkali metal dihydropyridines could be considered as a metal hydride vessel capable of release and uptake on demand, in a catalytic manner. Such a result would introduce s-block dihydropyridines as strong contenders in the metal-hydride catalyst catalogue.

2.6 Experimental

2.6.1 Synthesis

*Synthesis of [1-Li-2-*t*-Bu(NC₅H₅)] (1)*

Pyridine (1.36 mL, 17 mmol) was added to a Schlenk flask containing hexane (5 mL). *t*BuLi (10 mL, 1.7 M in hexane, 17 mmol) was added via syringe, giving a yellow solution. A pale yellow precipitate formed after standing overnight at -30°C that was filtered and collected (yield 2.02 g, 14.11 mmol, 83%).

¹H NMR (400.1 MHz, C₆D₁₂, 300 K): δ 6.85 (1H, d, ³J_{H-H} = 4.39 Hz, H5), 6.12 (1H, dd, ³J_{H-H} = 5.82, 8.39 Hz, H3), 4.92 (1H, br s, H4), 4.37 (1H, br s, H2), 3.12 (1H, br s, H1), 0.83 ppm (9H, s, CH₃).

¹³C NMR (100.6 MHz, C₆D₁₂, 300 K): δ 150.0 (C5), 127.9 (C3), 95.1 (C2 + C4, confirmed by HSQC), 66.1 (C1), 39.3 (*t*Bu quaternary), 25.6 ppm (CH₃ *t*Bu).

⁷Li NMR (155.5 MHz, C₆D₁₂, 300 K): δ -1.79 ppm.

Elemental analysis (%) for C₉H₁₄NLi: calcd: C 75.51, H 9.86, N 9.78; found: C 75.39, H 9.94, N 9.80.

*Synthesis of in-situ [1-Na-2-*t*-Bu(NC₅H₅)] and [1-Na-4-*t*Bu(NC₅H₅)] (2a and b)*

Pyridine (1.36 mL, 17 mmol) was added to a Schlenk flask containing hexane (20 mL). *t*BuLi (10 mL, 1.7 M in hexane, 17 mmol) was added via syringe, giving a yellow solution. NaOtBu (1.632 g, 17 mmol) was added via solid addition tube giving an instant beige suspension; this was allowed to stir overnight. The precipitate was

then filtered and washed (3 x 10 mL hexane). The solid was dried under vacuum and collected (yield 2.460 g, 15.57 mmol, 92%).

^1H NMR (400.1 MHz, d_8 -THF, 300 K): **1,2-isomer**: δ 6.78 (1H, d, $^3J_{\text{H-H}} = 5.07$ Hz, H5), 5.91 (1H, dd, $^3J_{\text{H-H}} = 5.65, 8.63$ Hz, H3), 4.18 (1H, t, $^3J_{\text{H-H}} = 5.36$ Hz, H4), 3.84 (1H, dd, $^3J_{\text{H-H}} = 4.08, 8.67$ Hz, H2), 3.19 (1H, d, $^3J_{\text{H-H}} = 4.11$ Hz, H1), 0.84 ppm (9H, s, CH_3). **1,4-isomer**: δ 6.20 (2H, d, $^3J_{\text{H-H}} = 7.53$ Hz, H1), 3.81 (2H, m, H2) overlapping with H2 of 1,2 isomer, 2.91 (1H, t, 3.63 Hz, H3), 0.70 ppm (9H, s, CH_3).

^{13}C NMR (100.6 MHz, d_8 -THF, 300 K): **1,2-isomer**: δ 152.3 (C5), 128.6 (C3), 91.1 (C2), 87.8 (C4), 68.9 (C2), 39.3 (tBu quaternary), 26.1 ppm (CH_3 tBu). **1,4-isomer**: resonances were too weak to assign.

Elemental analysis (%) for $\text{C}_9\text{H}_{14}\text{NNa}$: calcd: C 67.90, H 8.86, N 8.80; found: C 67.81, H 8.99, N 8.73.

Synthesis of [1-Na-2-tBu(NC_5H_5)] (2a)

Isolated **1** (0.143g, 1 mmol) was added to a Schlenk flask in a glovebox prior to adding hexane (10 mL). NaOtBu (0.096 g, 1 mmol) was added via solid addition tube, the resulting yellow suspension was left to stir for 4 hours, during which the colour changed from yellow to beige. The suspension was filtered and washed with hexane (5 mL). The isolated solid was collected (0.108 g, 0.68 mmol, 68%).

^1H NMR (400.1 MHz, d_8 -THF, 300 K): δ 6.78 (1H, d, $^3J_{\text{H-H}} = 5.08$ Hz, H5), 5.89 (1H, dd, $^3J_{\text{H-H}} = 5.80, 8.56$ Hz, H3), 4.16 (1H, t, $^3J_{\text{H-H}} = 5.30$ Hz, H4), 3.82 (1H, dd, $^3J_{\text{H-H}} = 4.42, 8.65$ Hz, H2), 3.20 (1H, d, $^3J_{\text{H-H}} = 4.06$ Hz, H1), 0.85 ppm (9H, s, CH_3).

^{13}C NMR (100.6 MHz, d_8 -THF, 300 K): δ 152.5 (C5), 128.7 (C3), 90.9 (C2), 87.5 (C4), 69.1 (C1), 39.4 (tBu quaternary), 26.1 ppm (CH_3 tBu).

Synthesis of in-situ [1-K-2-t-Bu($\text{C}_5\text{H}_5\text{N}$)] and [1-K-4-t-Bu($\text{C}_5\text{H}_5\text{N}$)] (3a and b)

Pyridine (1.36 mL, 17 mmol) was added to a Schlenk flask containing hexane (20 mL). tBuLi (10 mL, 1.7 M in hexane, 17 mmol) was added via syringe, giving a yellow solution. KOtBu (1.904 g, 17 mmol) was added via solid addition tube giving a yellow suspension; this was allowed to stir overnight. The precipitate was then filtered

and washed (3 x 10 mL hexane). The solid was dried under vacuum and collected (yield 2.743 g, 15.76 mmol, 93%).

^1H NMR (400.1 MHz, d_8 -THF, 300 K): **1,2-isomer**: δ 6.76 (1H, d, $^3J_{\text{H-H}} = 4.61$ Hz, H5), 5.87 (1H, dd, $^3J_{\text{H-H}} = 5.65, 8.43$ Hz, H3), 4.20 (1H, t, $^3J_{\text{H-H}} = 5.21$ Hz, H4), 3.73 (1H, dd, $^3J_{\text{H-H}} = 3.45, 8.24$ Hz, H2), 3.21 (1H, d, $^3J_{\text{H-H}} = 3.52$ Hz, H1), 0.86 ppm (9H, s, CH₃). **1,4-isomer**: δ 6.26 (2H, d, $^3J_{\text{H-H}} = 7.41$ Hz, H1), 3.87 (2H, m, $^3J_{\text{H-H}} = 5.65, 8.43$ Hz, H2), 2.85 (1H, t, $^3J_{\text{H-H}} = 3.72$ Hz, H3), 0.70 ppm (9H, s, CH₃).

^{13}C NMR (100.6 MHz, d_8 -THF, 300 K): **1,2-isomer**: δ 152.2 (C5), 129.0 (C3), 89.6 (C2), 87.3 (C4), 69.0 (C1), 38.8 (tBu quaternary), 26.2 ppm (CH₃ tBu). **1,4-isomer**: resonances too weak to assign.

Elemental analysis (%) for C₉H₁₄NK: calcd: C 61.66, H 8.05, N 7.99; found: C 61.93, H 8.38, N 8.08.

Synthesis of [1-K-2-t-Bu(NC₅H₅)] (3b)

Isolated **1** (0.143 g, 1 mmol) was added to a Schlenk flask in a glovebox prior to adding hexane (10 mL). KOtBu (0.112 g, 1 mmol) was added via solid addition tube, the resulting yellow suspension was left to stir for 4 hours. The suspension was filtered and washed with hexane (5 mL). The isolated solid was collected (0.127 g, 0.73 mmol, 73%).

^1H NMR (400.1 MHz, d_8 -THF, 300 K): δ 6.77 (1H, d, $^3J_{\text{H-H}} = 4.49$ Hz, H5), 5.86 (1H, dd, $^3J_{\text{H-H}} = 5.65, 8.39$ Hz, H3), 4.22 (1H, t, $^3J_{\text{H-H}} = 5.21$ Hz, H4), 3.69 (1H, dd, $^3J_{\text{H-H}} = 4.30, 8.59$ Hz, H2), 3.16 (1H, d, $^3J_{\text{H-H}} = 4.06$ Hz, H1), 0.86 ppm (9H, s, CH₃).

^{13}C NMR (100.6 MHz, d_8 -THF, 300 K): δ 152.1 (C5), 129.0 (C3), 88.9 (C2), 87.2 (C4), 69.3 (C1), 38.4 (tBu quaternary), 26.4 ppm (CH₃ tBu).

Synthesis of [K(1,2-t-Bu-DHP)(TMEDA)]₂ (4)

3 (0.174 g, 1 mmol) was added to a Schlenk flask in a glovebox. Hexane (5 mL) was added giving a yellow suspension. Excess TMEDA (2.55 mL, 17 mmol) was added to give a yellow solution. The Schlenk flask was then stored at -30°C and after 3 days the resulting crystals were filtered and collected (yield 0.134 g, 46%).

^1H NMR (400.1 MHz, d_8 -THF, 300 K): δ 6.76 (2H, d, $^3J_{\text{H-H}} = 4.65$ Hz, H5), 5.86 (2H, dd, $^3J_{\text{H-H}} = 5.65, 8.42$ Hz, H3), 4.21 (2H, d, $^3J_{\text{H-H}} = 5.12$ Hz, H4), 3.68 (2H, dd, $^3J_{\text{H-H}} = 3.69, 8.60$ Hz, H2), 3.16 (2H, d, $^3J_{\text{H-H}} = 3.37$ Hz, H1), 2.30 (8H, s, CH_2 TMEDA), 2.15 (24H, s, CH_3 TMEDA), 0.86 ppm (36H, s, CH_3 tBu).

^{13}C NMR (100.6 MHz, d_8 -THF, 300 K): δ 152.2 (C5), 129.0 (C3), 88.8 (C2), 87.2 (C4), 69.3 (C1), 58.8 (CH_2 TMEDA), 46.0 (CH_3 TMEDA), 38.4 (tBu quaternary), 26.4 ppm (CH_3 tBu).

Elemental analysis (%) for $\text{C}_{30}\text{H}_{60}\text{N}_6\text{K}_2$: calcd: C 61.80, H 10.37, N 14.41; found: C 61.49, H 10.50, N 13.97.

Synthesis of [$\{\text{K}(1,2\text{-}t\text{-Bu-DHP})(\text{PMDETA})\}_2$] (5)

3 (0.174 g, 1 mmol) was added to a Schlenk flask in a glovebox. Hexane (5 mL) was added giving a yellow suspension. PMDETA (0.45 mL, 3 mmol) was added to give a yellow solution. The Schlenk flask was then stored at 3°C and after 3 days the resulting crystals were filtered and collected (yield 0.284 g, 82%).

^1H NMR (400.1 MHz, d_8 -THF, 300 K): δ 6.76 (2H, d, $^3J_{\text{H-H}} = 4.72$ Hz, H5), 5.86 (2H, dd, $^3J_{\text{H-H}} = 5.61, 8.56$ Hz, H3), 4.21 (2H, t, $^3J_{\text{H-H}} = 5.05$ Hz, H4), 3.70 (2H, dd, $^3J_{\text{H-H}} = 3.31, 8.28$ Hz, H2), 3.17 (2H, d, $^3J_{\text{H-H}} = 3.54$ Hz, H1), 2.42 (8H, t, $^3J_{\text{H-H}} = 6.21$ Hz, CH_2 PMDETA), 2.30 (8H, t, $^3J_{\text{H-H}} = 6.14$ Hz, CH_2 PMDETA), 2.19 (6H, s, CH_3 PMDETA), 2.15 (24H, s, 4 x CH_3 PMDETA), 0.86 ppm (18H, s, CH_3 tBu).

^{13}C NMR (100.6 MHz, d_8 -THF, 300 K): δ 152.2 (C5), 129.0 (C3), 89.0 (C2), 87.2 (C4), 69.3 (C1), 58.7 (CH_3 PMDETA), 57.3 (CH_2 PMDETA), 46.0 (4 x CH_3 PMDETA), 43.1 (CH_2 PMDETA), 38.5 (tBu quaternary), 26.3 ppm (CH_3 tBu).

Elemental analysis (%) for $\text{C}_{36}\text{H}_{74}\text{N}_8\text{K}_2$: calcd: C 62.02, H 10.70, N 16.07; found: C 62.21, H 10.71, N 16.54.

Synthesis of [$\{\text{Na}(1,4\text{-}t\text{-Bu-DHP})(\text{PMDETA})\}_2$] (6)

2 (0.158 g, 1 mmol) was added to a Schlenk flask in a glovebox. Hexane (5 mL) was added giving a peach coloured suspension. PMDETA (0.42 mL, 2 mmol) was added to give an orange solution. The Schlenk flask was then stored at -30°C and after 3 days the resulting crystals were filtered and collected (yield 0.114 g, 34%).

^1H NMR (400.1 MHz, C_6D_{12} , 300 K): δ 6.91 (2H, d, $^3J_{\text{H-H}} = 4.81$ Hz, H5), 6.03 (2H, dd, $^3J_{\text{H-H}} = 5.61$, 8.64 Hz, H3), 4.35 (2H, t, $^3J_{\text{H-H}} = 5.12$, H4), 4.00 (2H, dd, $^3J_{\text{H-H}} = 3.32$, 8.22 Hz, H2), 3.10 (2H, d, $^3J_{\text{H-H}} = 3.59$, H1), 2.40 (8H, t, $^3J_{\text{H-H}} = 5.98$ Hz, CH_2 PMDETA), 2.31 (8H, t, $^3J_{\text{H-H}} = 5.98$ Hz, CH_2 PMDETA), 2.23 (6H, s, CH_3 PMDETA), 2.19 (24H, s, 4 x CH_3 PMDETA), 0.89 ppm (18H, s, CH_3 tBu).

^{13}C NMR (100.6 MHz, C_6D_{12} , 300 K): δ 153.6 (C5), 129.3 (C3), 92.6 (C2), 87.8 (C4), 68.6 (C1), 58.5 (CH_3 PMDETA), 56.8 (CH_2 PMDETA), 46.3 (4 x CH_3 PMDETA), 43.5 (CH_2 PMDETA), 38.8 (tBu quaternary), 27.0 ppm (CH_3 tBu).

Elemental analysis (%) for $\text{C}_{36}\text{H}_{74}\text{N}_8\text{Na}_2$: calcd: C 65.02, H 11.22, N 16.85; found: C 64.78, H 11.36, N 17.53.

Synthesis of [$\{\text{Na}(1,2\text{-}t\text{-Bu-DHP)}\}_2(\text{TMEDA})\}_2$] (7)

2 (0.158 g, 1 mmol) was added to a Schlenk flask in a glovebox. Hexane (5 mL) was added giving a peach suspension. TMEDA (0.15 mL, 1 mmol) was added to give an orange solution. The Schlenk flask was then placed in a Dewar flask containing hot water and after 24 h the resulting crystals were filtered and collected (yield 0.068 g, 31%).

^1H NMR (400.1 MHz, d_8 -THF, 300 K): δ 6.80 (4H, d, $^3J_{\text{H-H}} = 5.10$ Hz, H5), 5.91 (4H, dd, $^3J_{\text{H-H}} = 5.55$, 8.63 Hz, H3), 4.17 (4H, d, $^3J_{\text{H-H}} = 5.44$ Hz, H4), 3.84 (4H, dd, $^3J_{\text{H-H}} = 4.12$, 8.46 Hz, H2), 3.21 (4H, d, $^3J_{\text{H-H}} = 4.11$ Hz, H1), 2.30 (8H, s, CH_2 TMEDA), 2.15 (24H, s, CH_3 TMEDA), 0.84 ppm (36H, s, CH_3 tBu).

^{13}C NMR (100.6 MHz, d_8 -THF, 300 K): δ 152.4 (C5), 128.7 (C3), 91.1 (C2), 87.7 (C4), 69.0 (C1), 58.8 (CH_2 TMEDA), 46.0 (CH_3 TMEDA), 39.4 (tBu quaternary), 26.0 ppm (CH_3 tBu).

Elemental analysis (%) for $\text{C}_{48}\text{H}_{88}\text{N}_8\text{Na}_4$: calcd: C 66.48, H 10.00, N 12.92; found: C 65.72, H 10.24, N 13.28.

Synthesis of [$\{\text{K}(1,2\text{-}t\text{-Bu-DHP})(\text{THF})\}_\infty$] (8)

3 (0.174 g, 1 mmol) was added to a Schlenk flask in a glovebox. Hexane (5 mL) was added giving a yellow suspension. THF (0.08 mL, 50 mmol) was added to give a

yellow solution. The Schlenk flask was then stored at -30°C and after 24 hours the resulting crystals were filtered and collected (yield 0.118 g, 48%).

^1H NMR (400.1 MHz, d_8 -THF, 300 K): δ 6.77 (1H, d, $^3J_{\text{H-H}} = 4.81$ Hz, H5), 5.86 (1H, dd, $^3J_{\text{H-H}} = 5.71, 8.72$ Hz, H3), 4.22 (1H, t, $^3J_{\text{H-H}} = 5.41$ Hz, H4), 3.69 (1H, dd, $^3J_{\text{H-H}} = 3.38, 8.33$ Hz, H2), 3.62 (2.5H, t, $^3J_{\text{H-H}} = 6.53$ Hz, α -CH₂ THF), 3.16 (1H, d, $^3J_{\text{H-H}} = 3.47$ Hz, H1), 1.77 (2.5H, t, $^3J_{\text{H-H}} = 6.45$ Hz, β -CH₂ THF), 0.86 ppm (9H, s, CH₃).

^{13}C NMR (100.6 MHz, d_8 -THF, 300 K): δ 152.2 (C5), 129.0 (C3), 88.9 (C2), 87.2 (C4), 69.3 (C1), 68.0 (α -CH₂ THF), 38.4 (tBu quaternary), 26.4 (CH₃ tBu), 26.2 ppm (β -CH₂ THF).

Elemental analysis (%) for C₂₆H₄₄N₂O₂K₂: calcd: C 63.11, H 8.96, N 5.66; found: C 62.80, H 9.03, N 6.00.

2.6.2 TVA collection

2-*t*-butylpyridine

^1H NMR (400.1 MHz, CDCl₃, 300 K): δ 8.57 (1H, d, $^3J_{\text{H-H}} = 5.01$ Hz, H4), 7.60 (1H, t, $^3J_{\text{H-H}} = 7.70$ Hz, H2), 7.34 (1H, d, $^3J_{\text{H-H}} = 8.09$ Hz, H1), 7.10 (1H, dd, $^3J_{\text{H-H}} = 7.47, 4.83$ Hz, H3), 1.38 ppm (9H, s, CH₃).

2.6.3 Reduction of benzophenone

2 (0.158 g, 1mmol) was suspended in 10 ml of hexane. Benzophenone (0.182 g, 1 mmol) was added from a solid addition tube and dissolved after approximately 1 minute. An instant green suspension was obtained, which after approx. 1 minute turned to a pale green/blue solution. After 1 hour the solution started to turn yellow. Since no precipitate formed an internal standard, hexamethylbenzene (0.162 g, 1 mmol), was added to determine the yield (48%) by using the corresponding signal C-*H* signal at 5.91 ppm.

3 (0.174g, 1mmol) was suspended in 10 ml of hexane. Benzophenone (0.182 g, 1 mmol) was added from a solid addition tube and dissolved after approx. 1 minute. The yellow solution turned pale green/blue then, after approx. 1 hour, a white precipitate formed alongside a colourless solution. The precipitate was filtered, washed with hexane, dried *in vacuo* and collected (0.169 g, 76%).

^1H NMR (400.1 MHz, d_8 -THF, 300 K): δ ^1H NMR (400.1 MHz, d_8 -THF, 300 K): δ 5.85 (1H, s, C-H), 6.99 (2H, m, para-H), 7.10 (4H, m, meta-H), 7.26 (4H, m, ortho-H).

2.6.4 Crystallographic data and refinement details for compounds 4-8

	4	5	6	7	8
Empirical formula	$\text{C}_{30}\text{H}_{60}\text{N}_6\text{K}_2$	$\text{C}_{36}\text{H}_{74}\text{N}_8\text{K}_2$	$\text{C}_{36}\text{H}_{74}\text{N}_8\text{Na}_2$	$\text{C}_{48}\text{H}_{88}\text{N}_8\text{Na}_4$	$\text{C}_{26}\text{H}_{44}\text{N}_2\text{O}_2\text{K}_2$
Mol. Mass	583.04	697.23	665.02	869.25	494.85
Crystal system	monoclinic	monoclinic	monoclinic	monoclinic	triclinic
Space group	C 2/c	P 2/n	P 2 ₁ /n	P 2 ₁ /C	P -1
Temperature (K)	123	123	123	123	123
a/ Å	22.6958(10)	14.0503(6)	9.9788(9)	15.1838(8)	6.1733(4)
b/ Å	8.9464(5)	10.0747(4)	13.1357(10)	10.7957(5)	10.6514(7)
c/ Å	18.0264(9)	15.3534(5)	16.5894(15)	17.0882(9)	10.9928(7)
α /o	90	90	90	90	81.269(5)
β /o	94.489(4)	94.143(3)	104.163	106.129(5)	88.887(5)
γ /o	90	90	90	90	76.025(5)
V/Å ³	3649.0(3)	2167.63(15)	2108.4(3)	2690.8(3)	693.19(8)
Z	4	2	2	2	1
λ /Å	0.71073	0.71073	0.71073	0.71073	0.71073
Measured reflections	18020	9964	15209	26142	14420
Unique reflections	4611	4906	4446	6829	3183
R _{int}	0.0402	0.0333	0.0356	0.0390	0.0217
Observed rflns [I > 2 σ (I)]	3325	3593	3204	4827	2839
GooF	1.037	1.046	1.047	1.046	1.049
R [on F, obs rflns only]	0.0520	0.0475	0.0576	0.0562	0.0387
ωR [on F ² , all data]	0.1134	0.1015	0.1428	0.1533	0.1032
Largest diff. peak/hole e/Å ⁻³	0.28/-0.23	0.29/-0.18	0.75/-0.30	0.86/-0.52	0.84/-0.46

2.7 References

- [1] T. Anderson, *T. Roy. Soc. Edin.* **1849**, *16*, 123-136.
- [2] T. Anderson, *Liebigs Ann. Chem.* **1849**, *70*, 32-38.
- [3] T. Anderson, *Liebigs Ann. Chem.* **1851**, *80*, 44-55.
- [4] U. Eisner and J. Kuthan, *Chem. Rev.* **1972**, *72*, 1-42.
- [5] F. H. Allen, *Acta Crystallogr. Sect. B Struct. Sci.* **2002**, *58*, 380-388.
- [6] Y. He, D. Hu, M. Lv, L. Jin, J. Wu, S. Zeng, S. Yang and B. Song, *Chem. Cent. J.* **2013**, *7*, 76-81.
- [7] W. Zhang, X. Yang, W. Chen, X. Xu, L. Li, H. Zhai and Z. Li, *J. Agric. Food Chem.* **2010**, *58*, 2741-2745.
- [8] N. Pollak, C. Dölle and M. Ziegler, *Biochem. J.* **2007**, *402*, 205-218.
- [9] N. Edraki, A. R. Mehdipour and M. Khoshneviszadeh and R. Miri, *Drug Discov. Today*, **2009**, *14*, 1058-1066.
- [10] G. Swarnalatha, G. Prasanthi, N. Sirisha and C. Madhusudhana Chetty, *Int. J. Chem. Tech Res.* **2011**, *3*, 75-89.
- [11] Y. Kohari, Y. Okuyama, E. Kwon, T. Furuyama, N. Kobayashi, T. Otuki, J. Kumagai, C. Seki, K. Uwai, G. Dai, T. Iwasa and H. Nakano, *J. Org. Chem.* **2014**, *79*, 9500-9511.
- [12] R. M. Martin, R. G. Bergman and J. A. Ellman, *Org. Lett.* **2013**, *15*, 444-447.
- [13] N. Pedemonte, T. Diena, E. Caci, E. Nieddu, M. Mazzei, R. Ravazzolo, O. Zegarra-Moran and L. J. V. Galiotta, *Mol. Pharmacol.* **2005**, *68*, 1736-1746.
- [14] F. Becq, M. A. Mall, D. N. Sheppard, M. Conese and O. Zegarra-Moran, *J. Cyst. Fibros.* **2011**, *10*, S129-S145.
- [15] R. Budriesi, P. Ioan, A. Leoni, N. Pedemonte, A. Locatelli, M. Micucci, A. Chiarini and L. J. V Galiotta, *J. Med. Chem.* **2011**, *54*, 3885-3894.
- [16] E. M. P. Silva, P. A. M. M. Varandas and A. M. S. Silva, *Synthesis.* **2013**, *45*, 3053-3089.
- [17] P. T. Lansbury and J. O. Peterson, *J. Am. Chem. Soc.* **1963**, *85*, 2236-2242.
- [18] P. T. Lansbury and J. O. Peterson, *J. Am. Chem. Soc.* **1961**, *83*, 3537-3538.
- [19] P. T. Lansbury and J. O. Peterson, *J. Am. Chem. Soc.* **1962**, *84*, 1756-1757.
- [20] D. D. Tanner and C-M. Yang, *J. Org. Chem.* **1993**, *58*, 1840-1846.
- [21] K. Hensen, A. Lenke, T. Stumpf, M. Bolte, H. Fleischer, C. R. Pulham, R. O. Gould and S. Harris, *Inorg. Chem.* **1999**, *38*, 4700-4704.

- [22] K. Okada, M. Oda and R. Suzuki, *J. Chem. Soc., Chem. Commun.* **1995**, 2069-2070.
- [23] K. L. Miller, B. N. Williams, D. Beneitez, C. T. Carver, K. R. Ogilby, E. Tkatchouk, W. A. Goddard and P. L. Diaconescu, *J. Am. Chem. Soc.* **2010**, *132*, 342-355.
- [24] J. J. Sandoval, P. Palma, E. Álvarez, A. Rodríguez-Delgado and J. Cámpora, *Chem. Commun.* **2013**, *49*, 6791-6793.
- [25] Z. Jian, N. K. Hangaly, W. Rong, Z. Mou, D. Liu, S. Li, A. A. Trifonov, J. Sundermeyer and D. Cui, *Organometallics*, **2012**, *31*, 4579-4587.
- [26] T. I. Gountchev and T. D. Tilley, *Organometallics*, **1999**, *18*, 2896-2905.
- [27] D. Robert, P. Voth, T. P. Spaniol and J. Okuda, *Eur. J. Inorg. Chem.* **2008**, 2810-2819.
- [28] E. Kirillov, C. W. Lehmann, A. Razavi and J-F. Carpentier, *Eur. J. Inorg. Chem.* **2004**, 943-945.
- [29] Y. Zhang, J. Zhang, J. Hong, F. Zhang, L. Weng and X. Zhou, *Organometallics*, **2014**, *33*, 7052-7058.
- [30] C. M. Perez, A. Rodríguez-Delgado, P. Palma, E. Álvarez, E. Gutiérrez-Puebla and J. Cámpora, *Chem. Eur. J.* **2010**, *16*, 13834-13842.
- [31] T. R. Dugan, E. Bill, K. C. MacLeod, G. J. Christian, R. E. Cowley, W. W. Brennessel, S. Ye, F. Neese and P. L. Holland, *J. Am. Chem. Soc.* **2012**, *134*, 20352-20364.
- [32] R. A. Lewis, K. C. MacLeod, B. Q. Mercado and P. L. Holland, *Chem. Commun.* **2014**, *50*, 11114-11117.
- [33] F. Jaroschik, F. Nief, X-F. Le Goff and L. Ricard, *Organometallics*, **2007**, *26*, 3552-3558.
- [34] S. Labouille, F. Nief, X-F. Le Goff, L. Maron, D. R. Kindra, H. L. Houghton, J. W. Ziller and W. J. Evans, *Organometallics*, **2012**, *31*, 5196-5203.
- [35] M. S. Hill, D. J. MacDougall and M. F. Mahon, *Dalton Trans.* **2010**, *39*, 11129-11131.
- [36] E. C. Ashby and A. B. Goel, *J. Organomet. Chem.* **1981**, *204*, 139-145.
- [37] M. S. Hill, G. Kociok-Kohn, D. J. MacDougall, M. F. Mahon and C. Weetman, *Dalton Trans.* **2011**, *40*, 12500-12509.
- [38] J. Intemann, M. Lutz and S. Harder, *Organometallics*, **2014**, *33*, 5722-5729.

- [39] H. Xie, X. Hua, B. Liu, C. Wu and D. Cui, *J. Organomet. Chem.* **2015**, 798, 335-340.
- [40] P. Jochmann, T. S. Dols, T. P. Spaniol, L. Perrin, L. Maron and J. Okuda, *Angew. Chem. Int. Ed.* **2010**, 49, 7795–7798.
- [41] M. S. Hill, D. J. MacDougall, G. Kociok-Köhn, M. F. Mahon, and C. Weetman, *Organometallics*, **2015**, 34, 2590-2599.
- [42] M. Arrowsmith, M. S. Hill, T. Hadlington, G. Kociok-Köhn, and C. Weetman, *Organometallics*, **2011**, 30, 5556-5559.
- [43] C. Weetman, M. S. Hill, and M. F. Mahon, *Polyhedron*, **2016**, 103, 115-120.
- [44] J. Intemann, H. Bauer, J. Pahl, L. Maron and S. Harder, *Chem. Eur. J.* **2015**, 21, 11452-11461.
- [45] K. Ziegler and H. Zeiser, *Chem. Ber.* **1930**, 63, 1847-1851.
- [46] R. A. Abramovitch and B. Vig, *Can. J. Chem.* **1963**, 41, 1961-1965.
- [47] R. A. Abramovitch and G. A. Poulton, *Chem. Commun.* **1967**, 274-275.
- [48] C. S. Giam and J. L. Stout, *J. Chem. Soc. D., Chem. Commun.* **1969**, 142-142.
- [49] D. Barr, R. Snaith, R. E. Mulvey and D. Reed, *Polyhedron*, **1988**, 7, 665-668.
- [50] D. R. Armstrong, R. E. Mulvey, D. Barr, R. Snaith and D. Reed, *J. Organomet. Chem.* **1988**, 350, 191-205.
- [51] R. Levine and W. M. Kadunce, *Chem. Commun.* **1970**, 921-922.
- [52] W. Clegg, L. Dunbar, L. Horsburgh and R. E. Mulvey, *Angew. Chem. Int. Ed.* **1996**, 37, 753-755.
- [53] T. Wiklund, S. Olsson and A. Lennartson, *Monatsch. Chem.* **2011**, 142, 813-819.
- [54] C. Lichtenberg, T. P. Spaniol, L. Perrin, L. Maron and J. Okuda, *Chem. Eur. J.* **2012**, 18, 6448-6452.
- [55] S. D. Robertson, A. R. Kennedy, J. J. Liggat and R. E. Mulvey, *Chem. Commun.* **2015**, 51, 5452-5455.
- [56] A. Stasch, *Angew. Chem. Int. Ed.* **2012**, 51, 1930-1933.
- [57] D. R. Armstrong, C. M. M. Harris, A. R. Kennedy, J. J. Liggat, R. McLellan, R. E. Mulvey, M. D. T. Urquhart and S. D. Robertson, *Chem. Eur. J.* **2015**, 21, 14410-14420.
- [58] M. Lappert, P. Power, A. Protchenko, and A. Seeber, *Alkali Metal Amide*, in *Metal Amide Chemistry*, John Wiley & Sons, Ltd, Chichester, UK, **2008**.
Doi:10.1002/9780470740385.ch2

- [59] P. C. Andrews, D. R. Baker, R. E. Mulvey, W. Clegg and P. A. O'neil, *Polyhedron*, **1991**, 10, 1839-1841.
- [60] C. Glock, F. M. Younis, S. Ziemann, H. Görls, W. Imhof, S. Krieck and M. Westerhausen, *Organometallics*, **2013**, 32, 2649-2660.
- [61] P. C. Andrews, D. R. Armstrong, C. L. Raston, B. A. Roberts, B. W. Skelton and A. H. White, *J. Chem. Soc., Dalton Trans.* **2001**, 996-1006.
- [62] A. R. Kennedy, R. E. Mulvey, R. I. Urquhart and S. D. Robertson, *Dalton Trans.* **2014**, 43, 14265-14274.
- [63] W. Clegg, S. Kleditzsch, R. E. Mulvey and P. O'Shaughnessy, *J. Organomet. Chem.* **1998**, 558, 193-196.
- [64] A. R. Kennedy, J. Klett, C. T. O'Hara, R. E. Mulvey, and G. M. Robertson, *Eur. J. Inorg. Chem.* **2009**, 5029-5035.
- [65] C. Glock, H. Görls, and M. Westerhausen, *Eur. J. Inorg. Chem.* **2011**, 5288-5298.
- [66] D. R. Armstrong, D. V. Graham, A. R. Kennedy, R. E. Mulvey, and C. T. O'Hara, *Chem. Eur. J.* **2008**, 14, 8025-8034.
- [67] P. C. Andrews, D. R. Armstrong, W. Clegg, M. MacGregor and R. E. Mulvey, *J. Chem. Soc., Chem. Commun.* **1991**, 497-498.
- [68] K. Gregory, M. Bremer, W. Bauer and P. von Ragué Schleyer, *Organometallics*, **1990**, 9, 1485-1492.
- [69] J. A. Garden, A. R. Kennedy, R. E. Mulvey and S. D. Robertson, *Dalton Trans.* **2011**, 40, 11945-11954.
- [70] R. E. Mulvey and S. D. Robertson, *Angew. Chem. Int. Ed.* **2013**, 52, 11470-11487.
- [71] H.-W. Lerner, A. Scholz and M. Bolte, *Z. Anorg. Allg. Chem.* **2001**, 627, 1638-1642.
- [72] H. Bock, J-M, Lehn, J. Pauls, S. Holl and V. Krenzel, *Angew. Chem. Int. Ed.* **1999**, 38, 952-955
- [73] S. Krieck, H. Görls and M. Westerhausen, *Organometallics*, **2010**, 29, 6790-6800.
- [74] A. Torvisco, K. Decker, F. Uhlig and K. Ruhlandt-Senge, *Inorg. Chem.* **2009**, 48, 11459-11465.
- [75] P. Lorenzen, J. Kopf, F. Olbrich, U. Schumann and E. Weiss, *Angew. Chem. Int. Ed.* **1990**, 29, 1441-1444.
- [76] A. G. Avent, F. Antolini, P. B. Hitchcock, A. V. Khvostov, M. F. Lappert and A. V. Protchenko, *Dalton Trans.* **2006**, 919-927.

- [77] J. Barker, N. D. R. Barnett, D. Barr, W. Clegg, R. E. Mulvey and P. A. O'Neil, *Angew. Chem. Int. Ed.* **1993**, *32*, 1366-1368
- [78] W. Clegg, M. MacGregor, R. E. Mulvey and P. A. O'Neil, *Angew. Chem. Int. Ed.* **1992**, *31*, 93-95.
- [79] N. Kuhn, G. Henkel and J. Kreutzberg, *Angew. Chem. Int. Ed.* **1990**, *29*, 1143-1144.
- [80] J. Yu, X-J. Yang, Y. Liu, Z. Pu, Q-S. Li, Y. Xie, H. F. Schaefer and B. Wu, *Organometallics*, **2008**, *27*, 5800-5805.
- [81] F. Antolini, P. B. Hitchcock, A. V. Khvostov and M. F. Lappert, *Eur. J. Inorg. Chem.* **2003**, 3391-3400.
- [82] M. L. Cole, C. Jones and P. C. Junk, *J. Chem. Soc., Dalton Trans.* **2002**, 896-905.
- [83] P. C. Andrews, D. R. Armstrong, W. Clegg, F. J. Craig, L. Dunbar and R. E. Mulvey, *Chem. Commun.* **1997**, 319-320.
- [84] Macchioni, G. Ciancaleoni, C. Zuccaccia, and D. Zuccaccia, *Chem. Soc. Rev.* **2008**, *37*, 479-489.
- [85] D. Li, I. Keresztes, R. Hopson, and P. G. Williard, *Acc. Chem. Res.* **2009**, *42*, 270-280.
- [86] M. Sebban, L. Guilhaudis and H. Oulyadi, in *Lithium Compounds in Organic Synthesis: From Fundamentals to Applications*, ed. R. Luisi and V. Capriati, Wiley, Weinheim, **2014**, pp. 85-122.
- [87] R. Neufeld and D. Stalke, *Chem. Sci.* **2015**, *6*, 3354-3364.
- [88] A-C. Poppler, M. M. Meinholz, H. Fabhuber, A. Lange, M. John and D. Stalke, *Organometallics*, **2012**, *31*, 42-45.
- [89] S. E. Baillie, W. Clegg, P. Garcia-Alvarez, E. Hevia, A. R. Kennedy, J. Klett and L. Russo, *Organometallics*, **2012**, *31*, 5131-5142.
- [90] E. Hevia, A. R. Kennedy, R. E. Mulvey, D. L. Ramsay and S. D. Robertson, *Chem. Eur. J.* **2013**, *19*, 14069-14075.
- [91] C. Su, J. Guang, W. Li, K. Wu, R. Hopson and P. G. Williard, *J. Am. Chem. Soc.* **2014**, *136*, 11735-11747.
- [92] T. Tatic, S. Hermann, M. John, A. Loquet, A. Lange and D. Stalke, *Angew. Chem. Int. Ed.* **2011**, *50*, 6666-6669.
- [93] D. R. Armstrong, A. R. Kennedy, R. E. Mulvey and S. D. Robertson, *Dalton Trans.* **2013**, *42*, 3704-3711.
- [94] J. Guang, R. Hopson, and P. G. Williard, *J. Org. Chem.* **2015**, *80*, 9102-9107.

- [95] I. C. McNeill, *J. Polym. Sci. A-1 Polym. Chem.* **1966**, *4*, 2479-2485.
- [96] I. C. McNeill, *Eur. Polym. J.* **1967**, *3*, 409-421.
- [97] I. C. McNeill, *Eur. Polym. J.* **1970**, *6*, 373–395.
- [98] I. C. McNeill, L. Ackerman, S. N. Gupta, M. Zulfiqar and S. Zulfiqar, *J. Polym. Sci. Polym. Chem. Ed.* **1977**, *15*, 2381–2392.
- [99] L. Turnbull, J. J. Liggat and W. A. MacDonald, *Polym. Degrad. Stab.* **2013**, *98*, 2244-2258.
- [100] J. Geier, H. Rügger and H. Grützmacher, *Dalton Trans.* **2006**, 129-136.

Chapter 3: Lithium dihydropyridine catalysed dehydrogenative cyclisation of diamine boranes

3.1 Summary

This chapter introduces lithium dihydropyridine **1** to the catalytic arena. Selecting a catalytic manifold that has previously been restricted to a ruthenium catalyst, dehydrogenative cyclisation of diamine boranes to 1,3,2-borolidines, a competitive lithium alternative is discussed herein.

This study establishes the optimum conditions of the catalyzed cyclic reaction to be 70°C in *d*₆-benzene. Monitoring the reaction by ¹¹B and ¹H NMR spectroscopy and X-ray crystallographic studies of potential intermediate species namely [(*t*Bu)N(BH₃)(CH₂)₂N(H)(*t*Bu)Li.THF] **18**, [(*t*Bu)N(BH₃)(CH₂)₂N(H)(*t*Bu)Li.Py] **19**, [{(Me)N(BH₃)(CH₂)₂N(Me)₂Li.THF} ₂], **21** and [{(Me)N(BH₃)-(CH₂)₂N(Me)₂Li.Pyr} ₂] **22** aided in providing mechanistic insight, allowing a mechanism to be suggested.

Advancing on the synthesis of 1,3,2-borolidines, post arylation of the newly formed B-H functionality to a B-C_{phenyl} was developed, **23-26**.

3.2 Introduction

Of late there has been an explosion of main group catalysis in the literature, primarily due to the realization that main group compounds can mimic transition metal and lanthanide catalytic regimes.^[1] Hydroamination^[2] hydroboration and hydrosilylation,^[3-7] hydrogenation^[8] and dehydrogenative element-element bond formation,^[9] are all transformations which were once restricted to d- and f-block catalysis. These have now been achieved by main group (pre)catalysts, and the rare s-block example. Discussion of all main group catalysts is extensive and out of the scope of this chapter. Hence attention must be directed to the dehydrogenative E-E bond formation.

3.2.1 Dehydrocoupling catalysis

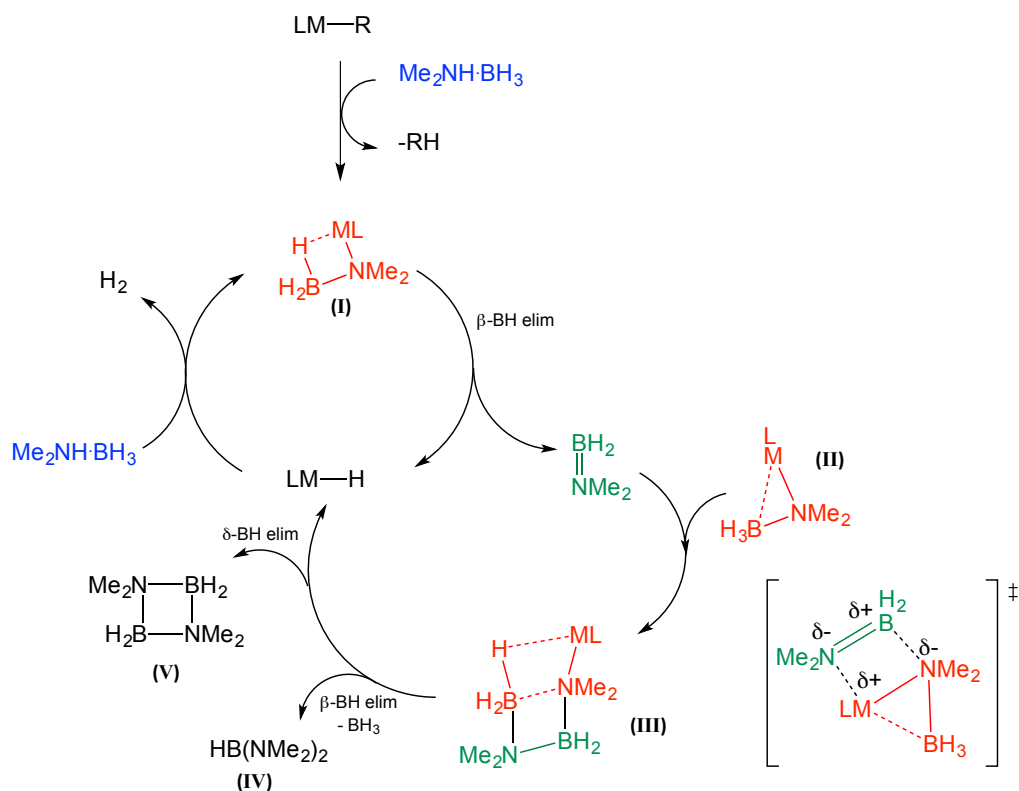
Dehydrocoupling is the formation of a new element-element bond from two E-H bonds, with concomitant loss of hydrogen. This is a valued synthetic pathway due to the clean and convenient removal of the gaseous by-product. In addition the production of hydrogen gas can be useful as an energy source for hydrogen storage applications.^[10] As a result one of the most advanced areas of catalytic heteronuclear dehydrocoupling, being driven by their potential application as a hydrogen transporter, is the dehydrogenation of amine-borane compounds.

Catalytic methods had primarily focused on transition metal-based species. However, today numerous main group d^0 complexes are successfully employed in stoichiometric and catalytic processes. Many research groups are invested in this area including those of Harder,^[11,12] Hill,^[13-16] Okuda^[17] and Wright.^[18-20] They typically exploit group 2 or group 13 metals more specifically, magnesium, calcium and aluminium. A common feature in the complexes is the presence of bulky ligands including β -diketiminato or silylamides. They have extensively studied the dehydrocoupling of the simple secondary amine borane, dimethylamine borane $\text{Me}_2\text{NH}\cdot\text{BH}_3$ (DMAB), probing its potential as a chemical storage vessel for hydrogen gas.

Hill reported a rare example of a group 1 (pre)catalyst, simply MHMDS (where M = Li, Na or K), which could effectively dehydrogenate DMAB.^[21] Subsequent reports by Panda^[22,23] employing the same alkali-metal (pre)catalyst for the catalyzed dehydrocoupling of pinacolborane and primary amines have also recently emerged.

Although s-block has the advantage of eliminating any Schlenk-type equilibria, these (pre)catalysts were let down from a practical point of view. s-Block (pre)catalysts typically suffer solubility issues, mainly due to the precipitation of group 1 metal hydride intermediates.

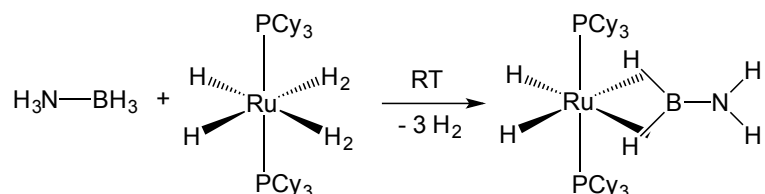
The general accepted mechanism for dehydrocoupling of DMAB is shown in [scheme 3.1](#) with an alkyl magnesium (pre)catalyst.^[13] The first step is generally accepted as a deprotonation of the dimethylamine borane by the alkylmagnesium species to obtain [LM(NMe₂)BH₃] (I) where a four membered ring is formed via Mg[⋯]H-B interactions. This undergoes elimination to produce a LM-H adduct and a BH₂=NMe₂ fragment (II). The insertion of this unsaturated species with (I) proceeds via the suggested transition state to reach the catalytic intermediate (III). This can then undergo further elimination to give either HB(NMe₂)₂ (IV) or (BH₂.NMe₂)₂ (V) regenerating the LM-H species that can react with a further equivalent of DMAB to release hydrogen and form the deprotonated DMAB (I).



Scheme 3.1: Generally accepted mechanism of group 2 promoted hydrogen release from Me₂NH.BH₃.^[13]

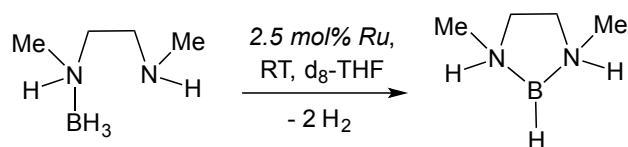
3.2.2 Dehydrogenative cyclisation

As discussed in the previous section the dehydrogenation of amine boranes has been extensively studied. However, Sabo-Etienne who previously found success in the stoichiometric dehydrogenation of ammonia borane by a bis(dihydrogen) ruthenium complex $[\text{RuH}_2(\eta^2\text{-H}_2)_2(\text{PCy}_3)_2]$ (Scheme 3.2), branched this work into a whole new field by exploring diamine-monoboranes.^[24]



Scheme 3.2: Sabo-Etienne's original stoichiometric dehydrogenation of ammonia-borane with a bis(dihydrogen) ruthenium complex.

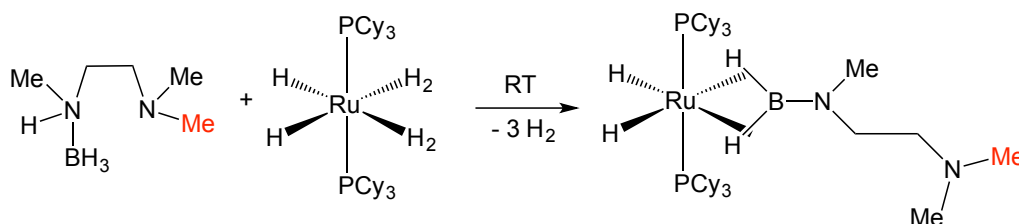
The ruthenium complex $[\text{RuH}_2(\eta^2\text{-H}_2)_2(\text{PCy}_3)_2]$, was employed in the dehydrogenative cyclisation of diamine-monoboranes, in catalytic quantities. Replacing the $\text{H}_3\text{N}\cdot\text{BH}_3$, with $\text{RR}'\text{NH}\cdot\text{BH}_3$ where $\text{R} = \text{methyl}$ and $\text{R}' = [(\text{CH}_2)_2\text{NMe}(\text{H})]$, incorporating a second NH moiety into the amine borane, interestingly resulted in the formation of a 1,3,2-diazaborolidine (Scheme 3.3). The influence of the second NH counterpart of the diamine borane was crucial in the reaction outcome, facilitating a novel cyclisation dehydrocoupling reaction. This was the first example of such a transformation.



Scheme 3.3: Sabo-Etienne's reported cyclisation of diamine monoboranes by employing a catalytic $[\text{RuH}_2(\eta^2\text{-H}_2)_2(\text{PCy}_3)_2]$.

They probed the influence of the second amino group, and found that extension of the carbon backbone did not alter the reaction outcome.^[25] However, they reported that when a tertiary amine such as $\text{R}' = (\text{CH}_2)_2\text{NMe}_2$ was present on the pendant amino

moiety, no dehydrogenated cyclisation occurred. Instead typical dehydrogenation of the BH₃ took place resulting in the loss of hydrogen and the formation of a complex where the nitrogen atom has no connectivity to the boron atom (Scheme 3.4).



Scheme 3.4: The influence of a tertiary amino moiety on the pendant group.

3.3 Aims of this chapter

From the literature, the pitfalls of group 1 (pre)catalysts for dehydrocoupling reactions tend to be the poor solubility of the metal hydride intermediates inhibiting the reaction. Overcoming this issue could result in an increase in reactivity and conversion. Since our development of a hexane soluble lithium dihydropyridine **1**, that is capable of acting as a metal hydride surrogate we wanted to introduce this to the group 1 (pre)catalyst family. This chapter aims at developing group 1 catalysed transformation of diamine-monoboranes to 1,3,2-diazaborolidines by:

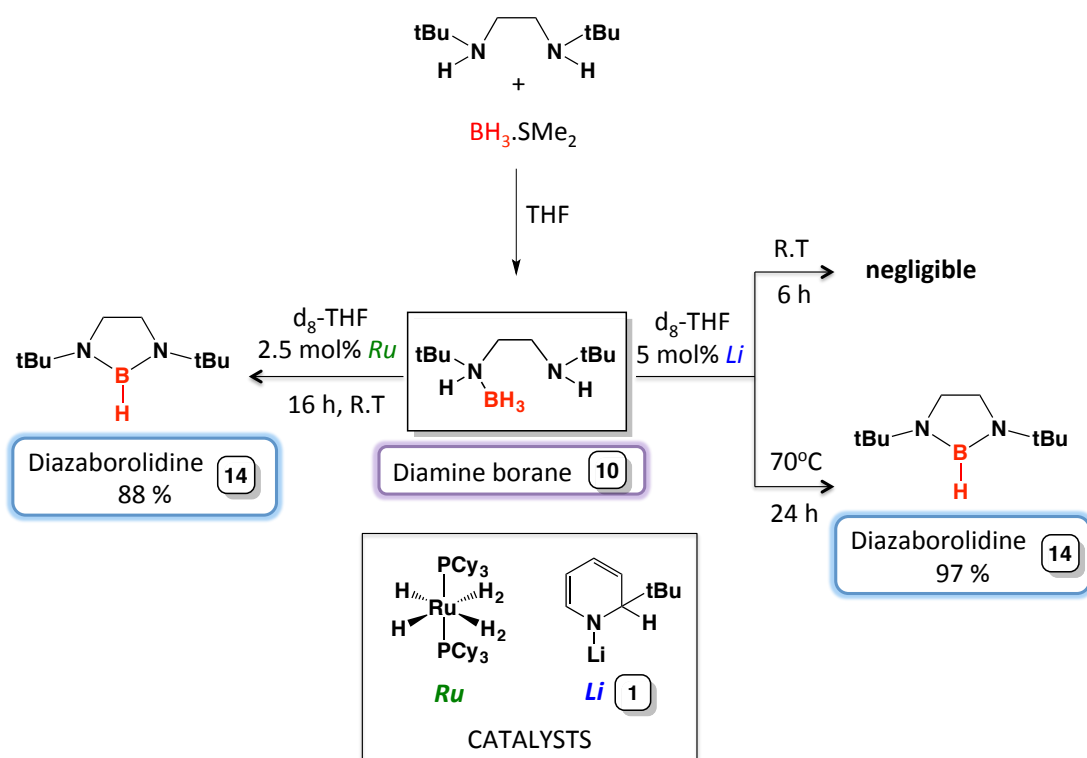
- Employing the LiDHP **1** as a catalyst to overcome solubility issues in the catalytic manifold.
- Probe the mechanism by NMR spectroscopy studies.
- Characterise isolated intermediates by X-ray crystallography.
- Post-functionalise the 1,3,2-diazaborolidine (B-H) products to synthetically more useful B-C products.

3.4 Results and discussion

3.4.1 Preliminary optimization studies

Given the precedence in the literature of *N*-(*tert*-butyl)(BH₃)-*N'*-*tert*-butylethylenediamine **10** to undergo dehydrogenative cyclisation and the simplicity of its

preparation, this was the starting point in this work. Sabo-Etienne previously reported the optimum conditions to catalyse the dehydrogenative cyclisation of **10**, to be 2.5 mol% of the ruthenium hydride precatalyst $[\text{RuH}_2(\eta^2\text{-H}_2)_2(\text{PCy}_3)_2]$ in $\text{d}_8\text{-THF}$ solution at room temperature.^[24] This yielded 88% of the *N,N'*-di-tert-butyl-1,3,2-diazaborolidine **14** in 16 hours. For comparison we started with **10** which could be isolated as a white solid in an almost quantitative yield from reaction of the parent diamine and $\text{BH}_3\cdot\text{SMe}_2$ in THF. Using isolated **10**, in a J. Youngs tube, an initial reaction was carried out in $\text{d}_8\text{-THF}$ solution along with 5mol% of LiDHP (pre)catalyst **1** (Scheme 3.5). The reaction was monitored by ^1H and ^{11}B NMR spectroscopy. Albeit hydrogen evolution was visible instantly upon addition of the catalyst, the reactivity at room temperature was very slow with barely any conversion after several hours.



Scheme 3.5: Comparison of dehydrogenative cyclisation reaction of **10** in $\text{d}_8\text{-THF}$ with Sabo-Etienne's ruthenium catalyst and our LiDHP catalyst (**1**).

Subsequently the reaction was repeated, heating the sample to 70°C and again monitoring over time. This was much more successful resulting in a 97% conversion in 24 hours, though granted this was still longer than the time required by the previously reported ruthenium catalyst.

Typically metal hydride catalysis is performed in d_8 -THF due to solubility problems in other solvents. However, considering the importance of Lewis base donors in alkali metal chemistry, specifically their influence on structure and reactivity, the solvent choice was re-evaluated. It was thought that d_8 -THF could be behaving as a donor towards catalyst **1** and deactivating it, having a negative effect on the reaction. Fortunately the lithium dihydropyridine catalyst, a metal hydride surrogate, overcomes common solubility issues being hydrocarbon soluble. This allowed us to move away from polar donating solvents. The reaction was replicated in d_6 -benzene and studied by NMR spectroscopy. Surprisingly this reduced the reaction time by 75% only requiring six hours at 70°C to reach a comparable conversion of 94% (Figure 3.1).

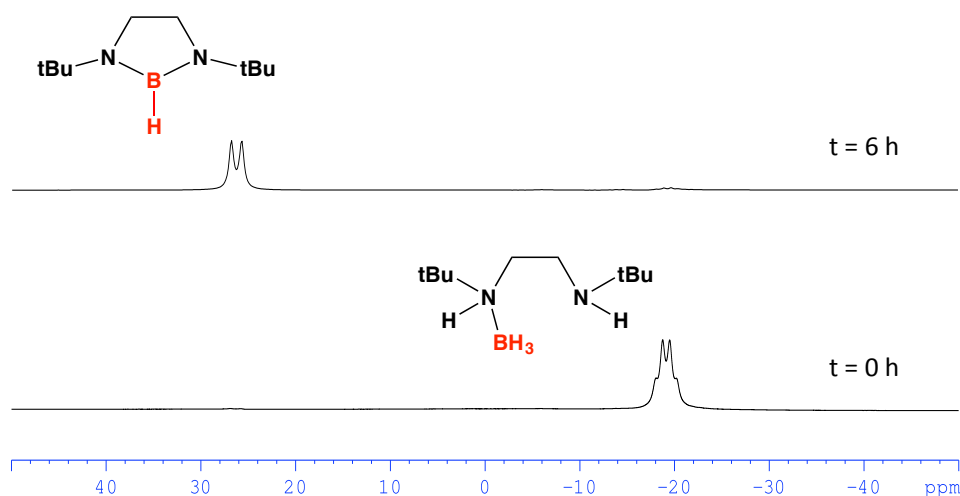
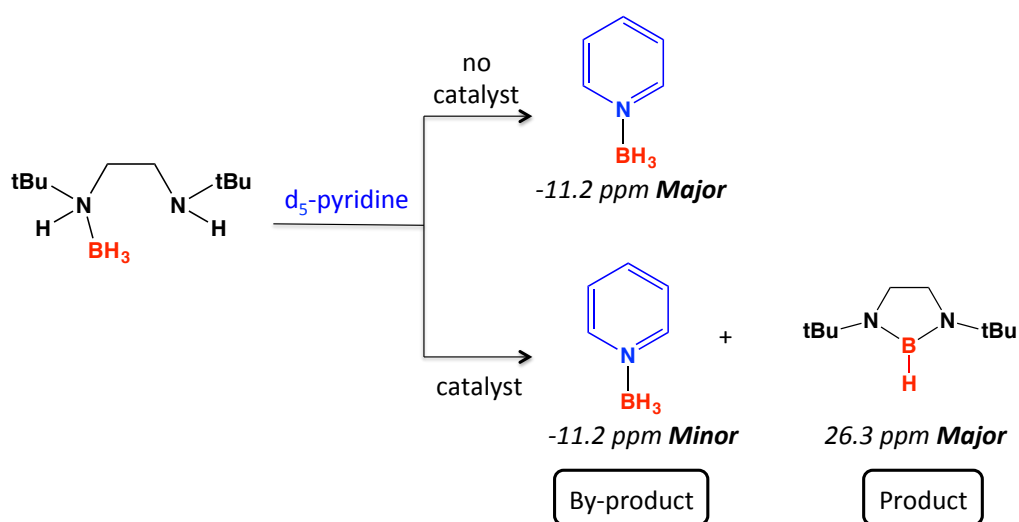


Figure 3.1: ^{11}B NMR spectra overlay of LiDHP (pre)catalysed dehydrogenative cyclisation of N-(*tert*-butyl)(BH_3)-N'-*tert*-butyl-ethylenediamine (**10**) in d_6 -benzene at 0 h with no conversion and at 6 h showing almost full conversion to cyclized product (**14**).

For completeness, to probe further the effect of bulk reaction solvents, d_5 -pyridine was also investigated. The outcome of this was unexpected with major influences to both the reaction time and product. Thus, it was found that in just 45 minutes full conversion of **10** was achieved. However, this was not yielding one product, as in the ^{11}B NMR spectrum two signals could be seen at 26.3 and -11.2 ppm in an approximate respective 3:2 ratio. The major signal represented by a broad doublet at 26.3 ppm was

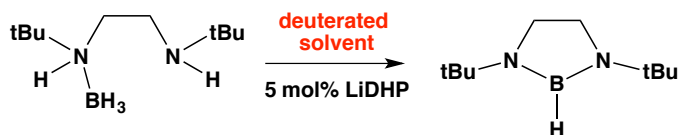
consistent with the cyclized product **14**, although the broad shoulder on the signal indicates the possibility of another product. The minor signal at -11.2 ppm was thought to be a pyridine·BH₃ adduct arising from a side reaction of the tert-butyl-diamineborane **10** with pyridine. To confirm this a control reaction with **10** in d₅-pyridine in the absence of catalyst was studied (Scheme 3.6). After a short time at room temperature, formation of pyridine·BH₃ was observed which reached full conversion after two hours at 70°C.



Scheme 3.6: Control reaction of d₅-pyridine and **10** in the presence and absence of catalyst **1**.

The abstraction of Lewis acidic BH₃ by Lewis basic pyridine was confirmed by ¹¹B NMR spectra where a quartet at -11.2 ppm was observed along with the concomitant release of the parent diamine *N,N'*-di-*tert*-butylethylenediamine present in the ¹H NMR spectrum. This highlighted that in the absence of a catalyst pyridine·BH₃ would be formed as the major product. However in the presence of catalyst, the side reaction could not be eliminated completely but only suppressed by the faster formation of product. Ultimately the formation of unwanted side products outweighed the advantage of an accelerated reaction time. The optimum reaction conditions for catalytic dehydrogenative cyclisation of **10** proved to be 70°C in C₆D₆ solution as summarized in table 3.1.

Table 3.1: Summary of solvent optimization for reaction of **10** with 5 mol% LiDHP catalyst **1**.



Catalyst	Solvent	Time (h)	Temp (°C)	Yield (%) ^a
<i>Ru</i>	d ₈ -THF	16	r.t	88
1	d ₈ -THF	24	70	97
1	d ₆ -benzene	6	70	94
1	d ₅ -pyridine	0.75	70	57 ^b

[a] = Conversion determined by ¹¹B NMR spectroscopy. [b] = major product from mixture of products obtained.

3.4.2 Extension to other diamine boranes

Following the successful cyclisation of (**10**), the scope of the catalysis was expanded to include varying R groups including isopropyl (**11**) and benzyl (**12**), and extending the carbon backbone length via the isopropyl analogue (**13**) (Figure 3.2). The isolation of these diamine boranes proved more complicated than the *tert*-butyl derivative due to their oily nature. That notwithstanding, the isolation of these was optimized to obtain a high purity starting material for the catalytic studies.

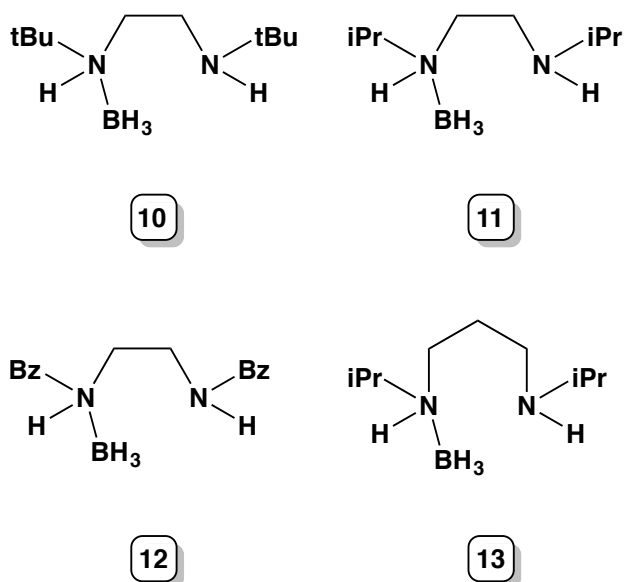


Figure 3.2: Substrate scope explored in LiDHP catalyzed dehydrogenative cyclisation.

Employing the optimised reaction conditions and monitoring by ^{11}B and ^1H NMR spectroscopy, these substrates followed the same pathway and gave the desired corresponding five or six membered cyclized products (**14-17**) (Figure 3.3). Increasing the steric bulk of the R group to benzyl slowed the reaction by four-fold (24 hours) to reach full conversion, whilst changing the R substituent to isopropyl required 48 hours to achieve a stagnant conversion of 77%. Interestingly, keeping with the isopropyl group, but increasing the backbone to a three-carbon chain, giving rise to a six-membered cyclized diazaborolidine, resulted in 97% conversion after 48 hours. These NMR yields as summarized in table 3.2 were comparable with those in the literature, with the benzyl derivative showing a considerable time improvement compared with the 72 hours required by Sabo-Etienne's ruthenium catalyst. However, the ruthenium catalyst proved more successful for the isopropyl analogue only taking eight hours to reach full conversion.

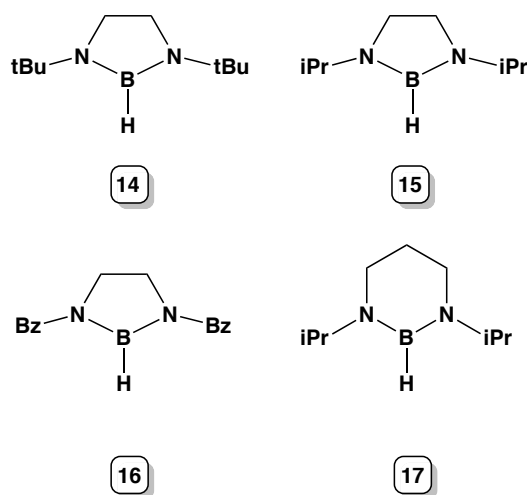
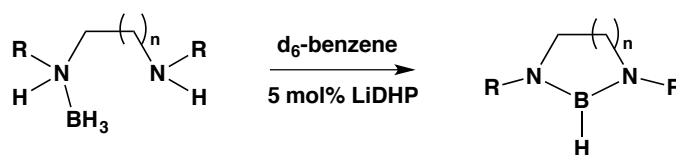


Figure 3.3: Chemdraw representation of the cyclized diazaborolidine products (**14-17**) synthesized from the corresponding diamine boranes (**10-13**).

The next step was to obtain isolated yields of these compounds. Unfortunately, this proved problematic because of the viscous waxy nature of these compounds. Extensive avenues were explored to try and isolate good yields of these materials but they proved unsuccessful due to inconsistency. The only one that was successfully collected was (**14**) *tert*-butyl diazaborolidine, which was distilled as a colourless oil from the residue of a Schlenk-scale reaction in a remarkable yield of 94%.

Table 3.2: Yields of catalysed dehydrogenative cyclisation of diamine boranes.



Compound	R	n	Time (h)	Yield (%) ^a	Isolated yield (%)
10	<i>tert</i> butyl	1	6	94	94
11	<i>isopropyl</i>	1	48	77	-
12	<i>benzyl</i>	1	24	96	-
13	<i>isopropyl</i>	2	48	97	-

[a]= Conversion determined by ¹¹B NMR spectroscopy.

3.4.3 Reaction mechanism by NMR spectroscopic studies

The mechanism was probed by NMR spectroscopic studies following the course of the reaction in the optimum solvent d₆-benzene. Looking at two intervals during the course of the reaction, namely prior to heating and after two hours heating at 70°C, gave insight to both the transformation of boron species present and the nature of the boron intermediate. Figure 3.4 shows the ¹¹B NMR spectrum recorded after ten minutes at room temperature prior to heating the sample. At this initial stage in the reaction three species can already be observed, through a quartet at -19.2 overlapping with another lower intensity quartet at -21.7 and a low intensity doublet at 26.2 ppm.

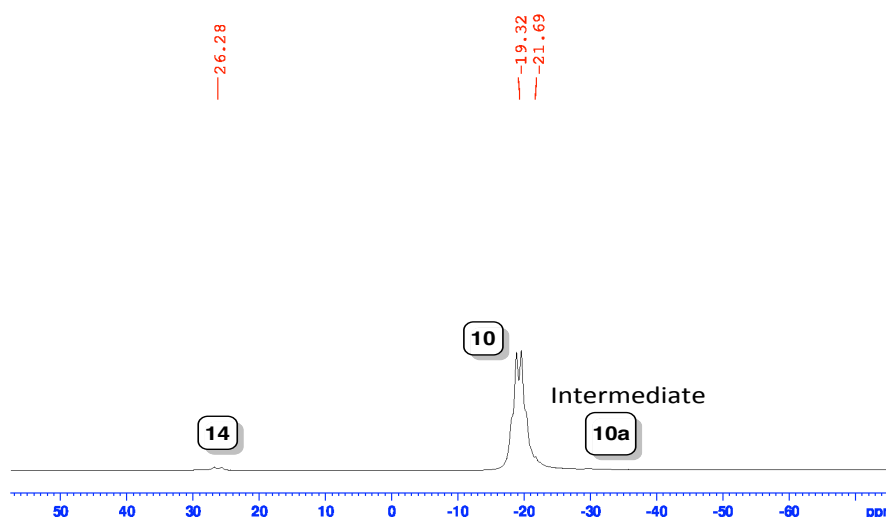
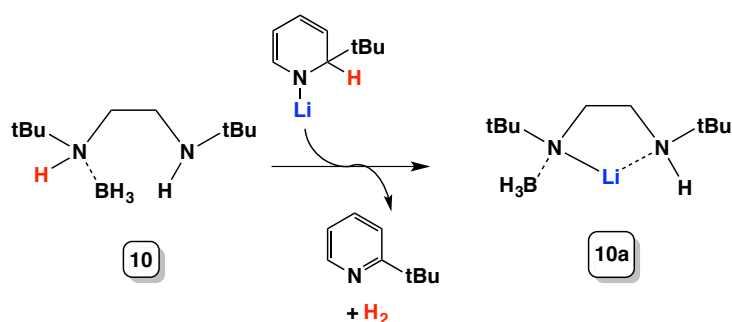


Figure 3.4: Mechanistic ¹¹B NMR study at 10 minutes at room temperature in d₆-benzene.

The signals at -19.2 and 26.2 ppm could be straightforwardly assigned, with the former being the starting material (**10**) and latter being early signs of product (**14**) formation. Enlarging this ^{11}B NMR spectrum revealed the additional presence of an overlapping quartet at -21.7 ppm, that proved insightful with regard to the first step of the catalytic pathway. It was assigned as a deprotonated form of diamine borane (**10a**), whereby the mostly acidic N-H hydrogen has been abstracted by the catalyst with the loss of 2-tert-butylpyridine and evolving hydrogen (Scheme 3.7). On searching the literature it was found there was precedence for this step as it has been previously seen in the dehydrocoupling of HNMe_2BH_3 with group 2 β -diketiminato complexes.^[12]



Scheme 3.7: Initial step in catalytic cycle: deprotonation of the diamine borane.

Investigating the ^{11}B NMR spectrum after 2 hours at 70°C displayed four new resonances in the spectrum at -38.8, -13.4, -5.8 and 38 ppm (Figure 3.5).

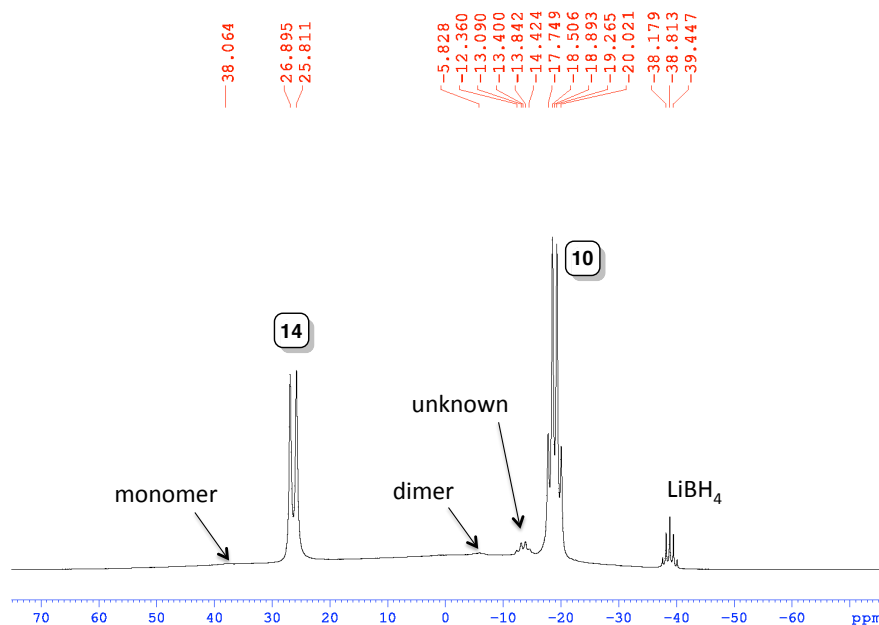
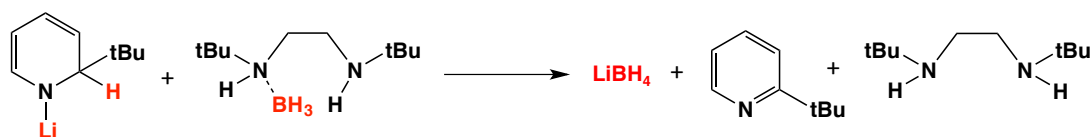


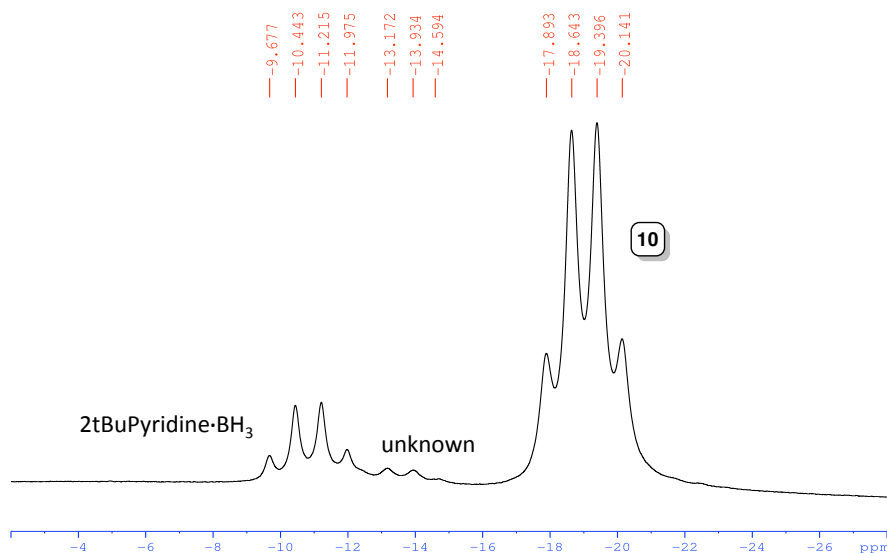
Figure 3.5: ^{11}B NMR spectrum run after 2 hours at 70°C .

The quintet at -38.8 ppm was assigned to be LiBH_4 that was thought to arise from a secondary reaction between LiDHP (**1**) and diamine borane (**10**) (Scheme 3.8). To determine if the formation of LiBH_4 via a BH_3 source and LiDHP **1** was possible a control reaction was carried out with $\text{BH}_3\cdot\text{THF}$ and LiDHP (**1**). This confirmed conversion to LiBH_4 by ^{11}B NMR spectroscopy. As this was a minor product it is presumed this pathway is slower than the competing deprotonation steps hence only minor quantities of LiBH_4 are present. For completeness, the catalytic activity of LiBH_4 was also investigated with **10** but it proved not as effective as **1**, with only 62% conversion after six hours and also gave a side product. This can be attributed to LiBH_4 being less soluble and the active hydride being less labile. Consequently it can be concluded the sole catalyst of the reaction is not LiBH_4 although the small quantity formed may aid the process.



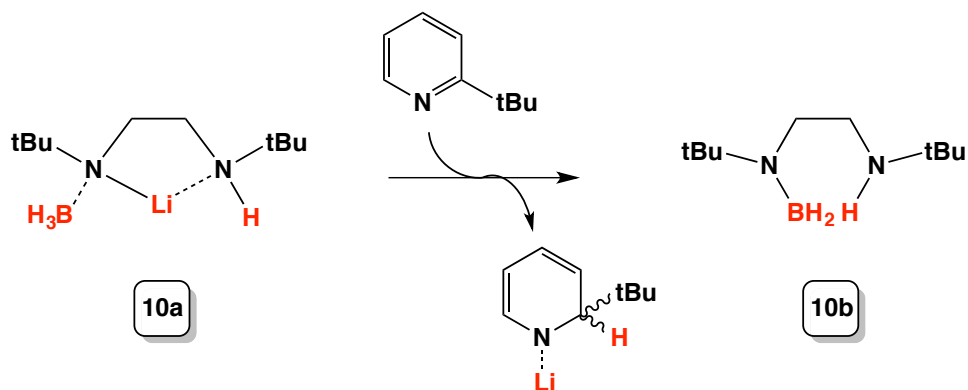
Scheme 3.8: Proposed formation of LiBH_4 from side reaction between catalyst and the diamine borane.

The quartet at -13.4 ppm remains unassigned. Initially it was thought to be the formation of 2-*tert*-butylpyridine. BH_3 as we know from the control reaction with d_5 -pyridine and **10**, pyridine can abstract BH_3 to form a pyridine BH_3 adduct (-11.2 ppm) (Scheme 3.6). The reaction of 2-*tert*-butylpyridine and $\text{BH}_3\cdot\text{SMe}_2$ showed a resonance around -9.0 ppm for 2-*tert*-butylpyridine. BH_3 . On replicating the reaction with 2-*tert*-butylpyridine and **10**, interestingly three signals appear (Scheme 3.9). One corresponds to **10**, another to 2-*tert*-butylpyridine. BH_3 and again the unknown species at -13.4 ppm. At this point the identity of the species is unknown however it can be concluded that it only forms in the presence of the diamine borane source.



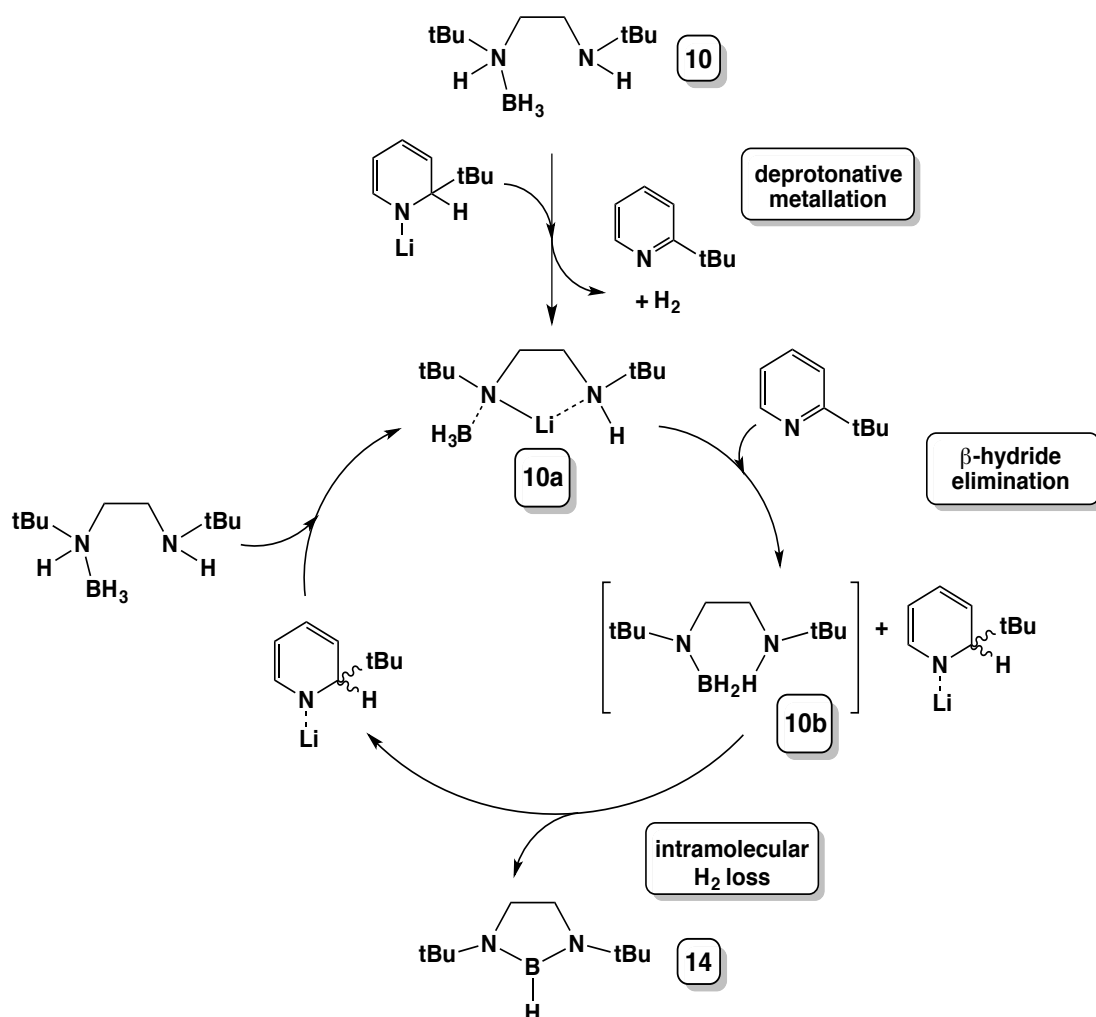
Scheme 3.9: ^{11}B NMR spectrum of **10** and 2-*t*BuPyr to shed light on unknown species at -13.4 ppm.

The pair of triplets at -5.8 and 38 ppm, which can be seen in the spectrum, aid in shedding light on the next step in the catalytic pathway. These can be attributed to a dimer/monomer equilibrium of a BH_2 species (**10b**), as previously seen by Sabo-Etienne with a similar methyl analogue. It is proposed that this step involves the addition of LiH from the deprotonated BH_3 lithium intermediate (**10a**) across 2-*tert*-butylpyridine. Although in scheme 3.10 it has been illustrated as a selective 1,2-addition, that is not necessarily always the case as will be explored later.



Scheme 3.10: Proposed second step; formation of BH_2 intermediate (**10b**) seen in monomer/dimer equilibrium from the deprotonated lithiated borane source (**10a**) and 2-*tert*-butylpyridine.

From the collective observations from these NMR studies a general catalytic mechanism can be proposed (Scheme 3.11). There are three key steps in this proposal, initially a deprotonative metallation as in scheme 3.7 to form **10a** with concomitant formation of 2-*tert*-butylpyridine and hydrogen evolution. This interestingly is in contrast to the mechanism proposed by Sabo-Etienne for their ruthenium catalysed system. From our hypothesis the second step involves a beta-hydride elimination to give the BH₂ intermediate **10b** with the addition of LiH over the *in-situ* generated 2-*tert*-butylpyridine as in scheme 3.10 to regenerate an active 1-lithiodihydropyridine species. Followed by the final step involving an intramolecular loss of hydrogen to generate the cyclized product. Due to the instability of the BH₂ intermediate **10b** it was not possible to isolate and study under the appropriate conditions to determine if this was a thermal or catalytic promoted step.



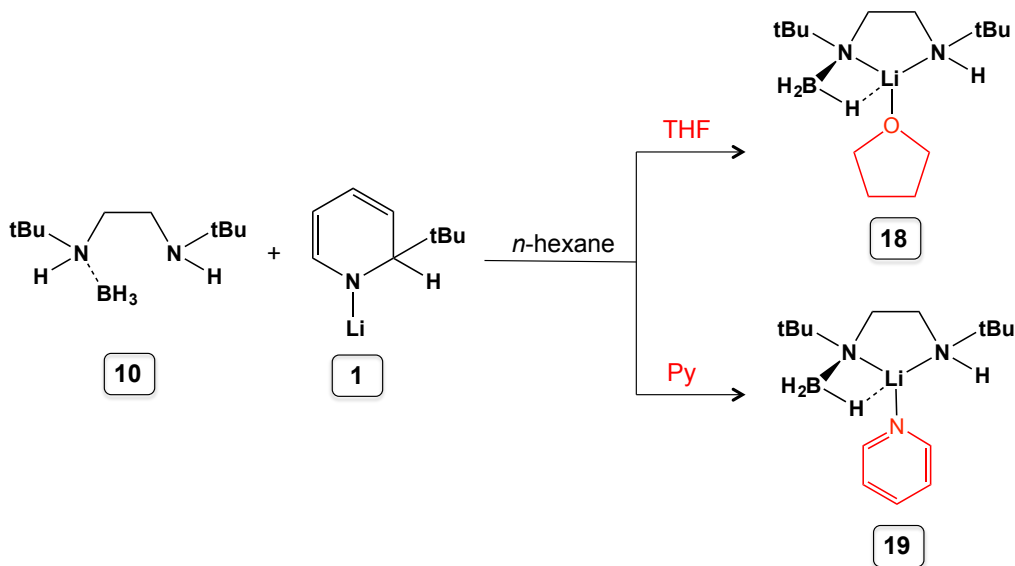
Scheme 3.11: Proposed catalytic cycle for catalytic dehydrogenative cyclisation of **10** with LiDHP **1** in C₆D₆

Table 3.3: Summary of ^{11}B species determined from ^{11}B NMR studies.

Compound	Chemdraw representation	Type of B species	^{11}B NMR signal in C_6D_6	Splitting pattern
10		BH_3	-19.2	quartet
10a		BH_3	-21.7	quartet
10b		BH_2	-5.8/38	triplet
14		BH	26.2	doublet
LiBH_4	-	BH_4	-38.8	quintet
unknown	-	BH_3	-13.4	quartet
$\text{Py} \cdot \text{BH}_3$		BH_3	-11.2	quartet
$\text{tBuPy} \cdot \text{BH}_3$		BH_3	-9.0	quartet

3.4.4 Structural evidence to support reaction mechanism

In a bid to support the suggested mechanism, the next step was an attempt at isolation of the proposed intermediates. Taking the first step of the proposed reaction, reacting **10** with the catalyst stoichiometrically (Scheme 3.12) in *n*-hexane resulted in a crop of crystals following the addition of either THF or pyridine.



Scheme 3.12: Chemdraw representation of the stoichiometric reaction of (**10**) and LiDHP (**1**) in *n*-hexane with either THF (**18**) or pyridine (**19**) added for crystallisation.

Gratifyingly, this resulted in the isolation of two essentially isostructural molecular structures, $[(t\text{Bu})\text{N}(\text{BH}_3)\text{-(CH}_2)_2\text{N}(\text{H})(t\text{Bu})\text{Li}^+\text{THF}]$ **18** and $[(t\text{Bu})\text{N}(\text{BH}_3)\text{-(CH}_2)_2\text{N}(\text{H})(t\text{Bu})\text{Li}^+\text{Py}]$ **19**, only varying by the donor ligand coordinated to the lithium atom (Figure 3.6). Both of the monomeric structures display a similar solid-state arrangement, where the lithium atom adopts a distorted trigonal pyramidal geometry. In a bidentate fashion, a deprotonated molecule of **10** is coordinated via its amino and amido nitrogen atoms to lithium along with a donor molecule (THF for **18** and pyridine for **19**) whilst the BH_3 on the amido nitrogen facilitates a hydridic $\text{B-H}\cdots\text{Li}$ interaction.

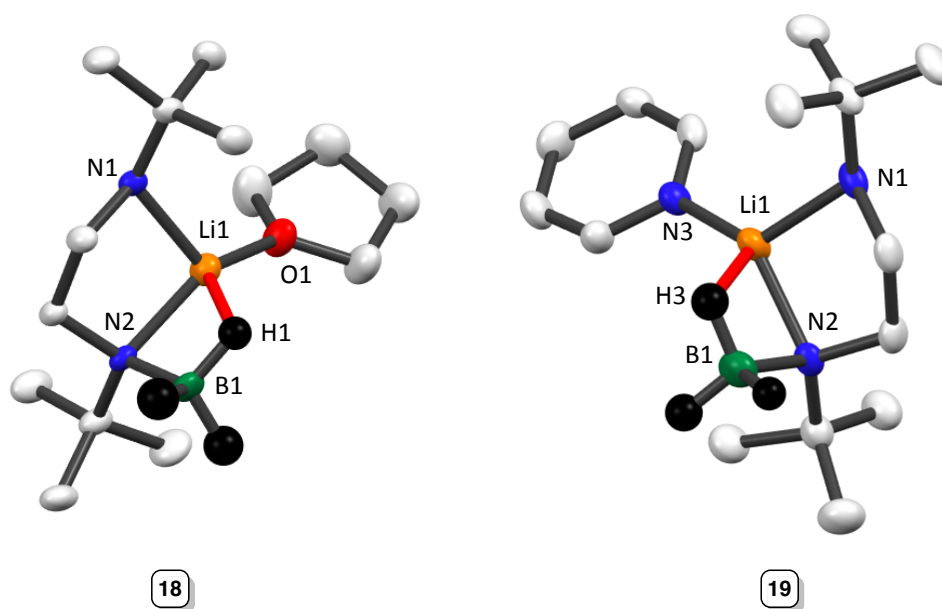


Figure 3.6: Molecular structure of $[(t\text{Bu})\text{N}(\text{BH}_3)(\text{CH}_2)_2\text{N}(\text{H})(t\text{Bu})\text{Li}\cdot\text{THF}]$ **18** and $[(t\text{Bu})\text{N}(\text{BH}_3)(\text{CH}_2)_2\text{N}(\text{H})(t\text{Bu})\text{Li}\cdot\text{Py}]$ **19**, with displacement ellipsoids at 50% probability level, hydrogen atoms omitted except those of the BH_3 moiety. Selected bond lengths and angles are summarized in table 3.4.

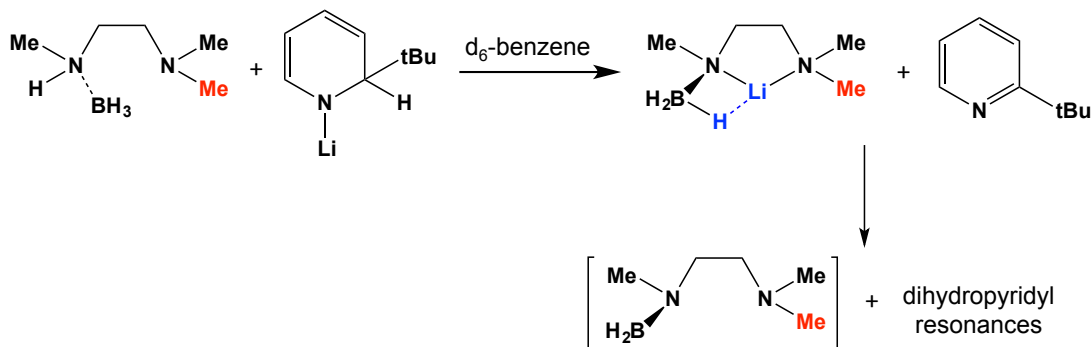
Table 3.4: Table of selected bond lengths and angles for compounds **18** and **19**.

Bond	Bond lengths (Å)		Angle	Bond angles (°)	
	18	19		18	19
Li1-N1	2.031(3)	2.025(11)	N1-Li1-N2	92.67(13)	93.4(5)
Li1-N2	1.969(3)	1.985(12)	N1-Li1-O1/N3	120.15(15)	126.4(6)
Li1-O1/N3	1.907(3)	2.040(11)	N2-Li1-O1/N3	136.30(17)	131.2(6)
Li1-H1/H3	1.894(18)	1.90(7)	N1-Li1-H1/H3	99.0(6)	99(2)
B1-N2	1.568(2)	1.581(9)	N2-Li1-H1/H3	70.0(6)	69(2)
B1-H1/H3	1.156(19)	1.14(7)	N3-Li1-H1/H3	125.1(6)	122(2)

N-(methyl)(BH_3)-*N'*-dimethylethylenediamine

In parallel an alternative diamine was selected *N*-(methyl)(BH_3)-*N'*-dimethylethylenediamine **20** as a substrate, where one of the nitrogen atoms contains two methyl groups and is thus incapable of eliminating hydrogen to allow cyclisation. It was anticipated that the dehydrogenation process would be arrested after deprotonation and elimination of LiH across 2-*tert*-butylpyridine to give rise to a new dihydropyridyl species and a BH_2 intermediate analogous to **10b**.

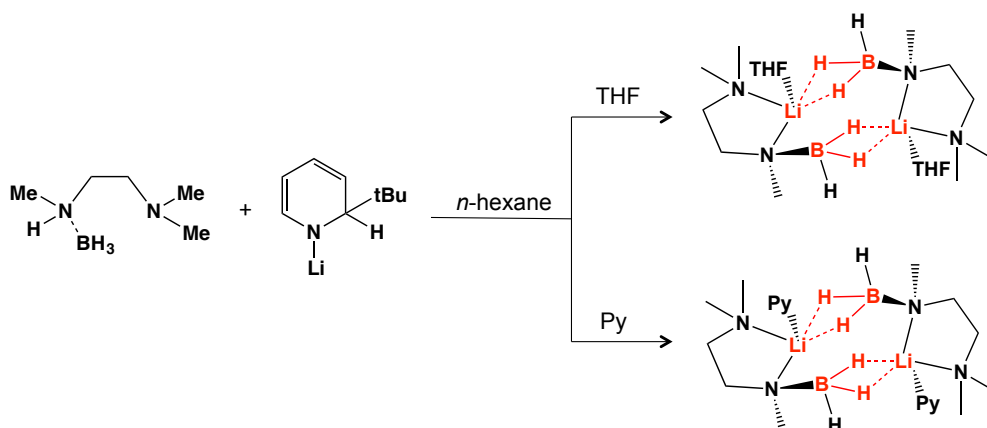
Provisional stoichiometric solution studies of *N*-(methyl)(BH₃)-*N'*-dimethylethylenediamine **20** and LiDHP **1** in d₆-benzene were carried out in a J. Youngs NMR tube and the ¹H and ¹¹B NMR spectra were recorded.



Scheme 3.13: Stoichiometric reaction between **20** and LiDHP **1**.

The ¹H NMR spectrum taken promptly after mixing displayed multiple resonances in the ¹H NMR (3-6.5 ppm) correlating to more than one dihydropyridyl species, the identity of which has not been conclusively determined, except that the original LiDHP is no longer present, indicating its role as a pre-catalyst for the initial deprotonation. This suggests that there is more than one active dihydropyridyl compound, all of which are likely to play an active role in the catalytic regime. Prolonged heating of the mixture resulted in several more dihydropyridyl resonances along with aromatic resonances corresponding to 2-*tert*-butylpyridine after 2.5 hours at 70°C. This spectroscopic data presents compelling evidence that deprotonation of N-H, followed by the addition of LiH across the *in-situ* generated 2-*tert*-butylpyridine are key reaction steps.

In a quest for structural evidence for this reaction, the stoichiometric reaction of **20** and LiDHP **1** in *n*-hexane with the required addition of THF and pyridine to aid crystallization was performed (Scheme 3.14). This resulted in the isolation and characterization of two compounds [$\{(Me)N(BH_3)(CH_2)_2N(Me)_2Li \cdot THF\}_2$] **21** and [$\{(Me)N(BH_3)(CH_2)_2N(Me)_2Li \cdot Pyr\}_2$] **22** by X-ray crystallography, only differing by the solvating Lewis donor molecule (Figure 3.7). In contrast to the previously obtained structures, a centrosymmetric dimeric motif was observed, albeit the monomeric unit is comparable to that previously discussed.



Scheme 3.14: Chemdraw representation of the stoichiometric reaction of **(20)** and LiDHP **(1)** in *n*-hexane with either THF **(21)** or pyridine **(22)** added for crystallisation.

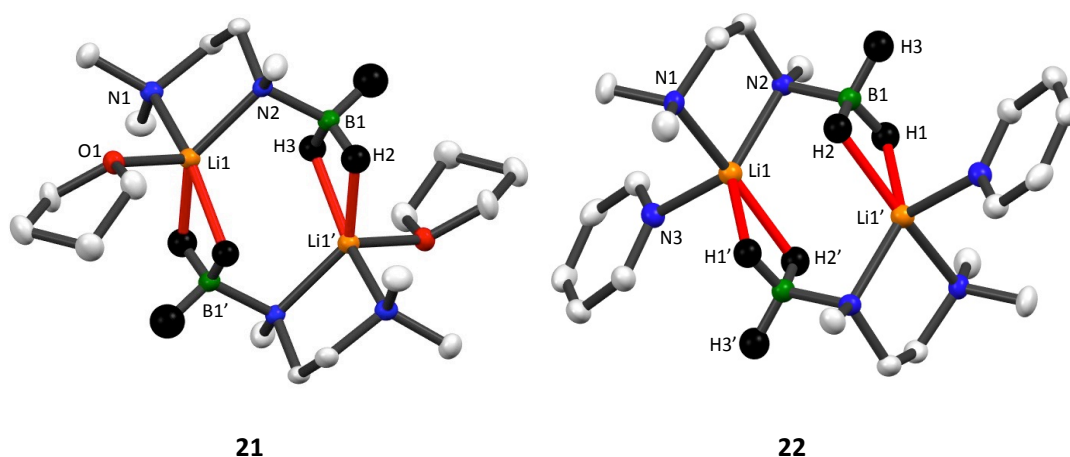


Figure 3.7: Molecular structures [$\{(\text{Me})\text{N}(\text{BH}_3)(\text{CH}_2)_2\text{N}(\text{Me})_2\text{Li}.\text{THF}\}_2$], **21** (left) and [$\{(\text{Me})\text{N}(\text{BH}_3)(\text{CH}_2)_2\text{N}(\text{Me})_2\text{Li}.\text{Pyr}\}_2$], **22** (right) with displacement ellipsoids at 50% probability level, all hydrogen atoms except those attached to boron are omitted for clarity and Li-H interactions are highlighted in red. Symmetry transformations used to generate equivalent atoms labelled ‘: -*x*, 1-*y*, -*z*. Selected bond lengths (Å) and bond angles (°) are summarized in table 3.5.

In this instance the lithium atom adopts a distorted square-pyramidal geometry with the deprotonated didentate diamine borane and monodentate donor ligand (THF or Py). Within the monomeric unit there are no internal $\text{Li}\cdots\text{H}$ interactions, instead there are two hydridic $\text{Li}\cdots\text{H}$ interactions between the lithium atom and a hydride of the symmetry equivalent BH_3 moiety sewing both monomeric counterparts together.

Notably, one is considerably shorter than the other [H2-Li1' 2.074(10) versus H3-Li1' 1.962(13) Å], giving rise to the dimeric composition.

Table 3.5: Summary of bond lengths and angles for compounds **21** and **22**.

Bond lengths (Å)			Bond angles (°)		
Bond	21	22	Angle	21	22
Li1-N1	2.156(2)	2.163(2)	N1-Li1-N2	89.24(6)	87.79(7)
Li1-N2	2.039(2)	2.055(2)	N1-Li1-O1/N3	105.92(6)	102.75(7)
Li1-O1/N3	1.984(2)	2.098(2)	N2-Li1-O1/N3	111.24(7)	117.92(8)
Li1-H2'	2.074(10)	2.107(11)	N1-Li1-H3'/H1'	96.0(4)	99.4(3)
Li1-H3'/H1'	1.962(13)	1.960(13)	N1-Li1-H2'	149.4(4)	152.9(4)
B1-N2	1.555(1)	1.558(1)	N2-Li1-H3'/H1'	139.0(3)	136.7(4)
B1-H1	1.15(1)	1.17(1)	N2-Li1-H2'	108.7(4)	105.5(4)
B1-H2	1.14(1)	1.16(1)	H2'-Li1-O1/N3	90.8(3)	102.1(4)
B1-H3	1.14(1)	1.16(1)	H3'/H1'-Li1-O1/N3	106.3(3)	91.9(4)

Interestingly the isolated crystalline yields of these compounds were low, in the region of 24-34%, most likely due to the formation of 2-*tert*-butylpyridine allowing further reactivity with a lithium hydride source to obtain dihydropyridyl species. An alternative preparation was studied replacing the LiDHP (**1**) by the common organolithium reagent *n*BuLi as the deprotonating source. This approach resulted in improved yields of **18**, **19**, **21** and **22** in the region of 48-81%.

This structural evidence supported the proposed catalytic cycle. Firstly, the complexes isolated represent valid reaction intermediates of the suggested first step of the catalytic cycle, whereby the acidic N-H functionality of the diamine borane is deprotonated. Looking at the structural parameters in particular B-H \cdots Li interactions, the proposed active Li-H distances range from [1.894(18)-1.962(13) Å] which are all shorter than the reported Li-H contact [2.043Å] in solid lithium hydride. This suggests that within these complexes the hydride is activated and inclined to add across pyridine to regenerate the active dihydropyridyl catalytic species (as in the transformation of **10a** to **10b** in scheme 3.11).

To complete the structural study and for comparison of solution state structure, the solution aggregation state of compounds **18** and **21** were explored by DOSY NMR spectroscopy studies to determine if the structural assembly was retained in solution. Employing Stalke's method in d_8 -THF, the aggregation state was assessed. In the case of **18** (Figure 3.8), the estimated molecular weight was determined to be 297 g/mol with a 9% error. When considering the expected molecular weight of 264.19 g/mol for the solid-state structure, this estimation is considerably larger than the anticipated value for a monomeric unit. When other possible species are considered (Table 3.6), it can be proposed that this value is still closer to a monomeric derivative rather than a dimeric structure. A reasonable suggestion is the possibility of solvation-desolvation with a further molecule of THF leading to a species with a higher molecular weight of 336.30 g/mol with a molecular weight in the region of entry 2 and 3 of table 3.6. For this molecule it would appear that it retains its structural integrity in solution with an equilibrium of solvation-desolvation of a further molecule of THF.

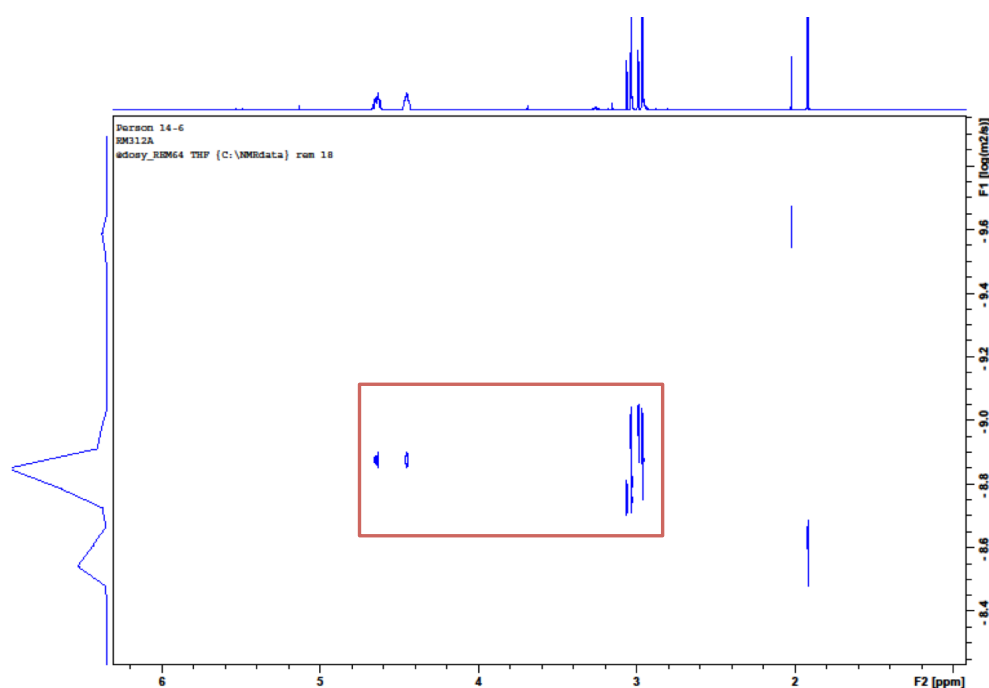
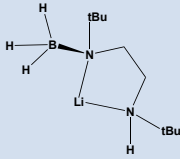
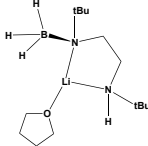
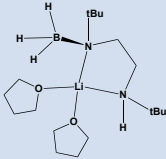
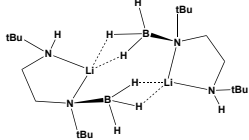


Figure 3.8: ^1H DOSY NMR spectrum of **18** in d_8 -THF.

Table 3.6: Possible aggregation species for the DOSY spectroscopy analysis of **18** in d_8 -THF.

Entry	Possible species	Molecular weight (g/mol)	Δ MW from actual MW (g/mol)
1		192.08	-104.9
2		264.19	-32.81
3		336.30	+39.3
4		384.16	+87.16

Studying complex **21**, again in d_8 -THF, the ^1H DOSY spectrum was obtained (Figure 3.9). In this case the estimated molecular weight was calculated to be 237 g/mol with a 9% error, considerably lower than the expected solid-state structure (entry 1, table 3.7). Upon analysing the data, two plausible explanations can be suggested. However, due to the deviations in DOSY it is important that we treat these values with caution. One reason could be the loss of THF molecules (entry 2 and 3, table 3.7) from the crystal structure arising from the sample being subjected to vacuum during isolation. Considering this when calculating the molecular weight, a closer value of 243.89 g/mol would be expected, opposed to the much higher value of 388.11 g/mol when both THF molecules are included. This suggests that the dimeric motif remains in solution with the absence of donor molecules. However, looking at an alternative, it is possible that the opposite occurs. Instead of desolvation of the THF molecules, there could be solvation of an extra THF molecule to a monomeric entity as in entry 4 and 5 of table 3.7. Due to the closeness of results it is not possible to confidently assign the aggregation state of compound **21** in solution by DOSY NMR spectroscopy studies.

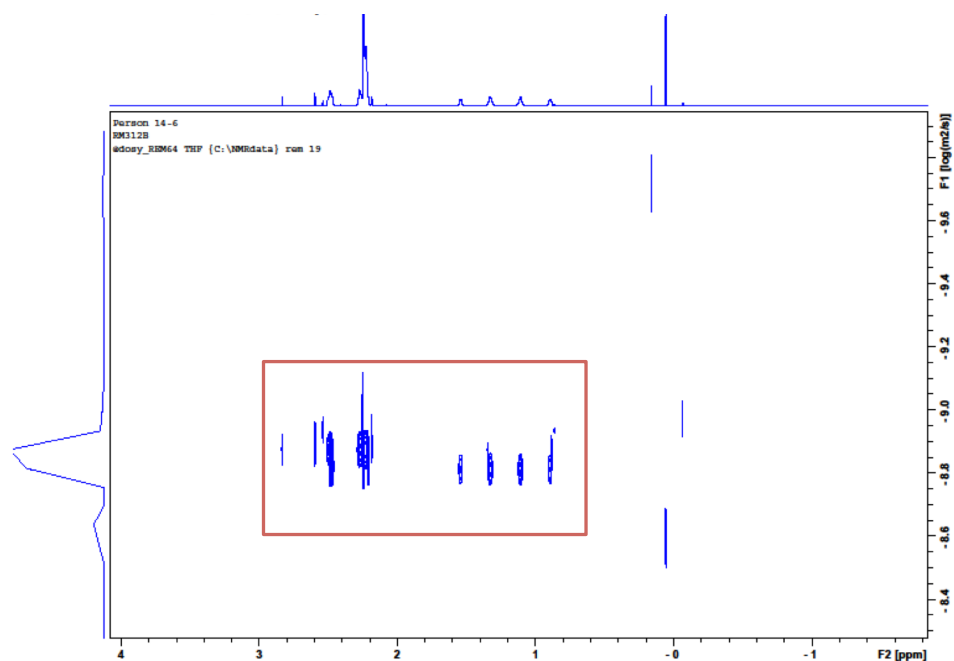
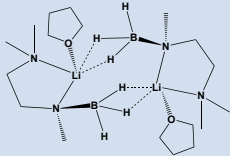
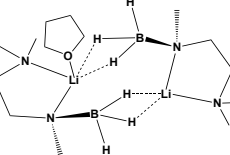
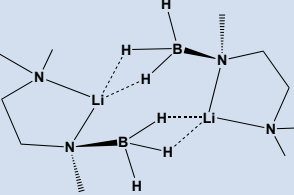
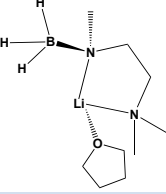
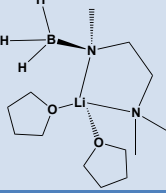


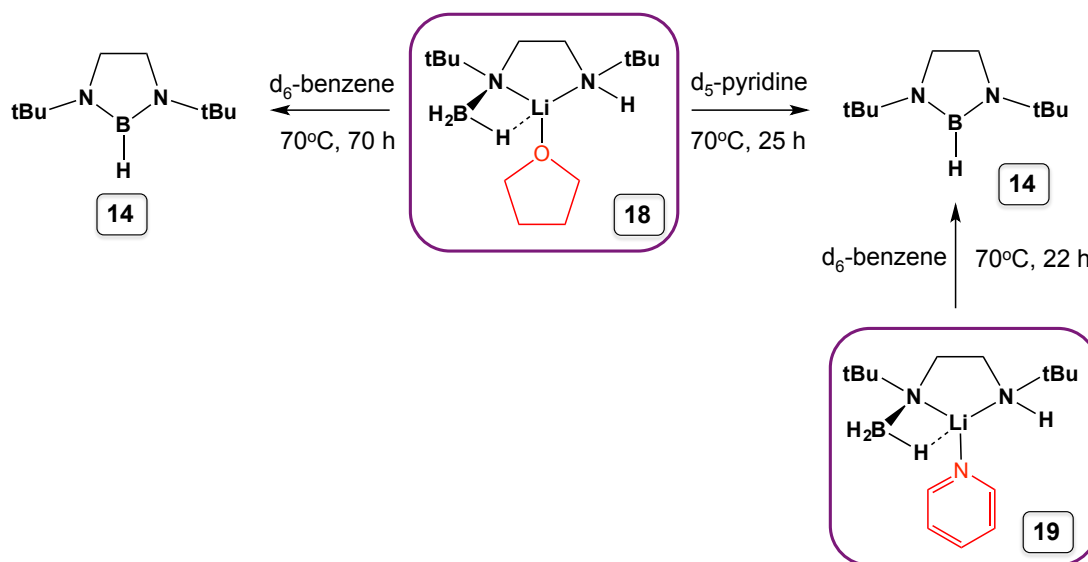
Figure 3.9: ^1H DOSY NMR spectrum of **21** in d_8 -THF.

Table 3.7: Possible DOSY species

Entry	Possible species	Molecular weight (g/mol)	Δ MW from actual MW (g/mol)
1		388.11	+151.11
2		316.37	+79.37
3		243.89	+6.89
4		194.05	-42.95
5		266.16	+29.16

3.4.5 Reactivity studies of isolated intermediates

Exploiting the ability to isolate reaction intermediates **18** and **19**, a series of experiments were conducted to further probe the mechanistic details. Since **18** contains a molecule of THF we decided to study the influential role of the solvent choice. Taking isolated **18** in d_6 -benzene or d_5 -pyridine and following the reaction by ^{11}B NMR spectroscopy the cyclized product was obtained. However, they required extended reaction times of 70 and 25 hours, respectively (Scheme 3.15).



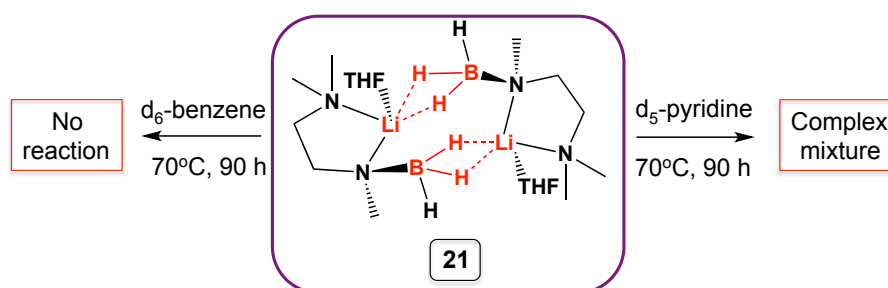
Scheme 3.15: Reaction of intermediate **18** in d_6 -benzene and d_5 -pyridine and intermediate **19** in d_6 -benzene.

From monitoring the reaction by ^{11}B NMR in d_6 -benzene the transformation of **18** to **14** was observed by the decrease in intensity of the starting material characterized by a quartet resonance at -21.7 ppm and the formation of the product represented by a doublet at 26.3 ppm. It can be presumed that the reaction proceeds as expected via a LiH elimination, as evidenced by a slight amount of precipitate observed, followed by a thermally induced dehydrogenation. The clean transformation to the product with no intermediates visible in the NMR timescale is surprising in contrast to the catalytic reaction where several intermediate species were observed, this may indicate a slow LiH release followed by a rapid cyclisation.

In d_5 -pyridine the reaction was completed in 25 hours, almost three times as fast as in d_6 -benzene. This can be attributed to the THF being displaced by the bulk solvent

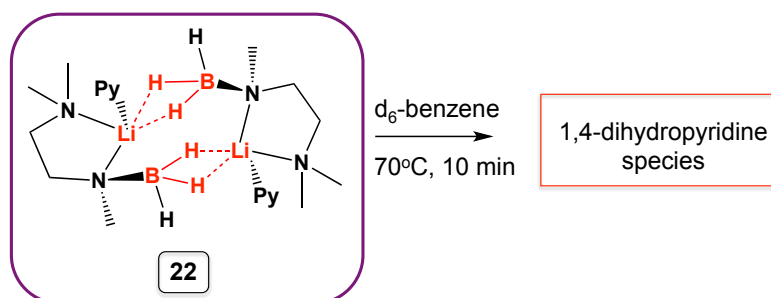
pyridine. This new arrangement is primed for the Li-H addition across pyridine to generate a dihydropyridyl species. This is confirmed when the reaction of **19**, containing a pre-organised solvated pyridine, in d_6 -benzene requires a similar but slightly shorter timescale of 22 hours. Relating the ^1H NMR data, the presence of resonances attributable to dihydropyridyl species were observed although with low integration values.

Moving to **21**, again because of its inability to cyclise it provided an opportunity to study the role of pyridine after the initial deprotonation. In d_6 -benzene, taking the THF solvate **21** and heating at 70°C , even after 90 hours no reaction was observed. However, in d_5 -pyridine after 90 hours at 70°C there was no starting material remaining, just a complex mixture of products (Scheme 3.16).



Scheme 3.16: Study of **21** in d_6 -benzene and d_5 -pyridine.

Interestingly starting with the pyridine solvate **22** in d_6 -benzene after 10 minutes, there was little change mainly the formation of a 1,4-dihydropyridine species in the ^1H NMR spectrum, to which further heating of 72 hours had no effect (Scheme 3.17).



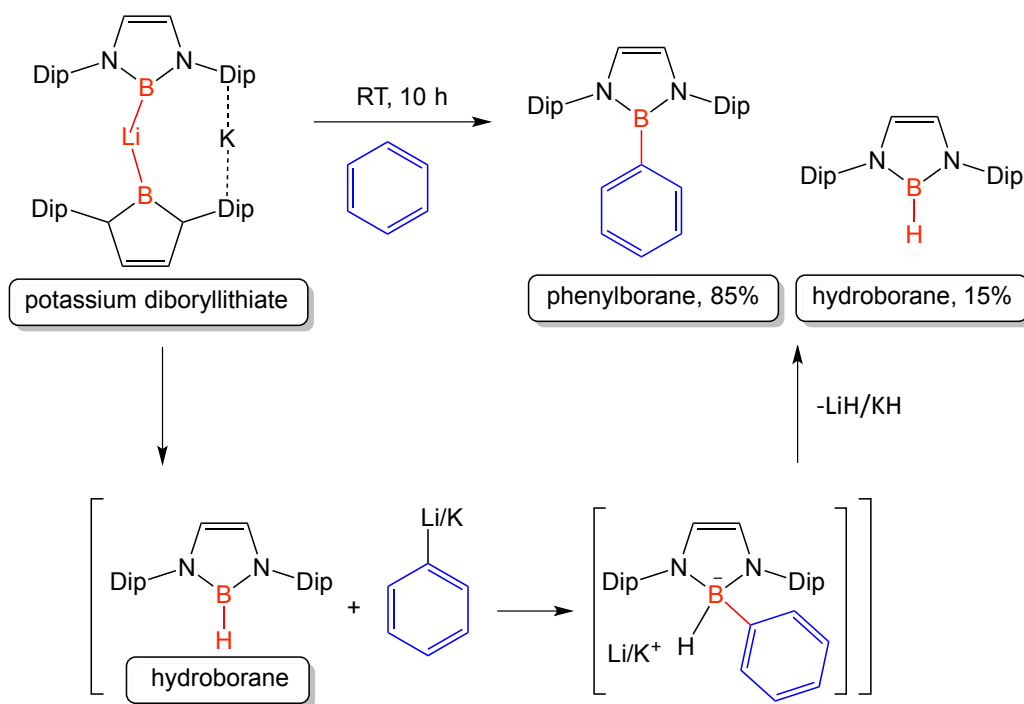
Scheme 3.17: Study of **22** in d_6 -benzene at 70°C .

The reactivity studies with the proposed reaction intermediates, compounds **18**, **19**, **21** and **22**, illustrate the negative effect of donor solvents d_8 -THF and d_5 -pyridine and help to explain the requirement for a non-coordinating solvent such as d_6 -benzene for success in these reactions.

3.3.6 Postsynthetic functionalization of 1,3,2-diazaborolidine

As most boron precursors are typically used *in-situ*, the functionalization of these 1,3,2-diazaborolidine species was explored. Due to the importance of Suzuki-Miyaura cross-coupling reactions^[26] the goal was to synthesise a nitrogen based boronate ester that could be potentially interesting in this field as an alternative to the typical oxygen congeners. Consequently, it was decided to try to transform the newly formed B-H bond for a synthetically more practical and useful B-C bond.

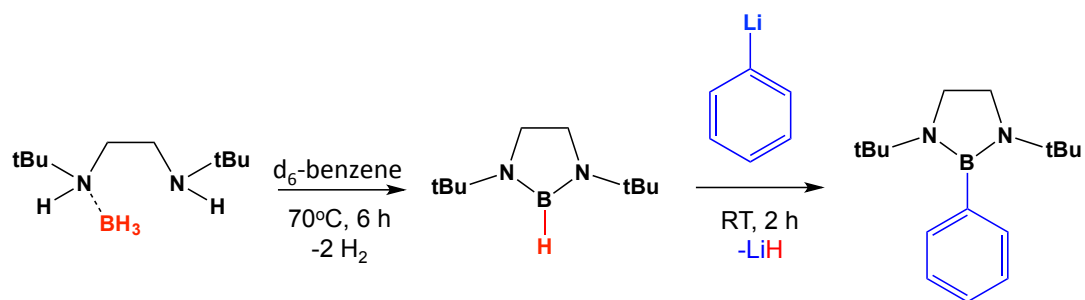
Interestingly Nozaki and co-workers have reported extensive studies on boryllithium chemistry^[27,28] and most recently a potassium diboryllithiate,^[29] which was found to deprotonate benzene, which ultimately led to the unprecedented isolation of a phenylborane derivative (Scheme 3.18).



Scheme 3.18: Nozaki's synthesis of diboryllithiate and subsequent deprotonation of benzene.

This work inspired the route for our attempted B-H transformation, since the formation of the phenylborane was thought to proceed via a similar cyclized hydroborane intermediate. Interestingly, the potassium diboryllithiate when left for 10 hours at room temperature in benzene, acted as a superb base deprotonating benzene to yield a hydroborane and metallated benzene. The hydroborane then subsequently reacted with the *in-situ* formed phenyllithium or phenylpotassium to yield the phenylborane product in an 85% yield with the concomitant elimination of Li/K-H. In this case the reaction of the hydridoborane with phenyllithium or phenylpotassium doesn't seem to have been studied experimentally but instead extensive DFT calculations support the suggested reaction pathway. However, a previous study by Nozaki with the monometallic boryllithium derivative has been reported to deprotonate toluene and result in a benzyl borane via the same hydridoborate intermediate.^[30]

Given that we developed a synthesis of similar cyclized B-H derivatives, we decided to explore this methodology experimentally starting from an intermediate stage. In a similar manner to Nozaki, having a one-pot synthesis, it was decided to follow the catalytic protocol to obtain the cyclized product to which phenyllithium could be added (Scheme 3.19). A desirable feature of this transformation is the ¹¹B NMR spectrum handle allows the monitoring of each step.



Scheme 3.19: Post-synthetic functionalization of cyclized product.

This was initially tested with **10**, the standard cyclisation protocol was carried out in a J. Youngs tube in d_6 -benzene, after which phenyllithium was added. After two hours at room temperature the formation of a new B-C_{phenyl} bond was established by the diagnostic singlet resonance at 31.8 ppm in the ¹¹B NMR spectrum, indicating the presence of the desired phenyl borolidine, **23**. Approximately 80% conversion was observed by ¹¹B NMR spectroscopy. This was repeated for **11-13** on NMR scale to test the versatility of this procedure to varying sterics around the B-H functionality. All

four compounds, **10-13**, showed high conversion to the phenylated products **23-26** (Figure 3.10) in yields of over 60%, hence their ease of isolation was next to be explored.

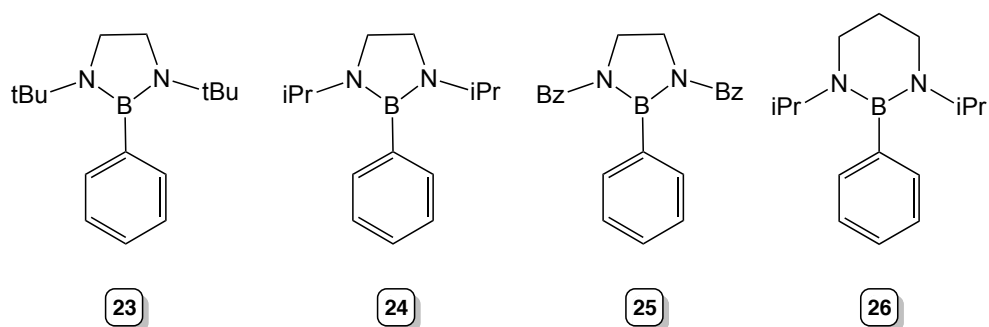
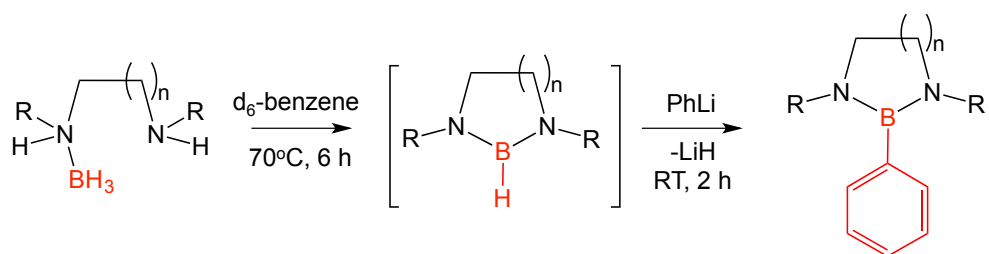


Figure 3.20: Phenyl-diazaborolidine products **23-26**.

Upon moving to a Schlenk scale reaction these reaction conditions were replicated in toluene rather than d_6 -benzene. The new compounds **23-26** could be isolated straightforwardly. For compounds **10**, **11** and **12**, isolated yields of 70%, 61 and 81% respectively of the phenyl product were obtained (entry 1, 2 and 3 in table 3.8). However, for compound **13** there were some complications with which resulted in a mixture of starting material and product, whereby the B-H product could not be separated from the B-phenyl product. A 3:1 ratio of phenylborane:hydroborane was observed in ^{11}B NMR of the isolated material. These were all fully characterized by NMR spectroscopy.

Table 3.8: Isolated yields of B-H to B-C transformation.



Starting material	Product	Isolated yield (%)
10	23	70
11	24	61
12	25	81
13	26	38

For the purpose of confirming the new B-C functionality installed, following the conversion of **10** to **23** in a Schlenk tube, the product was crystallised from a toluene/hexane mixture at -68°C . The expected molecular structure was obtained (Figure 3.11) with the replacement of the boron hydride bond with a new boron carbon bond. An interesting feature is the arrangement of the phenyl group relative to the plane of the borolidine ring whereby it sits in an orthogonal position with a dihedral angle of 85° . This can be attributed to the bulky *tert*-butyl groups on the nitrogen atoms of the ring.

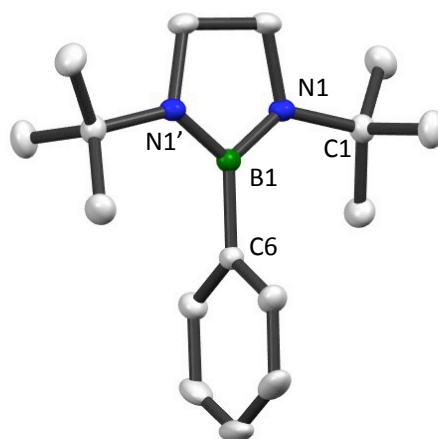


Figure 3.11: Molecular structure of **23** with displacement ellipsoids at 50% probability level, hydrogen atoms omitted for clarity. Symmetry transformations used to generate equivalent atoms labelled ‘: $x, +y, 0.5-z$. Selected bond lengths (\AA) and bond angles ($^{\circ}$): B1-N1, 1.4285(12); B1-C6, 1.578(2); N1-B1-N1’, 109.68(12); N1-B1-C6, 125.16(6).

3.5 Conclusions and future work

The demand for converting transition metal catalysis to more abundant metal catalysis is always present in synthetic chemistry. The cyclisation of diamine boranes to give potentially synthetically useful 1,3,2-diazaborolidine precursors were only accessible via a ruthenium based catalytic manifold. Here an alternative lithium dihydropyridine based (pre)catalyst has been delivered into the catalytic arena, which can compete on a similar playing field. Many aspects of this reaction have been explored, with a key finding being its necessity for non-coordinating solvent namely d_6 -benzene to achieve optimum catalytic performance. The deeper understanding of how lithium

dihydropyridine acts as a (pre)catalyst via solution and structural studies, has allowed the appreciation of the key role 2-*tert*-butylpyridine has in the reaction mechanistically, acting as a storage/release vessel of lithium hydride on demand.

The scope of this catalytic regime does not appear to be restricted; herein four substrates of varying steric requirements (*tert*butyl, *isopropyl* and *benzyl*) have been successfully cyclized, although not isolated. Developing on this, the B-H bond has been converted to a more synthetically practical B-C bond upon reaction with phenyllithium under mild conditions within short reaction times of two hours. An added benefit of these new B-C precursors was their isolation proved much simpler than that of the B-H derivative.

Further developments on this work can be made in different avenues, primarily these reactions could be employed in Suzuki-Miyaura cross-coupling reactions to compare their reactivity patterns with those in the literature. Extension of the aryllithium scope is crucial for its applicability in cross coupling reactions. For example if using a dilithiated species would this result in a di-borated species, akin to Nozaki's diborylxylene,^[30] which then has two sites for cross coupling reactivity (Figure 3.12). Could we exploit bimetallic synergic chemistry to access challenging metallated compounds to convert them to attractive organic boron species upon reaction with the cyclized diazaborolidine?

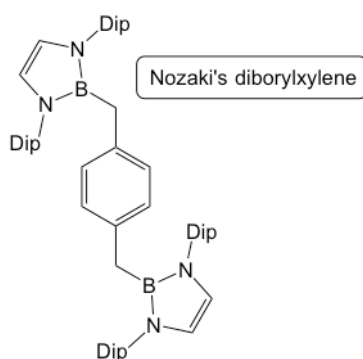


Figure 3.12: Nozaki's diborylxylene.

3.6 Experimental

3.6.1 General catalytic procedure

Catalytic dehydrogenative cyclisation of diamine monoboranes with 5 mol% of **1**

Diamine borane (0.5 mmol) and ferrocene (9.3 mg, 0.05 mmol) were placed in a J. Youngs NMR tube and dissolved in d_6 -benzene and NMR data were recorded. **1** (3.6 mg, 5 mol%) was then added and the NMR sample was then heated for the prescribed period and the reaction monitored via ^1H and ^{11}B spectroscopy.

3.6.2 Synthesis of starting materials and characterisation of new compounds

Synthesis of Compound **10**^[25]

To a solution of *N,N'*-di-*tert*butylethylenediamine (1.25 mL, 5.8 mmol) in 2 mL of THF, $\text{BH}_3\cdot\text{THF}$ (5.8 mL of a 1M THF solution, 5.8 mmol) was added at room temperature. The reaction was allowed to stir for 20 hours. The solvent was removed by vacuum and the white solid was isolated (0.734 g, 68%).

Synthesis of Compound **11**^[25]

To a solution of *N,N'*-diisopropylethylenediamine (1.05 mL, 5.8 mmol) in 2 mL of THF, $\text{BH}_3\cdot\text{THF}$ (5.8 mL of a 1M THF solution, 5.8 mmol) was added at -50°C . The reaction was allowed to stir for 20 hours. The solvent was removed by vacuum and replaced with 5 mL of toluene and 5 mL of hexane. Any slight precipitate was filtered through celite and glass wool. The solvent was then removed yielding a yellow oil (0.567 g, 62%).

Synthesis of Compound **12**^[25]

To a solution of *N,N'*-dibenzylethylenediamine (1.37 mL, 5.8 mmol) in 2 mL of THF, $\text{BH}_3\cdot\text{THF}$ (5.8 mL of a 1M THF solution, 5.8 mmol) was added at -50°C . The reaction was allowed to stir for 20 hours. The solvent was removed by vacuum and replaced with 5 mL of toluene and 5 mL of hexane resulting in a white suspension. This was filtered through celite and glass wool. The pale yellow solution collected was dried under vacuum to remove the solvent, producing a yellow oil (0.804 g, 55%).

Synthesis of Compound 13

To a solution of *N,N'*-diisopropyl-1,3-propanediamine (1.14 mL, 5.8 mmol) in 2 mL of THF, BH₃·THF (5.8 mL of a 1M THF solution, 5.8 mmol) was added at -50°C. The reaction was allowed to stir for 20 hours. The solvent was removed by vacuum and replaced with 5 mL of toluene and 5 mL of hexane. Any precipitate was filtered through celite and glass wool. The solvent was then removed under vacuum leaving a colourless oil (0.57 g, 57%).

¹H NMR (400.1 MHz, C₆D₆ 300K): δ 6.61 (1H, br s), 2.90 (1H, m), 2.75-2.62 (1H, m), 2.53-2.24 (4H, m), 2.13 (1H, m) and 1.99-1.82 (2H, m) ppm.

¹¹B NMR (128.4 MHz, C₆D₆ 300K): δ -18.78 (q, ¹J_{B-H} 92.6 Hz, BH) ppm.

Synthesis of Compound 14

The general catalytic procedure was employed with 0.186 g of **10**.

¹H NMR (400.1 MHz, C₆D₆ 300K): δ 3.12 (4H, s, CH₂) and 1.17 (18H, s, *t*Bu) ppm.

¹¹B NMR (128.4 MHz, C₆D₆ 300K): δ 26.3 (d, ¹J_{B-H} 140.6 Hz, BH) ppm.

Schlenk scale up for isolated yield

10 (93 mg, 0.5 mmol) and **1** (3.6 mg, 5mol%) were stirred in benzene (1 mL) in a Schlenk flask at 70 °C for 6 h. Benzene was removed by distillation at atmospheric pressure (oil bath temp – 90 °C). A second colourless oil was collected via distillation (oil bath temp 105 °C) and was confirmed by NMR studies as **14**. Yield 86 mg, 94%.

¹H NMR (400.1 MHz, C₆D₆ 300K): δ 3.13 (4H, s, CH₂), 1.18 (18H, s, *t*Bu) ppm.

¹¹B NMR (128.4 MHz, C₆D₆ 300K): δ 26.4 ppm (d, ¹J_{B-H} 138.2 Hz, BH) and -18.8 ppm (q, ¹J_{B-H} 94.8 Hz, BH₃) corresponding to a small amount of starting diamine borane.

Synthesis of Compound 15

The general catalytic procedure was employed with 0.079 g of **11**.

¹H NMR (400.1 MHz, C₆D₆ 300K): δ 3.11 (2H, overlapped m, CH), 3.08 (4H, s, CH₂) and 1.10 (12H, s, CH₃) ppm.

¹¹B NMR (128.4 MHz, C₆D₆ 300K): δ 26.7 (d, ¹J_{B-H} 141.2 Hz, BH) ppm.

Synthesis of Compound 16

The general catalytic procedure was employed with 0.127 g of **12**.

^1H NMR (400.1 MHz, C_6D_6 300K): δ 7.28-7.14 (8H, m, Ar C-H), 7.14-7.03 (2H, m, Ar C-H), 4.08 (2H, s, CH_2 benzyl) and 2.89 (2H, s, CH_2 backbone) ppm.

^{11}B NMR (128.4 MHz, C_6D_6 300K): δ 29.5 (d, $^1J_{\text{B-H}}$ 132.2 Hz, BH) ppm.

Synthesis of Compound 17

The general catalytic procedure was employed with 0.086 g of **13**.

^1H NMR (400.1 MHz, C_6D_6 300K): δ 3.34 (2H, m, CH), 2.71 (4H, t, CH_2 backbone), 1.66 (2H, m, CH_2 backbone) and 1.08 (12H, s, CH_3) ppm.

^{11}B NMR (128.4 MHz, C_6D_6 300K): δ 25.8 (d, $^1J_{\text{B-H}}$ 131.9 Hz, BH) ppm.

Synthesis of Compound 18

10 (186 mg, 1 mmol) was dissolved in hexane (3 mL) and *n*BuLi (0.63 mL, 1 mmol 1.6M in hexane) was added, resulting in precipitation of a white solid after several minutes. After 30 min. stirring THF was added dropwise until a colourless solution was obtained. Crystals suitable for single crystal X-ray diffraction studies were grown after standing the solution at $-20\text{ }^\circ\text{C}$ for 24 h. Yield 193 mg, 73%.

Elemental analysis (%) calculated for $\text{C}_{14}\text{H}_{34}\text{N}_2\text{B}_1\text{Li}_1\text{O}_1$: C 63.65, H 12.97, N 10.60; found: C 63.61, H 13.01, N 10.42.

^1H NMR (400.1 MHz, C_6D_6 300K): δ 3.57 (4H, br t, OCH_2 -THF), 2.67 (4H, br s, CH_2CH_2 -diamine), 1.41 (4H, br t, $(\text{CH}_2)_2$ -THF), 1.40 (9H, s, *t*Bu), 1.06 (9H, s, *t*Bu), 0.56 ppm (1H, t, $^3J_{\text{H-H}}$ 7.05 Hz, NH).

^{11}B NMR (128.4 MHz, C_6D_6 300K): δ -21.7 ppm (q, $^1J_{\text{B-H}}$ 86.7 Hz, BH_3).

^7Li NMR (155.5 MHz, C_6D_6 300K): δ 0.13 ppm.

^{13}C NMR (100.6 MHz, C_6D_6 300K): δ 67.8 (THF), 53.5 (*t*Bu quaternary), 51.6 (CH_2), 50.7 (CH_2), 42.8 (*t*Bu quaternary), 29.2 (CH_3 -*t*Bu), 28.4 ppm (CH_3 -*t*Bu).

Synthesis of Compound 19

10 (186 mg, 1 mmol) was dissolved in hexane (3 mL) and *n*BuLi (0.63 mL, 1 mmol 1.6M in hexane) was added, resulting in precipitation of a white solid after several

minutes. After 30 min. stirring pyridine was added dropwise until a colourless solution was obtained. Crystals suitable for single crystal X-ray diffraction studies were grown after standing the solution at -20 °C for 24 h. Yield 169 mg, 62%.

Elemental analysis (%) calculated for C₁₅H₃₁N₃B₁Li₁: C 66.44, H 11.52, N 15.49; found: C 66.26, H 11.19, N 15.30.

¹H NMR (400.1 MHz, C₆D₆ 300K): δ 8.52 (2H, m, CH-Pyr), 6.95 (1H, tt, ³J_{H-H} 7.68 Hz; ⁴J_{H-H} 1.93 Hz, CH-pyr), 6.64 (2H, m, CH-Pyr), 2.75 (4H, br s, CH₂CH₂-diamine), 1.41 (9H, s, *t*Bu), 1.01 (9H, s, *t*Bu), 0.54 ppm (1H, t, ³J_{H-H} 8.27 Hz, NH).

¹¹B NMR (128.4 MHz, C₆D₆ 300K): δ -21.3 ppm ¹J_{B-H} 84.9 Hz

⁷Li NMR (155.5 MHz, C₆D₆ 300K): δ 0.52 ppm

¹³C NMR (100.6 MHz, C₆D₆ 300K): δ 150.1 (pyr), 135.8 (pyr), 123.7 (pyr), 53.5 (*t*Bu quaternary), 51.6 (CH₂), 50.7 (CH₂), 43.0 (*t*Bu quaternary), 29.3 (CH₃-*t*Bu), 28.8 ppm (CH₃-*t*Bu).

Synthesis of Compound 20^[25]

To a solution of *N,N,N'*-trimethylethylenediamine (0.75 mL, 5.8 mmol) in 2 mL of THF, BH₃.THF (5.8 mL of a 1M THF solution, 5.8 mmol) was added at -50°C. The reaction was allowed to stir overnight. The following day the solvent was removed by vacuum and replaced with 5 mL of toluene and 5 mL of hexane. Any precipitate was filtered through celite and glass wool. The solution collected was dried under vacuum to remove the solvent, producing a colourless oil (0.422 g, 63%).

Synthesis of Compound 21

20 (116 mg, 1 mmol) was dissolved in hexane (3 mL) and *n*BuLi (0.63 mL, 1 mmol 1.6M in hexane) was added, resulting in precipitation of a white solid after several minutes. After 30 min. stirring THF was added dropwise until a colourless solution was obtained. Crystals suitable for single crystal X-ray diffraction studies were grown after standing the solution at -20 °C for 24 h. Yield 112 mg, 81%.

Elemental analysis (%) calculated for C₁₀H₃₂N₄B₂Li₂: C 49.25, H 13.23, N 22.97; found: C 49.51, H 12.28, N 22.92. Consistent with loss of 2 x THF upon drying *in vacuo*.

¹H NMR (400.1 MHz, C₆D₆ 300K): δ 2.64 (3H, br s, CH₃-diamine), 2.45 (2H, br s, CH₂-diamine), 2.34 (2H, br s, CH₂-diamine), 2.01 ppm (1H, s, 2xCH₃-diamine).

¹¹B NMR (128.4 MHz, C₆D₆ 300K): δ -17.9 ppm ¹J_{B-H} 83.3 Hz

⁷Li NMR (155.5 MHz, C₆D₆ 300K): δ 0.56 ppm

¹³C NMR (100.6 MHz, C₆D₆ 300K): δ 68.0 (THF), 58.6 (CH₂), 57.1 (CH₂), 48.0 (CH₃), 45.0 (2xCH₃), 25.6 ppm (THF).

Synthesis of Compound 22

20 (116 mg, 1 mmol) was dissolved in hexane (3 mL) and *n*BuLi (0.63 mL, 1 mmol 1.6M in hexane) was added, resulting in precipitation of a white solid after several minutes. After 30 min. stirring, pyridine was added dropwise until a colourless solution was obtained. Crystals suitable for single crystal X-ray diffraction studies were grown after standing the solution at -20 °C for 24 h. Yield 96 mg, 48%.

Elemental analysis (%) calculated for C₂₀H₄₂N₆B₂Li₂: C 59.74, H 10.53, N 20.90; found: C 59.31, H 11.04, N 20.96.

¹H NMR (400.1 MHz, C₆D₆ 300K): δ 8.53 (2H, m, CH-Pyr), 6.95 (1H, tt, ³J_{H-H} 7.60 Hz; ⁴J_{H-H} 1.80 Hz, CH-pyr), 6.64 (2H, m, CH-Pyr), 2.71 (3H, br s, CH₃-diamine), 2.56 (2H, br s, CH₂-diamine), 2.43 (2H, br s, CH₂-diamine), 1.98 ppm (1H, s, 2xCH₃-diamine).

¹¹B NMR (128.4 MHz, C₆D₆ 300K): δ -17.0 ppm ¹J_{B-H} 77.6 Hz

⁷Li NMR (155.5 MHz, C₆D₆ 300K): δ 0.96 ppm

¹³C NMR (100.6 MHz, C₆D₆ 300K): δ 150.1 (pyr), 135.7 (pyr), 123.6 (pyr), 58.9 (CH₂), 57.6 (CH₂), 48.3 (CH₃), 45.2 ppm (2xCH₃).

Synthesis of Compound 23

10 (372 mg, 2 mmol) and **1** (14 mg, 5 mol%) were dissolved in toluene (2 mL) and heated at 80 °C for 7h to ensure *in situ* conversion to **14**. Phenyllithium (168 mg, 2 mmol) was added and the reaction stirred overnight. Hexane (5 mL) was added and the reaction placed at -70 °C. After 24 hours, colourless crystals suitable for X-ray diffraction studies formed of **23**. Yield 361 mg, 70%.

¹H NMR (400.1 MHz, C₆D₆ 300K): δ 7.42 (2H, m, CH-phenyl), 7.20-7.10 (3H, m, CH-phenyl), 3.19 (4H, s, CH₂), 1.03 ppm (18H, s, CH₃).

¹¹B NMR (128.4 MHz, C₆D₆ 300K): δ 31.8 ppm (s, BPh).

¹³C NMR (100.6 MHz, C₆D₆ 300K): δ 132.7 (C-Ph), 127.4 (C-Ph), 126.9 (C-Ph), 51.8 (quaternary C-tBu), 45.2 (CH₂), 30.9 ppm (CH₃-tBu).

Synthesis of Compound 24

11 (462 mg, 3 mmol) and **1** (21 mg, 5 mol%) were dissolved in toluene (4 mL) and heated at 80 °C for 48 h to ensure *in situ* conversion to **15**. Phenyllithium (252 mg, 4 mmol) was added and the reaction stirred overnight. Hexane (5 mL) was added and the reaction placed at -70 °C. After 24 hours, colourless crystals formed. These were isolated at low temperature by decanting the solution from the solid. **24** exists as a colourless oil at room temperature. Yield 421 mg, 61%.

¹H NMR (400.1 MHz, C₆D₆ 300K): δ 7.54 (2H, d, CH-phenyl), 7.32 (2H, m, CH-phenyl), 7.25 (1H, t, CH-phenyl), 3.60 (2H, septet, CH(CH₃)₂), 3.16 (4H, s, CH₂), 0.98 ppm (12H, d, CH(CH₃)₂).

¹¹B NMR (128.4 MHz, C₆D₆ 300K): δ 31.6 ppm (s, BPh).

¹³C NMR (100.6 MHz, C₆D₆ 300K): δ 132.9 (C-Ph), 128.1 (C-Ph), 126.9 (C-Ph), 45.2 (CH₂), 41.9 (CH-CH₃)₂, 22.0 ppm (CH(CH₃)₂).

Synthesis of Compound 25

12 (1.640 g, 4 mmol) and **1** (29 mg, 5 mol%) were dissolved in toluene (4 mL) and heated at 80 °C for 24 h to ensure *in situ* conversion to **16**. Phenyllithium (336 mg, 4 mmol) was added and the reaction stirred overnight. Hexane (5 mL) was added and the reaction placed at -70 °C. After 24 hours, colourless crystals formed and were isolated by filtration. Yield 1.052 g, 81%.

¹H NMR (400.1 MHz, C₆D₆ 300K): δ 7.68 (2H, m, CH-phenyl), 7.21 (11H, m, CH-phenyl), 7.10 (2H, m, CH-phenyl), 4.14 (4H, s, CH₂), 3.03 ppm (4H, s, CH₂).

¹¹B NMR (128.4 MHz, C₆D₆ 300K): δ 32.7 ppm (s, BPh).

¹³C NMR (100.6 MHz, C₆D₆ 300K): δ 141.1 (C-Ph), 133.2 (C-Ph), 128.8 (C-Ph), 128.7 (C-Ph), 128.4 (C-Ph), 127.6 (C-Ph), 126.9 (C-Ph), 51.4 (benzyl CH₂), 48.4 ppm (CH₂).

Synthesis of Compound 26

13 (420 mg, 2.5 mmol) and **1** (18 mg, 5 mol%) were dissolved in toluene (4 mL) and heated at 80 °C for 48 h to ensure *in situ* conversion to **17**. Phenyllithium (156 mg, 2.5 mmol) was added and the reaction stirred overnight. Hexane (5 mL) was added and the reaction placed at -70 °C. After 24 hours a white solid formed. These were isolated at low temperature by decanting the solution from the solid. The reaction product mixture exists as a waxy white solid in a 3:1 ratio of **26:17**. Combined yield 421 mg, 38%.

3.6.3 Crystallographic data and refinement details for compounds **18**, **19**, **21**, **22** and **23**.

	18	19	21	22	23
Empirical formula	LiON ₂ C ₁₄ BH ₃₄	LiN ₃ C ₁₅ BH ₃₁	Li ₂ O ₂ N ₄ C ₁₈ B ₂ H ₄₈	Li ₂ B ₂ N ₆ C ₂₀ H ₄₂	C ₁₆ H ₂₇ B ₁ N ₂
Mol. Mass	264.18	271.18	388.10	402.09	258.2
Crystal system	monoclinic	monoclinic	triclinic	monoclinic	monoclinic
Space group	P 2 ₁ /c	P n	P -1	P 2 ₁ /c	C 2/c
Temperature (K)	123.1	122.9	122.6	123	158.3
a/ Å	6.1321(6)	8.4263(19)	8.4191(6)	8.4964(11)	14.5259(12)
b/ Å	15.8714(15)	6.2044(9)	8.8743(7)	9.8471(10)	10.3281(7)
c/ Å	18.017(2)	16.977(3)	9.7883(8)	15.8260(19)	11.2033(10)
α/o	90	90	67.501(8)	90	90
β/o	93.743(10)	100.745(19)	72.307(7)	104.836(12)	110.814(10)
γ/o	90	90	72.253(7)	90	90
V/Å ³	1749.7(3)	872.0(3)	628.76(10)	1279.9(3)	1571.1(2)
Z	4	2	1	2	4
λ/Å	0.71073	0.71073	0.71073	0.71073	0.71073
Measured reflections	17408	6136	12110	12683	3789
Unique reflections	4579	3083	3436	3477	1906
R _{int}	0.0512	0.0704	0.0257	0.0248	0.0151
Observed rflns [I > 2σ(I)]	3317	2109	2911	2965	1636
Goof	1.038	1.061	1.111	1.049	1.027
R [on F, obs rflns only]	0.0668	0.0753	0.0401	0.0419	0.0426
ωR [on F ² , all data]	0.1750	0.2117	0.1461	0.1150	0.1158
Largest diff. peak/hole e/Å ⁻³	0.37/-0.23	0.29/-0.21	0.31/-0.18	0.34/-0.24	0.41/-0.20

3.7 References

- [1] P. Power, *Nature*, **2010**, *463*, 171-177.
- [2] M. R. Crimmin, I. J. Casely and M. S. Hill, *J. Am. Chem. Soc.* **2005**, *127*, 2042-2043.
- [3] M. Arrowsmith, M. S. Hill, T. Hadlington, G. Kociok-Köhn, C. Weetman, *Organometallics*, **2011**, *30*, 5556-5559.
- [4] M. Arrowsmith, T. Hadlington, M. S. Hill, G. Kociok-Köhn, *Chem. Commun.* **2012**, *48*, 4567-4569.
- [5] J. Intemann, M. Lutz, S. Harder, *Organometallics*, **2014**, *33*, 5722-5729.
- [6] J. Intemann, H. Bauer, J. Pahl, L. Maron, S. Harder, *Chem. Eur. J.* **2015**, *21*, 11452-11461.
- [7] C. Weetman, M. D. Anker, M. Arrowsmith, M. S. Hill, G. Kociok-Köhn, D. J. Liptrot and M. F. Mahon, *Chem. Sci.* **2016**, *7*, 628-641.
- [8] J. Spielmann, F. Buch, S. Harder, *Angew. Chem. Int. Ed.* **2008**, *47*, 9434-9438.
- [9] R. L. Melen, *Chem. Soc. Rev.* **2016**, *45*, 775-788.
- [10] E. M. Leitao, T. Jurca, I. Manners, *Nat. Chem.* **2013**, *5*, 817-829.
- [11] J. Spielmann, M. Bolte, and S. Harder, *Chem. Commun.* **2009**, 6934-6936.
- [12] J. Spielmann, D. F.-J. Piesik, S. Harder, *Chem. Eur. J.* **2010**, *16*, 8307-8318.
- [13] D. J. Liptrot, M. S. Hill, M. F. Mahon, D. J. MacDougall, *Chem. Eur. J.* **2010**, *16*, 8508-8518.
- [14] M. S. Hill, G. Kociok-Köhn and T. P. Robinson, *Chem. Commun.* **2010**, *46*, 7587-7589.
- [15] M. S. Hill, M. Hodgson, D. J. Liptrot and M. F. Mahon, *Dalton Trans.* **2011**, *40*, 7783-7790.
- [16] M. S. Hill, D. J. Liptrot, D. J. MacDougall, M. F. Mahon and T. P. Robinson, *Chem. Sci.* **2013**, *4*, 4212-4222.
- [17] H. J. Cowley, M. S. Holt, R. L. Melen, J. M. Rawson and D. S. Wright, *Chem. Commun.* **2011**, *47*, 2682-2684.
- [18] M. M. Hansmann, R. L. Melen and D. S. Wright, *Chem. Sci.* **2011**, *2*, 1554-1559.
- [19] R. J. Less, H. R. Simmonds, S. B. J. Dane and D. S. Wright, *Dalton Trans.* **2013**, *42*, 6337-6343.
- [20] P. Cui, T. P. Spaniol, L. Maron, J. Okuda, *Chem. Eur. J.* **2013**, *19*, 13437-13444.
- [21] P. Bellham, M. S. Hill, G. Kociok-Köhn, *Dalton Trans.* **2015**, *44*, 12078-12081.

- [22] A. Harinath, S. Anga and T. K. Panda, *RSC Adv.* **2016**, *6*, 35648-35653.
- [23] S. Anga, Y. Sarazin, J-F. Carpentier, and T. K. Panda, *ChemCatChem.* **2016**, *8*, 1373-1376.
- [24] C. J. Wallis, H. Dyer, L. Vendier, G. Alcaraz, and S. Sabo-Etienne, *Angew. Chem. Int. Ed.* **2012**, *51*, 3646-3648.
- [25] C. J. Wallis, G. Alcaraz, A. S. Petit, A. I. A. I. Poblador-Bahamonde, E. Clot, C. Bijani, L. Vendier, and S. Sabo-Etienne, *Chem. Eur. J.* **2015**, *21*, 13080-13090.
- [26] N. Miyaura, A. Suzuki, *Chem. Rev.* **1995**, *95*, 2457-2483.
- [27] Y. Segawa, M. Yamashita, K. Nozaki, *Science*, **2006**, *314*, 113-115.
- [28] Y. Segawa, Y. Suzuki, M. Yamashita, and K. Nozaki, *J. Am. Chem. Soc.* **2008**, *130*, 16069-16079.
- [29] T. Ohsato, Y. Okuno, S. Ishida, T. Iwamoto, K. Lee, Z. Lin, M. Yamashita, and K. Nozaki, *Angew. Chem. Int. Ed.* **2016**, *55*, 11426-11430.
- [30] N. Dettenrieder, Y. Aramaki, B. M. Wolf, C. Maichle-Mössmer, X. Zhao, M. Yamashita, K. Nozaki, and R. Anwander, *Angew. Chem. Int. Ed.* **2014**, *53*, 6259-6262.

Chapter 4: Lithium dihydropyridine catalysed hydroboration of carbonyls

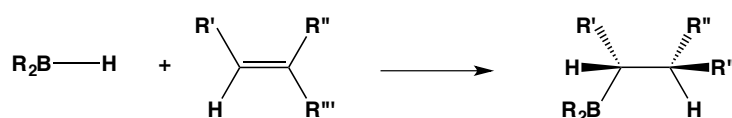
4.1 Summary

Herein, the extension of our lithium dihydropyridines catalytic capabilities is extended to hydroboration of carbonyl species, to prepare synthetically useful boronate esters for further chemical transformations. The standard conditions used for this is 5 mol% of **1** in 0.5ml of d_6 -benzene. The reactions were monitored by NMR spectroscopy and the yields determined by 1H NMR resonances relative to an internal standard hexamethylcyclotrisiloxane. Almost quantitative conversion was observed typically within 15 minutes at room temperature except in the case of the sterically hindered mesitaldehyde and 2,4,6-trimethylacetophenone, which require more forcing conditions, $70^\circ C$ for 24 hours.

Control reactions were probed which resulted in the isolation of [HBpin.NC₅H₅] **27**, an acceptor-donor adduct characterised by X-ray crystallography. Further NMR spectroscopy studies allowed the proposal of two potential reaction pathways, including the traditionally accepted route.

4.2 Introduction

Hydroboration, the syn-addition of a boron hydrogen bond across an unsaturated carbon-carbon, carbon-oxygen or carbon-nitrogen bond, typically in an anti-Markovnikov fashion (Scheme 4.1), is one of the most important synthetic tools in organic chemistry. The resulting organoborane product may by itself not seem that particularly significant but it is rarely the ultimate goal. It is the potential of these compounds when combined with further synthetic transformations that makes them powerful synthetic precursors. For example, organoboranes are employed in the complicated synthesis of natural products such as the anti-tumour agent fostriecin.^{1,2}



Scheme 4.1: Simple schematic of a typical hydroboration reaction of an alkene.

The pioneer of this work was H. C. Brown who in 1939 unveiled an uncatalysed reduction of aldehydes and ketones using diborane.³ These reactions were considered the beginning of the now widespread synthesis and applications of organoborane compounds. Brown later extended this work to alkenes,⁴ which was briefly followed by reports from Köster⁵ on alkene hydroboration with alkylboranes. Brown's contribution to organoborane chemistry was recognised in 1979 when he was awarded the Nobel Prize in Chemistry jointly with Wittig.⁶

"for their development of the use of boron- and phosphorus-containing compounds, respectively, into important reagents in organic synthesis"

The choice of hydroborating reagent is essential when performing a hydroboration reaction, as a major problem for these reagents can be their lack of regioselectivity and susceptibility to decomposition. Although there are many commercial boron reagents available, there are a few reagents that have been studied in much more detail. Representative examples of boranes, cyclic dialkylboranes and cyclic dialkoxyboranes are shown in figure 4.1.

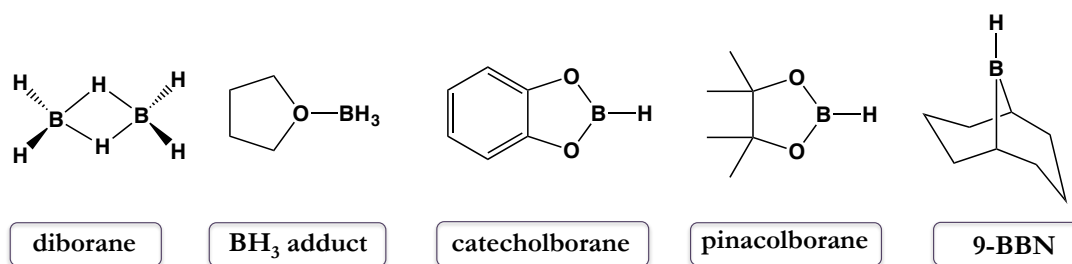
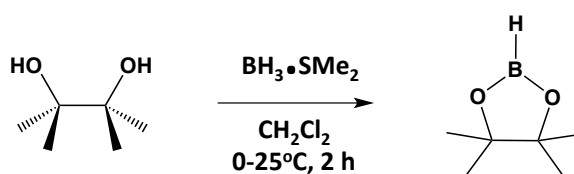


Figure 4.1: Popular commercially available hydroborating reagents.

The simplest boron hydride, diborane (B_2H_6) with its three-centre two-electron bonding is an exceptionally unstable toxic gas. However, due to its Lewis acidic nature it readily forms BH_3 adducts with Lewis basic donors such as tetrahydrofuran (THF) and dimethylsulfide (Me_2S). Although these are used extensively, the development of dialkylboranes and dialkoxyboranes, which exhibit improved regioselective and chemoselective properties, has been key to the expansion of the hydroboration landscape. To date one of the most popular hydroborating reagents is the dimeric dialkylborane 9-BBN, whose inability to engage in dehydroboration enhances its thermal stability, whilst its steric bulk allows it to react in a regioselective manner.⁷⁻⁹ Cyclic dialkoxyboranes such as pinacolborane (HBpin) and catecholborane (HBCat) also have their place in the synthetic toolbox as they can withstand harsher conditions. Knochel was the first to introduce pinacolborane as a hydroborating reagent¹⁰ from the simple reaction of pinacol and dimethylsulfideborane (Scheme 4.2). It was found that HBpin had some advantages over catecholborane including better functional group tolerance, higher regioselectivity and in most cases the resulting boronic ester would be stable enough for its isolation and purification by column chromatography.¹¹



Scheme 4.2: Knochel's synthesis of pinacolborane.

Despite the fact there are many boron reagents to exploit in hydroboration chemistry, with many being considered the standard protocol, there is still a major driving force to advance this chemistry. One of the main reasons for this is that the resulting

organoborane product, such as alkyl and alkenyl boronic esters (Figure 4.2) are extremely valuable precursors in pharmaceutical synthesis.¹² Such boron intermediates can be employed in organic transformations including C-C bond formation via Suzuki-Miyaura couplings¹³⁻¹⁹ to access more complex molecules, synthesizing optically active alcohols,²⁰⁻²² asymmetric synthesis¹¹ and in the preparation of alkylmagnesium reagents from alkenes.²³ Consequently there is a demand to have a collection of hydroborating reagents that can selectively hydroborate compounds such as alkenes, alkynes, carbonyls, nitriles and pyridines whilst maintaining functional group tolerance, so the synthesis of organoboranes is unlimited, and further functionalization and construction of complex molecules is accessible.

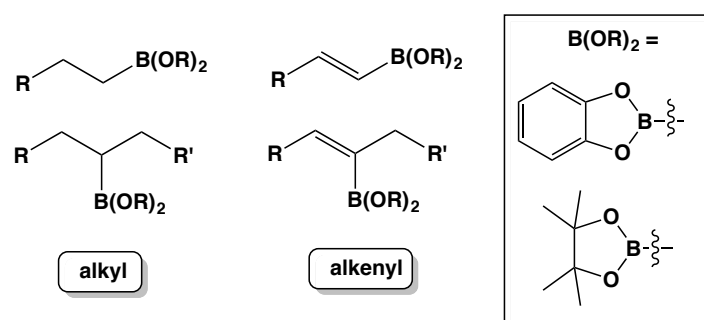
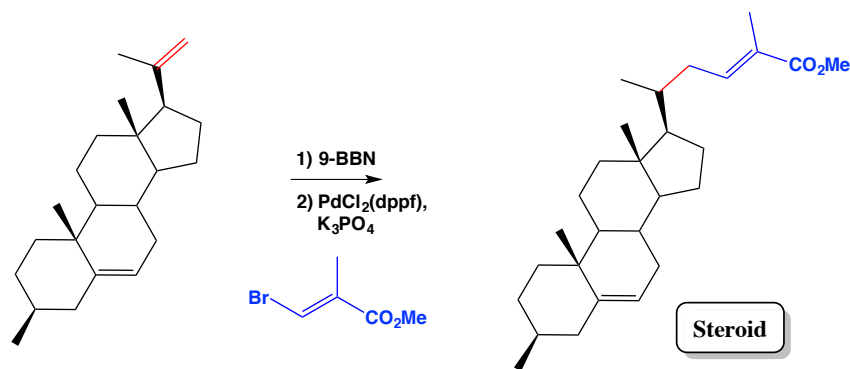


Figure 4.2: Simplistic representations of internal and terminal, alkyl and alkenyl boronic esters.

Studies of uncatalysed hydroborations were inconsistent, as in certain situations they could give rise to a regioselective product whereas in other instances it could result in multiple products, with the hydroborating reagent playing a big role in the outcome.⁹ An example of an effective uncatalysed hydroboration is the synthesis of a steroid molecule as shown in [scheme 4.3](#). An initial regioselective hydroboration of the terminal alkene functionality takes place by 9-BBN, which is then followed by a palladium catalyzed Suzuki-Miyaura cross-coupling reaction to obtain the desired compound.²⁴

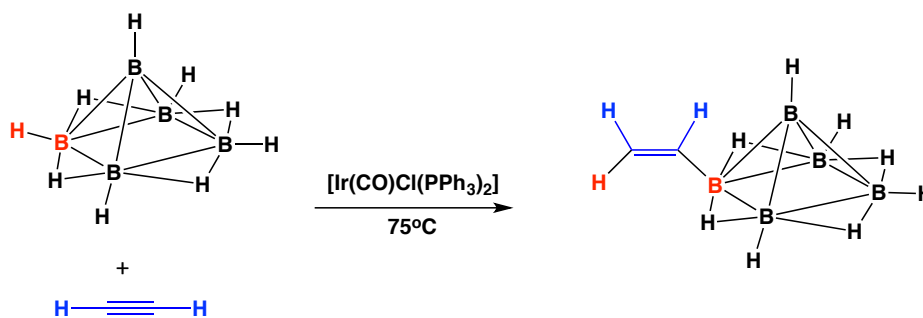


Scheme 4.3: Two-step synthesis of a steroid: namely hydroboration followed by a Suzuki-Miyaura cross coupling reaction.

This appears to be a straightforward synthesis but in other cases with for instance functional group considerations and steric influences, uncatalysed hydroboration can be unpredictable and lack the required level of control. As a result this area expanded immensely, and consequently catalytic systems evolved to maintain a level of control in hydroboration chemistry.

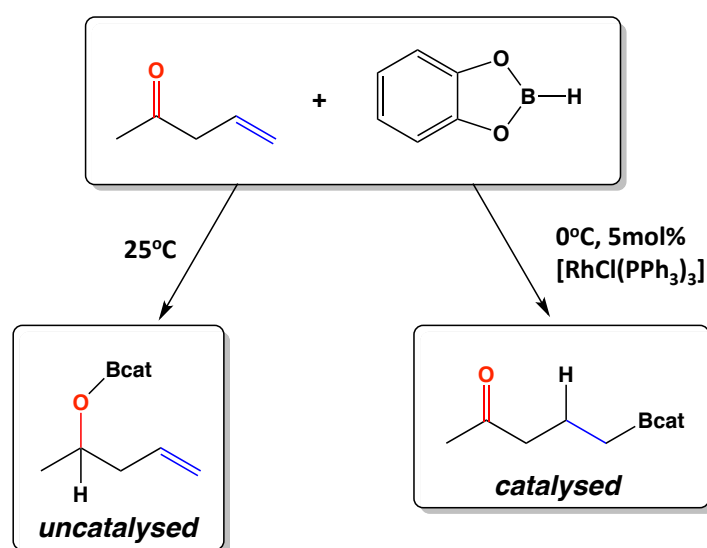
4.2.1 Summary of catalysed hydroboration reactions

The development of catalytic hydroboration has an interesting beginning. Männig and Nöth reported the first rhodium-catalyzed hydroboration utilising Wilkinson's catalyst²⁵ in 1985 following in the footsteps of transition metal catalysed hydrosilylation and hydrocyanation which at that point were already well known. However, Wilczynski and Sneddon had previously reported transition metal catalysed hydroboration in 1981 giving rise to alkenylboranes,²⁶ albeit from a different perspective (Scheme 4.4). They were interested in the synthesis and development of carboranes, studying the effect of iridium and cobalt catalysts on the reactions of alkynes with small carboranes such as pentaborane B₅H₉.^{27,28} Their inspiration for this work was in line with Männig and Nöth, wanting to expand the method of transition metals catalyzed addition reactions to BH systems but with a different end target. A rhodium catalysed hydroboration in the area of carboranes²⁹ followed in 1984 but it is apparent that the research of Männig and Nöth specifically targeted the development of hydroboration chemistry with an eye to its application in organic transformations.



Scheme 4.4: First transition metal catalyzed hydroboration of acetylene.

The catalysed hydroboration using Wilkinson's catalyst $[\text{RhCl}(\text{PPh}_3)_3]$, which successfully hydroborated alkenes and alkynes, turned out to be a milestone in the field when it was employed with a bifunctional molecule. Interestingly, catalyzed or uncatalysed hydroboration of substrate 5-hexene-2-one resulted in two different products (Scheme 4.5). It was established that using the rhodium catalyst activated the C=C double bond enabling selective rapid hydroboration of the alkene preferentially to the more active ketone functionality, which would typically be hydroborated in the absence of a catalyst. This seminal discovery stimulated interest in the community, with reports emerging probing the mechanistic detail and scope,³⁰⁻³² varying the rhodium catalyst,³³ and intuitively the comparison of iridium analogues of Wilkinson's catalyst.³⁴⁻³⁶



Scheme 4.5: Comparison of uncatalysed and rhodium catalysed hydroboration of 5-hexene-2-one with catecholborane in THF.

Rhodium catalyzed hydroborations continue to attract attention in the literature. Some recent key developments include the extension to pyridine,³⁷ to stilbene derivatives³⁸ and an alternative route to terminal alkenyl boronic esters from alkenes instead of alkynes.³⁹ It is the excellent efficiency of rhodium and iridium catalysts that makes them highly popular in organic transformations.

However, because of environmental and sustainable concerns and the heavy extent that these catalysts are used in synthesis, the race is on to find greener, more abundant and cheaper alternatives to these precious metal catalysts. This race has resulted in many alternative metal catalysts being developed including those based on the transition metals, zirconium,^{40,41} iron,^{42,43} copper,⁴⁴⁻⁴⁶ cobalt,⁴⁷ ruthenium,^{48,49} titanium,⁵⁰ zinc⁵¹ and manganese,⁵² on the p-group elements, aluminium,^{53,54,55} and silicon,⁵⁶ the alkaline earth metal, magnesium⁵⁷⁻⁵⁹ and recently with lanthanum catalysts.^{60,61} This long list of examples was able to hydroborate many different substrates including alkenes, alkynes, carbonyls, imines, pyridines, esters, but it is perhaps the magnesium pre-catalyst $\text{Dipp}^{\text{Mg}}\text{NacnacMgBu}$ ($\text{Dipp}^{\text{Mg}}\text{Nacnac} = \text{Ar}^*\text{NC}(\text{Me})\text{CHC}(\text{Me})\text{NAr}^*$; $\text{Ar}^* = 2,6\text{-}i\text{Pr}_2\text{-C}_6\text{H}_3$), which has shown the greatest versatility in substrate scope being extended to nitriles,⁶² isonitriles,⁶³ carbodiimides⁶⁴ and pyridine.⁶⁵ Given that this work is building on catalyzed carbonyl hydroboration; a comprehensive discussion follows on those specific catalysts in [section 4.2.2](#). However, there are general reviews of the current developments in catalytic hydroboration in the literature.^{66,67}

It must also be mentioned that it is possible to carry out efficient hydroborations using alternative catalysts such as metal-hydridotriphenylborates $[(\text{L})\text{M}][\text{HBPh}_3]$. Okuda originally reported alkali metal versions where $\text{M} = \text{Li}, \text{Na}, \text{K}$.⁶⁸ This is interesting as alkali metal catalysts are exceptionally scarce in hydroboration chemistry, even though LiBH_4 is known to promote the sluggish hydroboration of alkenes with HBcat .⁶⁹ A magnesium derivative soon followed⁷⁰ which exhibited more versatility being capable of hydroborating a suite of unsaturated substrates (nitriles, imine, esters, amides, CO_2 , isocyanates) unlike the alkali-metal versions that only displayed activity for carbonyls and CO_2 . In the past five years approaches to catalysing hydroboration have expanded including Lewis acid catalysis with Pier's borane,⁷¹⁻⁷³ employing stabilizing N-heterocyclic carbene boranes⁷⁴ and bulky organoboranes.⁷⁵

4.2.2 Catalysed hydroboration of carbonyls

More specifically this work will focus on carbonyl species hence a selection of relevant catalysts from the literature including transition metal^[46,49,76] and main group derivatives has been depicted in figure 4.3. From those in the literature Hill's nacnac supported magnesium hydride catalyst^[58] (A), Rivard's carbene supported zinc hydride^[51] catalyst, Roesky's nacnac supported aluminium monohydride^[53] catalyst (F) are most relatable to our proposed group 1 (pre)catalyst. A common theme throughout the range of catalysts is the presence of a metal hydride bond as the active species, although this is typically formed within the first step of the catalytic cycle.

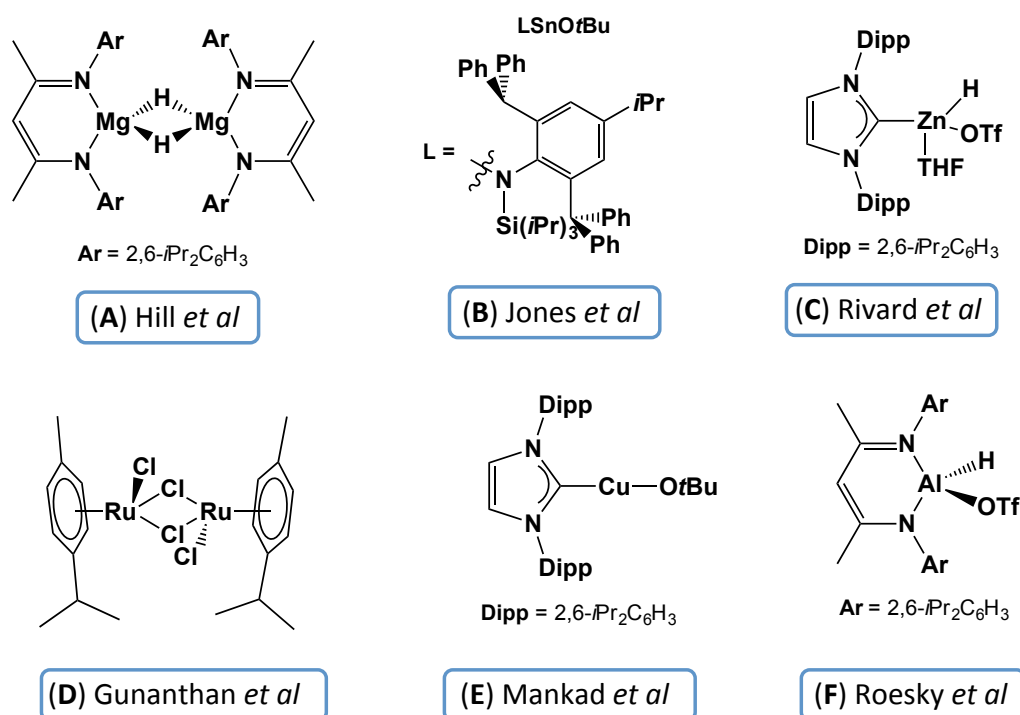
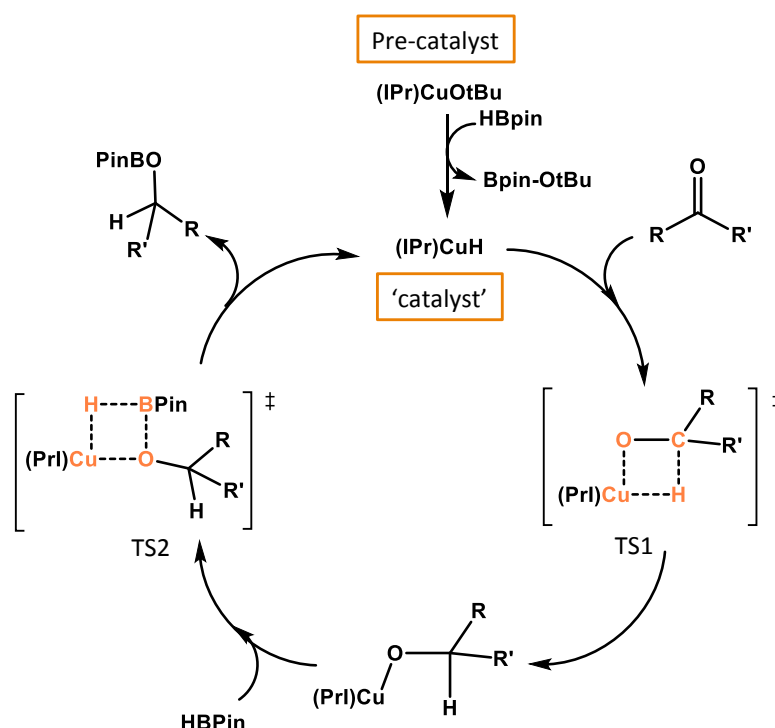


Figure 4.3: A selection of catalysts reported to hydroborate carbonyl species.^[46, 49, 51, 53, 58, 76]

Within the field of hydroboration there is a commonly accepted mechanism that has been postulated by many groups via a σ -bond metathesis type pathway. There have been many reports on this type of cycle, with calculations performed on the aluminium catalyst (F) supporting this route.^[53] Intermediate species have been isolated by X-ray crystallography in some cases. One of the latest research groups to agree with this type of mechanism is Mankad *et al*, employing a sterically

encumbered ligand supported copper *tert*butoxide, [LCuOtBu] (pre)catalyst.^[46] This is illustrated in [scheme 4.6](#) where the first step is the conversion of LCuOtBu (pre)catalyst to an active copper hydride species which can then reduce the carbonyl functionality, via TS1 ([scheme 4.6](#)). This copper intermediate species then undergoes a σ -bond metathesis with HBpin as in TS2 ([scheme 4.6](#)) to eliminate the desired boronate ester and regenerate the copper hydride catalyst.



Scheme 4.6: Generally accepted hydroboration of carbonyl mechanism with HBpin as reported by Mankad employing LCuOtBu as a catalyst.^[46]

4.3 Aims of this chapter

Following the success of the lithium dihydropyridine, LiDHP, **1**, catalysing the dehydrogenative cyclisation of diamine boranes in chapter 3, it was decided to test the versatility of our catalyst by attempting to extend its catalytic competence to hydroboration reactions. Therefore, the plan for this involved:

- Employing optimised conditions from the reactions outlined in chapter 3.
- Catalytic hydroboration of aldehydes.
- Catalytic hydroboration of ketones.
- Compare reaction pathway with that proposed from the literature.

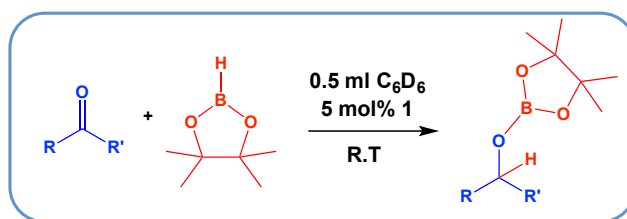
4.4 Results and discussion

The results within this chapter focus on two main substrate groups, aldehydes and ketones. A series of hydroboration reactions with a selection of these carbonyl compounds were studied with pinacolborane (HBpin). These hydroborated products are useful precursors to access alcohols without the requirement of a stoichiometric reducing agent.

4.4.1 Hydroboration of ketones

The idea for this section of work came from the provisional hydrometallation study with benzophenone,^[77] whereby compound **1** stoichiometrically reduced the carbonyl bond, yielding the lithiated alcohol Ph₂C(H)OLi **9** as a hexane insoluble precipitate. Comparing with the literature this insertion of the unsaturated carbonyl functionality by a metal hydride source mirrored the first step in the proposed catalytic regime. This step was followed by a metathesis step with HBpin. Hence it was decided to test the catalytic performance of **1** in a typical ketone hydroboration reaction, to determine if the LiH eliminated during the metathetical step would add across the 2-*tert*butylpyridine present to regenerate **1** or a derivative of it.

In a J. Youngs tube the solution combining benzophenone along with HBpin and 5 mol% of the LiDHP catalyst **1** in 0.5 mL of d₆-benzene, was monitored by ¹¹B NMR spectroscopy. This was a straightforward conversion to follow by ¹¹B NMR spectroscopy, as both the starting material and product had distinct NMR handles, a doublet at 28.4 ppm for HBpin and the new B-O bond formed product gave rise to a singlet typically in the region of 22-23 ppm. For preliminary reactions the conversion was calculated by the consumption of HBpin along with the identity of the product RR'CHOBpin resonance in both the ¹¹B and ¹H NMR spectra. In the case of benzophenone a conversion of greater than 99% was observed in the ¹¹B NMR spectrum within a short reaction time of 30 minutes. Encouraged by this promising result, the scope of ketones was expanded, to probe the influence of electron donating groups, electron withdrawing groups and possible steric factors. The NMR yields reported were calculated relative to an internal standard, hexamethylcyclotrisiloxane, [C₆H₁₈O₃Si₃]. The findings are summarized in Table 4.1.

Table 4.1: Catalytic hydroboration of ketones using **1** as a (pre)catalyst in d_6 -benzene.

Entry	Ketone	Time (h)	Yield by $^1\text{H NMR}$ (%) ^a
1		0.5	97
2		0.25	>99
3		0.25	>99
4		0.25	>99
5		0.25	97
6		0.25	>98
7		24 ^b	89

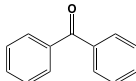
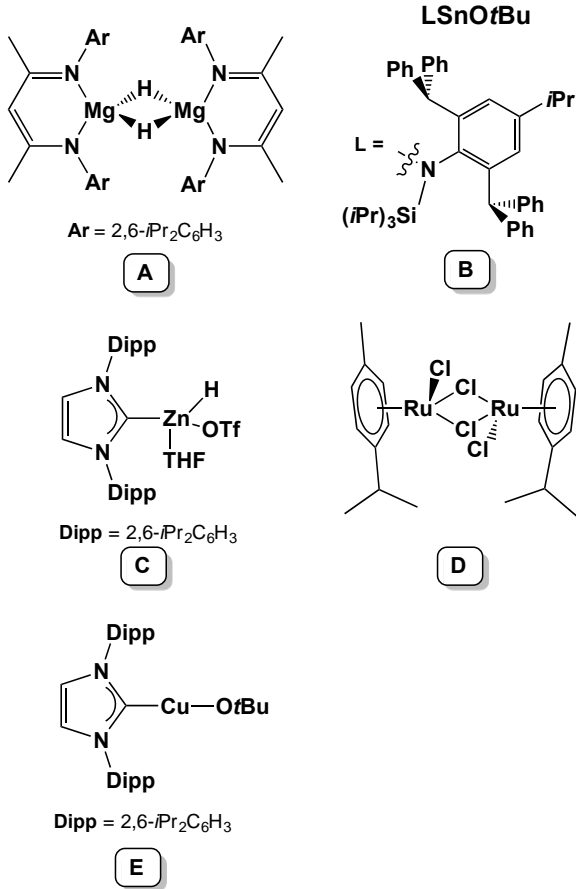
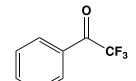
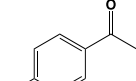
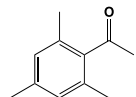
^a = yield determined by formation of $\text{RR}'\text{CHOBpin}$ in $^1\text{H NMR}$ spectrum relative to internal standard hexamethylcyclotrisiloxane. ^b = heated at 70°C .

Table 4.1 entries 1-7 highlight the robustness and stability of the catalytic reaction to several functional groups. Variations of substituted acetophenones were examined, 2-phenylacetophenone (entry 2), 2,2,2-trifluoroacetophenone (entry 3), 4-iodoacetophenone (entry 4) and 2,4,6-trimethylacetophenone (entry 7), all of which underwent successful hydroboration. Hydroboration of the alkyl-aryl ketone 2-phenylacetophenone achieves full conversion within 15 minutes. However some key points regarding the capabilities of the catalyst can be taken here when comparing the other derivatives. For example, hydroboration of 2,2,2-trifluoroacetophenone and 4-iodoacetophenone gave quantitative yields within 15 minutes (entry 3 and 4),

highlighting the tolerance of halides, with no lithium-halogen exchange being observed under these reaction conditions. In contrast, moving to the more sterically encumbered 2,4,6-trimethylacetophenone (entry 7) a notable influence of having methyl substituents in the ortho-position of the carbonyl was observed, with forcing reaction conditions required, namely 70°C for 24 hours. This can be attributed to the steric hindrance in this ketone, which appears to slow down the process either by inhibiting the hydrometallation step and/or by preventing the reformation of the active catalytic species. Acetylferrocene and 2-benzoylpyridine also cleanly convert to the hydroborated product in yields of greater than 95% within a short reaction time of 15 minutes. A noteworthy feature here is the selectivity observed with 2-benzoylpyridine which exclusively hydroborates at the ketone functionality. Given the nature of our catalyst **1**, to release and uptake lithium hydride across a pyridyl species, no interference with the pyridyl ring of the substrate was observed. From this study of ketones, the LiDHP catalyst stands as a strong competitor in the catalytic arena. Some key catalysts that have been reported to carry out these reactions catalytically have been compared with our results in table 4.2.

As summarised in table 4.2 it can be seen that the yields are competitive with those in the literature,^[46,49,51,58,76] the most noteworthy difference is the catalyst loading which in the case of **1** was limited to 5 mol% for practical accuracy opposed to reactivity. In the case of benzophenone, entry 1-1e table 4.2, shows the various catalyst loadings that can be employed, with some as low as 0.1 mol%. This comes with a slight penalty as in entry 1e the loading has been reduced to 0.1 mol% but it requires double the reaction time compared with **1**. The tin (pre)catalyst [LSnOtBu] where L = N(Ar)(SiⁱPr₃), Ar = C₆H₂{C(H)Ph₂}₂ⁱPr-2,6,4) outperforms catalyst **1** slightly, where it performs the hydroboration of 2,2,2-trifluoroacetophenone in less than 10 minutes at room temperature with as little as 0.1 mol%, compared to 15 minutes with 5 mol% for **1**. Again in entry 3 and 3a it can be seen the only changing factor is the catalyst loading which in our case employing 5 mol% results in a four-fold improvement on reaction time. Hill's alkyl magnesium catalyst A (entry 4a) outperforms catalyst **1** for 2,4,6-trimethylacetophenone. Although it requires longer reaction times than those required

Table 4.2: Comparison of catalyst **1** with reported comparable catalysts of hydroboration of ketones.

Entry	Substrate	Catalyst	Catalyst Loading (mol%)	Temperature	Time (h)	Yield (%)	Chemdraw representation of catalysts
1		1	5	RT	0.5	97	 <p>Ar = 2,6-<i>i</i>Pr₂C₆H₃</p> <p>Dipp = 2,6-<i>i</i>Pr₂C₆H₃</p>
1a		A	0.1	RT	2	98	
1b		B	0.5	RT	2.5	95	
1c		C	1	RT	0.25	91	
1d		D	0.1	60 °C	15	65	
1e		E	0.1	RT	1	94	
2		1	5	RT	0.25	>99	
2a		B	0.5	RT	<0.15	>99	
3		1	5	RT	0.25	>99	
3a		E	0.1	RT	1	>99	
4		1	5	70 °C	24	89	
4a		A	1	RT	1.25	93	
4b		D	0.1	60 °C	15	89	

for other ketones (1.25 h) and a slightly higher catalyst loading (1 mol%), this NacNac supported catalyst still displays improved reaction conditions than our catalyst **1** (5 mol% and 24 hours at 70°C).

4.4.2 Hydroboration of aldehydes

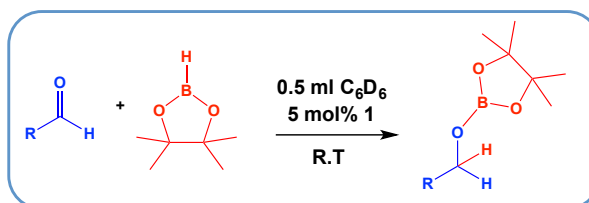
Next we turned our attention to aldehydes, adopting the same conditions as before, namely 5 mol% catalyst loading in 0.5ml of d₆-benzene at room temperature unless otherwise required. A range of aromatic substituted benzaldehydes were tested as summarised in table 4.3: these were benzaldehyde (entry 1), 2-methoxybenzaldehyde (entry 2), 4-bromobenzaldehyde (entry 3) and mesitaldehyde (entry 4). All of these aldehydes were cleanly converted to the protected alcohol in almost quantitative yields. A comparison can be made between them. The unsubstituted benzaldehyde reaches a yield of about 99% in 15 minutes, but placing a methoxy group in one of the *ortho* positions decreases the yield ever so slightly to 93% in 15 minutes, which could be attributed to a weak steric and/or coordination effect of the electron donating substituent. In the case of 4-bromobenzaldehyde, a 99% yield was observed confirming the functional group tolerance of the catalyst. Again when the aromatic group is heavily substituted such as in mesitaldehyde (entry 4) a considerably extended reaction time of 24 hours was necessary to overcome the steric hindrance. Moving to 2-naphthaldehyde and ferrocene carboxaldehyde (entries 5 and 6), greater than 95% conversions to the hydroborated product were recorded.

The scope of aldehydes covers a broad mixture of those presented in the literature. Again when comparing the values with those previously reported as a benchmark, the main difference is the higher catalyst loading employed in our conditions.^[46,49,51,58,76] The main aim from this work was to establish that lithium could be utilised in another catalytic system. The results employing our catalyst are compared and summarised with those in the literature in table 4.4, where we can conclude the yields are in the same ballpark as those achievable with tin, ruthenium, copper and magnesium.

In some cases it is notable that the increased catalyst loading decreases the reaction time for example, entry 3-3c, where Jones's [LSnOtBu] catalyst (0.05 mol%) requires over four hours, Gunanathan's [$\{\text{Ru}(p\text{-cymene})\text{Cl}_2\}_2$] catalyst (0.1 mol%) takes three

hours and Mankad's copper (pre)catalyst [(IPr)CuOtBu] (0.1 mol%) takes one hour to obtain only 89% compared to full conversion within 0.25 hours when **1** (5 mol%) is employed.

Table 4.3: Catalytic hydroboration of aldehydes using **1** as a (pre)catalyst.

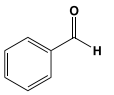
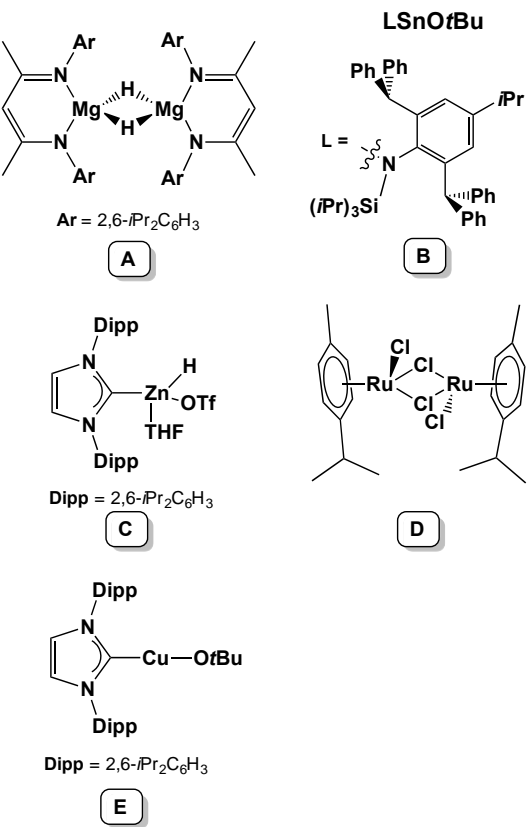
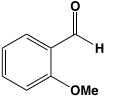
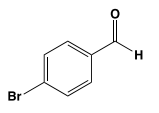
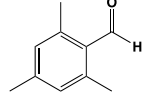
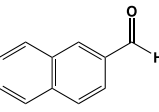
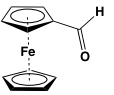


Entry	Aldehyde	Time (h)	Yield by ¹ H NMR (%) ^a
1		0.25	>99
2		0.25	93
3		0.25	>99
4		24 ^b	>99
5		0.25	98
6		0.25	>99

^a = yield determined by formation of RCH₂OBpin in ¹H NMR spectrum relative to internal standard hexamethylcyclotrisiloxane. ^b = heated at 70°C.

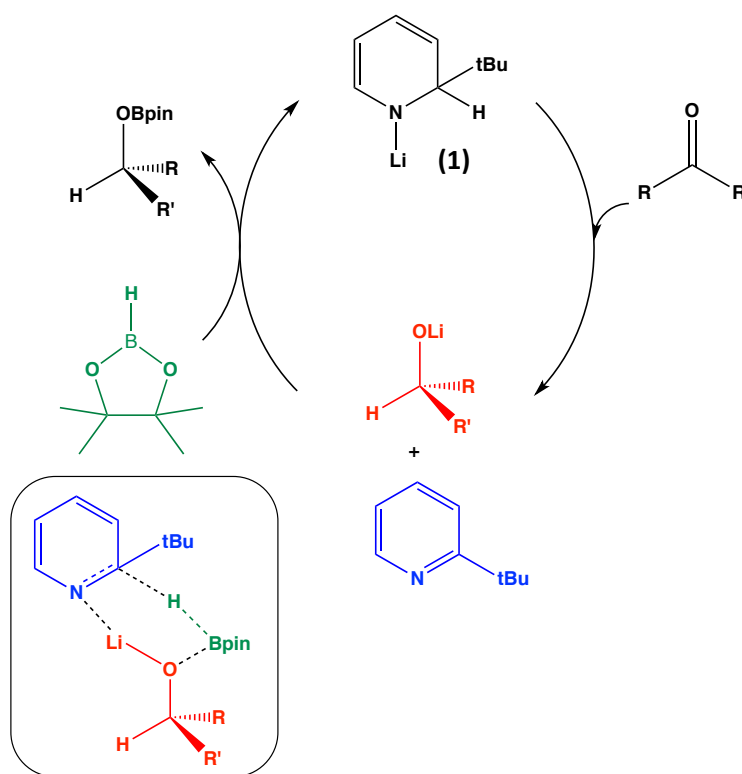
There is a trend with sterically demanding substituted aromatics whereby the hydroboration is sluggish. For mesitaldehyde, all the catalysts discussed require longer reaction times, though **1** cannot compete with these conditions, as it requires 24 hours at 70°C. 2-Naphthaldehyde displays a reasonable improvement in reaction time, at 0.25 hours compared with four hours for the ruthenium catalyst. The performance of **1** with the organometallic substituted aldehyde, ferrocene carboxaldehyde essentially mirrors that of the magnesium catalyst (see entries 6 and 6a) in realising a 99% yield after 15 minutes.

Table 4.4: Comparison of catalyst **1** with reported comparable catalysts of hydroboration of aldehydes.

Entry	Substrate	Catalyst	Cat Loading (mol%)	Temp	Time (h)	Yield (%)	Chemdraw representation of catalysts
1		1	5	RT	0.5	97	 <p>Ar = 2,6-<i>i</i>Pr₂C₆H₃</p> <p>Dipp = 2,6-<i>i</i>Pr₂C₆H₃</p> <p>Dipp = 2,6-<i>i</i>Pr₂C₆H₃</p>
1a		A	0.05	RT	0.25	95	
1b		B	1	RT	1.5	>99	
2		1	5	RT	0.25	>99	
2a		A	0.5	RT	1	97	
3		1	5	RT	0.25	>99	
3a		B	0.05	RT	4.5	>99	
3b		D	0.1	RT	3	>99	
3c		E	0.1	RT	1	87	
4		1	5	70°C	24	89	
4a		A	0.5	RT	1.25	96	
4b		D	0.1	RT	4	>99	
4c		E	0.1	RT	1	96	
5		1	5	RT	0.25	98	
5a		D	0.1	RT	4	99	
6		1	5	RT	0.25	>99	
6a		A	0.05	RT	0.2	98	

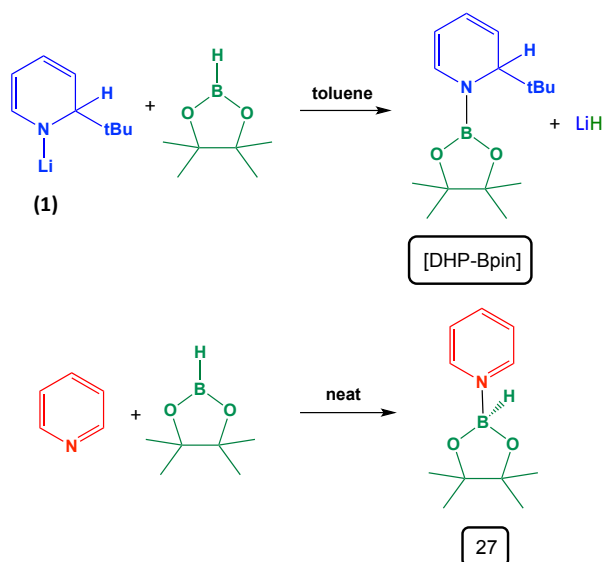
4.4.3 Proposed reaction pathway

Taking into account the typically accepted reaction pathway for hydroboration of carbonyls as discussed in section 4.2.2, it would be reasonable to propose the mechanism depicted in [scheme 4.7](#) for the dihydropyridine system. The first step involves the reduction of the carbonyl functionality to give a hydrolithiated species and the rearomatised co-product 2-*tert*-butylpyridine. This would then be followed by a metathesis step with HBpin to form the hydroborated product and regenerate the catalyst.



Scheme 4.7: Proposed reaction mechanism for hydroboration of carbonyls based upon literature.^[46,53,58]

In an attempt to shed light on the pathway for this transformation, a series of control reactions were carried out. As a starting point the reactivity of catalyst **1** towards HBpin was tested by a stoichiometric reaction in toluene solution ([Scheme 4.8](#)). As it is known that dihydropyridine species and their parent aromatic counterparts would be present during the course of the reaction, the reactivity between HBpin and pyridine was also investigated to determine if there was the possibility of side reactions involving hydroboration of pyridines ([Scheme 4.8](#)).



Scheme 4.8: Stoichiometric reaction HBpin with **1** (top) or pyridine (bottom).

The stoichiometric reaction between the catalyst **1** and HBpin in toluene resulted in a complete transelementation giving lithium hydride and [DHP-Bpin] as confirmed by ^1H and ^{11}B NMR spectroscopic analysis. As can be observed in figure 4.4 the original five dihydropyridine resonances corresponding to **1** have disappeared and have been replaced by five new dihydropyridyl resonances attributed to the installation of a Bpin moiety on the DHP ring with elimination of LiH.

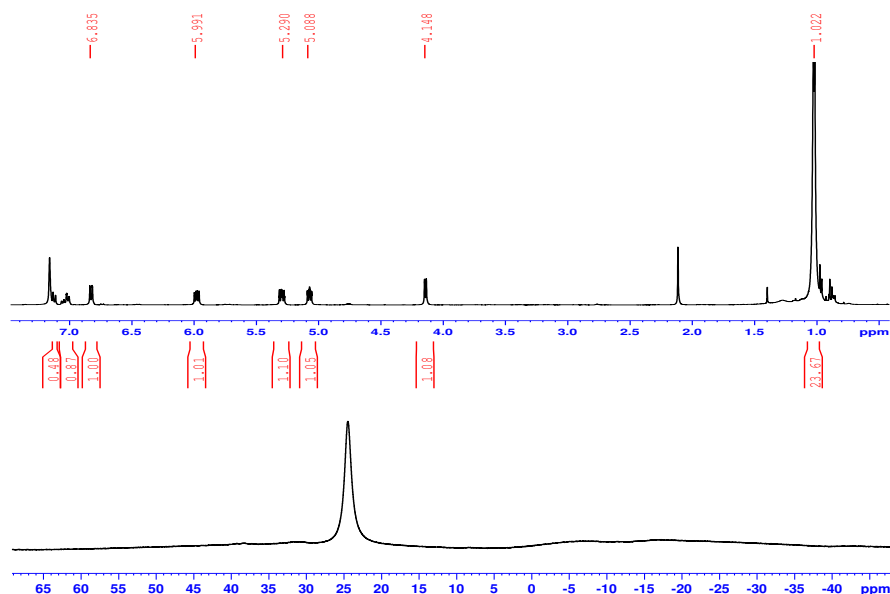


Figure 4.4: ^1H (top) and ^{11}B (bottom) NMR spectra illustrating transformation of HBpin to [DHP-Bpin] upon reaction with **1**.

Additionally, the ^{11}B NMR spectrum is indicative of a new species showing as a singlet observed at δ 24.5 ppm typical of a B-N bond in a hydroborated pyridine complex, (ca. 24ppm).^[75]

The reaction of pyridine and HBpin was probed next, as hydroboration of pyridine was considered to be a potential side reaction, although not thought to occur readily. Thus, stoichiometric reaction of neat pyridine and HBpin resulted in a colourless liquid that upon cooling to -30°C resulted in a crop of colourless crystals. X-ray crystallographic studies of these crystals revealed the molecular structure to be of the unknown simple donor-acceptor adduct $[\text{HBpin}\cdot\text{NC}_5\text{H}_5]$ **27**, thereby supporting the view that hydroboration and concomitant dearomatisation do not readily occur. The adduct shown in figure 4.5 was isolated in a 57% yield. This modest yield reflects more the volatile nature of the product rather than an incomplete reaction. The boron atom B1 assumes a distorted tetrahedral geometry with respect to N1, O1, O2 and H1 with bond angles spanning the range $103.4(9)$ - $116.7(9)^\circ$. Surprisingly given the relative simplicity of this adduct, a search of the Cambridge structural database^[78] revealed zero matches for a $\text{HB}(\text{O})_2$ unit bonded to pyridine.

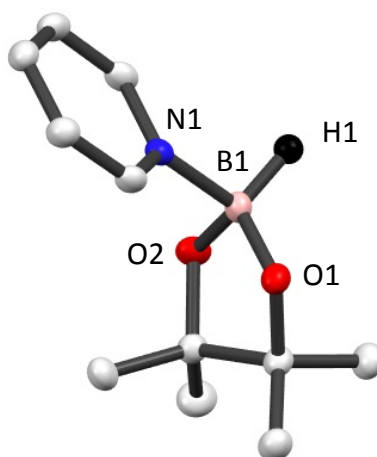
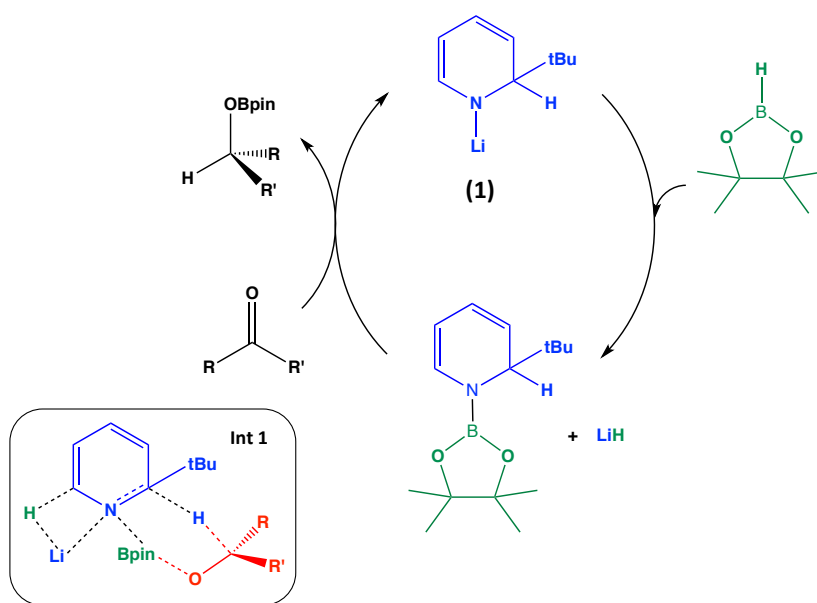


Figure 4.5: Molecular structure of **27** with displacement ellipsoids at 30% probability level, hydrogen atoms other than that attached to boron are omitted for clarity. Selected bond lengths (\AA) and bond angles ($^\circ$): B1-N1, 1.651(2), B1-O1, 1.442(2); B1-O2, 1.452(2); B1-H1, 1.164(18); N1-B1-O1, 107.76(13); N1-B1-O2, 108.41(13); N1-B1-H1, 103.4(9); O1-B1-O2, 107.45(15); O1-B1-H1, 116.7(9); O2-B1-H1, 112.6(9).

NMR spectroscopic analysis of these crystals proved challenging due to the sensitive nature of the species, which decomposed to an oil when placed under vacuum before storing in an inert atmosphere glovebox. ^{11}B NMR spectra of the sample revealed two products, a doublet at 28.3 ppm attributed to the desired product **27** and a singlet at 23.9 ppm suggesting some hydroboration of pyridine can occur over time. The ^1H NMR spectrum was consistent with this interpretation as it contains three aromatic signals correlating to pyridine at 8.53, 7.01, and 6.68 ppm. There are also some very weak resonances in the region of 3-6 ppm that could be proposed to be hydroborated dearomatised pyridine.

Concluding these reactions an alternative concerted pathway could be postulated including the formation of [DHP-Bpin]. As illustrated in [scheme 4.9](#), the first step would involve a transelementation, where the Bpin would anchor itself on the dihydropyridyl ring with the elimination of lithium hydride. Addition of the substrate at this stage would result in an intermediate such as ([Int 1](#) [scheme 4.9](#)) that would release the product and regenerate the catalyst. A control reaction with *in-situ* [DHP-Bpin] and benzophenone was monitored to determine if the transformation to the hydroborated product would occur. The ^{11}B NMR spectrum revealed a singlet at δ 23 ppm corresponding to the protected benzhydrol.



Scheme 4.9: Alternative postulated pathway for catalytic hydroboration of carbonyls by **1**.

An aspect of this catalytic manifold that deems it unlikely to be the dominant mechanism is based upon consideration of the elimination of lithium hydride. At this stage there is no free parent pyridine to uptake the lithium hydride and maintain its solubility, hence it could be predicted that polymeric aggregates could form that would precipitate from the reaction solution. As a result, one may expect the catalytic system in [scheme 4.7](#) to be the favoured route as lithium hydride is generated in the presence of an aromatic parent pyridine, which it can readily add across to form a dihydropyridine derivative that could continue the catalytic regime.

4.5 Conclusions and future work

This study establishes another catalytic regime usually performed by transition metal catalysts that lithium can mimic. Other main group catalysts have demonstrated the catalytic hydroboration of carbonyls and here we add lithium to the list. Considering the simplicity and cost effectiveness of the preparation of the lithium dihydropyridine catalyst, the slightly higher catalyst loading required is not off-putting, given the exceptionally high yields and functional group tolerance exhibited. The only significant downside of this catalyst is its decrease in reactivity when there is steric hindrance around the carbonyl functionality, though this can be overcome by heating the reaction mixture to 70°C. At the moment this reaction is limited to carbonyl substrates, but given the demands of boronic esters in cross coupling reactions it would be invaluable to extend this to unsaturated hydrocarbons, and more challenging inactivated substrates including nitriles and imines.

The mechanism for this transformation would be in agreement with the typical insertion/metathesis route proposed in the literature, albeit in this case the pyridine and dihydropyridine play a crucial role in acting as a metal hydride transport vessel for uptake and release, respectively. A potential second pathway has been suggested proceeding via a [DHP-Bpin] intermediate species. Unfortunately due to the rapid reactivity of these transformations, a kinetic experimental study was not feasible to provide greater insight into the mechanism. However, this could be a topic that is probed in the future exploring the active dihydropyridine species within catalytic systems.

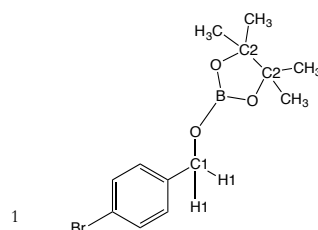
4.6 Experimental

4.6.1 General catalytic hydroboration procedure

The typical protocol involved adding the substrate (0.5 mmol) to a J. Youngs tube along with 0.5 mL of 0.1M solution of the internal reference standard hexamethylcyclotrisiloxane (10 mol%) and the first ^1H NMR data recorded. HBpin (0.5 mmol, 73 μL) was added along with **1** (5 mol%, 3.6 mg), and then the reaction was monitored by ^1H and ^{11}B NMR spectroscopy.

4.6.2 Characterisation of hydroborated aldehydes

4-bromobenzaldehyde

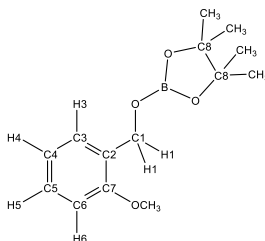


^1H NMR (400.1 MHz, C_6D_6 , 300K): δ 7.22 (2H, d, $^3J_{\text{H-H}} = 8.31$ Hz, Ar-H), 6.93 (2H, d, $^3J_{\text{H-H}} = 8.31$ Hz, Ar-H), 4.73 (2H, s, H1, C1), 1.03 (12H, s, CH_3 of Bpin) ppm.

^{11}B NMR (128.38 MHz, C_6D_6 , 300K): δ 22.8 (s, Bpin) ppm.

^{13}C NMR (100.62 MHz, C_6D_6 , 300K): δ 138.9 (quat Ar-C), 131.7 (Ar-C), 128.7 (Ar-C), 121.5 (quat Ar-C), 82.9 (C2), 66.1 (C1), 24.7 (CH_3 of Bpin) ppm.

2-methoxybenzaldehyde

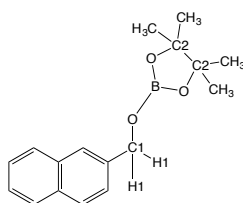


^1H NMR (400.1 MHz, C_6D_6 , 300K): δ 7.66 (1H, d, $^3J_{\text{H-H}} = 7.29$ Hz, H3), 7.07 (1H, t, $^3J_{\text{H-H}} = 8.12$ Hz, H5), 6.89 (1H, t, $^3J_{\text{H-H}} = 7.46$ Hz, H4), 6.48 (1H, t, $^3J_{\text{H-H}} = 8.18$ Hz, H6), 5.29 (2H, s, H1), 3.24 (3H, s, OCH_3), 1.05 (12H, s, CH_3 of Bpin) ppm.

^{11}B NMR (128.38 MHz, C_6D_6 , 300K): 22.9 (s, OBpin) ppm.

^{13}C NMR (100.62 MHz, C_6D_6 , 300K): δ 156.8 (C7), 128.4 (C5), 127.5 (C3), 120.8 (C4), 110.1 (C6), 82.7 (C8), 62.6 (C1), 54.7 (OCH_3), 24.7 (CH_3 of Bpin) ppm.

2-naphthaldehyde

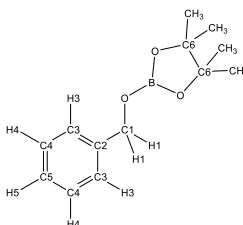


¹H NMR (400.1 MHz, C₆D₆, 300K): δ 7.77 (1H, s, Ar-*H*), 7.62-7.56 (3H, m, Ar-*H*), 7.39 (1H, d, Ar-*H*), 7.25-7.21 (2H, m, Ar-*H*), 5.10 (2H, s, H1), 1.05 (12H, s, CH₃ of Bpin) ppm.

¹¹B NMR (128.38 MHz, C₆D₆, 300K): δ 22.9 (s, OBpin) ppm.

¹³C NMR (100.62 MHz, C₆D₆, 300K): δ 137.5 (quat Ar-C), 134.0 (quat Ar-C), 133.4 (quat Ar-C), 128.4 (Ar-C), 128.3 (Ar-C), 128.0 (Ar-C), 126.2 (Ar-C), 125.9 (Ar-C), 125.7 (Ar-C), 125.3 (Ar-C), 82.8 (C2), 67.1 (C1), 24.7 (CH₃ of Bpin) ppm.

Benzaldehyde

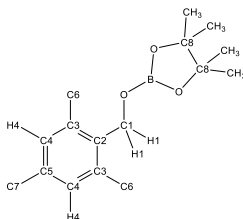


¹H NMR (400.1 MHz, C₆D₆, 300K): δ 7.30 (2H, d, H3), 7.17-7.09 (2H, m, H4), 7.08-7.02 (1H, m, H5), 4.95 (2H, s, H1), 1.04 (12H, s, CH₃ of Bpin) ppm.

¹¹B NMR (128.38 MHz, C₆D₆, 300K): δ 22.8 (s, OBpin) ppm.

¹³C NMR (100.62 MHz, C₆D₆, 300K): δ 140.0 (C2), 128.6 (C4), 127.6 (C5), 127.1 (C3), 82.7 (C6), 67.0 (C1), 24.7 (CH₃) ppm.

Mesitaldehyde

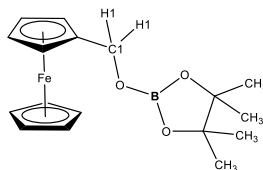


¹H NMR (400.1 MHz, C₆D₆, 300K): δ 6.71 (2H, br s, H4), 4.99 (2H, s, H1), 2.34 (6H, s, *o*-CH₃), 2.10 (3H, s, *p*-CH₃) and 1.03 (12H, s, CH₃ of Bpin) ppm.

¹¹B NMR (128.38 MHz, C₆D₆, 300K): δ 22.6 (OBpin) ppm.

^{13}C NMR (100.62 MHz, C_6D_6 , 300K): δ 136.9 (quat Ar-C), 132.1 (quat Ar-C), 128.4 (Ar-C), 81.6 (C8), 60.6 (C1), 23.8 (CH_3 of Bpin), 20.1 (CH_3) and 18.7 (CH_3) ppm.

Ferrocenecarboxaldehyde



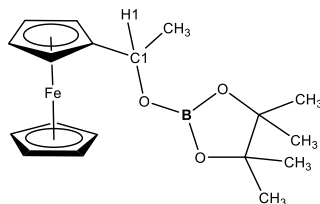
^1H NMR (400.1 MHz, C_6D_6 , 300K): δ 4.74 (2H, s, H1), 4.20 (2H, t, H), 3.98 (5H, s, Cp ring), 3.95 (2H, t, H), 1.07 (12H, s, CH_3 of Bpin) ppm.

^{11}B NMR (128.38 MHz, C_6D_6 , 300K): δ 22.6 (OBpin) ppm.

^{13}C NMR (100.62 MHz, C_6D_6 , 300K): δ 86.1 (C2), 82.6 (C6), 69.0 (C4), 68.8 (C5), 68.5 (C3), 63.4 (C1), 24.8 (CH_3 of Bpin) ppm.

4.6.3 Characterisation of hydroborated ketones

Acetylferrocene

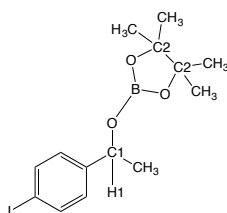


^1H NMR (400.1 MHz, C_6D_6 , 300K): δ 5.28 (1H, q, H), 4.34 (1H, m, H), 4.08 (1H, m, H), 4.06 (5H, s, Cp ring), 3.97-3.95 (2H, m, H), 1.49 (3H, d, CH_3), 1.09 (12H, s, CH_3 of Bpin) ppm.

^{11}B NMR (128.38 MHz, C_6D_6 , 300K): δ 22.5 (OBpin) ppm.

^{13}C NMR (100.62 MHz, C_6D_6 , 300K): δ 92.5 (quat Cp-C), 82.6 (C2), 69.3 (Cp ring), 68.0 (Cp-C), 67.5 (Cp-C), 66.1 (Cp-C), 24.8 (CH_3 of Bpin), 24.0 (CH_3) ppm.

4-iodoacetophenone

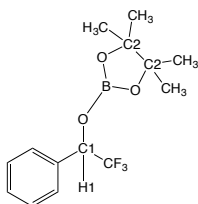


$^1\text{H NMR}$ (400.1 MHz, C_6D_6 , 300K): δ 7.43 (2H, d, Ar-H), 6.87 (2H, d, Ar-H), 5.21 (1H, q, H1), 1.32 (3H, d, CH_3) and 1.00 (12H, d, CH_3 of Bpin) ppm.

$^{11}\text{B NMR}$ (128.38 MHz, C_6D_6 , 300K): δ 22.5 (OBpin) ppm.

$^{13}\text{C NMR}$ (100.62 MHz, C_6D_6 , 300K): δ 137.7 (Ar-C), 127.7 (Ar-C), 92.7 (quat Ar-C), 82.7 (C2), 72.3 (C1), 25.6 (CH_3) and 24.7 (CH_3 of Bpin) ppm.

2,2,2-trifluoroacetophenone

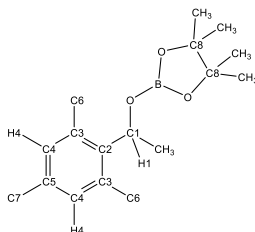


$^1\text{H NMR}$ (400.1 MHz, C_6D_6 , 300K): δ 7.41-7.35 (2H, m, H), 7.06-6.99 (3H, m, H), 5.56 (1H, q, H), 0.95 (12H, d, CH_3 of Bpin) ppm.

$^{11}\text{B NMR}$ (128.38 MHz, C_6D_6 , 300K): δ 22.9 (OBpin) ppm.

$^{13}\text{C NMR}$ (100.62 MHz, C_6D_6 , 300K): δ 133.9 (quat Ar-C), 129.5 (Ar-C), 128.7 (Ar-C), 127.9 (Ar-C), 83.7 (C2), 75.1 (C1), 24.4 (CH_3 of Bpin) ppm.

2,4,6-trimethylacetophenone

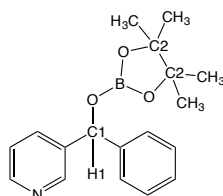


$^1\text{H NMR}$ (400.1 MHz, C_6D_6 , 300K): δ 6.73 (2H, br s, H4), 5.87 (1H, br s, H1), 2.48 (6H, br s, *o*- CH_3), 2.10 (3H, br s, *p*- CH_3), 1.54 (3H, br s, CH_3) and 0.99 (12H, br s, CH_3 of Bpin) ppm.

$^{11}\text{B NMR}$ (128.38 MHz, C_6D_6 , 300K): δ 22.4 (OBpin) ppm.

¹³C NMR (100.62 MHz, C₆D₆, 300K): δ 137.4 (quat Ar-C), 136.1 (quat Ar-C), 135.8 (quat Ar-C), 130.3 (Ar-C), 82.4 (C8), 70.3 (C1), 24.7 + 24.5 (CH₃ of Bpin), 22.0 (CH₃), 20.8 (*o*- + *p*-CH₃) ppm.

2-benzoylpyridine

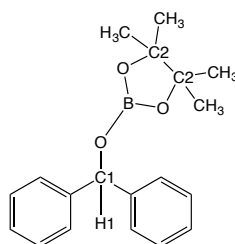


¹H NMR (400.1 MHz, C₆D₆, 300K): δ 8.29 (1H, d, Py-H), 7.52 (2H, d, Ar-H), 7.06 (2H, t, Ar-H), 6.98 (2H, m, Py-H), 6.59 (1H, t, Ar-H), 6.14 (1H, s, H1) and 1.28 (12H, s, CH₃ of Bpin) ppm.

¹¹B NMR (128.38 MHz, C₆D₆, 300K): δ 16.2 (OBpin) ppm

¹³C NMR (100.62 MHz, C₆D₆, 300K): δ 162.2 (quat Ar-C), 143.5 (Ar-C), 142.8 (quat Ar-C), 139.1 (Ar-C), 128.6 (Ar-C), 127.8 (Ar-C), 127.1 (Ar-C), 123.1 (Ar-C), 120.5 (Ar-C), 81.0 (C2), 78.7 (C1) and 24.9 (CH₃ of Bpin) ppm.

Benzophenone

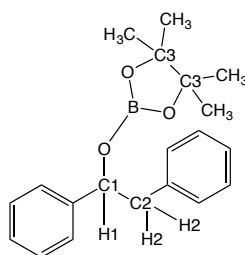


¹H NMR (400.1 MHz, C₆D₆, 300K): δ 7.45 (4H, d, Ar-H), 7.09 (4H, t, Ar-H), 7.00 (2H, t, Ar-H), 6.43 (1H, s, H1), 0.98 (12H, s, CH₃ of Bpin) ppm.

¹¹B NMR (128.38 MHz, C₆D₆, 300K): δ 22.9 (OBpin) ppm.

¹³C NMR (100.62 MHz, C₆D₆, 300K): δ 143.9 (quat Ar-C), 128.6 (Ar-C), 127.5 (Ar-C), 127.0 (Ar-C), 82.8 (C2), 78.6 (C1), 24.6 (CH₃ of Bpin) ppm.

2-phenylacetophenone



^1H NMR (400.1 MHz, C_6D_6 , 300K): δ 7.33 (2H, d, Ar-H), 7.16-7.10 (6H, m, Ar-H), 7.09-7.01 (2H, m, Ar-H), 5.47 (1H, q, H1), 3.08-2.89 (2H, m, H2), 0.89 (12H, d, CH_3 of Bpin) ppm.

^{11}B NMR (128.38 MHz, C_6D_6 , 300K): δ 22.1 (OBpin) ppm.

^{13}C NMR (100.62 MHz, C_6D_6 , 300K): δ 143.7 (quat Ar-C), 138.7 (quat Ar-C), 130.3 (Ar-C), 128.5 (Ar-C), 128.4 (Ar-C), 127.6 (Ar-C), 126.5 (Ar-C), 126.3 (Ar-C), 82.5 (C3), 78.0 (C1), 46.6 (C2), 24.5 (CH_3 of Bpin) ppm.

4.6.3 Crystallographic data and refinement details of compound 27

Table 4.5: Crystallographic data and refinement details for compound 27.

	27
Empirical formula	$\text{C}_{11}\text{H}_{16}\text{BNO}_2$
Mol. Mass	207.1
Crystal system	monoclinic
Space group	C c
Temperature (K)	119.5
a/ Å	17.3528(17)
b/ Å	7.5795(4)
c/ Å	11.1117(13)
α/o	90
β/o	126.698(16)
γ/o	90
$V/\text{Å}^3$	1171.8(3)
Z	4
$\lambda/\text{Å}$	0.71073
Measured reflections	5806
Unique reflections	2672
Rint	0.0337
Observed rflns [$I > 2\sigma(I)$]	2324
GooF	1.038
R [on F, obs rflns only]	0.0402
ωR [on F^2 , all data]	0.0884
Largest diff. peak/hole $e/\text{Å}^{-3}$	0.21/-0.18

4.7 References

- [1] A. J. J. Lennox and G. C. Lloyd-Jones, *Chem. Soc. Rev.* **2014**, *43*, 412-443.
- [2] D. Gao and G. A. O'Docherty, *Org. Lett.* **2010**, *12*, 3752-3755.
- [3] H. C. Brown, H. I. Schlesinger, and A. B. Burg, *J. Am. Chem. Soc.* **1939**, *61*, 673-680.
- [4] H. C. Brown and B. C. S. Rao, *J. Am. Chem. Soc.* **1956**, *78*, 5694-5695.
- [5] B. M. Trost and I. Fleming, in *Comprehensive Organic Synthesis selectivity, strategy & Efficiency in Modern Organic Chemistry*, Vol. 8 Reduction, Pergamon, Oxford, **1993**.
- [6] "The Nobel Prize in Chemistry 1979". Nobelprize.org. Nobel Media AB 2014. Web. 25 Jan 2017. http://www.nobelprize.org/nobel_prizes/chemistry/laureates/1979/
- [7] R. Köster, *Angew. Chem. Int. Ed.* **1960**, *72*, 626-627.
- [8] J. A. Soderquiet and H. C. Brown, *J. Org. Chem.* **1981**, *46*, 4599-4600.
- [9] E. R. Burkhardt and K. Matos, *Chem. Rev.* **2006**, *106*, 2617-2650.
- [10] C. E. Tucker, J. Davidson, and P. Knochel, *J. Org. Chem.* **1992**, *57*, 3482-3485.
- [11] C. M. Crudden and D. Edwards, *Eur. J. Inorg. Chem.* **2003**, 4695-4712.
- [12] I. P. Query, P. A. Squier, E. M. Larson, N. A. Isley, and T. B. Clark, *J. Org. Chem.* **2011**, *76*, 6452-6456.
- [13] A. Suzuki, *Angew. Chem. Int. Ed.* **2011**, *50*, 6722-6737.
- [14] N. Miyaura and A. Suzuki, *Chem. Rev.* **1995**, *95*, 2457-2483.
- [15] M. Shimizu, C. Nakamaki, K. Shimono, M. Schelper, T. Kurahashi and T. Hiyama, *J. Am. Chem. Soc.* **2005**, *127*, 12506-12507.
- [16] A. Suzuki, *Chem. Commun.* **2005**, 4759-4763.
- [17] F. Liron, C. Fosse, A. Pernolet and E. Roulland, *J. Org. Chem.* **2007**, *72*, 2220-2223.
- [18] N. A. Weires, E. L. Baker and N. K. Garg, *Nature Chem.* **2016**, *8*, 75-79.
- [19] K. M. Logan and M. K. Brown, *Angew. Chem. Int. Ed.* **2017**, *56*, 851-855.
- [20] F. Almqvist, L. Torstensson, A. Gudmundsson and T. Frejd, *Angew. Chem. Int. Ed.* **1997**, *36*, 376-377.
- [21] A. J. Blake, A. Cunningham, A. Ford, S. J. Teat and S. Woodard, *Chem. Eur. J.* **2000**, *6*, 3586-3594.
- [22] I. Sarvary, F. Almqvist and T. Frejd, *Chem. Eur. J.* **2001**, *7*, 2158-2166.
- [23] M. A. Reichle and B. Breit, *Angew. Chem. Int. Ed.* **2012**, *51*, 5730-5734.

- [24] N. Miyaura, T. Ishiyama, H. Sasaki, M. Ishikawa, M. Satoh, and A. Suzuki, *J. Am. Chem. Soc.* **1989**, *111*, 314-321.
- [25] D. Männig and H. Nöth, *Angew. Chem. Int. Ed.* **1985**, *24*, 878-879.
- [26] R. Wilczynski and L. G. Sneddon, *Inorg. Chem.* **1981**, *20*, 3955-3962.
- [27] R. Wilczynski and L.G. Sneddon, *Inorg. Chem.* **1982**, *21*, 506-514.
- [28] T. Davan, E. W. Corcoran Jr. and L. G. Sneddon, *Organometallics*, **1983**, *2*, 1693-1694.
- [29] J. D. Hewes, C. W. Kreimendahl, T. B. Marder and M. F. Hawthorne, *J. Am. Chem. Soc.* **1984**, *106*, 5757-5759.
- [30] D. A. Evans and G. C. Fu, *J. Org. Chem.* **1990**, *55*, 2280-2282.
- [31] D. A. Evans, G. C. Fu and B. A. Anderson, *J. Am. Chem. Soc.* **1992**, *114*, 6679-6685.
- [32] K. Burgess, W. A. van der Donk, S. A. Westcott, T. B. Marder, R. T. Baker and J. C. Calabrese, *J. Am. Chem. Soc.* **1992**, *114*, 9350-9359.
- [33] S. A. Westcott, H. P. Blom, T. B. Marder and R. T. Baker, *J. Am. Chem. Soc.* **1992**, *114*, 8863-8869.
- [34] D. A. Evans, G. C. Fu and A. H. Hoveyda, *J. Am. Chem. Soc.* **1992**, *114*, 6671-6679.
- [35] T. Ohmura, Y. Yamamoto and N. Miyaura, *J. Am. Chem. Soc.* **2000**, *122*, 4990-4991.
- [36] Y. Yamamoto, R. Fujikawa, T. Umemoto and N. Miyaura, *Tetrahedron*, **2004**, *60*, 10695-10700.
- [37] K. Oshima, T. Ohmura and M. Suginome, *J. Am. Chem. Soc.* **2012**, *134*, 3699-3702.
- [38] D. R. Edwards, Y. B. Hleba, C. J. Lata, L. A. Calhoun and C. M. Crudden, *Angew. Chem. Int. Ed.* **2007**, *46*, 7799-7802.
- [39] M. Morimoto, T. Miura, and M. Murakami, *Angew. Chem. Int. Ed.* **2015**, *54*, 12659-12663.
- [40] S. Pereira and M. Srebnik, *Organometallics*, **1995**, *14*, 3127-3128.
- [41] S. Pereira and M. Srebnik, *J. Am. Chem. Soc.* **1996**, *118*, 909-910.
- [42] L. Zhang, D. Peng, X. Leng and Z. Huang, *Angew. Chem. Int. Ed.* **2013**, *52*, 3676-3680.
- [43] J. Y. Wu, B. Moreau and T. Ritter, *J. Am. Chem. Soc.* **2009**, *131*, 12915-12917.
- [44] D. Noh, H. Chea, J. Ju and J. Yun, *Angew. Chem. Int. Ed.* **2009**, *48*, 6062-6064.

- [45] Y. Sasaki, Y. Horita, C. Zhong, M. Sawamura and H. Ito, *Angew. Chem Int. Ed.* **2011**, *50*, 2778-2782.
- [46] S. Bagherzadeh and N. Mankad, *Chem. Commun.* **2016**, *52*, 3844-3846.
- [47] L. Zhang, Z. Zuo, X. Leng and Z. Huang, *Angew. Chem. Int. Ed.* **2014**, *53*, 2696-2700.
- [48] L. Koren-Selfridge, H. N. Londino, J. K. Vellucci, B. J. Simmons, C. P. Casey and T. B. Clark, *Organometallics*, **2009**, *28*, 2085-2090.
- [49] A. Kaithal, B. Chatterjee and C. Gunanathan, *Org. Lett.* **2015**, *17*, 4790-4793.
- [50] A. A. Oluyadi, S. Ma and C. N. Muhoro, *Organometallics*, **2013**, *32*, 70-78.
- [51] P. A. Lummis, M. R. Momeni, M. W. Lui, R. McDonald, M. J. Ferguson, M. Miskolzie, A. Brown and E. Rivard, *Angew. Chem. Int. Ed.* **2014**, *53*, 9347-9351.
- [52] G. Zhang, H. Zeng, J. Wu, Z. Yin, S. Zheng, and J. C. Fettinger, *Angew. Chem. Int. Ed.* **2016**, *55*, 14369-14372.
- [53] Z. Yang, M. Zhong, X. Ma, S. De, C. Anusha, P. Parameswaran and H. W. Roesky, *Angew. Chem. Int. Ed.* **2015**, *54*, 10225-10229.
- [54] A. Bismuto, S. P. Thomas and M. J. Cowley, *Angew. Chem. Int. Ed.* **2016**, *55*, 15356-15359.
- [55] Z. Yang, M. Zhong, X. Ma, K. Nijesh, S. De, P. Parameswaran and H. W. Roesky, *J. Am. Chem. Soc.* **2016**, *138*, 2548-2551.
- [56] M. K. Bisai, S. Pahar, T. Das, K. Vanka and S. S. Sen, *Dalton Trans.* **2017**, *46*, 2420-2424.
- [57] J. Intemann, M. Lutz and S. Harder, *Organometallics*, **2014**, *33*, 5722-5729.
- [58] M. Arrowsmith, T. J. Hadlington, M. S. Hill and G. Kociok-Köhn, *Chem. Commun.* **2012**, *48*, 4567-4569.
- [59] D. Mukherjee, A. Ellern and A. D. Sadow, *Chem. Sci.* **2014**, *5*, 959-964.
- [60] A. S. Dudnik, V. L. Weidner, A. Motta, M. Delferro and T. J. Marks, *Nature Chem.* **2014**, *6*, 1100-1107.
- [61] V. L. Weidner, C. J. Barger, M. Delferro, T. L. Lohr and T. J. Marks, *ACS Catal.* **2017**, *7*, 1244-1247.
- [62] C. Weetman, M. D. Anker, M. Arrowsmith, M. S. Hill, G. Kociok-Köhn, D. J. Liptrot and M. F. Mahon, *Chem. Sci.* **2016**, *7*, 628-641.
- [63] C. Weetman, M. S. Hill and M. F. Mahon, *Chem. Commun.* **2015**, *51*, 14477-14480.
- [64] C. Weetman, M. S. Hill and M. F. Mahon, *Chem. Eur. J.* **2016**, *22*, 7158-7162.

- [65] M. Arrowsmith, M. S. Hill, T. Hadlington and G. Kociok-Köhn, *Organometallics*, **2011**, *30*, 5556-5559.
- [66] S. J. Geier, C. M. Vogels and S. A. Westcott, *Current Developments in the Catalyzed Hydroboration Reaction*, in *Boron Reagents in Synthesis*, **2016**, ACS Symposium Series, Vol. 1236, p209-225.
- [67] M. S. Hill, D. J. Liptrot and C. Weetman, *Chem. Soc. Rev.* **2016**, *45*, 972-988.
- [68] D. Mukherjee, H. Osseili, T. P. Spaniol and J. Okuda, *J. Am. Chem. Soc.* **2016**, *138*, 10790-10793.
- [69] A. Arase, Y. Nunokawa, Y. Masuda and M. Hoshi, *J. Chem. Soc., Chem. Commun.* **1991**, 205-206.
- [70] D. Mukherjee, S. Shirase, T. P. Spaniol, K. Mashima and J. Okuda, *Chem. Commun.* **2016**, *52*, 13155-13158.
- [71] M. Fleige, J. Möbus, T. vom Stein, F. Glorius and D. W. Stephan, *Chem. Commun.* **2016**, *52*, 10830-10833.
- [72] P. Eisenberger, A. M. Bailey and C. M. Crudden, *J. Am. Chem. Soc.* **2012**, *134*, 17384-17387.
- [73] J. S. McGough, S. M. Butler, I. A. Cade and M. J. Ingleson, *Chem. Sci.* **2016**, *7*, 3384-3389.
- [74] T. Taniguchi and D. P. Curran, *Angew. Chem. Int. Ed.* **2014**, *53*, 13150-13154.
- [75] X. Fan, J. Zheng, Z. H. Li and H. Wang, *J. Am. Chem. Soc.* **2015**, *137*, 4916-4919.
- [76] T. J. Hadlington, M. Hermann, G. Frenking and C. Jones, *J. Am. Chem. Soc.* **2014**, *136*, 3028-3031.
- [77] S. D. Robertson, A. R. Kennedy, J. J. Liggat and R. E. Mulvey, *Chem. Commun.* **2015**, *51*, 5452-5455.
- [78] The Cambridge Structural Database, C. R. Groom, I. J. Bruno, M. P. Lightfoot and S. C. Ward, *Acta. Cryst.* **2016**, *B72*, 171-179.

Chapter 5: Bimetallic dihydropyridines: synthetic approach and structural exploration

5.1 Summary

Within this chapter six new bimetallic dihydropyridine structures are characterized by X-ray crystallography, namely [(1-Na-4-benzyl-NC₅H₅)₄(LiOtBu)₄(NaH)], **28**, [THF·Li(TMP)Al(*i*Bu)₂(2*t*Bu-NC₅H₅)] **29**, [(THF)₂Li(2*t*BuNC₅H₅)(*i*Bu)₃] **30**, [{K(18-C-6)(THF)₂ }⁺ {Al(2-*t*BuNC₅H₅)(TMP)(*i*Bu)₂ }⁻] **31**, [(PMDETA)K(2-*t*BuNC₅H₅)Zn(*t*Bu)₂], **32** and [{K(18-C-6)(THF)₂ }⁺ {Zn(*t*Bu)₂(2-*t*BuNC₅H₅) }⁻], **33**. This set of new compounds comprises one tetralithium pentasodium alkoxide-amide, two lithium aluminates, one potassium aluminate, and two potassium zincates. Discussion focuses on a structural description of each compound and comparisons with related compounds in the literature, along with potential applications.

5.2 Introduction

As outlined in **chapter 2**, dihydropyridines as a research topic is receiving much attention. Following our expansion into s-block, the next natural progression for this work was to develop mixed-metal dihydropyridines. Extensive studies have confirmed the special cooperative synergic chemistry that can be achieved upon combining two metals, with regards to metallation, nucleophilic addition and other reaction types (**Chapter 1, section 1.2**). However, the bimetallic chemistry of dihydropyridines remained virtually unexplored until this present study.

5.3 Aims of this chapter

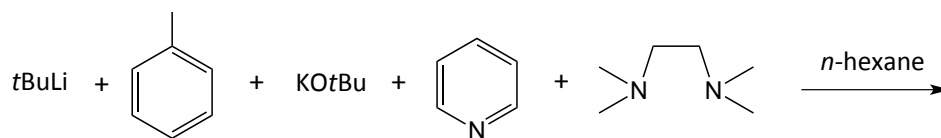
Building on our previous findings in **chapter 2**, where we have synthesised and structurally characterized monometallic dihydropyridines, the intention is now to use these as precursors to develop the bare area of bimetallic dihydropyridine systems by:

- Developing synthetic pathways to bimetallic dihydropyridines.
- Probe bimetallic dihydropyridines that combine aluminium or zinc with an alkali metal in the same compound.
- Isolate and characterise such bimetallic systems by X-ray crystallography.

5.4 Results and discussion

5.4.1 X-ray crystallographically characterised s-block bimetallic dihydropyridines

The first mixed alkali-metal dihydropyridine arose as a serendipitous result by an undergraduate student working on the project previously.¹ The original aim was to prepare benzyl lithiodihydropyridines, and employ the transmetallation approach to obtain the heavier sodium and potassium derivatives. Interestingly when the reaction was performed *in-situ* (**Scheme 5.1**) an unexpected novel discovery was obtained. What in turn occurred was the encapsulation of the by-product LiOtBu from the transmetallation step, by a 1,4-potassium-benzylidihydropyridine cage (**Figure 5.1**) analogous to the trimetallic Li-Na-K amido-alkoxide cage complex previously reported by Mulvey.²



Scheme 5.1: Serendipitous preparation of [(1-K-4-benzyl-NC₅H₅)₄(TMEDA)₄(LiOtBu)₂].

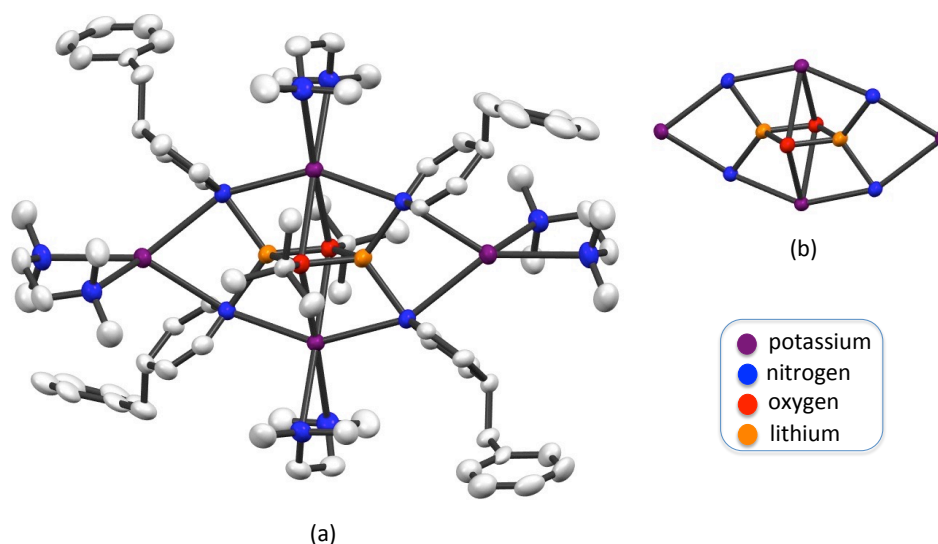
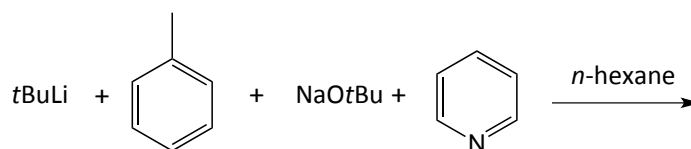


Figure 5.1: Structure of first mixed alkali-metal dihydropyridine compound [(1-K-4-benzyl-NC₅H₅)₄(TMEDA)₄(LiOtBu)₂], (a) full view and (b) with dihydropyridine and TMEDA shrubbery removed to emphasise inner core of structure.

From this initial finding, many combinations were investigated varying the lithium, sodium and potassium components, but no further structural data could be obtained. However this is not that surprising given that the original compound suffers from reproducibility issues. A plausible reasoning for that could be related to the bidentate donor TMEDA as it has been well established that Lewis base donors have a powerful influence on structural arrangements. In this case TMEDA plays a crucial role in the stabilization of the potassium atom supporting the cage like structure, yet it must be considered that in the case of excess TMEDA it could have a diminishing effect and lead to the collapse of the intricate assembly.

Adopting the same method in the absence of TMEDA (Scheme 5.2) resulted in the growth of X-ray quality crystals at -30°C. Curious as to what would fulfill the coordination sphere of the sodium atom, the molecular structure was determined by X-

ray crystallography and shown to be $[(1\text{-Na-4-benzyl-NC}_5\text{H}_5)_4(\text{LiOtBu})_4(\text{NaH})]$ **28** (Figure 5.2).



Scheme 5.2: Synthesis of **28**, $[(1\text{-Na-4-benzyl-NC}_5\text{H}_5)_4(\text{LiOtBu})_4(\text{NaH})]$.

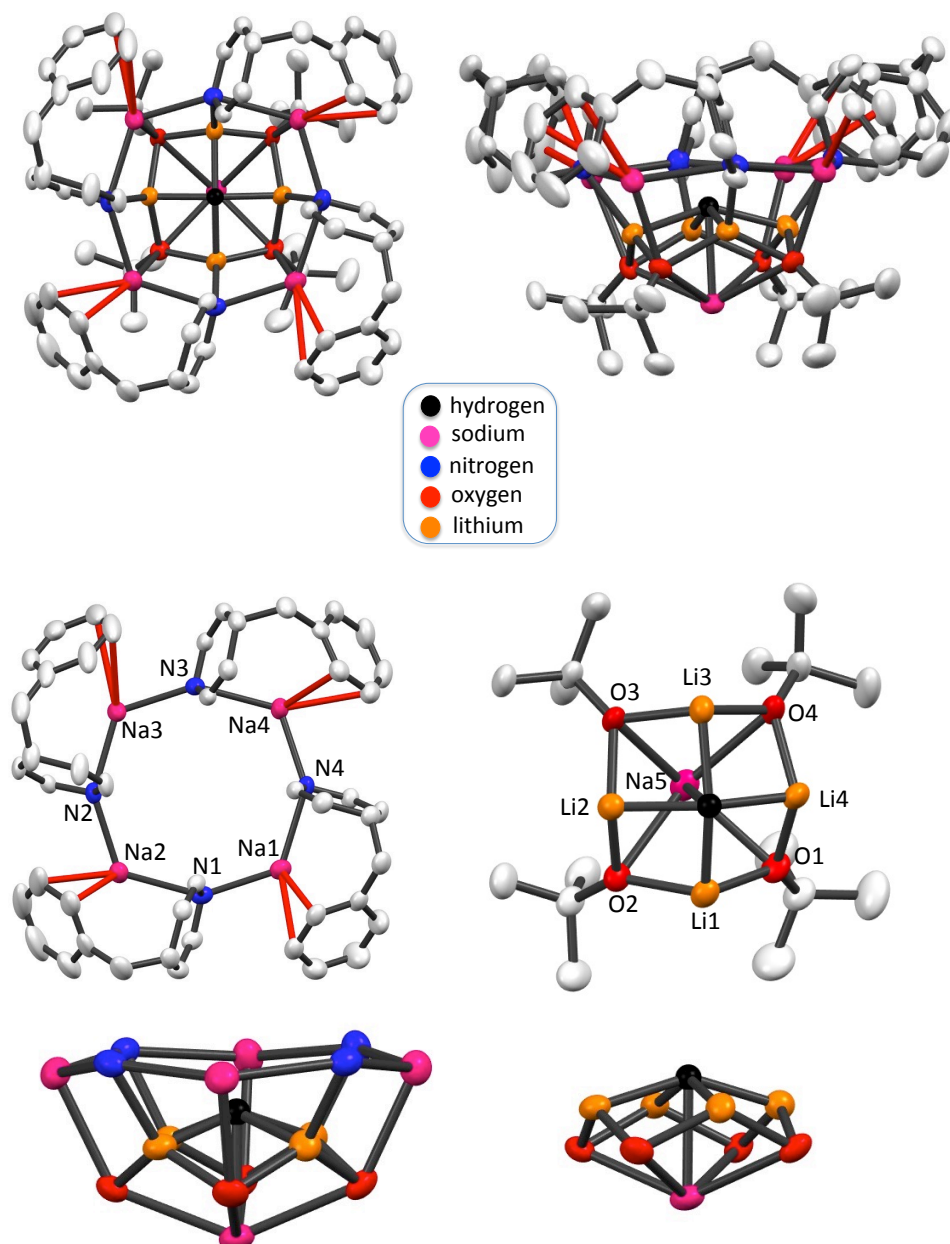


Figure 5.2: Molecular structure of $[(1\text{-Na-4-benzyl-NC}_5\text{H}_5)_4(\text{LiOtBu})_4(\text{NaH})]$, **28** with displacement ellipsoids at 50% probability level, hydrogen atoms omitted for clarity and relevant π -interactions highlighted in red. Table 5.1 gives selected bond lengths (in Å).

Solvent-free **28**, is the first alkali metal dihydropyridine system containing a direct metal-hydride bond as well as being a potential metal-hydride surrogate. The molecular structure arising from a metal-metal interchange reaction displayed a beautiful bowl-like structure. The tetralithium pentasodium mixed alkoxide-amide is an example of a molecular architecture based upon a templating seed³ (although not intentionally introduced), in this case a single molecule of NaH. When the organic shrubbery is removed, leaving the molecular skeleton, a 17-vertex inorganic Li₄Na₅N₄O₄ shell can be seen (Figure 5.2). The connectivity pattern is very organised, consisting of a series of stacked heteronuclear planes. The top layer is an octagonal (NaN)₄ ring, bearing the 1,4-benzylidihydropyridines. The Na-N bond lengths within the upper layer ranges from 2.456(2)-2.640(2) Å are in agreement with typical Na-N amido bond lengths. Each sodium atom in this ring is stabilized by cation- π interactions from the benzyl ring [mean Na-C bond length; 2.979 Å]. The middle layer is an eight-membered ring consisting of four lithium and four oxygen atoms, of the lithium *tert*butoxide. However this is arranged in a square-like fashion from an aerial view, though its true zig-zag arrangement of the lithium and oxygen atoms can be observed from a side-on perspective. The Li-O bonding within this core ring [1.891(4)-1.920(4)] is comparable with that previously seen in the lithium pentasodium mixed system [Li₄Na₄(*t*BuO)₄{Ph₂N(H)}₄(NaOH)(4-Me-Py)₄].³ The sodium atom of the templating seed (NaH) adopts the apical position in the bowl with the hydride sitting in an internal protected position. The sodium-hydride bond length 2.40(2) Å is comparable with those in the literature.^{4,5}

Table 5.1: Key bond distances within **28** (Å).

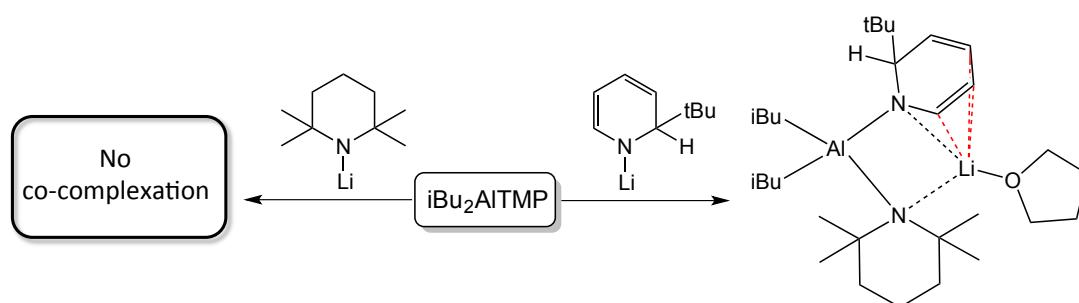
Bond	Bond length	Bond	Bond length	Bond	Bond length	Bond	Bond length
Na1-N1	2.500(2)	Na1-C1	2.968(2)	Li1-O1	1.911(3)	Na5-H1H	2.40(2)
Na1-N4	2.583(2)	Na1-C2	2.962(2)	Li1-O2	1.911(4)	Na5-O1	2.567(1)
Na2-N2	2.501(2)	Na2-C13	2.960(2)	Li2-O2	1.912(3)	Na5-O2	2.554(1)
Na2-N1	2.586(2)	Na2-C14	2.923(3)	Li2-O3	1.897(3)	Na5-O3	2.573(1)
Na3-N3	2.456(2)	Na3-C26	3.025(4)	Li3-O3	1.920(4)	Na5-O4	2.595(2)
Na3-N2	2.568(1)	Na3-C27	3.010(3)	Li3-O4	1.907(3)	Li1-H1H	2.06(2)
Na4-N4	2.500(2)	Na4-C37	2.958(3)	Li4-O4	1.901(3)	Li2-H1H	2.05(2)
Na4-N3	2.640(2)	Na4-C38	3.024(3)	Li4-O1	1.89194)	Li3-H1H	2.01(1)
Mean	2.542	Mean	2.979	Mean	1.906	Li4-H1H	2.07(1)

The molecular structure **28** provides a nice addition to the scarce family of template based mixed alkali metal cage molecules containing various alkoxide-amide^{2,3}/enolate⁶/oxide^{7,8} combinations. The novel feature in **28** compared with those previously reported examples is the encapsulation of a metal hydride opposed to a hydroxide anion.

5.4.2 Mixed alkali metal-aluminium dihydropyridines

On the quest to prepare a mixed metal dihydropyridine, pairing together a group 1 and a group 13 metal, the reaction between alkali metal dihydropyridines and diisobutylaluminium tetramethylpiperidine (*i*Bu₂AlTMP) were investigated. This aluminium reagent was selected for three main reasons; (i) the trans-metal trapping concept⁹ that has already emerged from the Mulvey group studies is based upon LiTMP and *i*Bu₂AlTMP (chapter 1); so this begged the question “could the lithium dihydropyridine act as an alternative to LiTMP”; (ii) from a structural perspective would these two monometallic species co-complex as in typical lithium aluminate chemistry,¹⁰ could this open up a new avenue to isolate rarer sodium and potassium aluminates and (iii) could the bulky ligands on the aluminium atom provide enough steric stability in the instance of preparing an aluminium hydride?

Starting with the lithium dihydropyridine **1** in hexane solution, addition of *i*Bu₂AlTMP with THF resulted in a crop of colourless crystals (Scheme 5.3). X-ray diffraction analysis revealed the molecular formula of these crystals to be [THF·Li(TMP)Al(*i*Bu)₂(2*t*Bu-NC₅H₅)] **29** (Figure 5.3).



Scheme 5.3: Comparison of reactivity of *i*Bu₂AlTMP with LiTMP versus that of LiDHP.

The central core of the structure exhibits a planar four-element ring (LiNAIN). The aluminium atom is now coordinated to four anions, two amido (from TMP and DHP ligands) and two alkyl (from *i*Bu ligands), in a slightly distorted tetrahedral geometry (mean angle, 109.25°). In a surprising rearrangement, the lithium atom has been displaced from its position on the dihydropyridine amido anion. It is now coordinated to the nitrogen atom of the bridging TMP anion, tucked under the dihydropyridine ring to take advantage of the π -interactions [2.391(5)–2.540(5) Å], whilst a molecule of THF completes its coordination sphere. This is comparable with some diamido-dialkyl lithium aluminate examples in the literature as highlighted in figure 5.4 (top, a^[11] and b^[12]) where the lithium atom is coordinated to two bridging amido groups and solvated by a molecule of THF.

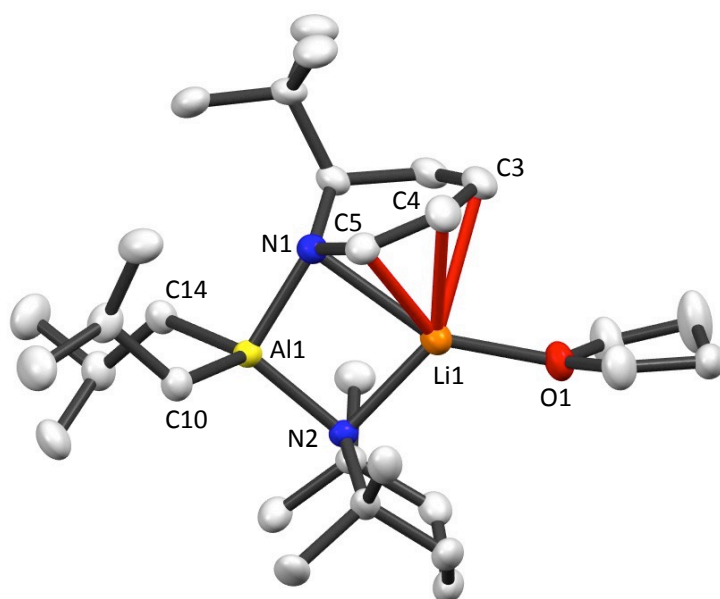


Figure 5.3: Molecular structure of **29** [THF·Li(TMP)Al(*i*Bu)₂(2*t*Bu-NC₅H₅)] with displacement ellipsoids at 50% probability level, hydrogen atoms omitted for clarity and π -interactions highlighted in red. The unit cell of **29** contains two crystallographic independent molecules with identical connectivity. One of these molecules is shown here. Selected bond lengths (Å) and bond angles (°): Al1-N1, 1.949(2); Al1-N2, 1.979(2); Al1-C10, 2.017(3); Al1-C14, 2.009(2); Li1-N1, 2.410(5); Li1-O1, 1.955(5); Li1-N2, 2.089(5); Li1-C3, 2.540(5); Li1-C4, 2.532(5); Li1-C5, 2.391(5); N1-Al1-C10, 108.91(9); N1-Al1-C14, 103.50(9); N1-Al1-N2, 100.08(8); C10-Al1-C14, 104.97(9); C10-Al1-N2, 115.72(9); C14-Al1-N2, 122.30(9).

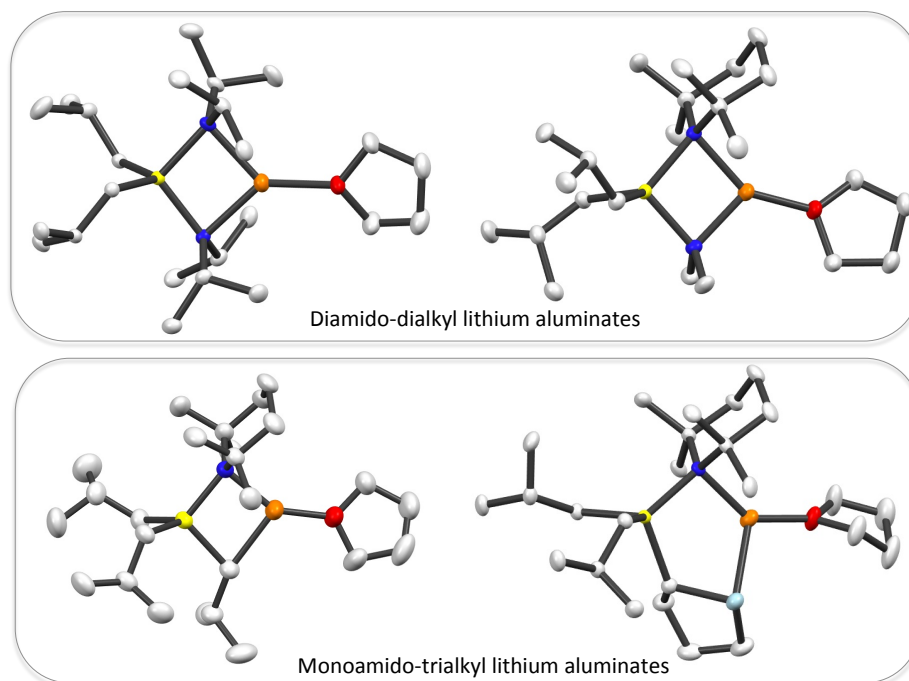


Figure 5.4: Literature examples of lithium aluminate structures comparable to **29** [top, (a) and (b)] and **30** [bottom, (c) and (d)]; orange =lithium, yellow = aluminium, red = oxygen, blue = nitrogen and pale blue = sulfur.

Notably here, it could be assumed that LiDHP **1** does not pose as an alternative to LiTMP, as in the concept-making trans-metal trapping system the criteria states the lithium and aluminium species must not co-complex to form an ate or else it will inhibit reactivity. Hence as the LiDHP is not sterically encumbered enough to prevent co-complexation it rules this out of consideration as a new member in the trans-metal-trap family. However, based on the same concept it could be suggested that this can be thought of as the first trans-metal trapping of an amido anion opposed to the carbanions trapped in all previous examples.^{13,14}

Since from a position of practicality *i*Bu₂AlTMP has to be pre-synthesised (albeit in a simple preparation), a commercially available aluminium reagent was trialled to test if a similar structural motif would be observed and react in a similar manner. There was also the consideration of how influential the TMP anion was in the reaction for facilitating the rearrangement of the lithium atom to switch to the vicinity of the π -interactions. Moving to a reagent with no amido ligands, triisobutylaluminium *i*Bu₃Al was selected, as its already documented in the literature.¹⁵ Following the same reaction conditions used with *i*Bu₂AlTMP; after several attempts X-ray quality crystals of

product **30** were obtained. In agreement with our expectations this was a tris-alkyl lithium aluminate that was isolated and characterized (Figure 5.5).

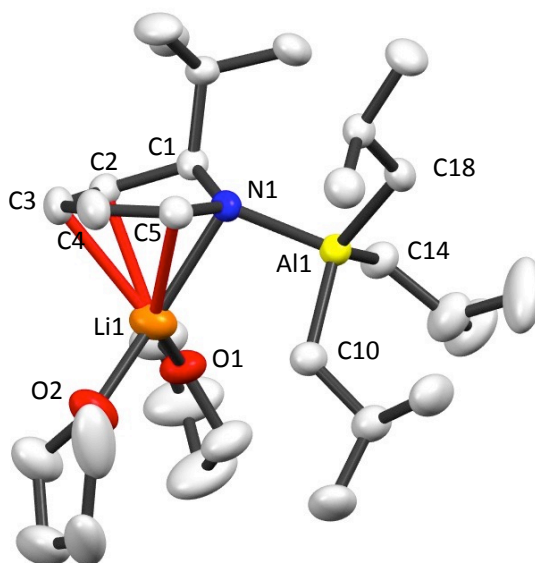


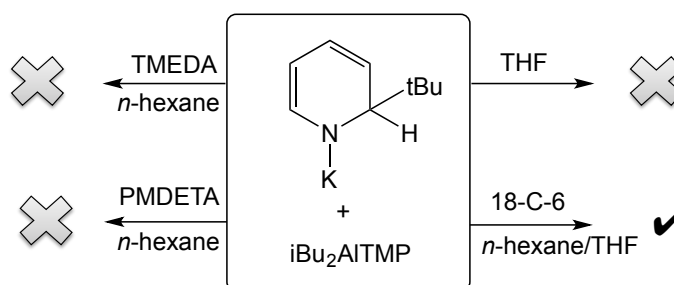
Figure 5.5: Molecular structure of $[(\text{THF})_2\text{Li}(2t\text{BuNC}_3\text{H}_5)(i\text{Bu})_3]$ **30** with displacement ellipsoids at 50% probability level, π -interactions highlighted in red, hydrogen atoms and minor disordered component on THF molecule and *i*Bu group have been omitted for clarity. Selected bond lengths (\AA) and bond angles ($^\circ$): Al1-N1, 1.958(2); Al1-C10, 2.019(3); Al1-C14, 2.004(3); Al1-C18, 2.011(2); Li1-N1, 2.326(4); Li1-O1, 1.961(5); Li1-O2, 1.923(5); Li1-C2, 2.491(5); Li1-C3, 2.493(6); Li1-C5, 2.430(5); N1-Al1-C10, 99.42(9); N1-Al1-C14, 106.8(1); N1-Al1-C18, 108.26(9); C10-Al1-C14, 111.7(1); C10-Al1-C18, 116.4(1); C14-Al1-C18, 112.9(1).

The framework in **30** is composed of a four-coordinate aluminium atom, in a familiar distorted tetrahedral environment. It is terminally bound to three *i*butyl groups and one amido dihydropyridine group. The dihydropyridine is partially bridging to the lithium atom via the nitrogen atom along with stabilizing cation- π interactions emanating from the olefinic region of the ring. Two molecules of THF are solvating the lithium atom to saturate its coordination sphere. Interestingly in this case the four-atom centre is not observed, as here there is no bond closing of the ring between Li1 and C10, with the separation distance measuring 3.025(5) \AA , considerably longer than that in $[\text{THF}\cdot\text{Li}(\text{TMP})\text{Al}(i\text{Bu})_3]^{10}$ [Figure 5.4 bottom, (c)] which is only 2.258(4) \AA . Again, the aluminium atom takes priority on deciding its coordination with the lithium atom

being displaced from an in-plane disposition of the dihydropyridine nitrogen atom. This is most noteworthy difference between **29** and **30**. In the case of triisobutylaluminium, where there are no bridging amido ligands available such as TMP, the lithium atom is more disconnected than in **29**. The lithium atom's only connectivity to the aluminum coordination sphere is via π -interactions with the HDP ligand. A comparable literature example by Westerhausen¹⁶ reveals a solvent-separated ion pair $[\text{Li}(\text{THF})_2\text{TMEDA}]^+ \{\text{Al}(\text{Ph})_3(\text{TMP})\}^-$, indicating that it is possible to obtain a solvent separated version of **30** upon adding a suitable donor ligand to cap the lithium atom. Attempts were made to prepare such a solvent-separated ion pair by employing TMEDA or 12-crown-4. Unfortunately this proved unsuccessful.

Extension to heavier alkali metals

Moving to the heavier alkali metals, sodium and potassium, it proved more challenging to prepare such mixed-metal dihydropyridines than with the lithium derivatives. Continuing with the original aluminium reagent, $i\text{Bu}_2\text{AlTMP}$, for sodium no mixed-metal systems could be crystallised. But the lack of sodium aluminates in the literature¹⁷ presents precedence for this failure. However, the reactivity with the potassium dihydropyridine derivative was more promising. Interestingly taking the potassium dihydropyridine **3a** in THF for solubility and reacting it with $i\text{Bu}_2\text{AlTMP}$, resulted in an oily solution. Various attempts at this were performed adding different Lewis base donor solvents to aid crystallization, including bulk THF, TMEDA, PMDETA and 18-crown-6, with only the last named resulting in crystallization.



Scheme 5.4: Outcome of various Lewis donors employed to aid crystallization of KDHP (**3**) and $i\text{Bu}_2\text{AlTMP}$.

Surprisingly, 18-crown-6 in the presence of THF yielded a crop of colourless crystals. A solvent-separated ion pair $[\text{K}(18\text{-C-6})(\text{THF})_2]^+ \{\text{Al}(2\text{-}i\text{BuNC}_5\text{H}_5)(\text{TMP})(i\text{Bu})_2\}^-$

31, was revealed by X-ray crystallographic determination (Figure 5.6). To the best of our knowledge this is the first solvent-separated ion pair (SSIP) motif in potassium aluminate chemistry.

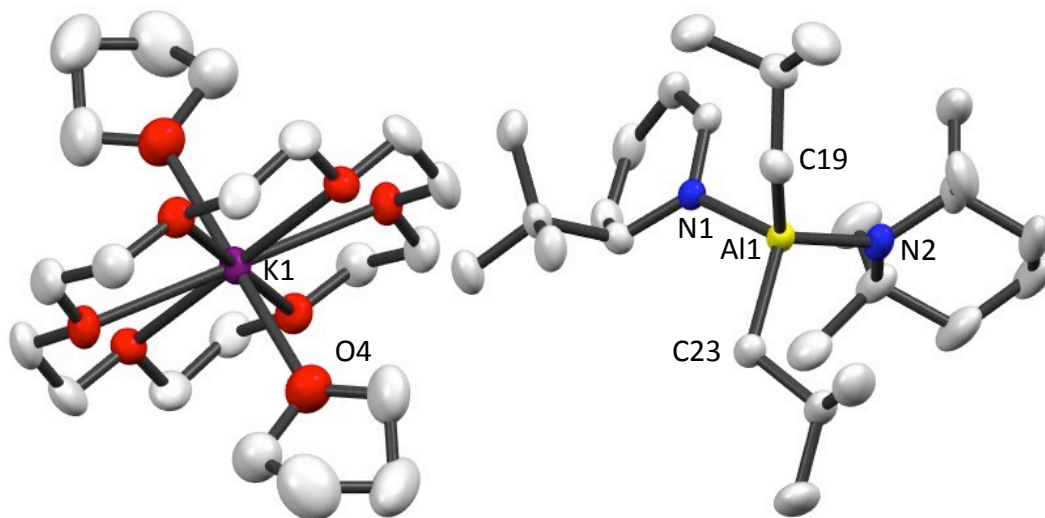


Figure 5.6: Molecular structure of **31** [$\{K(18-C-6)(THF)_2\}^+ \{Al(2-tBuNC_5H_5)(TMP)(iBu)_2\}^-$] with displacement ellipsoids at 50% probability level, hydrogen atoms, π -interactions and minor disordered component on THF molecule have been omitted for clarity. Selected bond lengths (Å) and bond angles ($^\circ$): Al1-N1, 1.939(2); Al1-N2, 1.901(2); Al1-C19, 2.020(2); Al1-C23, 2.026(2); N1-Al1-N2, 108.88(9); N1-Al1-C19, 103.94(9); N1-Al1-C23, 109.43(9); N2-Al1-C19, 120.2(1); N2-Al1-C23, 110.46(9); C19-Al1-C23, 103.4(1).

The SSIP motif can be discussed as two separate moieties. Its cationic moiety consists of an eight-coordinate potassium atom in a hexagonal bipyramid type arrangement. It is solvated by six oxygen atoms of the 18-crown-6 molecule in one plane whilst a further two THF molecules solvate above and below the plane forming the peaks. The average K-O bond lengths involving the 18-crown-6 are slightly longer (2.780-2.825 Å) than the K-O of the THF ligands [2.600(17) Å]. The four-coordinate anionic aluminum atom adopts an essentially tetrahedral geometry (mean bond angle; 109.4 $^\circ$). This complex anion contains two isobutyl groups, one TMP group and one 2-*tert*-butyldihydropyridine group.

Despite its simplicity, this structure is surprisingly unusual in terms of potassium aluminate chemistry. A search of the CSD structural database¹⁸ (Figure 5.7) highlights the lack of potassium aluminates in the literature with only nine hits for mono amido tris-alkyl potassium aluminates,¹⁹ four of which adopt the typical motif containing a 4 membered core (KNAIC) ring.²⁰ A report by Mulvey on these structures revealed the subtle structural differences that can be observed upon changing the amido anion from TMP, DMP and HMDS.²¹ Moving to our case of a diamido dialkyl potassium aluminates only three hits were discovered.^{16,22,23} Interestingly there are 12 examples in the structural database that contain both a potassium and aluminium fragment, however they bear interactions giving rise to a contacted ion pair type motif. Remarkably, none of them adopt a SSIP motif.

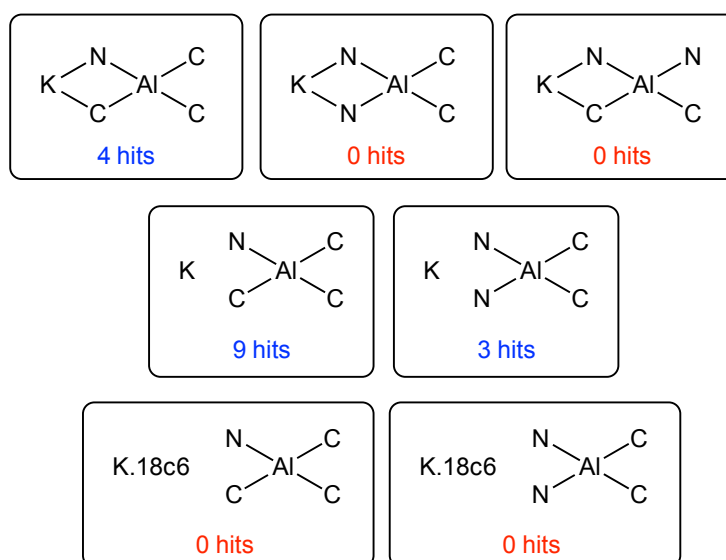


Figure 5.7: Hits obtained from CSD searches of potassium aluminate structures.

5.4.3 Mixed alkali metal - zinc dihydropyridines

Alkali-metal zincate compounds have been studied extensively,²⁴ most predominantly lithium and sodium examples. Pioneering examples include the lithium zincate by $\text{LiZn}(\text{Bu})_2(\text{TMP})$ reported by Kondo and Uchiyama,²⁵ and the sodium analogue $(\text{TMEDA})\text{NaZn}(\text{Bu})_2\text{TMP}$ developed by the Mulvey group.²⁶ On the other hand, potassium zincates are much more scarce in the literature in terms of those crystallographically characterized. The synergic reactivity observed with these zincate compounds provides an incentive to study and to gain a better understanding of how

potassium-mediated zincation operates. The successful potassium-mediated zincation of ethene,²⁷ substituted pyridines^{28,29} and ferrocene³⁰ has been reported. To date the reported potassium dialkylamidozincates follow the same design motif as lithium and sodium alkylamidozincates bearing the distinct four-element (AMNZnC) ring (Figure 5.8). There is structural exploration into various dialkylzinc compounds employed including ethyl, methyl and *n*-butyl but a similar study into the variation of the amido group appears to be absent in the literature.

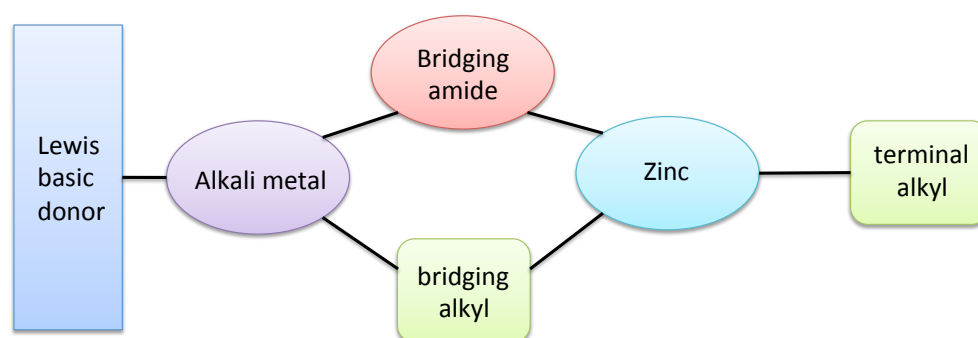


Figure 5.8: Typical alkali metal zincate motif.

Given the success of potassium dihydropyridines with aluminium, this was replicated with zinc to access a new series of potassium zincates. Keeping in theme with potassium-dialkyl-amido-zincates, the effect of replacing the amido group TMP with a dihydropyridine functionality was explored. This could lead to a potential new potassium zincate base that may display new reactivity, or react identically and hence provide a cheaper alternative to TMP. Another avenue for this work, more in keeping with the theme of this thesis, is the development of a potassium zincate that may act as an activated hydride surrogate. Would the complex result in a separate potassium, separate zinc or mixed-metal hydride surrogate species?

Firstly, a synthetic strategy was examined, adopting the same methodology as reported previously, by mixing a potassium amide, a dialkylzinc and a Lewis base donor in *n*-hexane. Employing our potassium dihydropyridine [1-K-2-*t*BuNC₅H₅] **3a** as the potassium amide, *di**tert*-butylzinc and the tridentate Lewis base donor PMDETA resulted in a crop of X-ray quality crystals upon cooling the solution to -30°C (Figure 5.9).

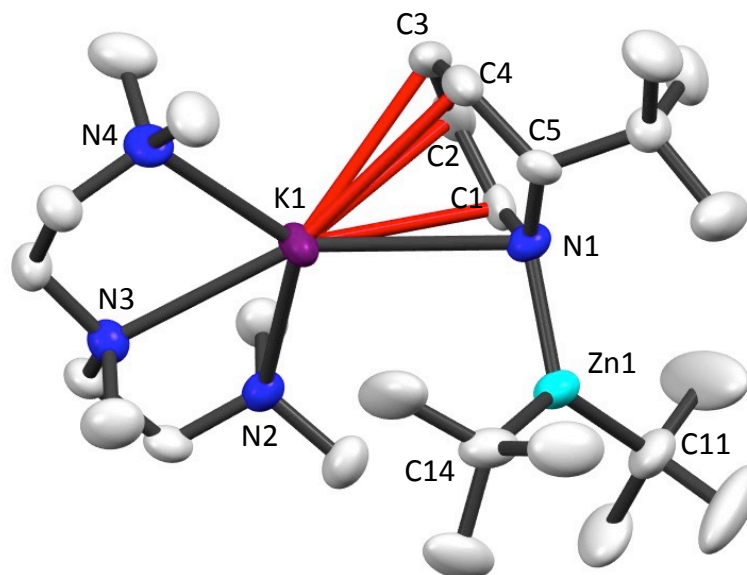


Figure 5.9: Molecular structure of [(PMDETA)K(2-*t*BuNC₅H₅)Zn(*t*Bu)₂], **32** with displacement ellipsoids at 50% probability level, π -interactions highlighted in red, hydrogen atoms and minor disordered component on *t*Bu group have been omitted for clarity. Selected bond lengths (Å) and bond angles (°): K1-N1, 3.072(4); K1-N2, 2.843(4); K1-N3, 2.847(4); K1-N4, 2.833(4); K1-C1, 3.020(5); K1-C2, 3.088(5); K1-C3, 3.058(4); K1-C4, 3.163(4); Zn1-N1, 2.022(3); Zn1-C11, 2.025(6); Zn1-C14, 2.055(7); C11-Zn1-C14, 130.3(2); C11-Zn1-N1, 115.6(2); C14-Zn1-N1, 114.0(2); Zn1-N1-C1, 121.7(3); Zn1-N1-C5, 122.0(3); C1-N1-C5, 116.4(4).

The new potassium zincate compound [(PMDETA)K(2-*t*BuNC₅H₅)Zn(*t*Bu)₂], **32** was found to have a contacted ion pair structure. The tricoordinated zinc atom occupies a trigonal geometry (mean bond angle; 120.03°) comprising a mixed alkyl and amido ligand set, made up of two terminal *tert*-butyl groups and one bridging dihydropyridine group. The potassium atom is to an extent removed from any coordination with the position of the alkyl groups on the zinc diminishing the possibility of the typical (KNZnC) ring. It has been chelated by three nitrogen atoms of PMDETA, whilst the other side of the atom is satisfied by π -interactions from the bridging dihydropyridine ring. The PMDETA in this case appears to be blocking any further aggregation of the potassium zincates.

In an effort to obtain a solvent separated ion pair motif, a crown ether was employed to take advantage of the higher denticity it offers. Following the same synthetic protocol

as used in the synthesis of **32**, replacing PMDETA by 18-crown-6 and adding THF to aid crystallisation, gave the desired product $[\{K(18-C-6)(THF)_2\}^+\{Zn(tBu)_2(2tBuNC_5H_5)\}^-]$, **33**, which was isolated straightforwardly at -30°C .

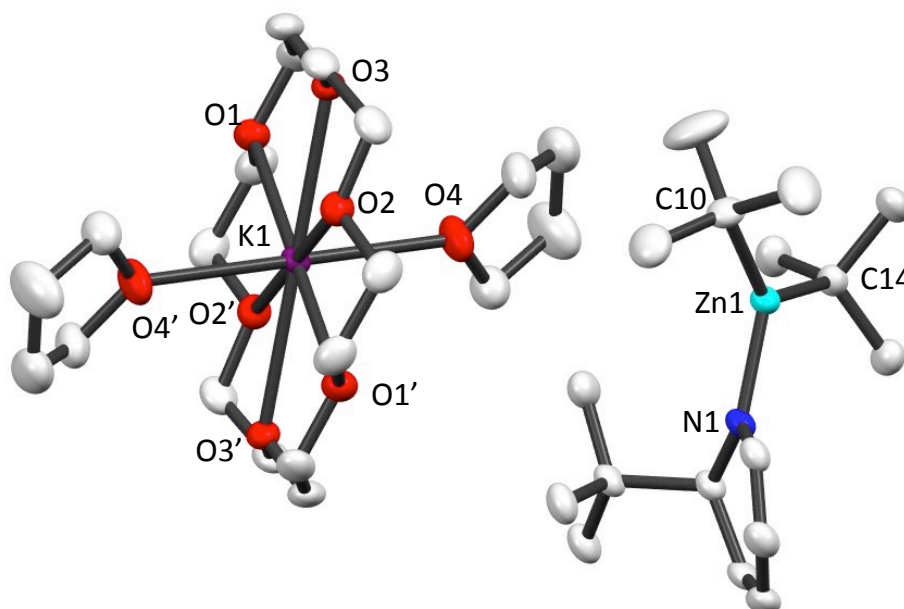


Figure 5.10: Molecular structure of **33** $[\{K(18-C-6)(THF)_2\}^+\{Zn(tBu)_2(2tBuNC_5H_5)\}^-]$ with displacement ellipsoids at 50% probability level, with hydrogen atoms omitted for clarity. The unit cell of **33** contains two crystallographic independent cationic fragments with identical connectivity. One of these molecules is shown here. Selected bond lengths (Å) and bond angles ($^\circ$): Zn1-N1, 2.001(2); Zn1-C10, 2.031(3); Zn1-C14, 2.036(2); C10-Zn1-C14, 129.0(1); C10-Zn1-N1, 114.45(9); C14-Zn1-N1, 116.37(9).

The rare SSIP potassium zincate motif (Figure 5.10) consists of a cationic moiety with a potassium atom solvated by eight oxygen atoms, six from 18-crown-6 and two from monodentate THF molecules. The anionic moiety composes two *tert*butyl and one dihydropyridine anions. This results in a distorted trigonal planar geometry, with angles subtended at the zinc atom (Zn1) ranging from 114.45 - 129.0° . The SSIP motif has been observed in potassium zincates previously, on the CSD structural database revealing only one example has been reported with 18-crown-6,³¹ but others exist where six monodentate THF donor molecules stabilise the potassium atom.³² Okuda reported a potassium zincate dihydropyridine structure,³³ which was the first example

of a dianionic tetrakis(amido)zincate to be characterized in the absence of chelating amido ligands (Figure 5.11). However, this structure differs slightly from that discussed here. As can be seen in figure 5.11, the zinc centre contains two dianionic ligands with charge balanced provided by two 18-crown-6 solvated potassium atoms. Noteworthy here is the interaction between the potassium atom and the olefinic functionality of the dihydropyridine ring, making this structure more comparable to the CIP motif in **32** although bearing the crown ether.

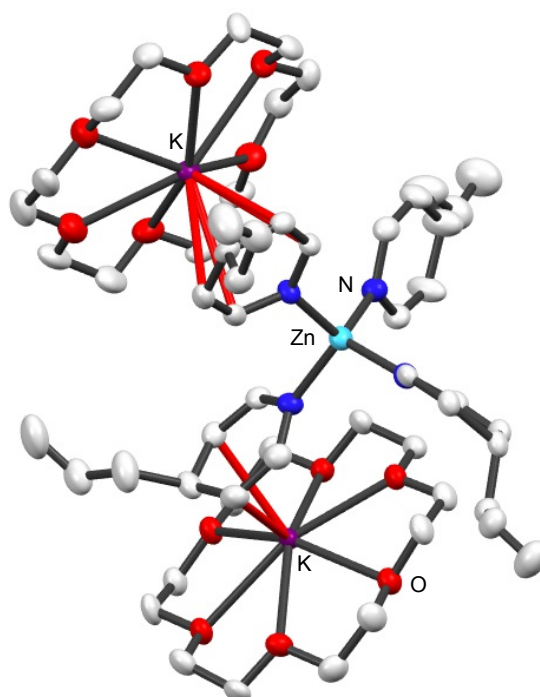


Figure 5.11: Structure of Okuda's dianionic tetrakis(amido)zincate, [$\{K(18-C-6)\}_2(Zn(NC_5H_5-4-C_3H_5)_4)$].

5.5 Conclusions and future work

The work discussed within this chapter has opened up the field of bimetallic dihydropyridines by providing a synthetic co-complexation pathway from our well-characterized monometallic dihydropyridines, to realize six new bimetallic dihydropyridine structural motifs.

The expansion of mixed alkali metal systems based on a templating architecture have briefly been touched upon, resulting in a reproducible tetralithium pentasodium mixed alkoxide-amide structure, though more work is required here to provide a reliable

systematic route to other alkali metal variations. The reactivity of **28** should be probed in terms of a hydride source to determine if this cage can function as a carrier to uptake and release NaH. Also, it would be interesting to test the limitations of this cavity, and determine what other small molecules could be encapsulated, or from a practical development if there are small molecules that have solubility issues, that the cage could trap and solubilise.

The incorporation of the group 13 metal aluminium into bimetallic dihydropyridine compositions has brought to the light the possibility of trans-metal-trapping amido anions as opposed to carbanions on which the concept was originally founded. From this result, it would be interesting to study the reactivity of *tert*butyllithium and other heterocycles that undergo non-selective addition reactions in the presence of *i*Bu₂AlTMP or *i*Bu₃Al to determine if these would trap and stabilize an amido anion. Also, aluminium hydrides are making a name for themselves in the field of catalytic hydroboration,³⁴⁻³⁶ so it would be interesting to explore these as a bimetallic lithium or potassium/aluminium hydride surrogates and compare their performance with those hydrides already studied in the literature.

The expansion of alkali metal dihydropyridines to potassium zincates has expanded the structural diversity within this intriguing family of heterobimetallic compounds. Their reactivity as an alternative potassium zincate base for potassium-mediated zincation should be explored to compare the influence of TMP in typical K-TMP-dialkyl-zincates. In alignment with the potassium aluminate, the corresponding potassium zincates should be explored as potassium/zinc hydride surrogates for potential catalytic roles. The comparison of compounds **31** and **33** in particular would be insightful to contrast aluminium and zinc in a closely related system.

5.6 Experimental

5.6.1 Synthesis of compounds 28-33

Synthesis of [(1-Na-4-benzyl-NC₅H₅)₄(LiOtBu)₄(NaH)] 28

NaOtBu (1.7 mmol, 0.1634 g) was added to a Schlenk along with 5 mL of toluene. To the colourless solution tBuLi (1.7 mmol, 1 mL of 1.7M solution) was added to give a bright orange suspension. Pyridine (1.7 mmol, 0.14 mL) was then added which resulted in an orange solution after a few minutes of stirring. This then changed to a green/brown coloured solution. Upon placing at -34°C, colourless crystals were deposited.

NMR characterization was attempted however due to the broadness further variable temperature studies will need to be performed to obtain a resolved ¹H NMR characterization.

*Synthesis of [THF·Li(TMP)Al(*i*Bu)₂(2*t*Bu-NC₅H₅)] 29*

LiDHP **1** (0.143g, 1 mmol) and *i*Bu₂AlTMP (0.28g, 1 mmol) were added to a Schlenk along with 10 mL of *n*-hexane at room temperature. This was left to stir for 10 minutes. To obtain a completely soluble solution, THF was added dropwise. This resulted in a colourless oil forming, from which crystals grew from at -30°C (0.08 g, 16%)

¹H NMR (400.1 MHz, C₆D₆, 300K): δ 7.20 (1H, overlap d₆-benzene, DHP), 5.64 (1H, m DHP), 4.92 (1H, br t, DHP), 4.70 (1H, br t, DHP), 3.81 (1H, br d, DHP), aliphatic region needs further NMR studies – most likely a complex equilibria typically observed with aluminium ‘ate’ species.

*Synthesis of [(THF)₂Li(2*t*BuNC₅H₅)(*i*Bu)₃] 30*

LiDHP **1** (0.143 g, 1 mmol) was added to a Schlenk flask along with 10 mL of *n*-hexane at room temperature. Triisobutylaluminium was then added (1 mL of 1M hexane solution, 1mmol) was added at -30 °C resulting in the precipitation of a white solid. Tetrahydrofuran (0.15 mL, 2 mmol) was added and the reaction mixture was solubilised. Upon cooling to -78 °C colourless crystals were deposited (0.029 g, 6%).

¹H NMR: (400.13 MHz, 298K, C₆D₆): δ 7.04-7.07 [1H, m, DHP], 5.91-5.94 [1H, m, DHP], 4.81-4.84 [1H, m, DHP], 4.71-4.74 [1H, m, DHP], 3.87 [1H, d, DHP], aliphatic region needs further NMR studies – most likely a complex equilibria typically observed with aluminium ‘ate’ species.

Synthesis of [$\{K(18-C-6)(THF)_2\}^+ \{Al(2-tBuNC_5H_5)(TMP)(tBu)_2\}^-$] **31**

KDHP **3a** (0.174g, 1 mmol) and *t*Bu₂AlTMP (0.28 g, 1 mmol) were added to a Schlenk along with 5 mL of hexane. 1 mL of THF was added to obtain a yellow/orange solution. 18-crown-6 (0.264g, 1 mmol) was then added causing an oil to form. This was left to stir for 1 hour before being placed at -30°C to aid crystallisation. A crop of crystals grew from the oil (0.575 g, 66%).

¹H NMR (400.1 MHz, C₆D₆, 300K): δ 7.30 (1H, d, DHP), 6.34 (1H, m, DHP), 4.93 (1H, m, DHP), 4.62 (1H, t, DHP), 4.47 (1H, d, DHP), again like compound **29** the aliphatic region needs further NMR studies – most likely a complex equilibria typically observed with aluminium ‘ate’ species.

Synthesis of [(PMDETA)K(2-*t*BuNC₅H₅)Zn(*t*Bu)₂] **32**

KDHP **3a** (0.174g, 1 mmol) was added to a Schlenk flask along with 10 mL of hexane. *t*Bu₂Zn (1 mL, 1 mmol) was then added, with no change to the beige suspension observed. This was left to stir for 15 minutes before adding PMDETA (0.21mL, 1 mmol) to obtain a brown oil in a yellow solution. This was placed at -30°C to aid crystallisation. A crop of yellow crystals grew from the oil (0.360 g, 68%).

¹H NMR (400.1 MHz, C₆D₆, 300K): δ 7.17 (1H, d, DHP), 6.09 (1H, m, DHP), 4.54 (2H, m, DHP), 3.98 (1H, d, DHP), 1.77 (12H, s, CH₃ PMDETA), 1.69 (8H, s, CH₂ PMDETA), 1.62 and 1.61 (21H, s overlapping, CH₃ PMDETA and *t*Bu₂Zn) and 1.29 (9H, s, *t*Bu DHP) ppm.

Elemental analysis (%): calcd: C 57.87, H 9.91, N 11.25; found: C 58.44, H 10.11, N 11.60.

Synthesis of [$\{K(18-C-6)(THF)_2\}^+ \{Zn(tBu)_2(2tBuNC_5H_5)\}^-$] **33**

KDHP **3a** (0.174g, 1 mmol) was added to a Schlenk flask along with 10 mL of hexane. tBu_2Zn (1 mL, 1 mmol) and 18-crown-6 (0.264g, 1 mmol) were then added. The beige suspension was left to stir for 15 minutes before adding 5 mL of THF was added to obtain an oil in the solution. This was placed at $-30^\circ C$ to aid crystallisation. A crop of yellow crystals grew from the oil (0.391g, 51%).

1H NMR (400.1 MHz, C_6D_6 , 300K): δ 7.30 (1H, br d, DHP), 6.25 (1H, m, DHP), 4.69 (1H, m, DHP), 4.35 (1H, m, DHP), 3.15 (24H, s, CH_2 of 18c6), 1.64 (18H, s, tBu of Zn) and 1.35 (9H, s, tBu of DHP) ppm.

Elemental analysis (%): calcd: C 56.25, H 9.912, N 2.26; found: C 56.25, H 9.12, N 2.26, for the abstraction of two THF molecules.

5.6.2 Crystallographic data and refinement details for compounds 28-33.

	28	29	30	31	32	33
Empirical formula	C ₆₄ H ₈₅ Li ₄ N ₄ Na ₅ O ₄	C ₆₀ H ₁₁₆ Al ₂ Li ₂ N ₄ O ₂	C ₂₉ H ₅₇ AlLiNO ₂	C ₄₆ H ₉₀ AlKN ₂ O ₈	C ₂₆ H ₅₅ KN ₄ Zn	C ₃₇ H ₇₂ KNO ₈ Zn
Mol. Mass	1117.06	993.40	485.70	865.27	528.21	763.42
Crystal system	Triclinic	Triclinic	Monoclinic	Triclinic	Monoclinic	Triclinic
Space group	P -1	P -1	P 2 ₁ /c	P -1	C c	P -1
Temperature (K)	154.9	122.9	153.9	161.9	123.5	125.1
a/ Å	15.8060(6)	10.6908(7)	16.8316(10)	11.0242(9)	14.8727(11)	12.1387(8)
b/ Å	15.8693(5)	16.3470(11)	9.1257(6)	11.5285(8)	12.6906(11)	13.7023(9)
c/ Å	16.2002(5)	18.8666(13)	20.9042(12)	20.5066(13)	17.7902(13)	14.6057(9)
α/o	71.625(3)	83.737(6)	90	101.189(6)	90	87.993(5)
β/o	83.505(3)	77.673(6)	97.224(6)	91.904(6)	110.620(6)	76.341(6)
γ/o	74.209(3)	77.967(6)	90	92.403(6)	90	65.360(6)
V/Å ³	3709.1(2)	3143.2(4)	3185.4(4)	2552.2(3)	3142.7(4)	2140.1(3)
Z	2	2	4	2	4	2
λ/Å	0.71073	0.71073	0.71073	0.71073	0.71073	0.71073
Measured reflections	31886	27359	17158	21510	13514	20325
Unique reflections	16047	13681	7797	11488	6232	10496
R _{int}	0.0288	0.0457	0.0416	0.0412	0.0636	0.0349
Observed rflns [I > 2σ(I)]	9618	7895	4701	7974	4085	7715
GooF	1.003	0.965	1.0331	1.066	0.885	1.041
R [on F, obs rflns only]	0.0539	0.0602	0.0710	0.0666	0.0477	0.0448
ωR [on F ² , all data]	0.1367	0.1486	0.2047	0.1809	0.0677	0.1050
Largest diff. peak/hole e/Å ⁻³	0.383/-0.186	0.391/-0.310	0.6916/-0.4722	0.476/-0.413	0.720/-0.528	0.481/-0.381

5.7 References

- [1] K. Anderson, Undergraduate thesis, University of Strathclyde, **2016**.
- [2] F. M. MacKenzie, R. E. Mulvey, W. Clegg, L. Horsburgh, *J. Am. Chem. Soc.* **1996**, *118*, 4721-4722.
- [3] A. R. Kennedy, J. G. MacLellan, R. E. Mulvey and A. Robertson, *J. Chem. Soc. Dalton Trans.* **2000**, 4112-4116.
- [4] S. Harder, *Chem. Commun.* **2012**, *48*, 11165-11177.
- [5] A. Stasch, *Chem. Commun.* **2015**, *51*, 5056-5058.
- [6] P. G. Williard and G. J. MacEwan, *J. Am. Chem. Soc.* **1989**, *111*, 7671- 7672.
- [7] W. Clegg, A. M. Drummond, R. E. Mulvey and S. T. Liddle, *Chem. Commun.* **1998**, 2391-2392
- [8] F. M. MacKenzie, R. E. Mulvey, W. Clegg and L. Horsburgh, *Polyhedron*, **1998**, *17*, 993-998.
- [9] D. R. Armstrong, E. Crosbie, E. Hevia, R. E. Mulvey, D. L. Ramsay and S. D. Robertson, *Chem. Sci.* **2014**, *5*, 3031-3045.
- [10] H. Naka, M. Uchiyama, Y. Matsumoto, A. E. H. Wheatley, M. McPartlin, J. V. Morey and Y. Kondo, *J. Am. Chem. Soc.* **2007**, *129*, 1921-1930.
- [11] R. E. Mulvey, D. R. Armstrong, B. Conway, E. Crosbie, A. R. Kennedy and S. D. Robertson, *Inorg. Chem.* **2011**, *50*, 12241-12251.
- [12] A. R. Kennedy, R. E. Mulvey, D. L. Ramsay and S. D. Robertson, *Dalton Trans.* **2015**, *44*, 5875-5887.
- [13] B. Conway, J. García-Álvarez, E. Hevia, A. R. Kennedy, R. E. Mulvey and S. D. Robertson, *Organometallics*, **2009**, *28*, 6462-6468.
- [14] E. Crosbie, P. García-Álvarez, A. R. Kennedy, J. Klett, R. E. Mulvey and S. D. Robertson, *Angew. Chem. Int. Ed.* **2010**, *49*, 9388-9391.
- [15] J. García Álvarez, E. Hevia, A. R. Kennedy, J. Klett and R. E. Mulvey, *Chem. Commun.* **2007**, 2402-2404.
- [16] J. Langer, S. Krieck, H. Görls, G. Kreisel, W. Seidel and M. Westerhausen, *New J. Chem.* **2010**, *34*, 1667-1677.
- [17] J. García-Álvarez, D. V. Graham, A. R. Kennedy, R. E. Mulvey and S. Weatherstone, *Chem. Commun.* **2006**, 3208-3210.
- [18] C. R. Groom, I. J. Bruno, M. P. Lightfoot and S. C. Ward, *Acta Cryst.* **2016**, *B72*, 171-179.

- [19] M. Schiefer, H. Hatop, H. W. Roesky, H-G. Schmidt, and M. Noltemeyer, *Organometallics*, **2002**, *21*, 1300-1303.
- [20] B. Conway, A. R. Kennedy, R. E. Mulvey, S. D. Robertson and J. García Álvarez, *Angew. Chem. Int. Ed.* **2010**, *49*, 3182-3184.
- [21] B. Conway, P. García-Álvarez, A. R. Kennedy, J. Klett, R. E. Mulvey and S. D. Robertson, *New J. Chem.* **2010**, *34*, 1707-1712.
- [22] T. Chlupaty, J. Turek, F. De Proft, Z. Ružičková and A. Ružička, *Dalton Trans.* **2015**, *44*, 17462-17466.
- [23] M. P. Coles, P. B. Hitchcock, A. V. Khvostov, M. F. Lappert and A. V. Protchenko, *Dalton Trans.* **2010**, *39*, 6426-6433.
- [24] R. E. Mulvey and S. D Robertson, in *FascinATES : mixed-metal ate compounds that function synergistically*, Organo-di-metallic compounds (or reagents), Topics in Organometallic Chemistry, Springer, **2014**.
- [25] Y. Kondo, M. Shilai, M. Uchiyama and T. Sakamoto, *J. Am. Chem. Soc.* **1999**, *121*, 3539-3540.
- [26] P. C. Andrikopoulos, D. R. Armstrong, H. R. L. Barley, W. Clegg, S. H. Dale, E. Hevia, G. W. Honeyman, A. R. Kennedy and R. E. Mulvey, *J. Am. Chem. Soc.* **2005**, *127*, 6184-6185.
- [27] A. R. Kennedy, J. Klett, R. E. Mulvey and D. S. Wright, *Science*, **2009**, *326*, 706-708.
- [28] B. Conway, D. V. Graham, E. Hevia, A. R. Kennedy, J. Klett and R. E. Mulvey, *Chem. Commun.* **2008**, 2638-2640.
- [29] W. Clegg, B. Conway, D. V. Graham, E. Hevia, A. R. Kennedy, R. E. Mulvey, L. Russo and D. S. Wright, *Chem. Eur. J.* **2009**, *15*, 7074-7082.
- [30] W. Clegg, B. Conway, P. García-Álvarez, A. R. Kennedy, J. Klett, R. E. Mulvey and L. Russo, *Dalton Trans.* **2010**, *39*, 62-65.
- [31] M. Irwin, T. Krämer, J. E. McGrady and J. M. Goicoechea, *Inorg. Chem.* **2011**, *50*, 5006-5014.
- [32] D. R. Armstrong, J. A. Garden, A. R. Kennedy, R. E. Mulvey and S. D. Robertson, *Angew. Chem. Int. Ed.* **2013**, *52*, 7190-7193.
- [33] C. Lichtenberg, T. P. Spaniol, L. Perrin, L. Maron and J. Okuda, *Chem. Eur. J.* **2012**, *18*, 6448-6452.
- [34] Z. Yang, M. Zhong, X. Ma, S. De, C. Anusha, P. Parameswaran and H. W. Roesky, *Angew. Chem. Int. Ed.* **2015**, *54*, 10225-10229.

- [35] Z. Yang, M. Zhong, X. Ma, K. Nijesh, S. De, P. Parameswaran and H. W. Roesky, *J. Am. Chem. Soc.* **2016**, *138*, 2548-2551.
- [36] V. K. Jakhar, M. Kr. Barman and S. Nembenna, *Org. Lett.* **2016**, *18*, 4710-4713.

Chapter 6: Closing Reflections

If we consider the bigger picture of science in the world, there are imminent global issues that are entrusting advancements in science to help overcome them. Global warming prevention, clean sustainable energy, fuel resources, endangered elements and green chemistry are some of the topics within the scientific community that ideally we would love to solve. However, there is the scenario that upon resolving one problem, it leads to the development of another. Hence there is a perpetual requirement to meet new demands as the world evolves. Although there are many research journals and research groups dedicated to sustainable development and green chemistry as a field, as a scientist our role is to continually provide new innovative tools that can have a positive contribution to the future of our planet.

Sustainable development: *“Meeting the needs of the present generation without compromising the ability of future generations to meet their own needs.”*

In organometallic chemistry, more specifically s-block, one of the first applications that would come to mind is C-H activation. So considering the fundamentals within our field we asked the question how can we incorporate an aspect of green chemistry into our work. Considering the twelve principles of green chemistry¹ (Figure 6.1), those highlighted in red were the main points incorporated in this work.

- | 12 Principles of Green Chemistry |
|---|
| 1. Waste prevention instead of remediation |
| 2. Atom efficiency |
| 3. Less hazardous/toxic waste |
| 4. Safer products by design |
| 5. Innocuous solvents and auxiliaries |
| 6. Energy efficient by design |
| 7. Preferably renewable raw materials |
| 8. Shorter synthesis (avoid derivitisation) |
| 9. Catalytic rather than stoichiometric reagents |
| 10. Design product for degradation |
| 11. Analytic methodologies for pollution prevention |
| 12. Inherently safer processes |

Figure 6.1: The twelve principles of Green Chemistry.

Typically, an alkali metal species would not be considered as a candidate in the design of a catalyst due to its inability to change oxidation state, its highly reactive nature and practical implications. However, there is a demand to develop alternative catalysts to mimic rare earth metals and this was one of the challenges bestowed upon here. Hence the work within this thesis aimed to introduce alkali metals, typically only thought of stoichiometric reagents, as catalytic entities. The precedence in the literature, with a surge of group 2 metal catalysts reacting successfully, provided encouragement and inspiration for this study.

This PhD thesis entitled, *Advancing Alkali Metal Dihydropyridine Chemistry: Syntheses, Structures and Applications*, started with the goal of developing an s-block “metal hydride” molecule that would have the potential to have catalytic activity, which would need to overcome the expected solubility issues of Group 1 metal hydride lattices and any practical implications of an organolithium compound.

By revisiting the simple atom efficient addition of an alkyllithium compound to pyridine, lithium dihydropyridines were synthesised and isolated from solution. The more reactive heavier alkali metal (sodium and potassium) dihydropyridine congeners have now successfully developed. These have been extensively characterised by X-ray crystallography, NMR spectroscopy, and thermal volatility analysis. Provisional thermal studies highlighted that although no direct metal-hydride bond was present it can still release an active soluble source of metal hydride. This indicated that the simplistic (Glasgow-born!) molecule pyridine, was acting as a transporting vessel that could release metal hydride. The next thing to establish was if the rearomatised alkylated pyridine was capable of up-taking the metal hydride to facilitate a soluble group 1 metal hydride catalytic cycle.

Not only was a range of potential alkali metal dihydropyridine catalysts prepared that displayed desirable properties; including simple efficient synthesis, commercially available reagents, non-toxic, safe to handle, but a full extensive study of the applicability of lithium dihydropyridines in catalytic regimes has been presented. In extensive detail, two catalytic manifolds, *catalytic dehydrogenative cyclisation of diamine boranes* and *catalytic hydroboration of carbonyls* have been discussed in this thesis. NMR spectroscopy and X-ray crystallographic studies have aided in the

understanding of these reaction pathways. Some key points to note is that in the case of the former catalytic cycle (chapter 3), our lithium dihydropyridine can mimic a ruthenium catalyst. Whilst in the latter catalytic regime (chapter 4) it stands as a strong competitor to those already in the literature.

Alkali-metal dihydropyridine catalysis is only the launching of this work. As discussed in chapter 5, new bimetallic systems, Li/Al, K/Al and K/Zn, have been unveiled that may exhibit unique catalytic properties, all of which need to be explored now. As Ekkehardt Hahn quoted “*the toolbox is only half full*” when we consider all of the possible polymetallic systems for reactivity in catalysis.²

On a wider outlook this study has added lithium to the list of non-conventional catalytic contenders. Although this is only a start on the plethora of organic transformations required in synthesis, alkali metals have now demonstrated their catalytic potential. Hopefully, this is the beginning of a rigorous study of catalytic transformations which dihydropyridines may be exploited in. Looking beyond the directly influenced future work of this project within the group, it can only be hoped that the findings described within this thesis will signify the beginning of a dramatic reappraisal of Group 1 catalysis, that they will earn a more permanent position in the catalytic arena of the future.

References

- [1] R. A. Sheldon, A. Arends and U. Hanefeld, *Green Chemistry and Catalysis*, Second Ed, John Wiley & Sons Ltd, Chapter 1, **2007**.
- [2] J. A. Gladysz, Z. T. Ball, G. Bertrand, S. A. Blum, V. M. Dong, R. Dorta, F. Ekkehardt Hahn, M. H. Humphrey, W. D. Jones, J. Klosin, I. Manners, T. J. Marks, J. M. Mayer, B. Rieger, J. C. Ritter, A. P. Sattelberger, J. M. Schomaker and V. Wing-Wah Yam, *Organometallics*, **2012**, *31*, 1-8.

Chapter 7: General experimental techniques and procedures

7.1 Schlenk techniques

All reactions were performed under protective argon inert atmosphere using Schlenk techniques. This involves using a Schlenk line; the main component is a glass manifold illustrated in [figure 7.1](#), this is attached to both a vacuum pump and an argon supply. The direction of the stopcock in the manifold allows the user to control whether they apply a vacuum or an inert gas to the Schlenk flask. At the vacuum end a cold trap is attached between the connection of the Schlenk line and the pump. This is emerged in liquid nitrogen to condense any solvent vapours, preventing them reaching the pump. Each Schlenk flask has a stopper and a tap in the sidearm. To prevent unwanted air/moisture entering the flask via these routes silicon grease is applied liberally to the stopper and the tap before carrying out the reaction. The purpose of the tap is to have control of the applied vacuum/gas into the Schlenk flask when it is connected to the line.



Figure 7.1: Typical Schlenk line set-up.

Before a Schlenk can be used, it has to be oven dried, overnight preferably. It must then be evacuated for 10 minutes to remove air and moisture and then refilled with argon; this process is repeated 3 times to ensure it is completely air-free. Solvents were added to the Schlenk tube via a needle and syringe also flushed with argon gas.

7.2 Glovebox manipulation

An MBraun glovebox fitted with an inert gas recirculation and purification system (figure 7.2) was used for the weighing and storage of air/moisture sensitive solid starting materials and preparing NMR samples. The glovebox contains two different sized ports to access the main chamber, which must be purged with argon before opening to the main chamber.

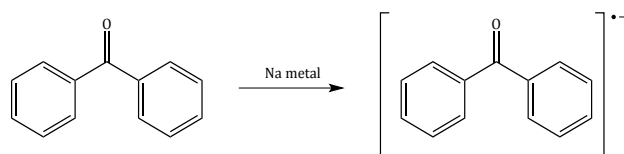


Figure 7.2: MBraun glovebox used for the inert atmosphere work within this thesis.

7.3 Solvent and reagent purification

All solvents used in the preparations were distilled over sodium and benzophenone under an inert nitrogen atmosphere to ensure they were anhydrous and oxygen free. Sodium and benzophenone is a routinely used drying agent^[1] as the benzophenone

undergoes a one electron reduction (Scheme 7.1) with sodium to generate the highly reactive benzophenone ketyl radical, which then reacts with water and oxygen.



Scheme 7.1: Reduction of benzophenone to the benzophenone ketyl radical

The formation of the ketyl radical is indicated by an intense royal blue colour. This is also indicative that the solvent is dry and under oxygen free conditions. Once the solvents are dry, they can be transferred to the reaction via an argon flushed syringe.

A freeze pump thaw methodology^[1] was employed to remove any oxygen from deuterated solvents, d_6 -benzene and d_8 -THF. The solvent is placed in a J. Youngs ampule and then the sealed flask is placed in liquid nitrogen to freeze the solvent. It is then placed under vacuum whilst thawing to room temperature. This was repeated three times. The resulting solution was then stored over 4Å molecular sieves.

The reagents used within this thesis were purchased from Sigma Aldrich, Alfa Aesar or Fluorochem and were typically used as received. The diamines in chapter 3 and the aldehydes and ketones in chapter 5 were stored over 4Å molecular sieves prior to use.

7.4 Analytical procedures

7.4.1 NMR Spectroscopy

All NMR spectra were recorded on a Bruker AV3, AV400 or DRX 500, operating at 400.03, 400.13 or 500.13 MHz for ^1H , 100.62, 100.60 and 125.77 MHz for ^{13}C and 155.50 MHz for ^7Li referenced against LiCl in D_2O at 0.00 ppm. Correlation spectroscopy was obtained by COSY (correlation spectroscopy) and HSQC (heteronuclear single quantum correlation) NMR methods. DOSY (diffusion ordered spectroscopy) NMR experiments were performed on a Bruker AV400 NMR spectrometer.

7.4.2 X-ray Crystallography

Single crystal X-ray diffraction data were recorded on either an Oxford Diffraction Xcalibur E or Oxford Diffraction Gemini S diffractometer using graphite-monochromatic $\text{Mo}_{\text{K}\alpha}$ or $\text{Cu}_{\text{K}\alpha}$ radiation (0.71073 and 1.54180 Å respectively). The structures were solved and refined to convergence on F^2 using all independent reflections by the full-matrix least squares method using SHELXL-2014/7^[2,3] or by the GaussNewton algorithm using OLEX2.^[4]

7.4.3 Elemental Analysis

Elemental analysis (CHN) was performed on a Perkin Elmer 2400 elemental analyser to determine the elemental composition of new compounds reported within this thesis. Samples were prepared in triplicate in the glove-box and sealed in an air tight box for transportation to avoid decomposition.

7.5 Preparation of common starting materials

7.5.1 Preparation of $n\text{BuNa}$ ^[5]

To a suspension of NaOtBu (3.84 g, 40 mmol) in 50 mL of *n*-hexane, $n\text{BuLi}$ (25 mL of a 1.6 M heptane solution, 40 mmol) was added slowly at 0°C. The white suspension was left to stir overnight before filtering to collect the white solid (typical yield: 2.4 g, 75%).

7.5.2 Preparation of $\text{KCH}_2\text{SiMe}_3$

To a suspension of KOtBu (3.37, 30 mmol) in *n*-hexane (20 mL) $\text{LiCH}_2\text{SiMe}_3$ (30 mL of a 1M pentane solution, 30 mmol) was added dropwise. This was left to stir overnight before filtering to collect the white solid (typical yield: 2.99 g, 79%).

7.5.3 Preparation of $t\text{Bu}_2\text{Zn}$ ^[6]

To a suspension of anhydrous ZnCl_2 (5.45 g, 40 mmol) in 80 mL of diethyl ether, at 0°C, $t\text{BuLi}$ (48 mL of a 1.7 M heptane solution, 80 mmol) was then added. The resulting suspension was then protected from light to prevent decomposition by covering the Schlenk tube with a black bag and allowing to stir for 2-3 hours. The suspension was then filtered through celite and glass wool. The colourless solution is then placed under vacuum to remove the majority of the diethyl ether. The remaining

solution is then transferred to sublimation apparatus via cannula. The remaining solvent is then removed under vacuum. Chilled isopropanol (-30°C) was then placed in the cool finger and continually maintained whilst the $t\text{Bu}_2\text{Zn}$ is subliming. Once complete the sublimation apparatus is transferred to a glovebox to collect the purified $t\text{Bu}_2\text{Zn}$ (typical yield: 5.0 g, 69%). This is then stored in a Schlenk tube as a 1M hexane solution at -30°C.

7.5.4 Preparation of $i\text{Bu}_2\text{AlTMP}$

$n\text{BuLi}$ (12.5 mL of a 1.6 M hexane solution, 20 mmol) was added to a Schlenk tube containing 50 mL of hexane. TMP(H) (3.4 mL, 20 mmol) was then added dropwise. This was allowed to stir for 15 minutes before adding $i\text{Bu}_2\text{AlCl}$ (3.8 mL, 20 mmol). The white suspension was allowed to stir at room temperature for 1 hour before filtering through celite and glass wool to remove LiCl . The hexane was removed by vacuum and the remaining yellow oil was stored in the glove box (typical yield: 5.04g, 90%).

7.6 References

- [1] D. F. Shriver, M. A. Drezdon, *The Manipulation of Air-Sensitive Compounds*, 2nd ed., Wiley, New York, **1986**.
- [2] G. M. Sheldrick, *Acta. Crystallogr.* **2008**, *A64* 112-122.
- [3] G. M. Sheldrick, *Acta. Crystallogr.* **2015**, *C71*, 3-8.
- [4] O. V. Dolomanov, L. J. Bourhis, R. J. Gildea, J. A. K. Howard, H. Puschmann, *J. Appl. Crystallogr.* **2009**, *42*, 339-341.
- [5] C. Schade, W. Bauer, P. V. Schleyer, *J. Organomet. Chem.* **1985**, *295*, C25-28.
- [6] P. C. Andrikopoulos D. R. Armstrong, H. R. L. Barley, W. Clegg, S. H. Dale, E. Hevia, G. W. Honeyman, A. R. Kennedy and R. E. Mulvey, *J. Am. Chem. Soc.* **2005**, *127*, 6184-6185.